CRANFIELD UNIVERSITY

M ELSDEN

A Transport Model For Dispersed Two-Phase Flows: Development and Implementation

SCHOOL OF MECHANICAL ENGINEERING

PH.D THESIS

CRANFIELD UNIVERSITY

SCHOOL OF MECHANICAL ENGINEERING

Academic Year 1994-5

M ELSDEN

A Transport Model For Dispersed Two-Phase Flows: Development and Implementation

Supervisor: P Hutchinson

May 1995

Abstract

Two-phase flows are found in many industrial and natural processes, from the combustion chambers of aero-engines to silt transport in rivers. The interaction between the two, or more, phases is extremely complex and is not amenable to analytical solution. Though equations exist to describe the behaviour of each of the phases, the direct solution of these equations, for all but the simplest flows, is beyond current computer power. Because of this much work is being done to develop computationally tractable models which are capable of predicting the behaviour of these flows well.

This thesis presents a new form of model based on a joint Eulerian-Lagrangian approach. This model is termed a transport model and consists of solving the second phase conservation equations in an Eulerian frame while introducing Lagrangian effects though a particle diffusion coefficient.

This thesis consists of three parts. First the development of the method used to obtain particle diffusion coefficients is presented and tested against available experimental data. This is followed by a discussion of the Eulerian calculation procedure used for both the carrier and discrete phase. Finally the linking of the two calculation procedures is discussed in detail and the model's performance is evaluated against both experimental data and a range of other models found in the literature.

The transport model is shown to perform well in predicting the chosen test-cases. Further, the results are shown to be comparable to, or better than, those of the other models considered.

One of the main benefits of the model is its low computational overhead. All calculations presented here were performed on a desktop personal computer.

Finally some recommendations are made for further work.

Acknowledgments

I would like to express my gratitude and appreciation to all the people who have made this work possible.

Special thanks must go to Prof. P. Hutchinson for all his help and guidance, which has been invaluable in the preparation of this thesis. Despite the many demands on his time, he has always been available when needed. Also thanks must go to Miss S. Gammons who has dealt with 'trouble' admirably.

My thanks also go to Stefan, Gangolf and the boys from Erlangen for some timely help.

Clearly a big thank you must also go to my parents whose support (financial and otherwise) and understanding was greatly appreciated.

Lastly I would like to thank all the friends and workmates who made my four years at Cranfield enjoyable.

List of Contents

Abstract i

Acknowledgements ii

List of Contents iii

List of Figures ix

Nomenclature xvi

Chapter 1 - Introduction.

1.1 Outline of Thesis 1

1.2 Introduction 1

1.3 Particle Equation of Motion 3

1.4 Modelling Approaches 6

1.4.1 Lagrangian Models 6

1.4.1.1 Turbulence Models 7

1.4.1.2 Turbulent Scales 8

1.4.2 Eulerian Models 10

1.4.2.1 Single Fluid Models 10

1.4.2.2 Two Fluid Models 11

1.4.2.3 Closure 12

1.4.2.3.1 Zero-Equation Models 12

1.4.2.3.2 One-Equation Models 13

1.4.2.3.3 Two-Equation Models 14

1.4.2.3.4 The Diffusion Approximation 15

1.4.3 Joint Models 15

1.4.4 The Transport Model 16

1.4.5 Other Considerations 16

1.5 Experimental Data 19

Chapter 2 - Lagrangian Calculation.

2.1 Introduction 22

2.2 Particle Equation of Motion 23
2.3 Solution of the Particle Equation of Motion 26
2.3.1 The Analytical Solution of HHD 27
2.3.2 Crossing Trajectory Effects 30
2.3.3 Vector Model 31
2.4 Turbulence Modelling 34
2.4.1 Relationship between Eulerian and Lagrangian Scales 35
2.4.2 Effect of Turbulent Scales 37
2.5 Particle Diffusion Coefficients 39
2.5.1 Calculation of Particle Diffusion Coefficients 39
2.5.2 Autocorrelation Functions 42
2.5.3 Convection Approximation 44
2.5.4 Empirical Correlation 46
2.6 Statistical Considerations 47
2.6.1 Non-Ergodicity of a Sequence of Random Signs 48
2.6.2 Implications for Diffusion Coefficient Calculations 50

Chapter 3 - Experimental Validation of Diffusion Coefficient Calculation
3.1 Introduction 59
3.2 Data of Snyder and Lumley 60
3.2.1 Discussion of Snyder and Lumley Results 62
3.2.2 HHD Model 63
3.2.3 Vector Model - No Convection 64
3.2.4 Vector Model - With Convection 65
3.2.5 Integration of Autocorrelation Function 66
3.3 Data of Wells and Stock 66
3.3.1 Discussion of Wells and Stock Results 68
3.3.2 Vector Model Comparison 70
3.3.3 Convection Time Comparison 71
3.4 Data of Elghobashi and Truesdell 71

3.4.1 Discussion of Elghobashi and Truesdell Results 73
3.4.2 HHD Model 74
3.4.3 Vector Model - No Convection 74
3.4.4 Vector Model - With Convection 74
3.4.5 Integration of Autocorrelation Function 75
3.5 Conclusions 75

Chapter 4 - Single Phase Calculation
4.1 Introduction 83
4.2 Conservation Equations 84
4.2.1 Mass Conservation 84
4.2.2 Momentum Conservation 86
4.2.3 Generalised Form 88
4.3 Reynolds Averaged Equations 88
4.3.1 Continuity Equation 89
4.3.2 Momentum Equation 90
4.4 Turbulent Closure 91
4.4.1 Turbulent Viscosity Models 91
4.4.2 Stress Models 93
4.4.3 Choice of Turbulent Closure Model 95
4.5 Boundary Conditions 96
4.5.1 Inlet Boundary Conditions 96
4.5.2 Outflow Boundary Conditions 97
4.5.3 Planes of Symmetry 97
4.5.4 Periodic Boundary Conditions 98
4.5.5 Solid Boundaries 98
4.6 Solution Procedure 100
4.6.1 Numerical Solution 101
4.6.2 Discritisation 102
4.6.3 The Control-Volume Formulation 103

4.6.4 Pressure Coupling 108
4.6.5 The Staggered Grid 109
4.6.6 The Pressure Equation 110
4.6.7 Solution Methods 111
4.6.8 The Solution Algorithm 112
4.7 Validation Calculations 113
4.8 Conclusions 115

Chapter 5 - Eulerian Calculation for Second Phase.

5.1 Introduction 122
5.2 Conservation Equations 123
5.2.1 Mass Conservation 124
5.2.2 Momentum Conservation 124
5.2.3 Generalised Form 126
5.3 Reynolds Averaged Equations 126
5.4 Closure Model 127
5.4.1 The Diffusion Approximation 128
5.4.2 Mean Transport Equations 129
5.5 External Forces 130
5.6 Boundary Conditions 131
5.6.1 Wall Boundaries 132
5.7 Solution Procedure 132

Chapter 6 - Complete Calculation.

6.1 Introduction 136
6.2 Solution Algorithm 136
6.3 Calculation of Particle Diffusion Coefficients 138
6.4 Mean Square Velocity Term 140
6.4.1 Importance of the Fluctuating Velocity Term 141
6.4.2 Empirical Correlation 142

6.5 Validation Calculation 143

Chapter 7 - Test-Case Calculations.

7.1 Introduction 152

7.2 Test-Case 1 -Confined Coaxial Jet 153

7.2.1 Experimental Setup 153

7.2.2 Experimental Results 154

7.2.3 Comparative Models 155

7.2.4 Comparison between Models and Experiment 156

7.2.4.1 Gas Flow Field 157

7.2.4.2 Case 1 - Heavy Particles 158

7.2.4.3 Case 2 - Light Particles 159

7.2.5 Transport Model Calculations 161

7.2.5.1 Gas Flow Field 162

7.2.5.2 Case 1 - Heavy Particles 163

7.2.5.3 Case 2 - Light Particles 164

7.2.6 Discussion of Results 165

7.3 Test-Case 2 - Horizontal Channel Flow 167

7.3.1 Experimental Setup 167

7.3.2 Gas Flow Field 168

7.3.3 Deposition Experiments 169

7.3.4 Flow Field Calculation 171

7.3.5 Particle Dispersion Calculation 172

7.3.6 Discussion of Results 174

7.4 Conclusions 178

Chapter 8 - Discussion, Conclusions and Recommendations for Future Work.

8.1 Discussion 210

8.1.1 Particle Diffusion Coefficient Calculations 210

8.1.2 Single Phase Calculation 212

8.1.3 Second Phase Eulerian Calculation 213
8.1.4 Complete Calculation 214
8.1.5 Comparison with Test-Cases 216
8.2 Conclusions 218
8.3 Recommendations for Future Work 219
References 221
Appendix I - Derivation of Vector Model 234
Appendix II - Quadratic Initial Form 254
Appendix III - Statistics of a Sequence of Random Signs 259
Appendix IV - Derivation of Second Phase Conservation Equations 264

List of Figures

Figure 2.1 : Crossing Effect Due to Gravity 52

Figure 2.2 : Comparison of Crossing Time (l_e/u_t) and Eddy Lifetime (t_e) with water droplet size for droplets falling at terminal velocity in air at NTP..... 52

Figure 2.3 : Vector Diagram for the Instantaneous Particle Velocity Relative to the Gas Velocity. 53

Figure 2.4 : Use of the E&T Fluid Point Displacement Curve to Obtain the Fluid Point Diffusion Coefficient. 53

Figure 2.5 : Schematic of Velocity and Length Scale Distributions 54

Figure 2.6(a) : Fluid Point Dispersion with Variable Scales 54

Figure 2.6(b) : Copper Dispersion with Variable Scales 55

Figure 2.7 : Comparison of Arbitrary Time 'Average' and Ensemble Average 55

Figure 2.8 : Comparison of Dispersion from Simulation and Integral of Autocorrelations 56

Figure 2.9 : Normalised Autocorrelation Functions 56

Figure 2.10 : Comparison of Correlation and Simulation Dispersion Curves 57

Figure 2.11 : Evaluation of a Range of Sequences Υ_n^2 57

Figure 2.12 : Evaluation of a Range of Sequences Ω_n 58

Figure 3.1 : Comparison of HHD Model - No Crossing, With S&L Data 77

Figure 3.2 : Comparison of HHD Model - With Crossing, With S&L Data 77

Figure 3.3 : Comparison of Vector Model - No Convection, with S&L Data 78

Figure 3.4 : Comparison of Vector Model - With Convection, with S&L 78

Figure 3.5 : Comparison of Integral of Autocorrelation Function
with S&L Data 79

Figure 3.6 : Normalised Autocorrelation Functions 79

Figure 3.7 : Comparison of Calculated 57μm Glass Particle with W&S Data
for a Range of Drift Velocities, v_d (m/s). 80

Figure 3.8 : Comparison of Calculated 5μm Glass Particle with W&S Data
for a Range of Drift Velocities, v_d (m/s) 80

Figure 3.9 : Comparison of HHD Model with E&T Fluid Point 81

Figure 3.10 : Comparison of Vector Model - No Convection, with E&T 81

Figure 3.11 : Comparison of Vector Model - With Convection,
with E&T Fluid Point 82

Figure 3.12 : Comparison of Integral of Autocorrelation Function with
E&T Fluid Point, Showing Corresponding Correlation Times..... 82

Figure 4.1 : Elementary Volume Flux 116

Figure 4.2 : Elementary Volume Stress 116

Figure 4.3 : Simple One-Dimensional Control Volume 117

Figure 4.4 : Simple Two-Dimensional Control Volume..... 117

Figure 4.5 : A Portion of the Staggered Grid 118

Figure 4.6 : Calculation Grid for Pipe Flow 118

Figure 4.7 : Comparison of Mean Velocity Profiles Across Pipe
(Re_D=50,000) 119

Figure 4.8(a) : Calculated Kinetic Energy Profile Across Pipe (Re_D=50,000) 119

Figure 4.8(b) : Calculated Dissipation Profile Across Pipe (Re_D=50,000) 120

Figure 4.9 : Comparison of Calculated and Measured Non-Dimensional
Radial Fluctuating Velocity in the Boundary Layer (Re_D=500,000) ... 120

Figure 4.10 : Normalised Relative Turbulence Intensities in a Pipe Flow,
$Re_D = 5\times10^5$, (from Laufer (1954))..... 121

Figure 5.1 : Elementary Volume Flux for Second Phase 134

Figure 5.2 : Elementary Volume Stress for Second Phase 134

Figure 5.3 : Example of the Convolution of the Probability Density Function $f_i(x)$, Papoulis (1984), Showing the Rapid Approach to a Normal Distribution Characteristic of a Diffusion Process..... 135

Figure 6.1 : Variation of Water Droplet Diffusion Coefficient With Turbulent Scales 144

Figure 6.2 : Concentration Profiles, Water, Using Simulation for Γ_p 145

Figure 6.3 : Concentration Profiles, Copper, Using Simulation for Γ_p 146

Figure 6.4 : Comparison of Interaction Time Scales, Water 147

Figure 6.5 : Comparison of Interaction Time Scales, Copper 147

Figure 6.6 : Comparison of Correlation and Simulation, Water, Without $\langle u_p^2 \rangle$ 148

Figure 6.7 : Comparison of Correlation and Simulation, Water, With $\langle u_p^2 \rangle$ 149

Figure 6.8 : Comparison of Correlation and Simulation, Copper, Without $\langle u_p^2 \rangle$ 150

Figure 6.9 : Comparison of Correlation and Simulation, Copper, With $\langle u_p^2 \rangle$ 151

Figure 7.1 : Schematic of Hishida and Maeda Flow Field 179

Figure 7.2 : Mean Axial Gas Velocity Profiles - Case 1 (Heavy Particles) 180

Figure 7.3 : Mean Radial Gas Velocity Profiles - Case 1 (Heavy Particles) 181

Figure 7.4 : Fluctuating Axial Gas Velocity Profiles - Case 1
(Heavy Particles) 182

Figure 7.5 : Fluctuating Radial Gas Velocity Profiles - Case 1
(Heavy Particles) 183

Figure 7.6 : Mean Axial Particle Velocity Profiles - Case 1 (Heavy Particles) 184

Figure 7.7 : Mean Radial Particle Velocity Profiles - Case 1 (Heavy Particles) 185

Figure 7.8 : Fluctuating Axial Particle Velocity Profiles - Case 1
(Heavy Particles) 186

Figure 7.9 : Fluctuating Radial Particle Velocity Profiles - Case 1
(Heavy Particles) 187

Figure 7.10 : Particle Mass Flux - Case 1 (Heavy Particles) 188

Figure 7.11 : Mean Axial Particle Velocity Profiles - Case 2
(Light Particles) 189

Figure 7.12 : Mean Radial Particle Velocity Profiles - Case 2
(Light Particles) 190

Figure 7.13 : Fluctuating Axial Particle Velocity Profiles - Case 2
(Light Particles) 191

Figure 7.14 : Fluctuating Radial Particle Velocity Profiles - Case 2
(Light Particles) 192

Figure 7.15 : Particle Mass Flux - Case 2 (Light Particles) 193

Figure 7.16 : Mean Axial Gas Velocity Profiles 194

Figure 7.17 : Mean Radial Gas Velocity Profiles 195

Figure 7.18 : Fluctuating Radial Gas Velocity Profiles 196

Figure 7.19 : Mean Axial Particle Velocity Profiles - Case 1 197

Figure 7.20 : Mean Radial Particle Velocity Profiles - Case 1 198

Figure 7.21 : Particle Mass Flux - Case 1 199

Figure 7.22 : Mean Axial Particle Velocity Profiles - Case 2 200

Figure 7.23 : Mean Radial Particle Velocity Profiles - Case 2 201

Figure 7.24 : Particle Mass Flux - Case 2 202

Figure 7.25 : Experimental Setup of Perkins et al 203

Figure 7.26 : Particle Deposition Profile, Experiment D1 204

Figure 7.27 : Particle Deposition Profile, Experiment D2 205

Figure 7.28 : Particle Deposition Profile, Experiment D3 206

Figure 7.29 : Particle Deposition Profile, Experiment D4 207

Figure 7.30 : Particle Deposition Profile, Experiment D5 208

Figure 7.31 : Angle of Incidence between Particle Trajectory and
Calculation Grid 209

Nomenclature

Alpha-Numeric

a,b ..... Coefficients in SIMPLE algorithm.

A_i ..... Drag pre-multiplier, i th realisation.

A_p ..... Cross-sectional area of particle.

C ..... Mean concentration of second phase.

c ..... $A_i l_e$, Concentration of second phase.

C_μ ..... k-ϵ model constant, standard value of 0.09.

$C_{1\epsilon}$ ..... Constant in ϵ equation, standard value 1.44.

$C_{2\epsilon}$ ..... Constant in ϵ equation, standard value 1.92.

C_D ..... Drag Coefficient.

D ..... Pipe diameter, Diffusive flux in SIMPLE algorithm.

D_{ij} ..... Symmetric part of stress tensor.

d_p ..... Diameter of particle.

E ..... Wall roughness parameter.

E_{ijk} ..... Third order alternating tensor.

F ..... Drag force $1/\tau_p$., Convective flux in SIMPLE algorithm.

F_e ..... External potential force.

f_i ..... Fluctuating density.

g ..... Gravitational acceleration.

h ..... Non-dimensional displacement length (HHD).

k ..... Turbulent kinetic energy, wavenumber.

l, L ..... Length scale or displacement.

L_u ..... Integral length scale (S&L).

M ..... Mesh sizes (S&L), (W&S).

m ..... Mass.

P ..... Peclet number.

R	.....	Pipe radius.
r	.....	Radial distance.
Re	.....	Reynolds number.
$_R$	.....	Lagrangian two-time autocorrelation function.
S	.....	Infinitesimal surface element.
s_i, S_i	.....	Random sign.
S_p	.....	Source terms.
t, T	.....	Time scale.
t_d	.....	Eddy decay time.
U,V	.....	Mean velocities.
u,v	.....	Velocities.
u_τ	.....	Wall friction velocity.
u_t	.....	Particle terminal velocity.
V	.....	Infinitesimal volume element.
v	.....	Non-dimensional particle velocity (HHD).
W	.....	Weighting function.
x,y	.....	Displacements.
x	.....	Absolute relative velocity $\lvert u_g - u_p \rvert$

Greek

α	.....	$(u_t+(u_t+x_{t-1})^{\frac{1}{2}})/x_{t-1}$
β	.....	$A_i u_t$
Γ	.....	Diffusion Coefficient.
γ	.....	$\alpha e^{\beta x}$,Coefficient of proportionality used in second phase wall boundary condition.
δ_{ij}	.....	Dirac delta function or Kronecker delta, as required.
Δx, Δy	.....	Computational cell sizes.

ϵ ..... $(\alpha-1)/(\alpha+1)$, or dissipation.

η ..... Mean.

θ ..... Incidence angle between flow field and calculation grid.

κ ..... von Kármán constant value 0.4.

λ ..... Turbulent micro-scale.

μ ..... Dynamical viscosity.

μ_T ..... Turbulent/Eddy viscosity.

ν ..... Kinematic viscosity.

ξ ..... Non-dimensional inertial interaction time (HHD).

P ..... Mean density.

ρ ..... Density.

σ ..... Standard deviation.

σ_ϵ ..... Constant in k-ϵ equations, standard value 1.3.

σ_{ij} ..... Stress tensor.

σ_k ..... Constant in k-ϵ equations, standard value 1.0.

τ ..... Interaction time.

τ_c ..... Particle correlation time.

τ_p ..... Particle relaxation time.

Φ ..... Mean of generalised variable.

ϕ ..... Generalised variable.

Ω, Υ^2 ..... Sequences of random signs.

Ω_k ..... Anti-symmetric part of stress tensor.

ϱ ..... Density ratio.

Sub-Scripts

c ..... Convection.

D ..... Pipe diameter.

e ..... Eulerian.

f ..... Fluid.

fp ..... Fluid point.

g ..... Gas.

i,j,k ..... Coordinate direction or i th realisation.

L ..... Lagrangian.

N,S,E,W ..... Cell boundaries.

n,s,e,w ..... Node labels.

nb ..... Neighbouring cell.

p ..... Particle.

T ..... Time mean, or turbulent quantity as appropriate.

ϕ ..... Generalised variable.

Ω, Υ^2 ..... Sequences of random signs.

Super-Scripts

$\rightarrow$ ..... Vector quantity.

' ..... Fluctuating value.

$-$ ..... Time average.

+ ..... Non-dimensional distance form the wall.

^ ..... Pseudo-velocity.

Other

$\langle\ \rangle$ ..... Ensemble average.

Chapter 1

Introduction

1.1 Outline of Thesis

This thesis presents the development and implementation of a new joint model for the prediction of dilute two phase flows. The work consists of three parts. First the calculation of particle diffusion coefficients using a Lagrangian simulation technique is presented in chapter 2. Results obtained are compared with a range of experimental results in chapter 3. The second part discusses the single phase flow field calculation procedure used throughout this work, and is presented in chapter 4. Derivation of the Eulerian second phase conservation equations is presented in chapter 5. Chapter 6 deals with issues arising from the linking of the three parts of the model together; namely the particle diffusion coefficient calculation, the carrier phase flow field and the solution of the Eulerian equations for the discrete phase. Chapter 7 compares the results obtained from the full model with experimental test-cases. Finally chapter 8 presents the discussions, conclusions and recommendations for future work.

1.2 Introduction

The wide occurrence of two phase flows in all areas of engineering means that the knowledge of their behaviour is both important and useful. They can be found in a large range of applications extending from weather prediction to spray drying. Many industrial processes have two-phase flow as one of their key features and, therefore, an improved understanding and ability to predict its behaviour is of key economic importance. These applications can be found in such diverse situations as the injection of fuel into the combustion chamber of diesel engines and the production of powdered milk. Therefore the ability to be able to predict the behaviour and characteristics of a given two-phase flow would be extremely useful.

Unfortunately the interaction process between the two (or more) phases found in all these flow situations is exceedingly complex. This is true even for the simplest cases. The coupling of the phases through the exchange of various properties intrinsically ties them together. Even in the case of an isothermal, non-reacting, dilute, mono-dispersed flow the coupling of the two phases makes the direct solution of the problem extremely difficult. Although equations are well established for both the particle and its carrier phase, solution of this simplest case is only possible with the use of the most powerful computers available today. This direct solution method very quickly becomes intractable. The extension of two phase flows into more physically realistic situations therefore, poses many problems. Much work is being conducted to develop viable modelling approaches to these problems, thus enabling the prediction of more complicated flow regimes while remaining computationally tractable.

Two-phase flows can take on a wide variety of forms, and the prediction of the distribution structure in these flows is in itself a formidable problem. One of the interesting areas in two-phase flows is that of dispersed flows consisting of droplets or particles entrained in a liquid or gas in a sufficiently low concentration that the interaction between the individual particles or droplets can be considered negligible. This class of two-phase flows is important in a wide range of industrial applications, spray driers and diesel engines for example. The work presented here is concerned with developing a better understanding of the interplay between phases in this specific area. In particular a new model is presented and tested against experimental data.

An overview of modelling approaches commonly used in the literature is given below. Two main types of modelling approach are to be found, which consist of either considering the dispersed phase as a continuous fluid or as discrete particles. The first approach deals with the second phase through the use of standard conservation equations with added terms to describe the interaction between the two-phases. Such a model is generally solved in a stationary frame and, therefore, is termed an Eulerian approach. The second form of model considers the behaviour of a single particle (or many simultaneous particles), its motion being coupled to the continuum phase through a particle equation of motion. This type of model is generally solved in a frame travelling with the particle and,

hence, is termed a Lagrangian approach. Each type of model has its advantages and disadvantages over the other. Both types of model are discussed in turn below.

First the development of the particle equation of motion is discussed. A currently accepted form is given and then some remarks on the relative importance of the individual terms are made. The use of this equation is common to both types of models considered here. The two distinct forms of modelling approach are then discussed in turn.

The Lagrangian approach is presented first. The need for the gas velocity at all particle locations is discussed together with common techniques used to obtain this velocity. The introduction of the required turbulence model leads on to a discussion of the scales of turbulence which are important when considering particle dispersion.

Secondly the Eulerian approach is introduced. The two main types of this form of model are presented and a more detailed description of the preferred form is given. The need for a closure model similar to that used in single phase flows is then discussed. Four types of closure method are presented varying in complexity and approach, and a preference indicated.

Joint models, which are developed to exploit the benefits and avoid the disadvantages of each of the above modelling approaches are then briefly discussed. The work presented here belongs to this category and is briefly outlined.

Further interesting effects which apply to all of the modelling approaches are treated separately. The effect of an external gravitational field is discussed together with its relation to other inertial effects. The possibility of particles dispersing more than their carrier fluid is introduced in this context and related to the form of the particle autocorrelation function.

The available experimental data is then discussed. Three general classes of experiment are considered, which vary from fundamental studies, through more complex experiments, to those representing real industrial processes.

1.3 Particle Equation of Motion

The interaction processes between the discrete and continuous phase are specified through the particle equation of motion. This equation was originally derived for a slow-

moving particle in a fluid at rest, around the turn of the century by Basset (1888), Boussinesq (1903) and Oseen (1927), based on the earlier work of Stokes, and as such is commonly known as the BBO equation. The applicability of this equation is limited, due to the large number of assumptions made in its derivation. It has therefore been the subject of much refinement. Tchen (1947) extended the original work to consider the relative motion between the fluid and the particle and his work has been subsequently refined by Corrsin and Lumley (1957), Buevich (1966), Lumley (1978a), Maxey and Riley (1983) and Auton (1983) among others. (For a more mathematical treatment of these refinements see chapter 2). The currently accepted form can be written as

$$\underset{(I)}{m_p \frac{du_{p_i}}{dt}} = \underset{(II)}{m_p F(u_{f_i}-u_{p_i})} + \underset{(III)}{m_f \frac{Du_{f_i}}{Dt}} + \underset{(IV)}{\frac{1}{2} m_f \left(\frac{Du_{f_i}}{Dt} - \frac{du_{p_i}}{dt} \right)} + \underset{(V)}{\frac{3}{2} d_p^2 (\pi \rho_f \mu)^{\frac{1}{2}} \int_{t_0}^{t} \frac{\frac{d}{d\tau}(u_{f_i}-u_{p_i})}{(t-\tau)^{\frac{1}{2}}} d\tau} + (m_p - m_f) g_i \tag{1.1}$$

where

$$F = \frac{1}{\tau_p} = \frac{3}{4} \frac{1}{d_p} \frac{\rho_f}{\rho_p} C_d |u_{f_i}-u_{p_i}| \quad ; \quad \frac{D}{Dt} = \left[\frac{\partial}{\partial t} + u_{f_j} \frac{\partial}{\partial x_j} \right]$$

The term on the LHS of equation (1.1) is the inertia force on the particle due to its acceleration. The terms on the RHS corresponds to: (i) the viscous and pressure drag force; (ii) the force due to pressure gradients and viscous stresses; (iii) the inertia force due to the added mass of fluid displaced by the particle; (iv) viscous forces due to unsteady relative acceleration between the particle and fluid (commonly known as the Basset History integral) and (v) the buoyancy or gravity force.

Equation (1.1) is extremely complicated and has no exact solution, except for the

trivial case. Lumley (1978b), showed that this particle equation of motion is only valid for low particle Reynolds numbers for which a Stokes approximation is valid. It was further shown that the validity of the equation, in turbulent flow, depends on the following criteria: (a) the particle Reynolds number (based on the fluctuating relative velocity) should be less than 0.5; (b) the flow in the vicinity of the particle should be homogeneous shear and (c) for a particle Reynolds number ≤ 10 the particle wake can be considered stable. Of these criteria (a) is clearly the most restrictive. This equation is commonly assumed to hold for flows that do not strictly adhere to (a) but for which the particle Reynolds number is small (typically < 5).

The complexity of this particle equation of motion has lead to many studies being conducted to investigate the relative importance of the force terms found on the right-hand side. Hjelmfelt & Mockros (1966) considered this equation under three types of approximation. The first approximation neglected the Basset history term, (iv), arising from wake effects, the second also neglected the added mass term, (iii), which allows for the difference in density of the two phases, and finally the pressure gradient effects were also neglected, (v). These three terms were shown to become important only for very high density ratios (i.e. the density of the fluid is comparable to that of the particulate phase) and for very small particles that act like fluid points. Ahamadi & Goldschmidt (1971) also considered the Basset History term and showed that when interest is focused on turbulent dispersion this term does indeed become negligible. This was found to be true, in real systems, if the relative velocity is bounded for all time. Vojir and Michaelides (1994) also investigated the influence of the Basset history integral and it was again shown to be negligible for a large range of flow situations.

Through these considerations many forces experienced by the particle can be neglected, for a wide range of flow situations. Thus (1.1) can be reduced to drag and gravity (buoyancy) terms only (terms (i) and (v)). Though this reduces the complexity of the equation it is still a nonlinear (if a quadratic drag term is used), differential equation. The need for knowledge of the instantaneous fluid velocity at all possible particle positions further complicates the solution. This knowledge is generally not available (though with the use of DNS and LES this is becoming possible for simple flow situations). Consequently,

a modelling approach is required in order to specify the fluctuating fluid velocity field.

The solution of equation (1.1) is common to both forms of model discussed here. The Lagrangian models use it to solve for the required particle trajectory and the Eulerian models use (1.1) to obtain the source terms required for the momentum exchange between the continuous and discrete phases.

The two types of model are discussed in more detail below.

1.4 Modelling Approaches

The two types of modelling discussed here fall into the categories of Lagrangian and Eulerian methods. Lagrangian methods consider the behaviour of a single particle (usually) described by a particle equation of motion, and use statistical averaging to obtain mean characteristics of the whole second phase. Eulerian methods, conversely, consider the discrete phase as a continuum and derive the mean properties of the flow field directly. The two forms of models are complementary in nature, Durst et al (1984), Crowe et al (1977), Adeniji-Fashola (1987), Mostafa and Montigia (1987). It is generally concluded that the Lagrangian approach gives more detailed information about the individual particle behaviour but becomes expensive to compute when particle-particle interactions are required, as is the case for less dilute flows. The Eulerian approach, conversely, is superior for flows of higher void fraction and allows more straightforward treatment of multiple particle interaction.

1.4.1 Lagrangian Models

The most common modelling approach is based on tracking an individual particle through a given flow field. This implies that the characteristics of the particle are solved for along a particle trajectory and therefore the representation is Lagrangian. Using equation (1.1), usually applying some simplifications, to describe the behaviour of a single particle in the given flow field enables the physics of the interaction process to be captured accurately. It is commonly accepted that the current form of the particle equation, (1.1), accurately

represents the behaviour of a given particle, if the conditions set out above are met. The reduced form of this equation, which is accurate for many flow situations, has a form that allows the straightforward use of common computational techniques. Thus, the numerical development of this type of model is relatively straightforward.

However, the main drawback of the Lagrangian approach is that a large number of particles needs to be averaged over to obtain statistically stationary mean characteristics (typically of the order of 10,000). While this presents few problems in the most simple cases the introduction of added effects greatly increases the computational cost.

In order to be able to solve for the required particle trajectories the fluctuating gas velocity must be specified for all particle locations. This is typically accomplished through the use of a turbulence model. The most common forms of this turbulence model are discussed below, as is the associated problem of the selection of scales of turbulence.

1.4.1.1 Turbulence Models

Many forms of model are used in the literature to specify the required instantaneous fluid velocity around the particle. It is generally accepted that the problem can be expressed, through Reynolds decomposition, as a superposition of the fluid mean and fluctuating velocities. The mean fluid velocity, which is generally known at all locations within the flow, acts to convect the particle. Thus, the specification of the instantaneous fluid velocity 'seen' by the particle reduces to a requirement to specify the fluctuating component at the desired location.

The most commonly used approach to this problem is the so called discrete eddy concept in which the particle is considered to interact with a sequence of discrete eddies which are used to represent the turbulent fluctuations. This model was used in a basic one dimensional form by Hutchinson et al (1971), see also Hutchinson and Brown (1974), where the eddy was considered to consist of a random (positive or negative) velocity equal to the gas turbulent intensity which remained constant throughout an interaction. The straightforward form of the model allowed the analytical solution of the particle equation of motion (see chapter 2). This idea was later extended by Gosman and Ioannides (1983).

A more realistic approximation to a turbulent eddy can be made by assuming a Gaussian velocity distribution with a zero mean and a standard deviation equal to the turbulent intensity, see Phythian (1975), Shuen et al (1985) among others. The basic assumption of the eddy characteristics remaining constant throughout an interaction (as made in the earlier models) was extended by Milojevic (1990) and Sommerfeld et al (1993) to allow for modification of the eddy characteristics experienced by the particle during an interaction. The modification is based on the local kinetic energy and dissipation associated with the current particle position. Such a model is highly dependent on the specification of the eddy characteristics for which a clear rationale is difficult to find. Further discussion of this topic is deferred to section 2.4.

1.4.1.2 Turbulent Scales

The above turbulence models require the specification of the characteristics of the representative eddy, with which the particle interacts. Because the particle equation of motion is solved along the trajectory of the particle the required scales are Lagrangian. This leads to further problems as, though the Eulerian scales of the flow are relatively straightforward to obtain, the relationship between the Lagrangian and Eulerian scales is not simple.

Various attempts have been made to relate the two scales see Corrsin (1963), Hinze (1975), though no consensus has been reached. The commonly followed procedure is to relate the required eddy characteristics to the flow kinetic energy and dissipation. The widespread use of the k-ϵ turbulence model, Launder and Spalding (1974), to calculate the turbulent carrier phase flow field has strengthened the case for this approach, as it specifies the relationship between the kinetic energy and dissipation of the flow and the flow scales, see equation (2.10). The scales thus defined are Eulerian. Because of this, and the lack of a commonly accepted relationship between these and the required Lagrangian scales, a wide range of expressions for both the eddy lifetime and length scale can be found in the literature. Common practice is to use the Eulerian scales given by Shuen et al (1985) which can be obtained directly from the k-ϵ values for the carrier phase. This implies an intrinsic

assumption that the particle travelling in a Lagrangian frame experiences the same scales as found in the stationary Eulerian frame, which is clearly in error. The Eulerian time scale corresponds to the time taken for an eddy to cross a stationary observation point, and is not necessarily equivalent to its decay time. Mostafa and Mongia (1987) and Desjonqueres et al (1988) both used a Lagrangian time scale to represent the eddy lifetime but its specification was rather arbitrary. The lack of a consensus regarding the correct specification of these scales adds a degree of freedom to this modelling technique which, though useful, reduces its universality.

Chung and Troutt (1988) suggested an alternative approach in which the carrier flow field was modelled using a vortex ring method. This was applied to the development of a round jet. Tracking the particles through such a flow field removes the need for the specification of the eddy scales as they are known a priori, since the characteristics of the turbulent vortices are calculated explicitly.

Sabnis et al (1987) and Sabnis et al (1988) avoided the problem of the requirement for a knowledge of the Lagrangian scales of the turbulence by converting the tracking approach to an Eulerian frame by coordinate scaling. This method also allows the interaction between the two phases to be incorporated straightforwardly.

Correct specification of the eddy decay time and length scale does not fully specify the interaction process. This eddy decay time specifies an upper bound on the possible particle-eddy interaction time, but as the inertial effects of the particle increase other time scales become important. The inertial crossing time due to the relative velocity between the particle and eddy is also important (as are crossing trajectory effects, see below). The general method for specifying this interaction time, Gosman and Ioannides (1983), Adeniji-Fashola (1988) and others, is to use the time taken for the particle to cross a given eddy (using the defined length scale) assuming the relative velocity from the previous interaction. This rather crude method is still widespread in the literature due to the difficulties in specifying this time more accurately. A more realistic method, extending the original idea of Hutchinson et al (1971) is presented in chapter 2.

It should be noted that the problem of the correct specification of the length and time scales is not unique to Lagrangian calculations, as they are also required in a range of

closure assumptions needed for the Eulerian representations as described below.

1.4.2 Eulerian Models

The second modelling approach is based in a stationary Eulerian frame. Eulerian models generally take two forms. First those where the flow is modelled as a single homogeneous fluid where the interaction between the two phases is represented by internal stresses. These are related, via constitutive equations, to the bulk properties of the medium. The second method consists of regarding the gas-particle flow as two interpenetrating continua. The governing equations for the particle cloud are obtained by averaging the conservation equations over a volume. The two methods are discussed below. The use of the second type of model leads to a closure problem similar to that encountered in single phase calculations. Various methods of performing this closure are also presented.

1.4.2.1 Single Fluid Models

Here we discuss the representation of the two phase flow as a single homogeneous medium where the interactive forces are represented by internal stresses. A fundamental difficulty of this approach is its inability to accurately represent phenomena present in the flow arising from the detailed interaction between the two phases. As a result, it has generally been superseded (and should be superseded) by the two fluid model discussed in the following section, and is only applied to the calculation of the behaviour of a passive scalar.

The original formulation is described in detail by Monin & Yaglom (1971), and also used by Michaelides (1984) to describe the heat transfer coefficients of gas-solid mixtures. The fluid was considered to have variable density and variable heat capacity, with the solid phase contributing to fluctuations in the mean properties of the flow. Momentum and energy equations were developed for the steady-state. New terms arose from the variable density and heat capacity and the extra terms lead to closure problems. These problems were resolved by consideration of the equations arising from a single phase flow, using a turbulent

mixing length approach. Non-dimensionalisation led to a system of non-coupled, nonlinear ordinary differential equations. The results were compared with experiment and it was shown that the model yielded useful information about the space-averaged flow coefficients but would not describe the interactions of the particles and phenomena associated with the exchange mechanisms between the two phases. The latter failure is not surprising as this form of model does not represent the actual physics of the interaction between phases in sufficient detail.

1.4.2.2 Two Fluid Models

This method consists of developing, through standard techniques, conservation equations for the properties of the dispersed phase. The following assumptions are generally made in the formation of these equations: (i) The particulate phase is dilute, so that interactions between the particles can be neglected, also the particles are assumed to be spherical and of uniform size, to enable ease of computation; (ii) Both the gaseous and particulate phase act macroscopically as continua, this together with the dilute assumption affects the size of the smallest control volume, i.e. it must be large enough to contain sufficient particles to satisfy the continuum approximation; (iii) The mean flow is steady and incompressible; (iv) Molecular diffusion, Brownian and gravity effects are assumed negligible compared with turbulent diffusion.

Marble (1970), Hinze (1972) and others, developed governing equations based on the above assumptions. It is noted that the correct treatment of both the second phase pressure and viscosity terms presents problems, due to the lack of a mechanism for particle interactions. The assumption of a dilute suspension, (i), implies no direct particle-particle interactions, further the assumption of only one-way coupling, made here, removes any possibility of indirect interaction. These points are dealt with in more detail in chapter 5.

The resultant equations for the second phase are very similar in form to those used in single phase flow calculations. This enables the application of the solution techniques available to single phase flow solvers. This convection diffusion form also helps the simultaneous solution of both phases thus enabling coupling effects to be implemented much

more easily than in the above tracking methods.

Unfortunately these equations, when averaged, exhibit the same closure problem as found in the single phase equations. This introduces the need for a closure approach, discussed below.

1.4.2.3 Closure

The closure problem is encountered in single phase modelling, after applying the Reynolds decomposition and averaging, and is due to the presence of the so-called Reynolds stress terms (see chapter 4). This problem is also encountered in the conservation equations for the discrete phase. It leads to the need to solve N equations containing N+1 unknowns (see chapter 5). In single phase calculations this closure is effected by the use of a turbulence model.

Again following the turbulence models of single phase calculations, four forms of closure model can be found in the literature. They fall into the general headings of: (i) Zero-equation models; (ii) One-equation models; (iii) Two-equation models and (iv) Diffusion approximation closures. These four forms of closure model are discussed below.

1.4.2.3.1 Zero-Equation Models

Early theories suggested the presence of solid particles decreases the eddy viscosity of the gas flow arising from dissipation of turbulence energy at the interface. Owen (1969) considered the transport of particles in a horizontal pipe, including electrostatically charged particles. Rough estimates of the effect of particles on the gas phase turbulence were made for various types of particle. The turbulent length scale was assumed to be unaffected, which lead to a reduction in the eddy viscosity of the carrier phase. These results lead to the development of several first-order closure schemes that modified the eddy viscosity for the single phase flow. Owen proposed two relationships dependent on the ratio of particle relaxation time to the turbulent time scale. Choi & Chung (1983) modified the results of Owen by deriving different expressions for the virtual laminar and eddy viscosity of the

second fluid. A Boussinesq eddy viscosity model was assumed, together with the model of Owen, to obtain these various correlations. The eddy viscosity of the second fluid was modelled using the ratio of eddy viscosities derived empirically by various authors; Soo (1956), Meeks and Jones (1973), Hinze (1975), Peskin (1975), O'Brien (1979). These empirical expressions were reduced to a single expression containing model dependent coefficients. The laminar kinematic viscosity of the secondary fluid was approximated by assuming the ratio of ν_f/ϵ_f of the second fluid is similar to that of the primary. The results, considered against the experiments of Boothroyd (1966), with low solid-gas loading ratios were shown to give satisfactory prediction of friction factors in pipes. This work was further extended, Chung, Sung & Lee (1986), to consider the flow through a Venturi tube. Again closure was achieved using a Boussinesq eddy viscosity model, and a similar model to that of Choi and Chung for the eddy viscosities. A new expression was used for the kinetic energy expression following Elghobashi & Abou-Arab (1983) (see section 1.4.2.3.3). The eddy viscosity ratio was as above. Results were compared with experimental data and other theoretical predictions. The agreement was found satisfactory for the pressure drop and the dependence on particle size and flow rate was well predicted.

Generally this form of model has been superseded by one and two equation models, discussed later.

1.4.2.3.2 One-Equation Models

Possibly the first attempt to use a one-equation model to study two phase flows was that of Dannon et al (1977) in which a k-l closure model was applied to a particle laden axi-symmetric jet. The length scale was specified algebraically and taken to be equivalent to that of the single-phase jet. For the kinetic energy equation, the diffusion and production terms were modelled by a conventional single-phase gradient model neglecting any triple correlations. The authors proposed a model for the fluctuating velocity correlation that contained the correct asymptotic behaviour. The model was shown to give poor results due to the inappropriate choice of length scale thus arbitrary modification of the production and dissipation terms was needed to reflect structural variations.

1.4.2.3.3 Two-Equation Models

Most studies of two-phase turbulence modelling use a transport equation for the turbulence length scale based on a modelled equation for the isotropic dissipation rate, ϵ. The exact form of this equation, including particle effects, consists of 67 terms. Elghobashi & Abou-Arab (1983) described a two-equation model for the prediction of two-phase flows. The two equations describe the conservation of turbulence kinetic energy and the dissipation rate of the energy for the carrier-fluid. Transport equations were derived from the instantaneous and mean flow equations, together with equtions for the kinetic energy and dissipation. Closure of the momentum equations was achieved by modelling the turbulent correlations that appear in the mean flow equations. Following Lumley (1975) (1978b) and Launder (1975), the strain-rate volume-fraction correlations that appear in the mean flow equations were neglected due to their relatively small magnitude. The closure of the kinetic energy equations was accomplished by modelling the correlations up to, and including, third order, those of fourth order being ignored, as was the contribution to the diffusion of turbulence energy by the pressure interaction. Closure of the dissipation equation (which consists of 67 terms, see above) was accomplished by modelling the correlation expressions present, neglecting all those of fourth order. These closure expressions accounted for the interaction between the two phases and its influence on the turbulence structure. Comparison with experimental data suggests that the model predicted the significant effects of the particles on the jet flow.

Several proposals have been made in the two-equation method for the modelling of the extra terms in the k and ϵ equations. Chen & Wood (1983) followed Dannon et al (1977) and proposed exponential forms for the added dissipation terms in both equations. A second order closure assumption was also used by Chung, Sung and Lee (1986).

Higher order closure assumptions can also be found in the literature. For example, Andresen (1990) developed equations for the correlation terms themselves. These models are similar in form to the algebraic and Reynolds stress closures of single phase calculations, but are not generally tractable for computational application.

1.4.2.3.4 The Diffusion Approximation

A further method of closure, which is adopted in this work, is that of a gradient diffusion approximation (Fickian), which requires knowledge of the particle diffusion coefficient. Taylor (1921) gave an expression relating the diffusion coefficient for a fluid point to the turbulent Lagrangian time scale. Snyder and Lumley (1971) showed that this idea applied to non-fluid point particles if the Lagrangian time scale used corresponded to that measured along the particle trajectory.

Reeks (1977) conducted a study based on the linearised, reduced particle equation of motion to develop an expression for the particle diffusion coefficient based on time, the aerodynamic response time of the particle and the correlation function for the velocity field. Using the turbulent energy spectrum developed by Phythian (1975) he showed that the diffusion coefficient approaches an asymptotic value for long times, and that the asymptotic value increases with aerodynamic response time and could exceed the diffusion coefficient of the fluid point. This surprising result arose as a result of both the Frenkiel functions, Frenkiel (1948), selected to represent the autocorrelations, and the lack of inclusion of crossing trajectory effects (see below).

The advantage of a gradient diffusion approximation for closure is that it can be directly incorporated into the two fluid models, by simplifying the correlations of fluctuating properties found in the Reynolds averaged second phase equations, using repeated application of the gradient diffusion assumption. Difficulties arise in the correct specification of the particle diffusion coefficient. The particle fluctuating velocity is usually set by using the particle Schmidt number, which relates the fluctuating velocity of the particle to that of the gas, as discussed by Durst et al (1984). Other, more complicated models exist, see for example Govan (1989)

1.4.3 Joint Models

The above discussion shows the complementary benefits of the Lagrangian and Eulerian methods. Lagrangian models give a good representation of the particle dynamics

found in dilute two-phase flows. However, the requirement for extensive averaging generates a large computational overhead for complex flow situations. The Eulerian approach ,conversely, contains a less explicit model for the particle dynamics, as this is only included in averaged form as source terms in the momentum equations for the second phase. However, the Eulerian models allow more straightforward extension to complex flows. Therefore, it seems advantageous to develop a model that captures the benefits of each modelling approach while avoiding the drawbacks. This idea leads to so-called joint models. The work presented here accomplishes this linkage through the use of an Eulerian two-fluid model for the second phase with the incorporation of Lagrangian effects in the diffusion coefficient of the particle. The model is termed a transport model and is discussed briefly below.

1.4.4 The Transport Model

The model presented here uses a method which combines the benefits of the two above approaches. The basic framework of the model is Eulerian being based on the conservation equations for the discrete phase. Lagrangian effects are introduced by a simulation calculation for the diffusion coefficient of the particles. As a result it is straightforward to include effects which are usually difficult to incorporate into an Eulerian description, such as crossing trajectories (see below).

The dynamical equation used in the Lagrangian calculation includes only the quadratic drag and gravity forces, which allows the development of an analytical solution (following Hutchinson et al (1971)) for the particle motion resulting from the interaction with a representative eddy.

A detailed discussion of the proposed model is presented in chapters 2, 5 and 6.

1.4.5 Other Considerations

Various important and interesting results arise from the above discussion and are treated separately here. Discussed first is the possibility of over diffusion of particles, i.e. the

ability of a particles to disperse more than a fluid point having the same initial conditions. This is followed by a discussion of the important effect of crossing trajectories and its influence on the over diffusion of a particle.

The inclusion of particle-particle and particle-wall effects is then addressed in the context of both of the above modelling approaches. Finally the inclusion of two-way coupling is examined, again with reference to both Lagrangian and Eulerian methods.

Over diffusion of particles has been observed both experimentally and numerically by a range of authors, Chung and Troutt (1988), Gouesbet et al (1984), Elghobashi and Truesdell (1992) among others, and has been closely linked to the presence of negative loops in the autocorrelation functions of the particles, and is clearly an inertial effect arising from the dependence of the behaviour of a heavy particle on its previous motion. This effect is first examined for the case of zero-gravity. Crossing trajectory effects are then introduced in to the discussion and shown to significantly reduce the possibility of over diffusion of heavy particles.

The DNS experiment of Elghobashi and Truesdell (1992) enabled the calculation of the dispersion of a range of types of particles both with and without gravity (for a detailed discussion of both the types of particles and flow field considered see chapter 3). In zero gravity, at short times, inertia effects were shown to enable the magnitude of the autocorrelation function of heavy particles to considerably exceed that of the fluid point. These inertial effects later lead to a faster decay rate of the autocorrelation function of the particles and hence gave rise to negative loops. It follows, see chapter 2, that the diffusivity of heavy particles, in zero-gravity, may thus exceed that of the fluid point initially but, due to the influence of negative loops, the reverse was noticed for long times.

The introduction of gravity clearly influences the above discussion, and acts as a damping force on the particle dispersion. The added inertial effect of crossing trajectories is discussed by Yudine (1959), Csanady (1963), Snyder and Lumley (1971), Meeks and Jones (1973), Pisman and Nir (1978), Nir and Pisman (1979), Wells and Stock (1983) and Shih and Lumley (1985), among others. Crossing trajectories dominate over the inertial effects giving rise to the observed over diffusion, by greatly reducing the mean particle-eddy interaction time. Consequently it becomes less likely that the autocorrelation function of the

particle can be greater than that of the fluid point, and also reduces the likelihood of negative loops. This is shown by the results of Elghobashi and Truesdell who observe a much reduced particle dispersion on the introduction of gravity, and no over diffusion is observed.

The effects of particle-particle interaction and particle-wall interactions have also been investigated, using Lagrangian techniques, by a variety of authors, see Sommerfeld and Krebs (1989), Sommerfeld (1990), Raju and Sirignano (1990), Kim et al (1991), Sommerfeld (1992), Silverman and Sirignano (1994) among others. These effects are very important as the mass loading increases or for confined flows. The use of Lagrangian techniques to investigate these effects leads to a good understanding of the properties of the interactions. The actual implementation of these effects into a tracking code increases the computational cost enormously as it generally requires the simultaneous tracking of a large number of particles. An alternative approach to the problem was recently proposed by Litchford and Jeng (1991) who proposed predicting the behaviour of a parcel of droplets by tracking a representative mean particle and approximating the variance found in the flow through a statistical formulation based on the linearised particle equation of motion. This approach was shown to give good results and to significantly reduce the computational cost. Including these effects into an Eulerian calculation would require the introduction of a mean effect on the complete discrete phase, and the implementation of new boundary conditions. Silverman and Sirignano (1994) proposed a useful method for introducing particle-particle interactions into an Eulerian approach through statistical averaging. The particle drag coefficient, together with other particle properties, is modified to take account of its neighbouring particles. These modifications were developed by considering early work into the interaction between two particles travelling either side-by-side or in tandem, Sirignano (1983), Chiang et al (1992) and Kim et al (1992), (1993).

Two-way coupling effects, in which account is taken of the effects of the particles on the carrier phase, also become important as the mass loading increases. These effects arise form the bi-lateral exchange of momentum between the two phases. The incorporation of this effect into the above tracking techniques generally requires global iteration of both the carrier phase solver and the particle tracking code. This is generally based on the particle

source in cell (PSIC) approach of Crowe et al (1977). This technique significantly increases the computational cost, as discussed above. Conversely, the ability of the Eulerian methods to solve for both phases simultaneously allows the whole flow field to be solved without resorting to this global iteration approach. Further, the specification of the inter-phase coupling terms is more straightforward since both phases are solved in the same frame.

1.5 Experimental Data

Experiments are the key way of developing insight into the physical processes involved in any aspect of nature and also form a basis for the evaluation and validation of computational models. In some limited cases it is also now possible to use direct numerical simulation (DNS) of flows to test approximate models. DNS results are used in this work in both chapters 2 and 3. Experimental investigations described in the literature vary in complexity between those which concentrate on simple flow situations and those which represent the more complex processes used in industrial applications. The more fundamental investigations are aimed at understanding simple situations in some detail. Conversely, the more industrially orientated experiments generally consider flows which involve a range of processes and are generally conducted in complex geometries. It should be noted here that the use of numerical results from DNS is restricted by current computer power to the most fundamental investigations.

Fundamental experiments are extremely useful in the development and the early validation of proposed models. They generally reduce the complex problems found in the real world to much simplified flows where effects can be studied individually. For the case of two-phase flows the simplest situation obtainable is that of the dispersion of a single particle of constant size in a homogeneous, isotropic, stationary turbulent flow. While this type of flow field cannot be found in nature, since homogeneous flows are generally non-stationary and stationary flows are generally non-homogeneous, it can be closely approximated by decaying grid generated turbulence. The decay characteristics of this type of turbulence are well known and through the application of a suitable temporal and spatial scaling can be treated as quasi-stationary. Also, corrections can be made to account for the

inhomogeneity found in the mean flow direction. It can also be considered isotropic, in planes perpendicular to the direction of mean flow.

As a result grid generated turbulence is studied in the fundamental experiments in this field for example, Snyder and Lumley (1971), Wells and Stock (1983) and the DNS data of Elghobashi and Truesdell (1992). Mickelsen (1955) and Vames and Hanratty (1988) used a similar approach in considering the core region of a pipe flow. Experiments of this type allow the measurement of the fundamental dispersion characteristic of a given particle for a simple flow field, which is needed in the early validation of any proposed model. Clearly, if a new model is unable to capture the correct behaviour in these simple situations it will almost certainly fail when applied to more complex problems.

The second type of experimental data allows the testing of developed models for more complicated and physically more realistic flow regimes. Generally these experiments are conducted with some industrial application in mind. Examples are given by Bendig et al (1991) for a two fluid atomizer; Neumann and Umhauser (1991) who were concerned with the spatial arrangement of particles in pipes; Sommerfeld and Qui (1991) for swirling confined flows and Kawazoe et al (1990) for fuel droplet size distributions.

Between the two extremes of experimental data lie experiments which, while incorporating more physical effects than the fundamental experiments, avoid the complexity of the second type of experiment. These intermediate types of experiment offer a stepping stone between the development of a model, using the results of the fundamental experimental results, and application to real life flow problems. Good examples are the range of experiments conducted by Fleckhaus et al (1987), Hishida and Maeda (1987), Hishida et al (1988), Hishida et al (1989) concerning the behaviour of particles in a range of simplified jet and shear flows. Another useful example is the experiment of Perkins et al (1994) which was conducted on a range of particles in a low speed horizontal wind tunnel.

The work presented here is at an early stage and as such has currently not been tested in complex flow situations. Therefore only comparison with the first two categories of data is presented. The calculations of the particle diffusion coefficients are compared to the experimental data of Snyder and Lumley (1971) and Wells and Stock (1983) together with the DNS data of Elghobashi and Truesdell (1992) in chapter 3 in order to validate the

calculation procedure. The full model is later tested against the more complex experimental data of Hishida and Maeda (1987) and Perkins et al (1994), chapter 7, in order to investigate the performance of the complete calculation procedure.

CHAPTER 2

Lagrangian Calculation

2.1 Introduction

The derivation of the particle diffusion coefficient calculation used in this work is described in this chapter.

The historical development of the particle equation of motion is discussed first. This leads to the currently accepted form of equation for the motion of the particle. The relative importance of each term in this equation is then discussed and various simplifications described. Use of these simplifications leads to the reduced equation of motion, which is used throughout this work.

The original work of Hutchinson, Hewitt and Dukler (1971), hereafter referred to as HHD, is then discussed in the context of the current work. This original model is then developed and extended to include the effect of crossing trajectories to give the so-called vector model.

The discrete eddy turbulence model of HHD is then discussed as is the development of a suitable set of scales for the representative eddy. The use of distributions on these scales is then described. A comparison is then made between the calculated particle diffusion coefficients from the two models.

A further exact method of calculation is developed based on the integral of the autocorrelation of the particle velocity. A self-consistency check is performed between the vector model and this exact method, and is shown to be satisfied.

An extension is then developed to enable the application of the diffusion approximation to the initial quadratic interaction region, through the use of an additional time scale. This convection time is considered a function of the particle autocorrelation functions. Finally in this section an empirical correlation is proposed to enable the direct calculation of particle diffusion coefficients without the need for simulation.

Finally a discussion is made concerning the ergodicity of the particle-eddy interaction

process. Consideration of a sequence of random signs illustrates that, in general, the calculation of the diffusion coefficient is non-ergodic, i.e. time and ensemble averages are not equivalent. The impact of this result on the calculation of particle diffusion coefficients is then discussed.

2.2 Particle Equation of Motion

To investigate the behaviour of a discrete particle, either solid, liquid or gaseous, suspended in a turbulent flow field it is useful to define an equation of motion for the particle. An equation of this type was first developed at the turn of the century using the work of Stokes by Basset (1888), Boussinesq (1903) and Oseen (1927), to give;

$$\frac{1}{6}\pi d_p^3 \rho_p \frac{du_{p_t}}{dt} = -\frac{1}{12}\pi d_p^3 \rho_g \frac{du_{p_t}}{dt} - 3\pi\mu d_p u_{p_t} + \frac{3}{2}\pi\mu\frac{d_p}{\sqrt{\pi\nu}} + \int_{t_0}^{t} \frac{du_{p_t}(\tau)}{\sqrt{t-\tau}} d\tau - \frac{1}{6}\pi d_p^3(\rho_p - \rho_g) g_t \tag{2.1}$$

In the form above the equation is only valid for slow motion of a spherical particle under the influence of gravity in a fluid initially at rest.

Tchen (1947) extended equation (2.1) to describe the motion of a particle in a fluid moving with a variable velocity to give

$$\frac{\pi}{6} d_p^3 \rho_p \frac{du_{p_t}}{dt} = 3\pi\mu d_p(u_{g_t} - u_{p_t}) + \frac{\pi}{6} d_p^3 \rho_g \frac{du_{g_t}}{dt} + \frac{1}{2}\frac{\pi}{6} d_p^3 \rho_g \left(\frac{du_{g_t}}{dt} - \frac{du_{p_t}}{dt} \right) + \frac{3}{2} d_p^2 \sqrt{\pi \rho_g \mu} \int_{t_0}^{t} \frac{\frac{du_{g_t}}{d\tau} - \frac{du_{p_t}}{d\tau}}{\sqrt{t-\tau}} d\tau + F_e \tag{2.2}$$

The term on the LHS of (2.2) corresponds to the force required to accelerate the particle.

The terms on the RHS are : the drag term according to Stokes' law; a term due to pressure gradients in the fluid surrounding the particle, due to the acceleration of the fluid; the added mass term i.e. the force to accelerate the apparent mass of the particle relative to the fluid; the Basset history integral, which accounts for the deviation of the flow pattern from steady state; and the final term F_e which corresponds to external potential forces and contains the gravity force of (2.1).

This equation has been much modified and extended since it was first proposed. Corrsin and Lumley (1956) showed that the second term in equation (2.2) must be corrected in order to apply the equation to a turbulent flow where the fluid velocity is a function of both time and space. Considering the pressure drop in the ambient fluid, and using the pressure term in the Navier-Stokes equations in a Lagrangian frame the new form becomes

$$\frac{\pi}{6} d_p^3 \rho_g \left[\frac{\partial}{\partial t} u_{g_i} + u_{g_j} \frac{\partial u_{g_i}}{\partial x_j} \right] - \frac{\pi}{6} d_p^3 \mu \frac{\partial^2 u_{g_i}}{\partial x_j \partial x_j}$$

Rearranging the resulting equation, following Hinze (1975), gives a term containing

$$\left\{ \frac{18\,\mu}{d_p^2} (u_g - u_p) + \rho_g (u_g - u_p) \frac{\partial u_g}{\partial x} \right\}$$

From the above it can be seen that the effect of the resulting non-linearity is negligible if

$$\rho_f \frac{\partial u_f}{\partial x} \ll \frac{\mu}{d_p^2} \quad or \quad \frac{d_p^2}{\nu} \frac{\partial u_f}{\partial x} \ll 1$$

which implies that the particle must be small and if the particle diameter, d_p, is treated as a unit length , then this can be written as $\frac{\partial u_f}{\partial x^*} \ll 1$ where $x^* = \frac{x}{d_p}$.

The viscous forces in the new pressure term must also be neglected to reduce the equation to a first order time dependent form. This requires that

$$u_p \frac{\partial u_f}{\partial x} \gg \nu \frac{\partial^2 u_f}{\partial x^2} \quad or \quad \frac{u_p}{\nu} \frac{\partial u_f / \partial x}{\partial^2 u_f / \partial x^2} \gg 1$$

It is generally assumed here and elsewhere that these requirements can be met (see Hinze (1975)).

It is possible to simplify equation (2.2) by neglecting various terms. Hjelmfelt and Mockros (1966) presented a review of these various simplifications. Three types of approximations were considered termed type I, type II and type III. These consisted of neglecting only the history term; neglecting the history and added mass terms and neglecting the history term, the added mass term and the pressure effect respectively. Only stationary cases were considered and the velocities were expressed as Fourier integrals, following Hinze (1975) (p. 357), allowing the difference between the various simplifications to be seen in phase angle and amplitude ratios.

Three density ratios, ρ_p/ρ_f, 1000, 2.65 and 8.6×10^{-5} were considered. It was shown that for low frequency fluid motions all approximations gave good results. This corresponds to large Stokes numbers and implies that the particles follow the fluid, as expected. At high frequencies neglecting the Basset history term produces larger errors than neglecting the added mass term. Neglecting the pressure gradient was shown to be very important for the lowest density ratio. The conclusion of the work was that only for very high density ratios and small particles were the terms considered found to be unimportant.

Ahmadi and Goldschmidt (1971) considered the importance of the Basset history integral only. The aim was to show that though this term is non-negligible when considering a transient response, as considered above, it does become negligible in a statistically stationary response. This implies that for sufficiently long times of motion the effect of the history term on the particle motion is not strong. It was shown that the Basset term does indeed become negligible after a sufficiently long time if the relative velocity is bounded for all time. This condition while not exact can be considered to hold in general, especially in a statistical sense where the probability of this bound being broken is very small.

Many further modifications to the original equation have been made within the

literature see Lumley (1957), Maxey and Riley (1983), Auton (1983). The resultant form currently in general use is:

$$m_p\frac{du_{p_i}}{dt} = m_pF(u_{g_i}-u_{p_i}) + m_f\frac{Du_{g_i}}{Dt} + \frac{1}{2}m_f\left(\frac{Du_{g_i}}{Dt}-\frac{du_{p_i}}{d_t}\right) + \frac{3}{2}d_p^2(\pi\rho_f\mu)^{\frac{1}{2}}\int_{t_0}^{t}\frac{\frac{d}{d\tau}(u_{g_i}-u_{p_i})}{(t-\tau)^{\frac{1}{2}}}d\tau + (m_p-m_f)g_i \qquad (2.3)$$

where

$$F = \frac{1}{\tau_p} = \frac{3}{4}\frac{1}{d_p}\frac{\rho_f}{\rho_p}C_d|u_{g_i}-u_{p_i}| \quad ; \quad \frac{D}{Dt} = \left[\frac{\partial}{\partial t}+u_{g_j}\frac{\partial}{\partial x_j}\right]$$

This is the equation used as a starting point for the following analysis and throughout the current work.

No exact and general solution of equation (2.3) is possible even in the trivial form of all but the drag term being neglected. This is due the non-linearity arising from the coupling between the gas and particle velocities. This said, it is possible to create a mathematical framework within which the simplified form of equation (2.3) can be solved in a statistical sense by introducing a turbulence model to represent the fluctuating gas velocity experienced by the particle.

2.3 Solution of the Particle Equation of Motion

To simplify equation (2.3) we limit our viewpoint to the behaviour of particles whose density is much greater than that of the carrier fluid. This assumption obviously excludes bubbles from the following work. This demarcation between bubble flows and particle flows (either solid or liquid) is a common one. The assumption of a particulate flow enables some useful approximations to be made in equation (2.3). The second, third and fourth terms on the RHS of equation (2.3) only become important if the density of the carrier fluid becomes

comparable to, or less than, that of the particle (which occurs in bubble flows). This leads to substantial simplification, reducing the equation of motion of the particle to.

$$\frac{du_{p_i}}{dt} = \frac{A_p \rho_g}{2m_p} C_D (u_{g_i} - u_{p_i}) |u_{g_i} - u_{p_i}| + g_i \qquad (2.4)$$

where A_p is the cross-sectional area of the particle and C_D is the particle drag coefficient.

In certain conditions it is possible to solve this equation analytically. This was first accomplished by Hutchinson, Hewitt and Dukler (1971). The original derivation forms the basis of the current work and as such will be outlined in the next section.

2.3.1 The Analytical Solution of HHD

The original work of HHD serves as the basis for the model presented here for the dispersion of a particle in a turbulent flow field. Therefore, the work of HHD is given below as a first step in the development of the current model.

The original paper was concerned with the deposition of water droplets on the interior of a vertically orientated pipe. This required the calculation of particle dispersions radially within the pipe together with the process of deposition. Of interest here is the method used to calculate the radial dispersion of the particles. The starting point, as mentioned above, was the reduced form of the particle equation of motion. Gravity forces were neglected since the dispersion considered was orthogonal to the gravitational field. This simplification though commonly found in the literature, will be shown later, to be in error. The turbulence was also considered isotropic in directions radial to the mean flow direction, thus enabling a one dimensional model to be applied to represent the particle dispersion in a plane perpendicular to the pipe axis. This resulted in the following one dimensional equation of motion.

$$\frac{du_p}{dt} = \frac{A_p \rho_f}{2m_p} C_D (u_g - u_p) |u_g - u_p| \qquad (2.4)$$

It is possible to apply this equation to only the fluctuating velocity component of the flow field as the mean convection direction of the particle is parallel to the pipe axis and therefore orthogonal to the considered dispersion. Consequently, the total particle velocity consisted of a superposition of the radial dispersion, obtained from the solution of the above equation, and the mean convective displacement in the direction of the pipe axis. A model is thus required for the gas fluctuating velocity. This is accomplished by using a discrete-eddy concept model in which the turbulence is considered to consist of a sequence of discrete eddies with which a particle interacts. A more detailed discussion of this model is found in the following section.

As mentioned above it is possible to solve equation (2.4) analytically under some limited conditions. This is possible if the gas velocity is assumed to be constant during a droplet-eddy interaction, thus simplifying the highly coupled nature of the gas and particle velocity and allowing convenient solution. Solving the equation (2.4) using non-dimensional parameters based on the pipe characteristics results in the following equations

$$v_{p_t} = s_t \left[1 - \frac{1 - s_t v_{p_{t-1}}}{1 + A_t \xi_t (1 - s_t v_{p_{t-1}})} \right] \qquad (2.5a)$$

$$h_t = \xi_t \left[1 - \frac{1}{A_t} \ln \left[1 + A_t (1 - s_t v_{p_t}) \right] \right] \qquad (2.5b)$$

$$\xi_i = \frac{e^{A_i} - 1}{A_i(1 - s_i v_{p_{i-1}})} \tag{2.5c}$$

using the following non-dimensional parameters

$$v = \frac{u_p}{u_e} \quad ; \quad h = \frac{l_p}{l_e} \quad ; \quad \xi = \frac{t}{t_e} \tag{2.6}$$

and the drag pre-multiplier

$$A_i = \frac{3}{8} C_D \frac{\rho_g}{\rho_p} \frac{l_e}{R} \frac{d_T}{d_p}$$

which is given in terms of the pipe radius, R, and diameter, d_T; s_i is the sign of the relative velocity between the particle and the gas, where the subscript i now refers to the i th interaction between particle and eddy.

It is possible to extend these equations to a more general form by rewriting the dependency on the pipe parameters in terms of the equivalent turbulence characteristics (see the first limiting case in Appendix I) to yield the following dimensional equations

$$u_{p_i} = u_g - \frac{u_g - u_{p_{i-1}}}{1 + A_i s_i (u_g - u_{p_{i-1}})\tau} \tag{2.7a}$$

$$l_{p_i} = u_g \tau - \frac{s_i}{A_i} \ln\left(1 + A_i s_i (u_g - u_{p_{i-1}})\tau\right) \tag{2.7b}$$

$$\tau = \frac{e^{l A_{p_i}} - 1}{A_i s_i (u_g - u_{p_{i-1}})} \tag{2.7c}$$

with A_i now being given by

$$A_i = \frac{3}{4}\frac{\rho_g}{\rho_p}\frac{1}{d_p}C_D$$

The two time equations derived above, (2.5c) and (2.7c), represent the inertial crossing time of the eddy by the particle. As such they represent only one possible interaction time scale. The other time scale used in the work of HHD was the eddy decay time. The shortest time scale will prevail thus the interaction time between the particle and eddy is obtained from:

$$t = MIN\,(t_{decay}, t_{inertial})$$

As mentioned previously the assumption that gravity can be ignored, made by HHD, is inappropriate and can lead to rather large errors. This is due to the so-called cross-trajectory effect that was not included in the original work. The following subsection discusses this effect.

2.3.2 Crossing Trajectory Effects

An important effect that needs to be included into the above calculation is that of crossing-trajectories. This effect was first proposed by Yudine (1959) and is concerned with the effect of the inclusion of a mean slip velocity between the particle and its carrier fluid (see figure (2.1)). This slip velocity can arise from various influences. The most common would be a velocity induced by an external potential field such as gravity, an electromagnetic field on a charged particle, or a form of injection velocity. The result of considering this effect is to introduce an extra time scale into the particle eddy interaction. This time scale becomes more influential in the interaction as the mean slip velocity increases. To show the importance of this effect the ratio of crossing time to turbulence time scale is shown in figure 2.2, for a water droplet in a specified turbulence field.

The importance of this effect shows that the simplification made in the work of HHD in ignoring the effects of gravity seriously over-predicts the particle dispersion since the interaction time between the particle and the eddy is generally over-predicted. The error increases as the particle relaxation time increases. This effect can be seen in the next chapter where calculations made using this model are compared with available experimental data.

To incorporate this effect into the particle dispersion calculations a psuedo-one-dimensional model has been developed which allows the inclusion of the effects of an arbitrarily orientated slip velocity. The only form of slip velocity included in this work is that of a gravity induced terminal velocity though it would be straightforward to extend the model to other forms of slip velocity. Development of this new, so-called vector model, is outlined in the next section.

2.3.3 Vector Model

To include the effect of an orthogonally orientated slip velocity into the calculation, while retaining the simple one-dimensional form of the original model, a new form of the particle equation of motion is developed. To accomplish this the reduced form of the particle equation of motion is used, as in the work of HHD but retaining the gravity term. This gives the following form.

$$\frac{d\vec{u}_p}{dt} = A_1(\vec{u}_g - \vec{u}_p)\,|\vec{u}_g - \vec{u}_p| + \vec{g} \qquad (2.8)$$

where A_1 represents the drag pre-multiplier, as before.

To reduce equation (2.8) to a one-dimensional form while retaining a dependence on orthogonal velocity, the vector form is resolved in the direction normal to gravity.

Consider the vector diagram shown in figure 2.3. The relative velocity between the particle and the eddy is given by:

$$(\vec{u}_g - \vec{u}_p) = (U - (U - u_p), u_g' - u_p')$$

$$= (u_t, u_g' - u_p')$$

where U represents the mean flow velocity and is assumed orthogonal to the dispersion direction. It follows that

$$|\vec{u}_g - \vec{u}_p| = (u_t^2 + (u_g' - u_p')^2)^{\frac{1}{2}}$$

The component of the drag force in the (gravity normal direction) is given by

$$A_t(u_g' u_p') |u'_g - u'_p| = A_t(u_t^2 + (u_g' - u_p')^2) \cos\theta$$

with

$$\cos\theta = \frac{u_g' - u_p'}{(u_t^2 + (u_g' - u_p')^2)^{\frac{1}{2}}}$$

$$A_t(u_g' - u_p')^2 = A_t(u_t^2 + (u_g' - u_p')^2) \frac{u_g' - u_p'}{(u_t^2 + (u_g' - u_p')^2)^{\frac{1}{2}}}$$

Hence

$$A_t(u_g' - u_p') = A_t(u_t^2 + (u_g' - u_p')^2)^{\frac{1}{2}} (u_g' - u_p')$$

Dropping the primes gives

$$\frac{du_p}{dt} = A_t\left(u_t^2+(u_g-u_p)^2\right)^{\frac{1}{2}}(u_g-u_p) \qquad (2.9)$$

Equation (2.9) is solved analytically in a similar manner to that proposed by HHD, which assumes a constant eddy velocity, u_g, throughout an interaction. This results in the following equations for the particle velocity and displacement after an eddy interaction together with the corresponding inertial interaction time. The full derivation of the equations is given in Appendix I.

$$u_{pi} = u_g + \frac{2u_t s_t c}{1-c^2} \qquad (2.9a)$$

$$l_{pi} = u_g\tau + \frac{u_t s_t}{\beta}\ln\left|\frac{1+\alpha e^{\beta t}}{1-\alpha e^{\beta t}}\frac{1-\alpha}{1+\alpha}\right| \qquad (2.9b)$$

$$\tau = \frac{1}{\beta}\ln\left|\frac{1}{\alpha}\frac{\epsilon e^{-\gamma}-1}{\epsilon e^{-\gamma}+1}\right| \qquad (2.9c)$$

where

$$\alpha = \frac{u_t+\left(u_t^2+x_{t-1}\right)^{\frac{1}{2}}}{x_{t-1}} \qquad \& \qquad \beta = A_t u_t$$

$$c = \alpha e^{\beta t}$$

$$\epsilon = \frac{1+\alpha}{1-\alpha} \qquad \& \qquad \gamma = \frac{\beta l_e}{u_t} = A_t l_e$$

and x_i represents the modulus of the relative velocity $|u_g-u_p|$

The behaviour of these new equations in the two limiting cases of $u_t \to 0$ and $u_t >> |u_g - u_p|$ is also investigated in Appendix I. The model is shown to recover the original model of HHD in the limit of small u_t together with the correct behaviour in the large u_t limit. The range of solution for the time equation is also discussed as problems may arise if it is attempted to solve (2.9c) for times greater than the eddy lifetime. This problem is avoided in the calculation by ensuring that the limiting time corresponding to the eddy decay time is never exceeded.

As in the model of HHD the time equation (2.9c) represents the inertial interaction time between the particle and eddy. The introduction of crossing effects leads to the use of a further time scale:

$$t = MIN\,(t_{decay}, t_{inertial}, t_{crossing}) = MIN\,(t_d, \tau, \frac{l_e}{u_t})$$

The above equations characterise the particle behaviour during a single interaction with a turbulent eddy while accounting for the effect of gravity. The equations require repeated solution, using sufficient interactions to assure statistical independence in order to obtain the mean particle behaviour through suitable averaging.

To solve these equations the instantaneous fluctuating gas velocity must be specified for each interaction. As noted previously, the gas velocity is represented by a modified form of the discrete eddy concept first proposed by HHD. The model for the turbulent eddy is discussed in the following section.

2.4 Turbulence Modelling

The need for the fluid instantaneous fluctuating velocity, together with the requirement that the gas velocity is constant throughout a particle-eddy interaction, leads intuitively to the development of the so-called discrete eddy concept. In this model the notion of a representative eddy is developed based on the turbulent scales present in the flow. A particle is then repeatedly interacted with representative eddies, by solution of equations (2.9a-c), to obtain the characteristic dynamical behaviour of the particles.

To implement the model it is necessary to specify characteristic scales for the eddies, i.e. size, velocity and lifetime. Many equations for the specification of these scales exist in the literature, Gosman and Ioannides (1981), Shuen et al (1985), Mostafa and Mongia (1987), Desjonqueres et al (1988) and Govan et al (1989) among others. Indeed it can be considered rather arbitrary which values are chosen provided they are consistent with each other and can be shown to lie within the inertial sub-range of the turbulent spectra of the flow. This will be discussed in more detail when the application of distributions to the chosen scales is described in section 2.4.2.

Here the standard equations for the particle velocity and length scales are set in the well-known k-ϵ turbulence model used in single phase computational fluid dynamics (see chapter 4):

$$u_e = \sqrt{\frac{2}{3}k} \quad ; \quad l_e = C_\mu^{\frac{3}{4}} \frac{k^{\frac{3}{2}}}{\epsilon} \quad ; \quad t_e = \frac{l_e}{u_e} \tag{2.10}$$

This choice of scales is commonly used in the literature and is made out of convenience. Moreover the approach is consistent throughout the calculation since the single phase flow field outlined later in this work is also computed using the k-ϵ model.

Use of equations (2.10) gives the Eulerian time scale for the eddy, that is the time taken for the eddy to cross a stationary observation point. Using this time to represent the lifetime of an eddy as seen by the particle is inappropriate. In fact this time represents the minimum of the eddy lifetime. The lifetime of the eddy experienced by the particle is obtained by considering the case of an observation point following the eddy from its birth to its decay. Thus, to specify the eddy lifetime the Lagrangian time scale is required. The relationship between Eulerian and Lagrangian time scales is discussed in the next section.

2.4.1 Relationship between Eulerian and Lagrangian Scales

As outlined above, a Lagrangian time scale is required to represent the eddy lifetime. Unfortunately, no simple relationship exists between the specified Eulerian scales and the required Lagrangian scales.

In the original work of HHD a crude estimate for this relationship was developed based on the pipe work of Laufer (1954), which gave:

$$t_d = 1.6\frac{l_e}{u_e}$$

Many other attempts have been made to derive a simple relationship between these Eulerian and Lagrangian time scales, Corrsin (1962), Hinze (1975), Graham and James (1994), Graham (1994). The resultant values vary considerably form author to author.

The relationship developed in this work uses data for the dispersion of a fluid point in a grid generated turbulent channel flow. This flow field is commonly used in experimental studies as it can be considered isotropic, homogeneous and is quasi-stationary (see chapter 3). The actual data used is from a numerical experiment using direct numerical simulation (DNS) performed by Elghobashi and Truesdell (1992). Their work was based on an earlier physical experiment of Snyder and Lumley (1971) in which the dispersion of a range of particles in a turbulent channel flow was considered. The original work, unfortunately, failed to produce reliable data for a fluid point. The corresponding numerical experiment rectified this problem. Both experiments are discussed in more detail in the next chapter.

The experimental data for the fluid point is extremely useful as it provides a full characterisation of the flow field. It is possible, within the framework of the model developed here, to define the characteristics of a fluid point analytically thus allowing various properties of the model to be investigated.

To derive a relationship between the Lagrangian and Eulerian time scale of the eddy the long time dispersion of the fluid point is considered. In the limit of large time the dispersion of a fluid point can be considered a diffusion process. The diffusion coefficient for a fluid point can be defined analytically by:

$$\Gamma_{fp} = \frac{1}{2}u_e^2 t_e = \frac{1}{2}u_e l_e = \frac{1}{2}\frac{l_e^2}{t_e} \qquad (2.11)$$

If this value is known from experimental data, together with the Eulerian velocity scale,

which simply corresponds to the turbulent velocity scale, a relationship between the Lagrangian and Eulerian time scale can be developed.

As mentioned earlier, the long time behaviour of the fluid point can be considered a diffusion process. This implies that the gradient of the curve of mean square displacement versus time, at large time, corresponds to twice the diffusion coefficient of the particle. Figure 2.4 shows the fluid point dispersion curve of Elghobashi and Truesdell (1992), which is used to obtain the fluid point diffusion coefficient .Use of the above analytical form, allows a value to be obtained for the eddy decay time.

As shown in figure 2.4 the experimental data of Elghobashi and Truesdell (1992) lead to a value of the Lagrangian time scale that is approximately 1.65 times greater than the corresponding Eulerian scale. Thus

$$t_L = 1.65\, t_e$$

This value is in remarkably close agreement with that found by HHD and falls well within the range of the other published values.

Though the method of derivation of this value is certainly justified, the accuracy of the value itself is open to question. The numerical data used in its derivation could lead to possible constraints on its validity, due to the scaling operations required in DNS simulation (see chapter 3). The question of whether it remains valid in other flow situations, such as boundary layers or shear layers is also in question. Regrettably very little experimental data exists from which to draw a firm conclusion.

Despite the above problems the relationship is assumed to remain valid for the purposes of the calculations described in this work. The chosen value fits well within the range found in the literature and the resulting dispersion of the fluid point, given in the next chapter, is in reasonable agreement with experimental data.

2.4.2 Effect of Turbulent Scales

Another important consideration is the effect of introducing a distribution of the various turbulent quantities, around the mean values obtained above. Many possible

distributions are possible while retaining the mean properties of the turbulent fluctuations. To investigate the effect of introducing statistical variation into the length, time and velocity scales two types of distributions were introduced.

Since it is generally considered that a turbulent flow exhibits properties that are close to Gaussian in distribution Batchelor (1953), Townsend (1956), Corrsin and Lumley (1956), a Normal distribution was implemented on the fluid velocity scale. The effect of this on the diffusion coefficient of the particles was investigated. In addition a 'box-distribution' was chosen to represent the possible variation in the eddy size encountered by the particle. Figure 2.5 shows schematic diagrams of the distributions.

The proposed velocity distribution was Gaussian with zero mean and a standard deviation equal to the fluid velocity scale, u_e (defined above). Thus the distribution exhibited the same mean characteristics as the simple $\pm u_e$ relationship used in the original work. To investigate the effect of this distribution on the dispersion of the discrete phase, two types of particles were used. The particles were chosen to represent the two extremes of the interaction process, i.e. a particle with a very small relaxation time that would follow the turbulent fluctuations exactly (a fluid point) and a particle with a relatively large relaxation time that would show appreciable inertial effects (a 46.5μm copper particle).

The effect of the introduction of the Gaussian velocity distribution on the dispersion of these two types of particles is shown in figure 2.6(a)-(b). The effect on the fluid point calculation is beyond the resolution of the graph and the two lines are coincident. The copper particle shows a small difference between the two calculations, which can, in part, be attributed to the finite number of iterations performed in the calculation of the diffusion coefficient. The error given is considered acceptable considering the extra computational cost required in the calculation of more iterations.

Secondly a 'box-distribution' was implemented around the original single length scale model proposed by HHD. The width of the distribution is shown in figure 2.5 to be $\pm\frac{1}{2}l_e$. This change in eddy size corresponds to a change in wavenumber of approximately two. The selected range keeps the eddy size within the energy containing range of the turbulent energy spectrum as required, but allows a relatively large variation in the eddy size experienced by the particle.

The effects of this distribution of length scales are shown in figure 2.6(a)-(b). As with the velocity distribution the effect on the fluid point calculation can be considered negligible. Similarly the effect on the copper particle is relatively small and can again be attributed to the approximation of a finite number of interactions in the simulation which leads to a small difference between the statistics of the two distributions

Following these results it was decided to include a Gaussian velocity distribution into the calculation. The added cost is modest and it gives a more realistic representation of the turbulent velocity distribution than the original $\pm u_g$ used by HHD. In particular, this form of distribution allows a particle eddy interaction that is no longer constrained to the case of $|u_p| \leq |u_g|$ as in the original model. Conversely the length scale distribution was discarded in favour of the simpler model of HHD since its effect is minimal.

2.5 Particle Diffusion Coefficients

As mentioned in the previous sections the aim of the calculations described here is the determination of particle diffusion coefficients. These can be derived from the statistical properties of the particle, which in turn, are obtained from the repeated solution of the above equations. The methods used, with some more specific consideration of the validity of representing the particle dispersion by a diffusion approximation, is discussed in the following section.

2.5.1 Calculation of Particle Diffusion Coefficients.

The calculation of the particle diffusion coefficient allows the dispersion of the particle to be obtained by application of a diffusion approximation

$$\langle x^2 \rangle = 2\Gamma t \qquad (2.12)$$

The diffusion coefficient of the particle may be obtained from one of the relationships below

$$\Gamma = \frac{1}{2}\langle u_p^2\rangle\langle t_l\rangle = \frac{1}{2}\frac{\langle l_p^2\rangle}{\langle t_l\rangle} = \frac{1}{2}\langle u_p\rangle\langle l_p\rangle \qquad (2.13)$$

These equations are only equivalent under the assumption of Eulerian scales. The transformation from one form to another depends on the triplet relationship

$$t_e = \frac{l_e}{u_e} \qquad t_L \neq \frac{l_e}{u_e}$$

This holds true when the Eulerian scales of the previous section are used. When a Lagrangian time scale is introduced, as required by the calculation, the triplet relationship breaks down.

In this work the equation for the particle diffusion coefficient is given by the second form of equation (2.13). The statistics required for the calculation of the particle diffusion coefficient are therefore the mean square displacement of the particle and the mean particle-eddy interaction time. This collapses to the analytical form for the fluid particle, equation (2.11), as required.

Multiple solutions of the particle-eddy interaction equations (equations 2.7a-c or 2.9a-c) are needed to obtain these statistical properties. Averaging procedures are then applied to obtain the required mean values. Two methods of averaging seem appropriate to compute mean values; namely time and ensemble averages. Time averaging would consist of calculating the behaviour of a single particle as it interacts with a large number (sufficient to ensure statistical stationarity) of random eddies and then averaging over these interactions. Ensemble averaging, alternatively, would consist of calculating the behaviour of a large number of particles as they interact with, perhaps, a smaller number of eddies and obtaining the average of the mean particle characteristics. Obviously the time averaging approach is preferable from a computational perspective and if the interaction process is ergodic the two forms of averaging would be equivalent. However, this has been found not to be the case, that is the ensemble and time averages for this type of interaction model are not equivalent. This will be dealt with in more detail in the next section.

The nonequivalence of time and ensemble averages means (see section 2.6) that the mean characteristics of the particle must be calculated using ensemble averages. This adds an appreciable calculation cost over the time averaging calculation. The difference in the calculated particle diffusion coefficient and hence the dispersion is shown in figure 2.7 for a range of particle types. The relaxation time, hence inertial effects, of the particles chosen varies across the range of interest. The difference between the two averaging processes increases as the particle relaxation time increases and can lead to up to an order of magnitude difference in the particle dispersion. The ensemble averaging approach has been shown to give the correct behaviour for all particle types considered (see section 2.5) and as such will be used throughout this work.

The assumption that the dispersion of the particles can be represented by a diffusion process is only strictly valid in the limit of long time, as mentioned in the previous section. Thus, though the gradient of the predicted dispersion curve may be correct for long times the short time displacement may be seriously over-predicted. This effect is again dependent on the particle relaxation time. The smaller the relaxation time of the particles the greater is its initial variation from the long time diffusive behaviour. This is due to the initial quadratic region of the interaction where the particle can be considered as being convected by the individual turbulent eddies and hence the displacement is of the form

$$\langle l_p \rangle = \langle u_p \rangle \langle t_l \rangle \quad \rightarrow \quad \langle l_p \rangle^2 = \langle u_p \rangle^2 \langle t_l \rangle^2$$

compared to

$$\langle l_p \rangle^2 = 2\Gamma_p \langle t_l \rangle$$

for a diffusion process.

A more accurate method of calculating the displacement of the particle as a function of time, which includes the initial quadratic region was first developed by Taylor (1921) and requires consideration of the particle autocorrelation function. This method allows both a check of self-consistency within the model and a means of developing an extension of the

diffusion approximation which more accurately represents the short time dispersion of the particle.

The next subsection discusses the use of the particle autocorrelation function.

2.5.2 Autocorrelation Functions

The particle two-time Lagrangian autocorrelation function is a measure of the memory effects exhibited in the motion of the particle, which is the amount of time over which the history of the particle motion influences its current behaviour. The non-dimensional form of this quantity can be defined as

$$R_L(\tau) = \frac{\overline{u_p(t)\,u_p(t+\tau)}}{u_p^2(t)}$$

which corresponds to the correlation between two particle velocities separated by a time interval, τ. This correlation function has been shown to exhibit some useful properties. Taylor (1921) showed that the particle's mean square displacement, due to its carrier fluid turbulent fluctuations, may be obtained from the particle autocorrelation function, through simple consideration of the particle kinetics, from

$$\overline{y^2(t)} = 2u_e^2 \int_0^t dt' \int_0^{t'} d\tau\, R_L(\tau) \qquad (2.14)$$

This equation can be simplified by performing a partial integration to give, Kampé de Fériet (1939)

$$\overline{y^2(t)} = 2u_e^2 \int_0^t d\tau\,(t-\tau) R_L(\tau) \qquad (2.15)$$

Equation (2.15) remains valid for all t and, as such, can capture the initial quadratic short

time behaviour of the displacement of the particle, unlike the diffusion approximation.

Furthermore it follows that the long time diffusion coefficient for the particle is given by

$$\Gamma = u_*^2 \int_0^{\infty} d\tau R_L(\tau) \qquad (2.16)$$

Equation (2.16) allows a useful check of self consistency within the model presented here. The particle autocorrelation function may be calculated using the sequence of interactions defined in the simulation and numerically integrated to obtain the diffusion coefficient. The results of this calculation are shown in figure 2.8, for a range of particle types. The dispersion curves corresponding to a constant diffusion coefficient agree closely. This implies that the model contains a high level of self consistency and that the ensemble averaging is carried out over sufficiently many samples.

The autocorrelation functions used in this comparison are shown in figure 2.9. The curves exhibit a roughly exponential decay profile. This has led many authors to postulate analytical forms for these functions, generally following Frenkiel (1948). Unfortunately these analytical forms generally fail to represent the required decay characteristics sufficiently well to be useful for the calculation of the diffusion coefficient of the particles. This lack of a reliable and consistent analytical representation of a particle autocorrelation function leads to a requirement for their numerical calculation.

The need for numerical calculation severely limits the usefulness of equations (2.15)-(2.16). In general a requirement to calculate the product of a large number of particle velocities over a large number of time steps so as to perform the required averaging is very time consuming. As a result the calculation of the autocorrelation functions as a route to the turbulent dispersion of the particles and the related diffusion coefficient is usually not appropriate. However, the detailed and precise description of the dispersion of the particles provided by equation (2.15) is a key to the development of the diffusion representation, especially in the short time region.

It is possible to reduce equation (2.15) into two distinct parts, one corresponding

to the initial quadratic region and a second corresponding to the constant diffusion form. The derivation of these equations can be found in Appendix II.

The cutoff point between the two forms corresponds to the correlation time for that particular particle, τ_c. A useful special case is that of a fluid point. Within the constraints of the eddy interaction model, outlined above, its Lagrangian autocorrelation function has the analytical form:

$$R(\tau) = \begin{cases} \langle v^2(t) \rangle \left(1 - \dfrac{\tau}{t_d} \right) & \tau \leq t_d \\ 0 & \tau > t_d \end{cases}$$

This allows the dispersion of a fluid point to be calculated analytically throughout. This special case is also presented in Appendix II.

The numerically calculated autocorrelation functions, shown in figure 2.9, have been used to develop a further extension to the diffusion form to improve its applicability in the short time region. This is discussed in the next subsection.

2.5.3 Convection Approximation

The initial interaction period is generally poorly represented by a diffusion approximation, as shown in the next chapter where a range of the models developed above is compared to experimental data. The poor performance of the model in this important initial region can lead to an over-prediction of the dispersion at long times. Consequently an additional refinement to the standard diffusion approximation has been developed, using the autocorrelation function representation discussed previously.

The basis for this refinement is the assumption that during the initial interaction period the effect of the turbulent flow on the particle is more convective than dispersive. To represent this a 'convection time' is chosen during which no diffusion is considered to take place.

The appropriate choice of convection time is dependent on the characteristics of the particle and most notably the particle relaxation time as mentioned above. The three

calculated autocorrelation functions, shown in figure 2.9, have been used to develop an empirical correlation for this convection time as a function of the particle relaxation time.

Since, within the constraints of the current model, the properties of a fluid point can be specified analytically it is possible to derive the convection time for a fluid point using these results.

The diffusion coefficient is defined, from equation (2.11), as

$$\Gamma_{fp} = \frac{1}{2}\frac{\langle l_p^2 \rangle}{\langle t_i \rangle} = \frac{1}{2}\frac{l_e^2}{t_L}$$

where t_i is the particle -eddy interaction time. This corresponds to half the gradient of the dispersion curve for a fluid point (at long time). Using the simple form for a straight line

$$y = mx + c$$

it is possible to find the correct value for the fluid point convection time from

$$\langle y^2 \rangle = 2\Gamma t + c$$

Given a known point, y_1^2, t_1 say, it is possible to specify c and therefore the convection time from

$$t_c = -\frac{c}{2\Gamma}$$

Using the fluid point data of Elghobashi and Truesdell (1992) (E&T) we obtain a value for the fluid point convection time of

$$t_c = 0.87\, t_L$$

This analytical solution is only possible because of the known properties of the fluid point. To obtain an empirical equation for this quantity a curve has been fitted through the times obtained from the numerical autocorrelations given in figure 2.9. The convection time was taken to be given by the half decay time of the autocorrelation function. This lead to the

following empirical correlation

$$\tilde{\tau}_c = c_{conv} \exp\left(\frac{-\tilde{\tau}_p^2}{2\sigma^2}\right) \quad , \quad c_{conv} = 0.35\, t_L \quad , \quad \sigma = 0.1\, t_L \tag{2.17}$$

This convection time corresponds to the time taken before the particle is allowed to disperse. The effect of the introduction of this time is shown in the next chapter where it is compared with the other methods of calculation derived here and experimental data.

Use of this time in the Eulerian calculation, outlined later, would correspond to a shift of the particle injection to a position corresponding to the point to which the particles will have been convected in time t_c under action of the mean velocity. Diffusion would then be considered from this position.

As can be seen in the comparison with experimental data in the next chapter the use of this convection time greatly enhances the accuracy of the diffusion approximation in the prediction of the displacement of the whole range of particles considered.

2.5.4 Empirical Correlation

Though the simulation method presented above is less costly computationally than the numerical integration of the autocorrelation function it is still a relatively time-consuming calculation. Therefore a simple empirical correlation has been developed that can be used to quickly calculate the diffusion coefficient of a particle.

The form for this empirical correlation is given by

$$\Gamma = \frac{1}{2} u_e^2 MIN\left(t_{decay}, \frac{l_e}{2u_t}\right) \tag{2.18}$$

Equation (2.18) has the standard form of the diffusion coefficient calculation in that it consists of a velocity scale multiplying a time scale. This is desirable since any empirical form should recover the correct expression for the fluid point which, as shown above, is known analytically. For the fluid point the first of the time scales on the RHS of (2.18) becomes dominant and, as a result, the correct diffusion coefficient is recovered. In the

opposite limit of a large, heavy particle the dominant time scale of the particle-eddy interaction is the crossing time. The second time scale on the RHS of (2.18) has this crossing time as its basic form but, unlike the simulation calculation, the Eulerian length scale is used. Also, a factor of two is introduced in the denominator. This extra factor of two serves to compensate for the over-prediction of the mean square particle velocity resulting from equating it to the turbulent fluctuating velocity. The exact reasons for this compensation are not yet clear though the form of the correlation implies that there is a close relationship between the ratio of the crossing time scale used in the correlation to the actual particle-eddy interaction time and that between the mean square fluctuating velocity of the gas and the particle.

Figure 2.10 shows a comparison of the dispersion obtained from the correlation and the simulation method for a range of particles and the fit can be seen to be surprisingly good.

Though this method of calculation is very cheap to compute, its validity is uncertain. Also the only result possible from this calculation is the particle diffusion coefficient. It will be shown in chapter 5 that the mean square fluctuating velocity of the particle is also required for later calculation.

While this empirical correlation is a useful tool for rapid calculation, its lack of physical insight into the processes involved in the particle-eddy interaction limits its use. It therefore is best considered a way of obtaining a good working approximation for the particle diffusion coefficient before a more robust, and expensive, method of calculation is used.

2.6 Statistical Considerations

As briefly mentioned above the statistics of the interaction process are of great interest. It has generally been assumed that the behaviour of a sequence of particle-eddy interactions, using a model like the one presented here, is ergodic in nature. During this investigation it has been discovered that this is not, in fact, the case. To illustrate this the behaviour of a sequence of random signs, which represents the simplest form of the interaction model, will be discussed.

2.6.1 Non-Ergodicity of a Sequence of Random Signs

During the course of this work an investigation was performed into the statistics of the particle-eddy interaction process arising out of the turbulence model discussed above. Initially, it was assumed that all the statistics of the interaction process could be determined from a single sample, if a sufficiently long time was considered, by time averaging. While simplifying the calculation, since it only requires computation of the behaviour of a single particle, the use of time averaging intrinsically assumes that the interaction process is ergodic.

The principle of ergodicity states (Papoulis (1984)):

"A stochastic process, x(t), is called ergodic if its ensemble averages equal appropriate time averages. Therefore, with probability 1, any statistic of x(t) can be determined from a single sample $x(t,\xi)$"

It is expressed mathematically below.

The ensemble average of a process x(t) is an estimate of the mean $\eta(t)$ and can be defined as:

$$\eta(t) = \frac{1}{n}\sum_{i=1}^{n} x(t,\xi_i)$$

The corresponding time average is given by:

$$\bar{x} = \lim_{T\to\infty} \frac{1}{2T}\int_{-T}^{T} x(t,\xi)\,dt$$

If $\eta(t)$ equals a constant, η, a mean ergodic process is one such that for

$$\eta_T = \frac{1}{2T}\int_{-T}^{T} x(t,\xi)\,dt \qquad \eta_T \to \eta \qquad as \qquad T \to \infty \tag{2.19}$$

where η_T is the mean obtained from time averaging. It follows from (2.19) that a process is mean ergodic iff its variance tends to zero as the time tends to infinity:

$$\sigma_T^2 \to 0 \quad as \quad T \to \infty \tag{2.20}$$

Therefore, to establish the ergodicity of a given process it is sufficient to investigate the behaviour of the variance of the process in the limit T→ ∞.

It is possible to reduce the particle-eddy interaction process, as considered here, to a sequence of random signs by correct non-dimensionalisation of the eddy characteristics and gives a sequence $\{\Omega_n\}$ where

$$\Omega_n = \frac{1}{n}\sum_{i=1}^{n} s_i \tag{2.21}$$

where s_i represents a random sign. A fluid point is also assumed in (2.21) as it is fully captured by the eddy and follows the fluid exactly. Use of this simplified form allows the statistics of the interaction process to be investigated analytically, and leads to the following statistics (see appendix III):

$$\overline{\Omega_n} = 0 \quad \& \quad \sigma_{\Omega_n}^2 = \frac{1}{n} \to 0 \quad as \quad n \to \infty \tag{2.22}$$

Since the variance of Ω_n tends to zero as n tends to infinity it follows from (2.20) that this sequence is ergodic.

For a diffusion process we require the mean square statistics of this interaction process, since:

$$\Gamma = \frac{1}{2}\frac{\langle l^2 \rangle}{\langle t \rangle}$$

In the simple case considered here, we therefore need to investigate the behaviour of the sequence $\{\Upsilon_n^2\}$ where

$$\Upsilon_n^2 = \frac{1}{n}\left(\sum_{i=1}^{n} s_i\right)^2 \tag{2.23}$$

Again it is possible to obtain these statistics analytically (see appendix III), and leads to the following:

$$\overline{\Upsilon_n^2} = 1 \quad \& \quad \sigma^2_{\Upsilon_n^2} = 2 - \frac{2}{n} \to 2 \quad as \quad n \to \infty \tag{2.24}$$

It is clear from (2.24) that the variance of Υ_n^2 fails to satisfy (2.20) and is therefore non-ergodic. This has large implications in the averaging procedure used to obtain the diffusion coefficients and is discussed below.

2.6.2 Implications for Diffusion Coefficient Calculation

The non-ergodicity of (2.23) implies that the calculation of the diffusion coefficients of the particles through (2.11) is itself non-ergodic. It follows, therefore, that the use of time averaging will not result in a statistically stationary average, irrespective of the number of realisations considered. This is shown graphically in figure (2.11) where equation (2.23) is plotted for a number of different sequences, s_1-s_5. Figure (2.11) clearly shows that the various sequences do not tends to a single value in the limit of large n, as is required. Conversely, applying ensemble averages to (2.23) does indeed lead to a statistically stationary average given sufficient elements in the ensemble, also shown in figure (2.11), due to the finite value of the variance in (2.24).

A similar plot for the ergodic sequence (2.21) is shown in figure (2.12), and all the plotted sequences can be seen to converge to a single value, which is equivalent to the value obtained from an ensemble average.

The effect of the choice of averaging method on the calculated diffusion coefficient, and therefore the particle dispersion, is shown in figure 2.7. Due to the lack of a unique time average for the particle diffusion coefficients, and hence dispersion, the time averaged particle statistics, plotted in figure 2.7, are obtained from an arbitrary number of particle-

eddy interactions (10,000). These 'averages' result in up to an order of magnitude difference in the predicted dispersion. This difference varies inversely with the particle relaxation time, since the higher the relaxation time of the particle the more its properties vary from those of the eddy, and all particle types show an appreciable difference between the two averaging methods. This is especially obvious in the copper particle calculation, the particle with the greatest inertial effects. The error is shown to lead to an order of magnitude reduction in the calculated dispersion.

The effect of the observed non-ergodicity of the particle-eddy interaction process is clearly important in the correct calculation of the diffusion coefficient of the particle, but its larger implications are still unclear. The result itself is surprising and could be of great importance in a large range of applications beyond those considered here. Further investigation of the more fundamental consequences of this result would be of great interest but are not pursued here.

Due to the above result all diffusion coefficient calculations throughout the remainder of this work are performed using ensemble averages.

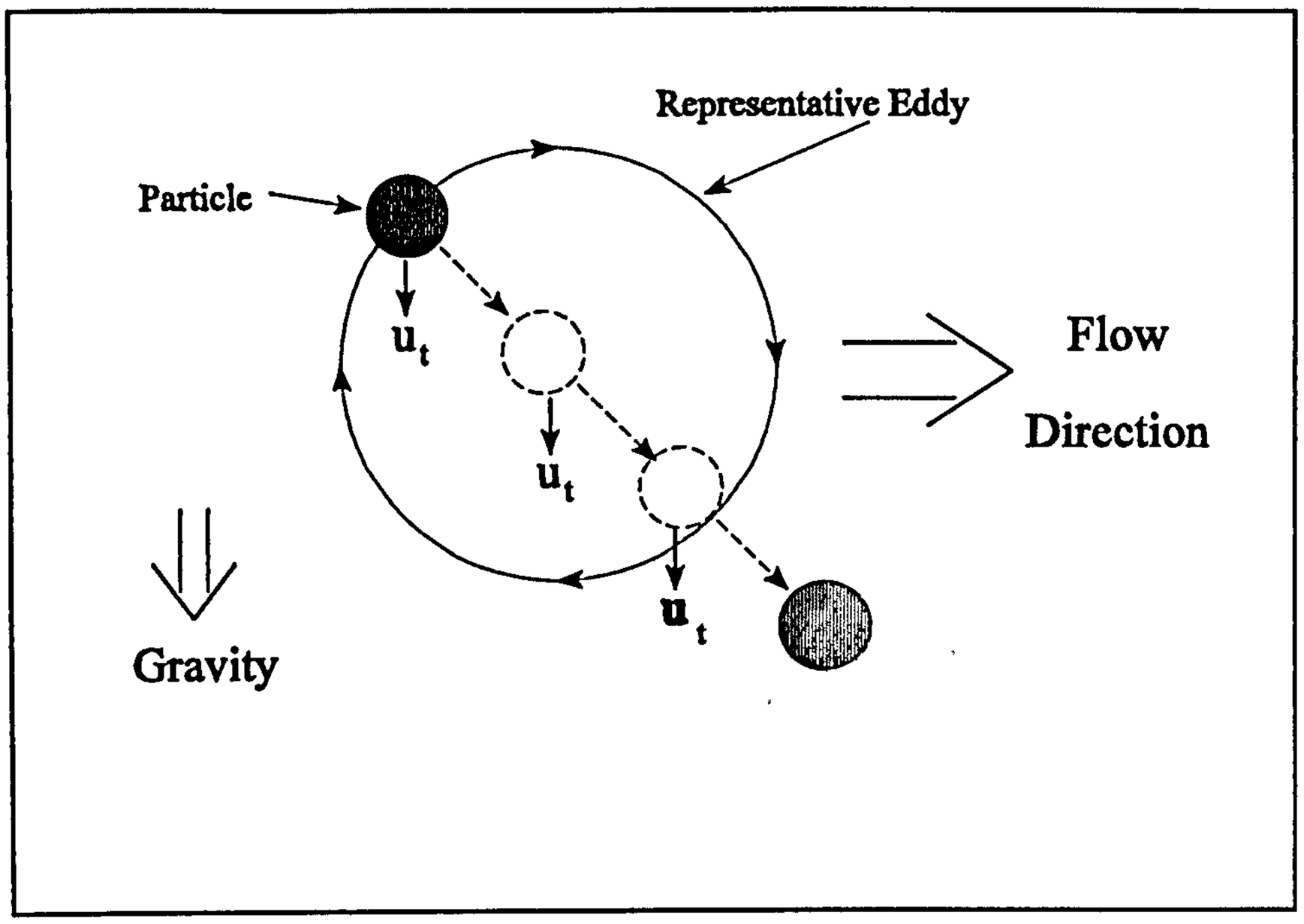

Figure 2.1 : Crossing Effect Due to Gravity

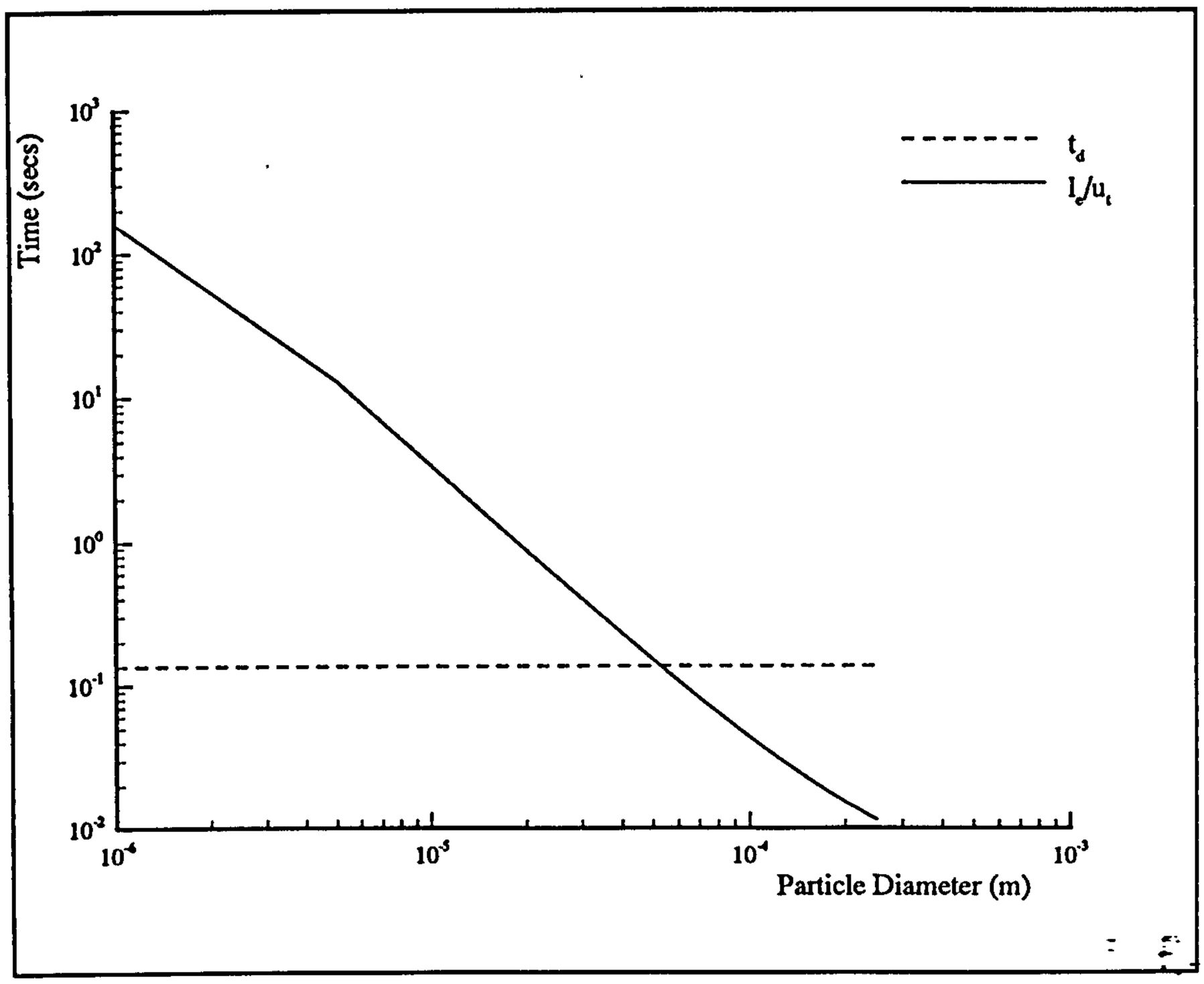

Figure 2.2 : Comparison of Crossing Time (l_e/u_t) and Eddy Lifetime (t_d) with water droplet size for droplets falling at terminal velocity in air at NTP.

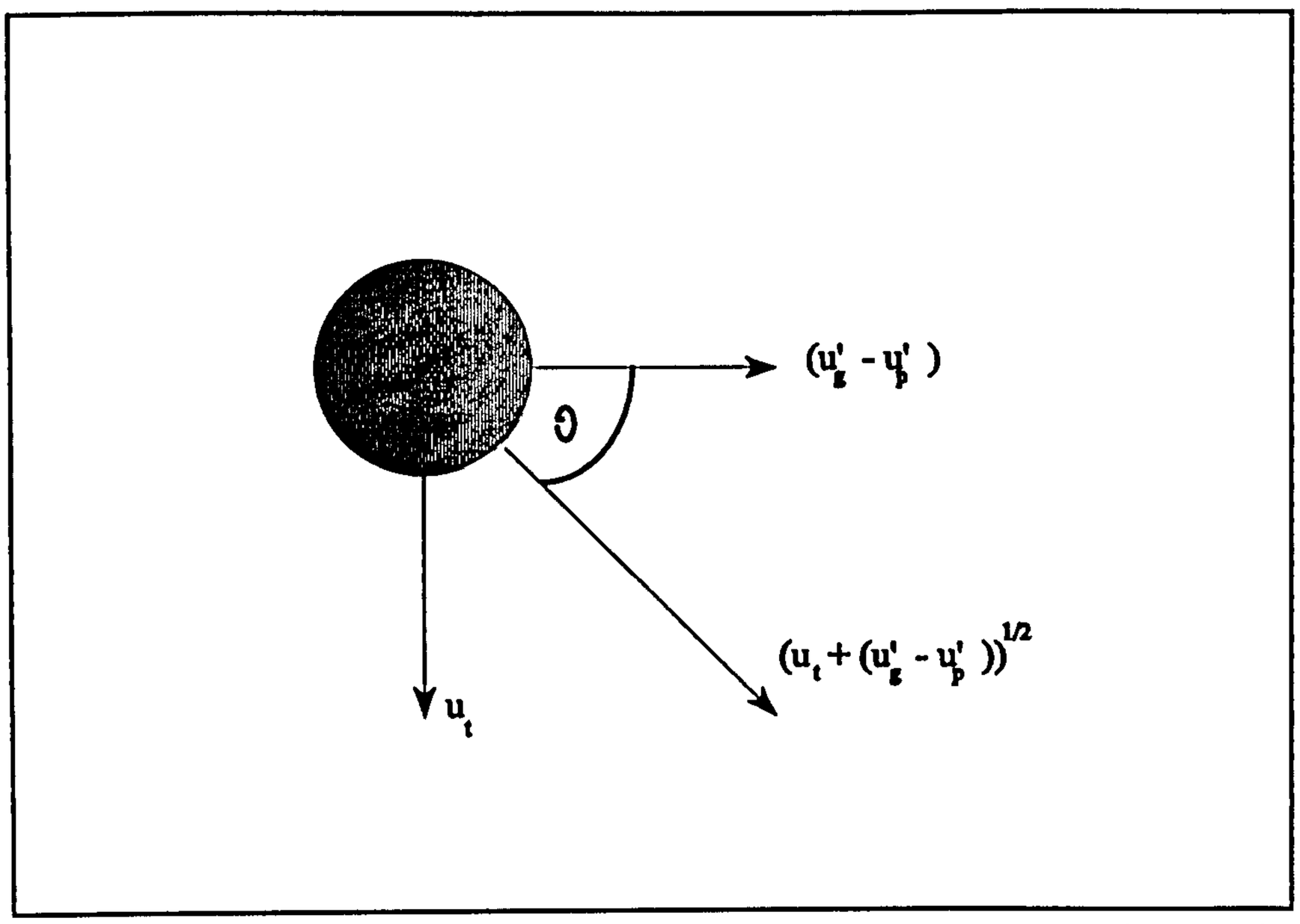

Figure 2.3 : Vector Diagram for the Instantaneous Particle Velocity Relative to the Gas Velocity.

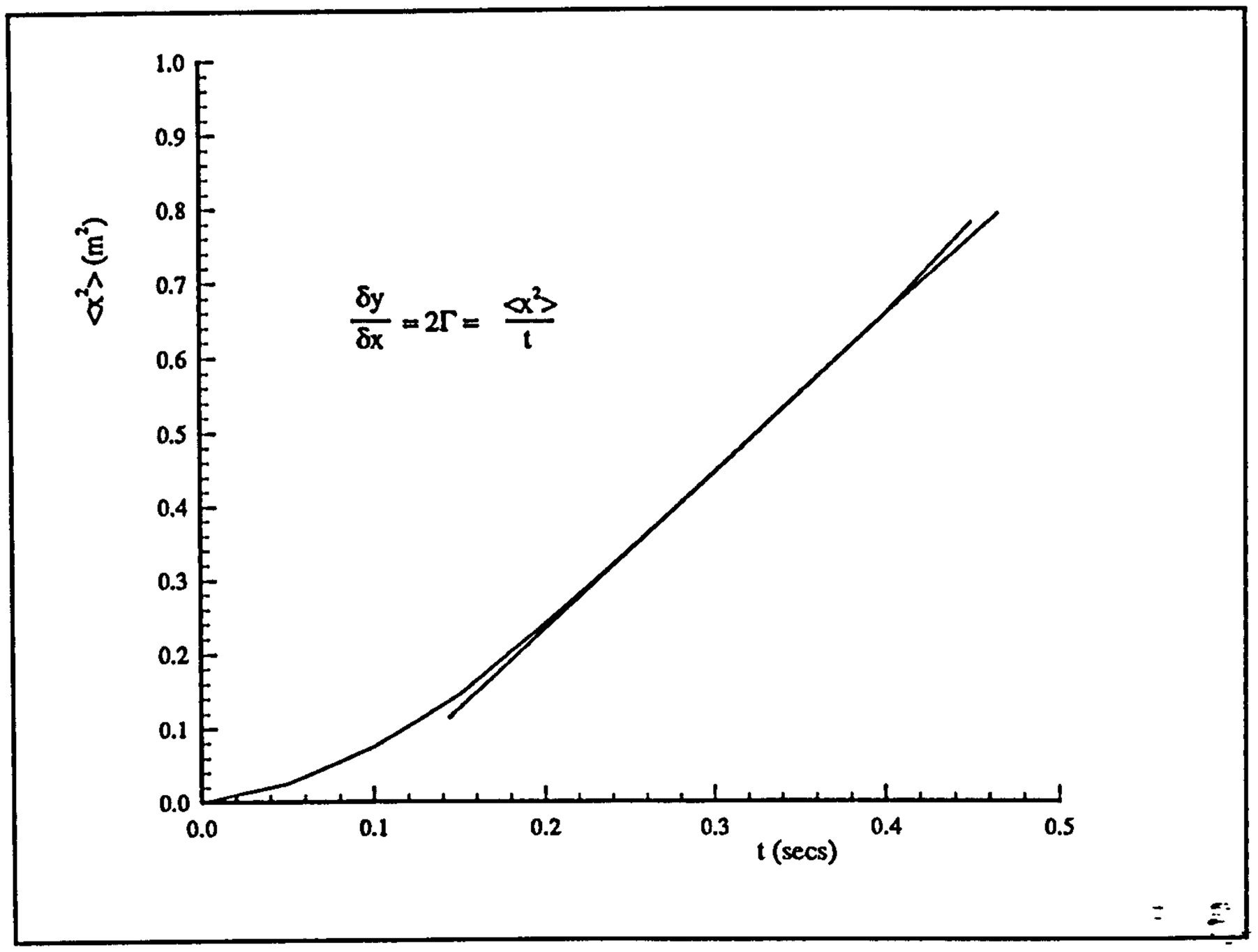

Figure 2.4 : Use of the E&T Fluid Point Displacement Curve to Obtain the Fluid Point Diffusion Coefficient.

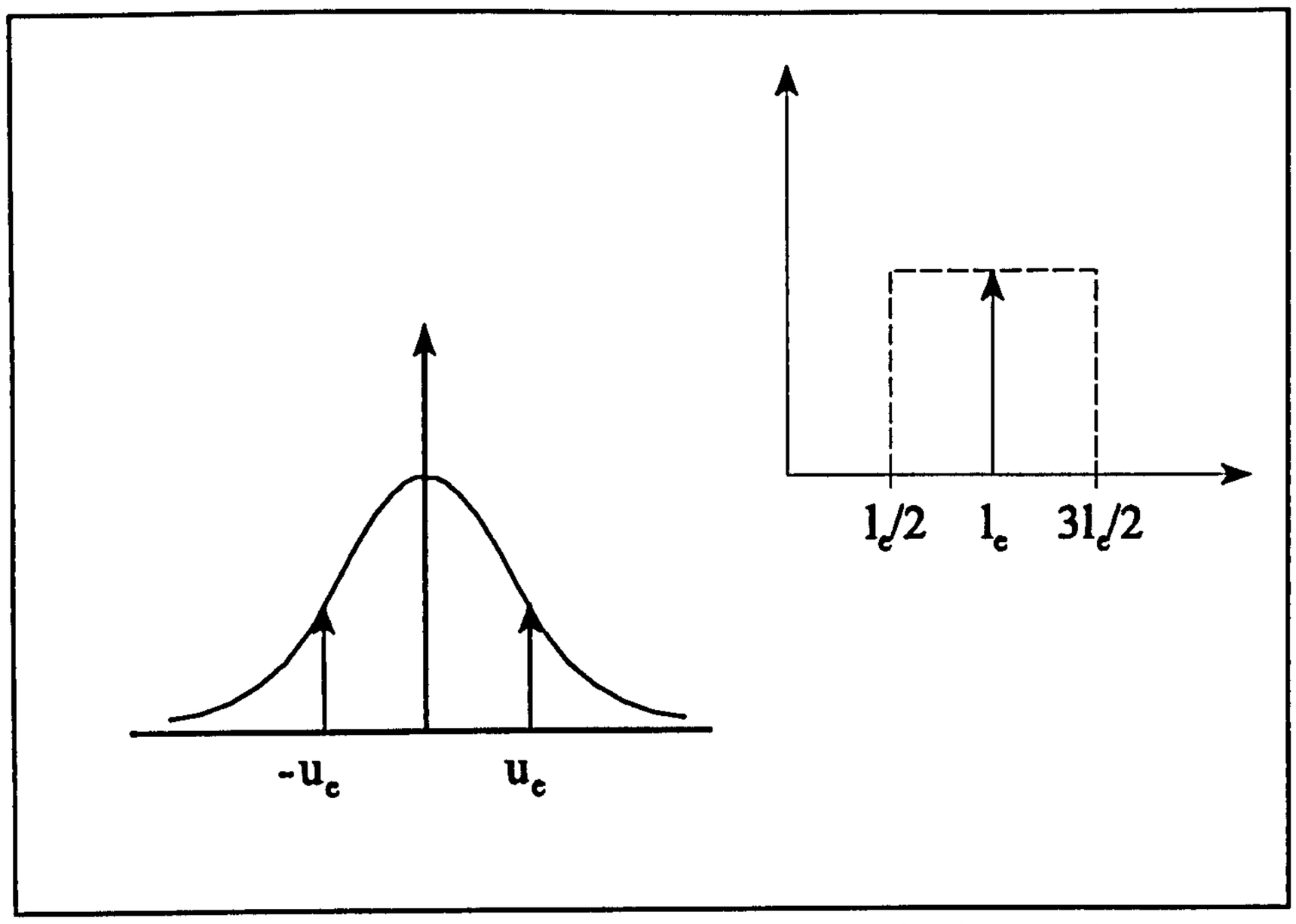

Figure 2.5 : Schematic of Velocity and Length Scale Distributions

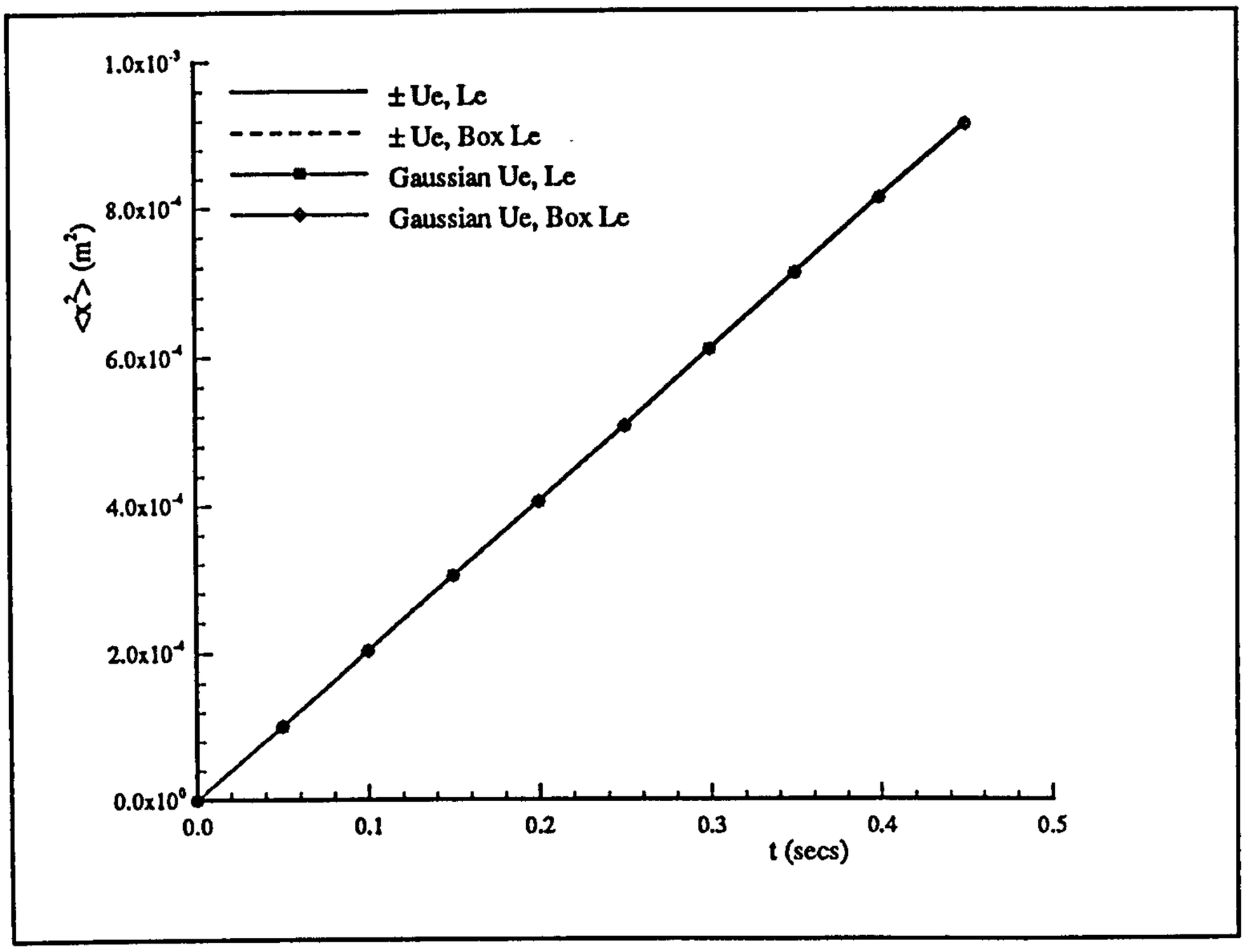

Figure 2.6(a) : Fluid Point Dispersion with Variable Scales

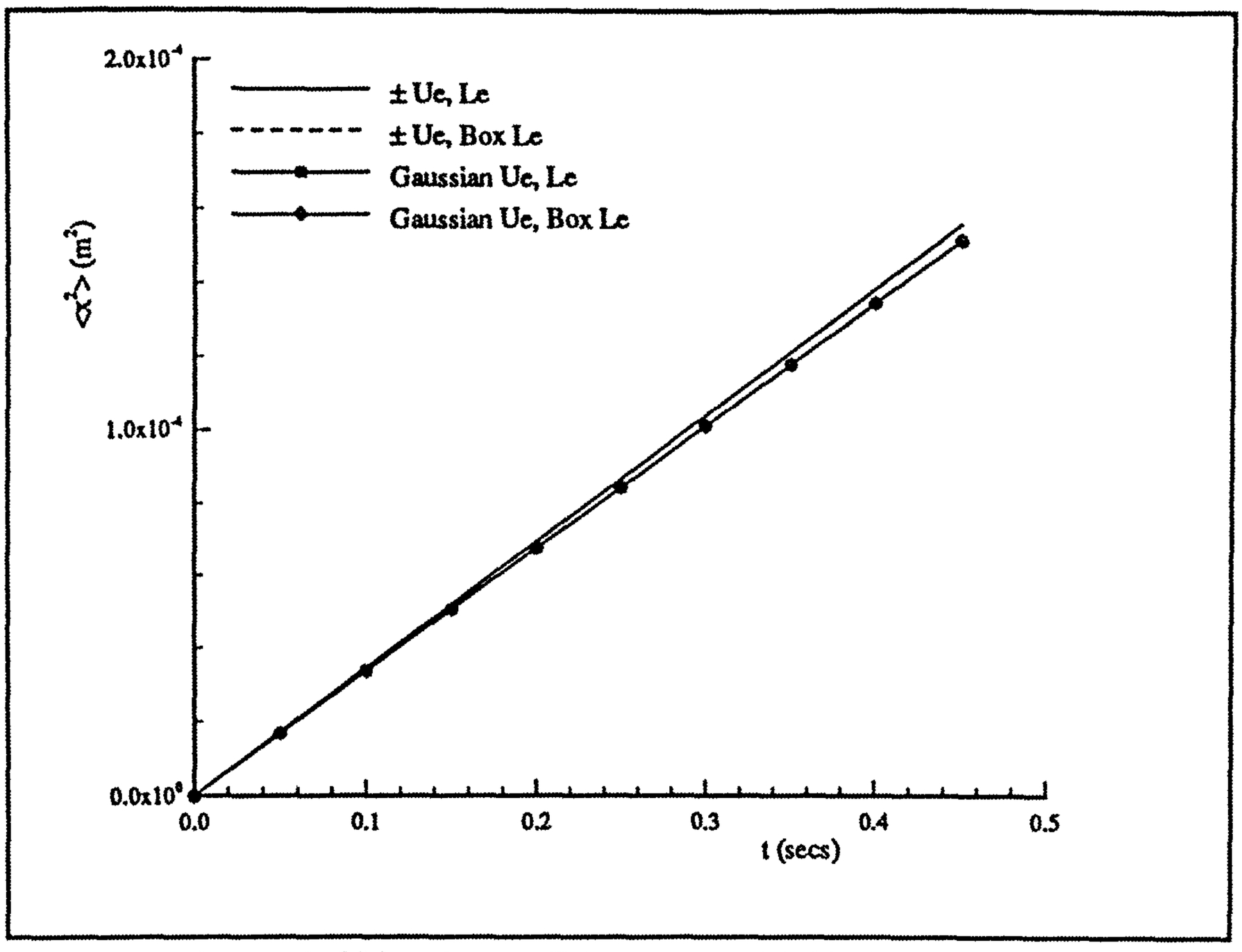

Figure 2.6(b) : Copper Dispersion with Variable Scales

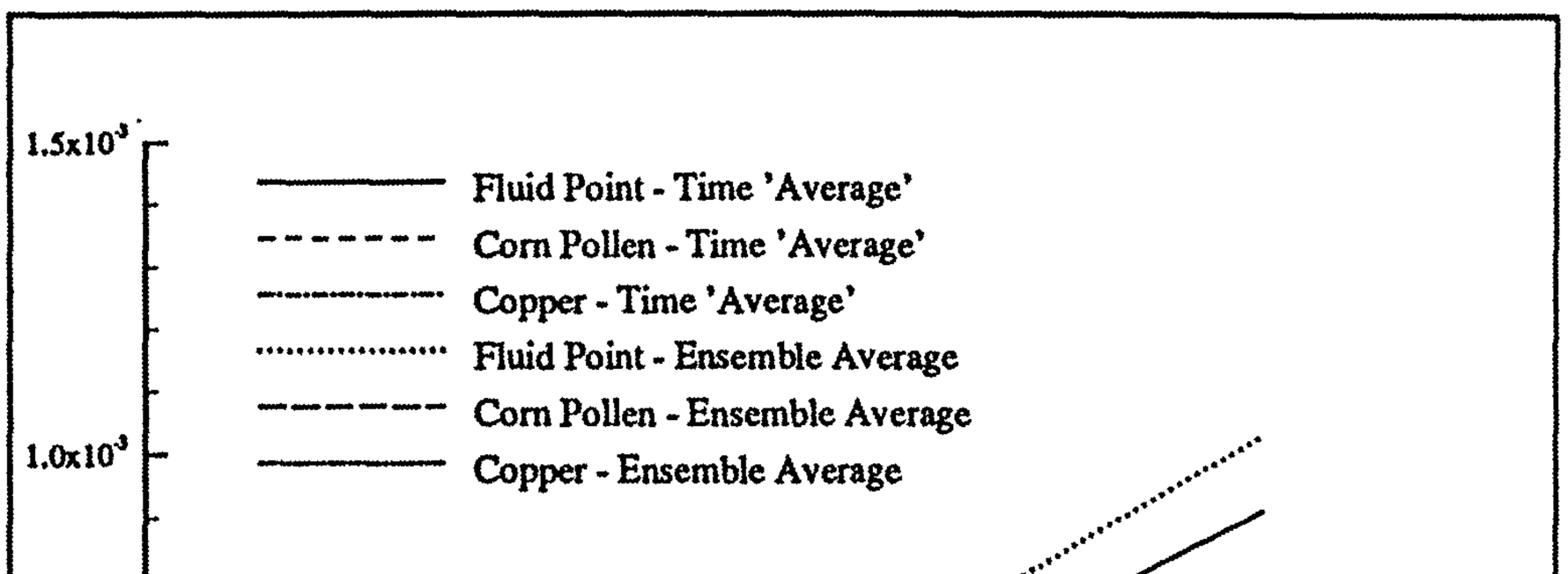

Figure 2.7 : Comparison of Arbitrary Time 'Average' and Ensemble Average.

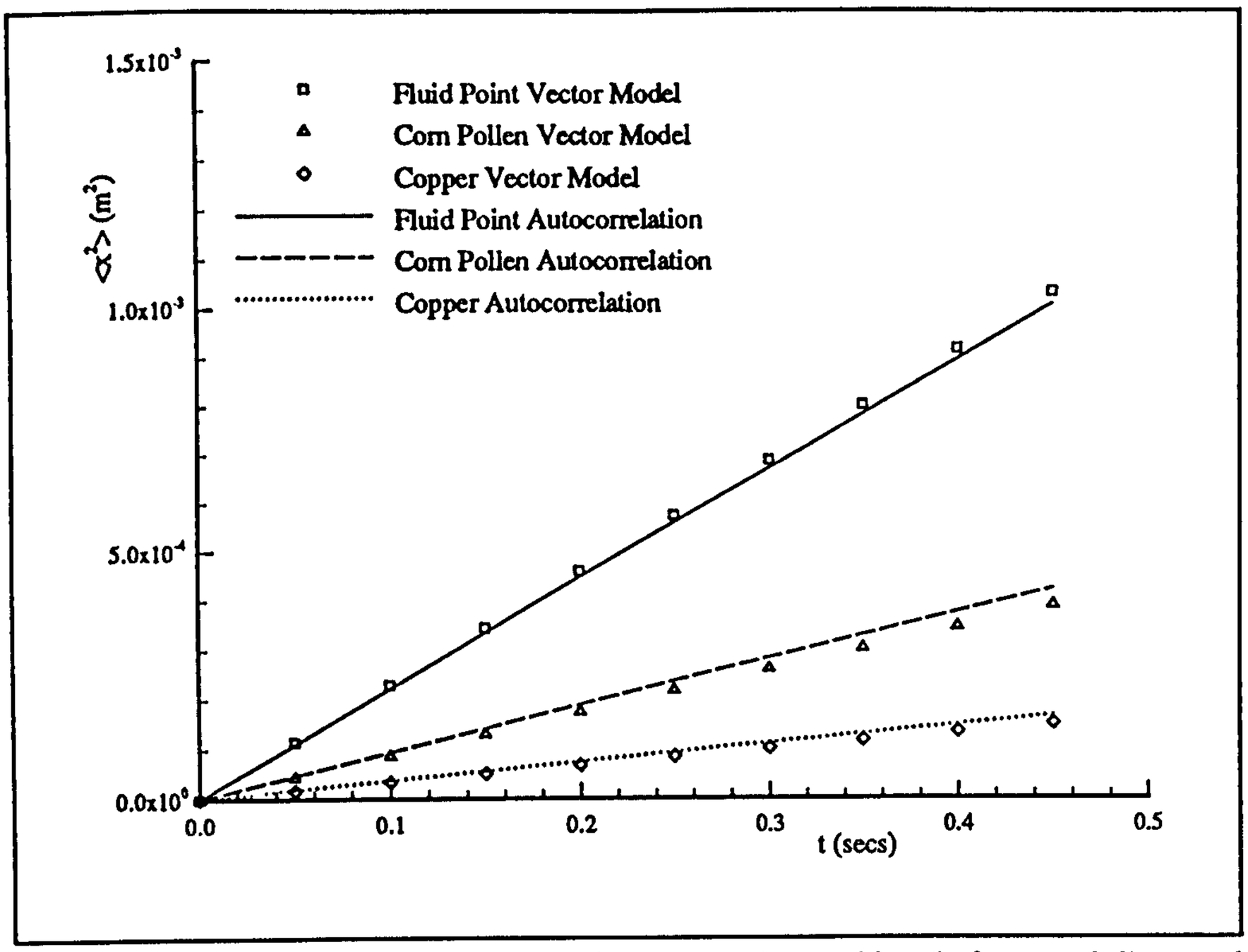

Figure 2.8 : Comparison of Dispersion from Simulation and Integral of Autocorrelations

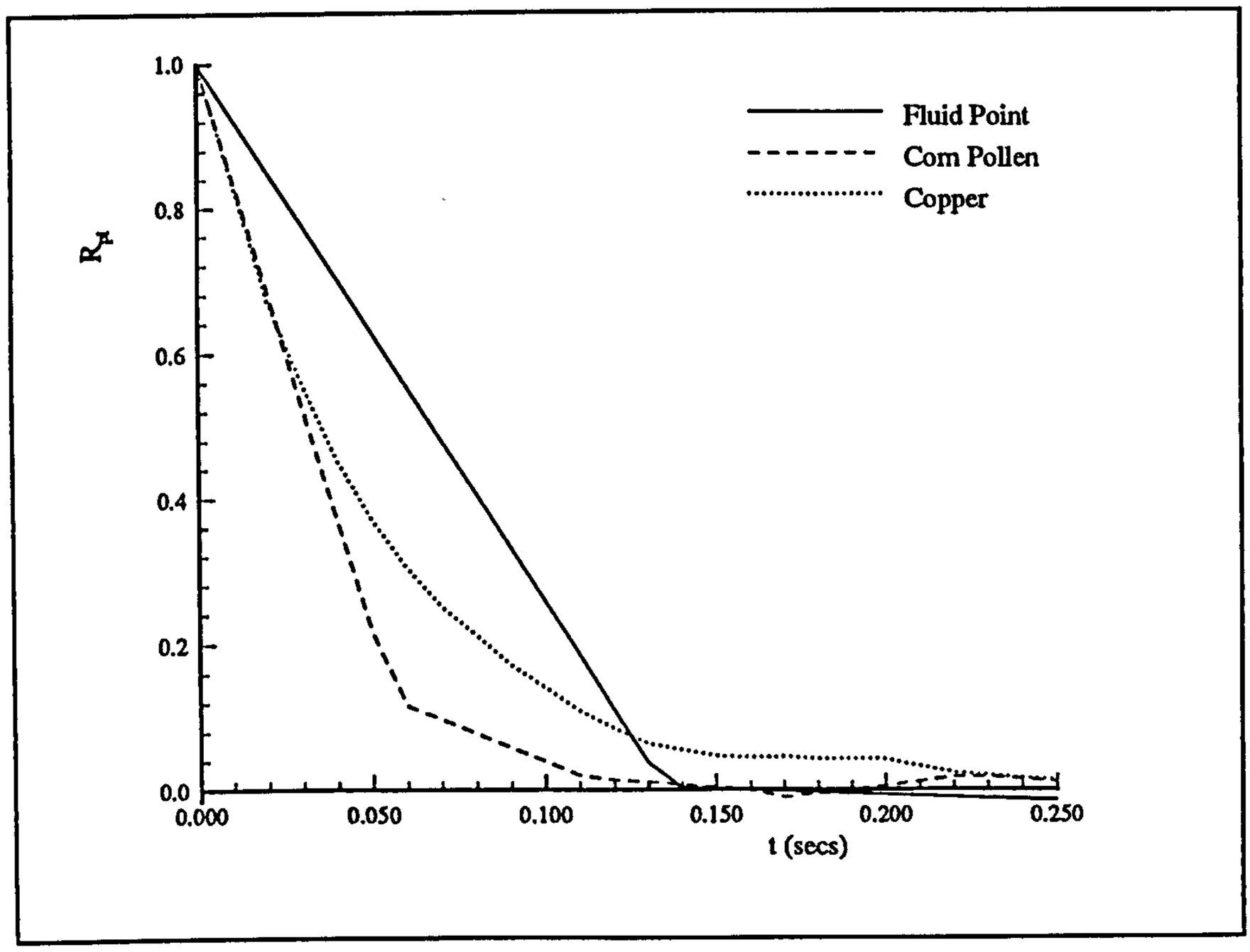

Figure 2.9 : Normalised Autocorrelation Functions

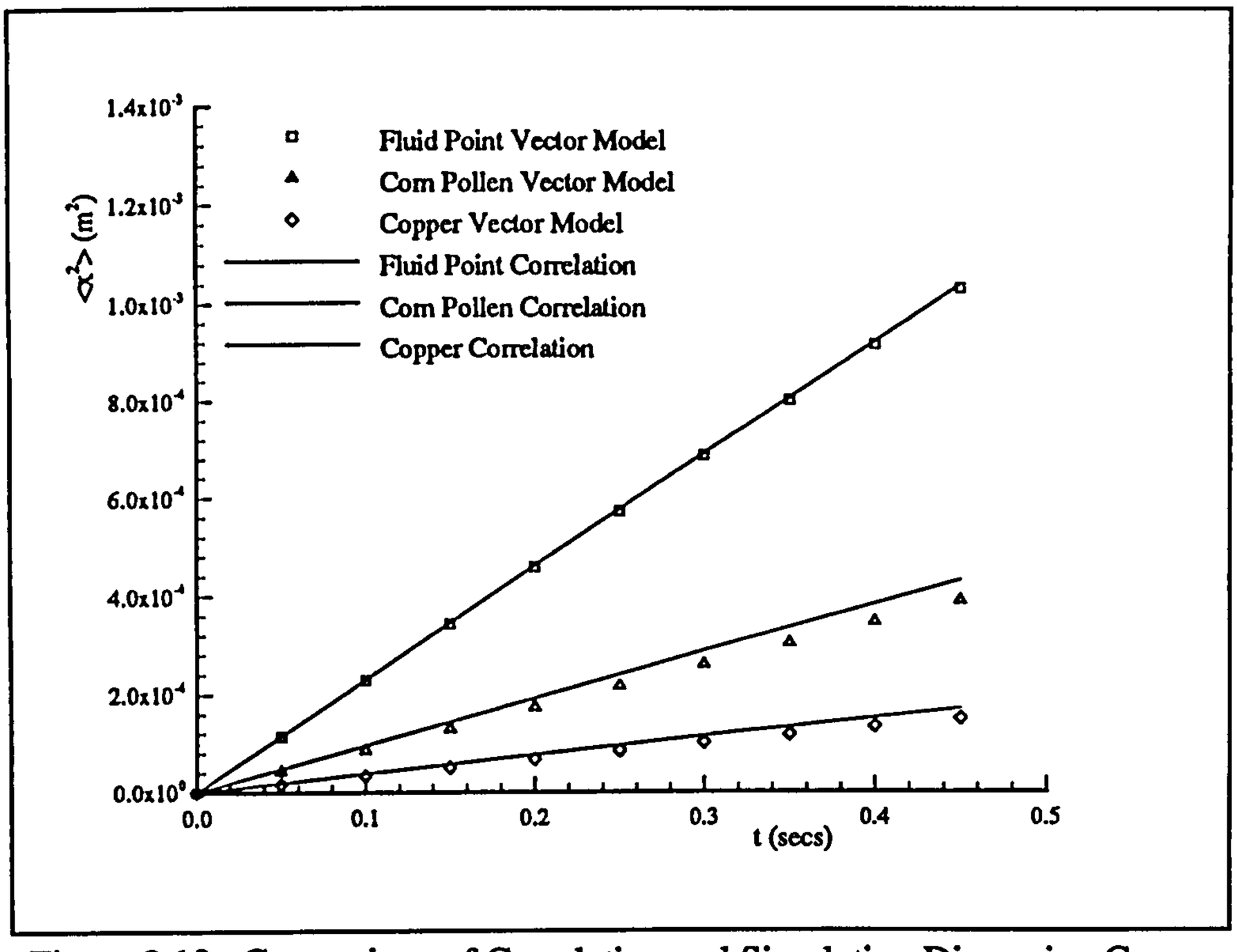

Figure 2.10 : Comparison of Correlation and Simulation Dispersion Curves

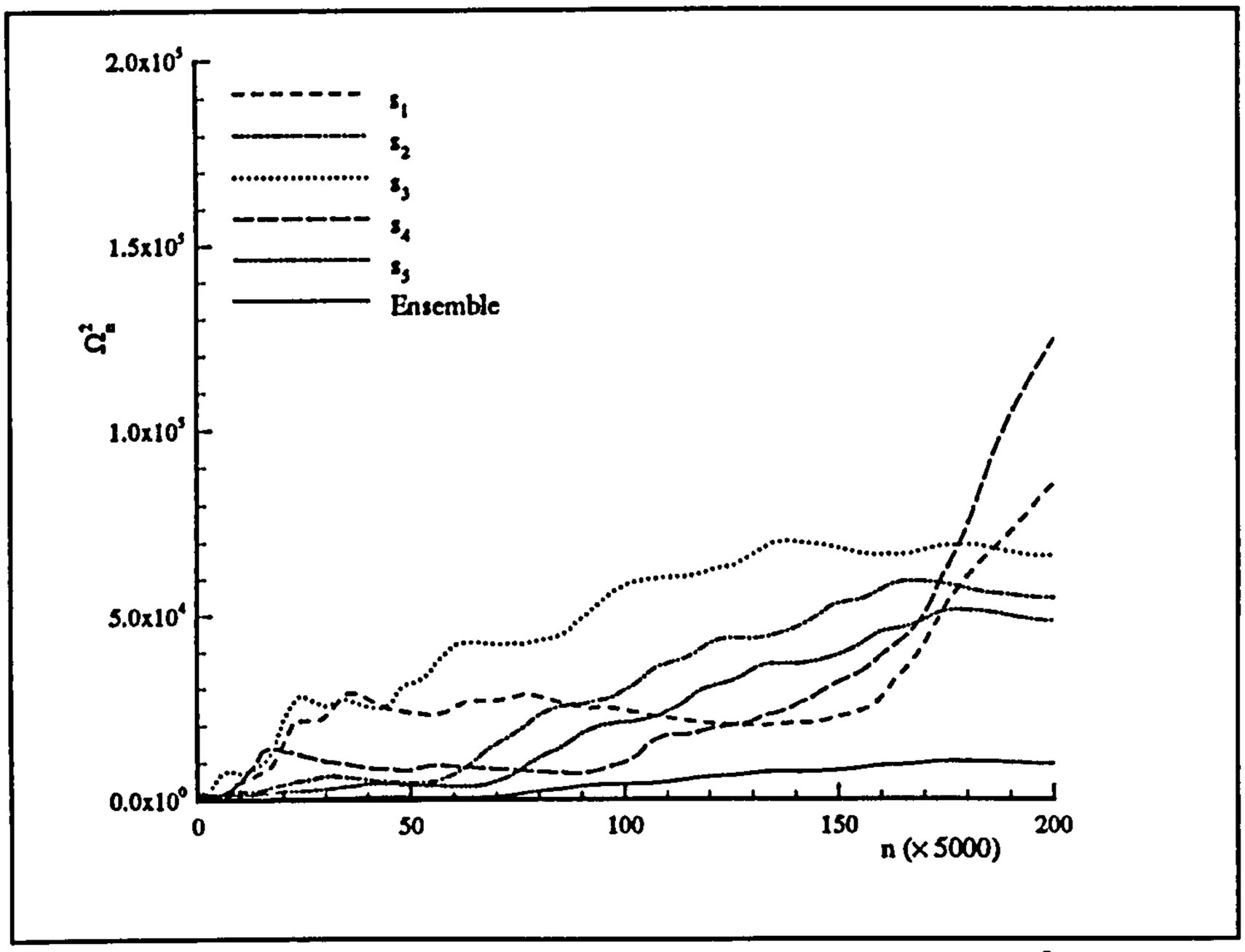

Figure 2.11 : Evaluation of a Range of Sequences Υ_n^2.

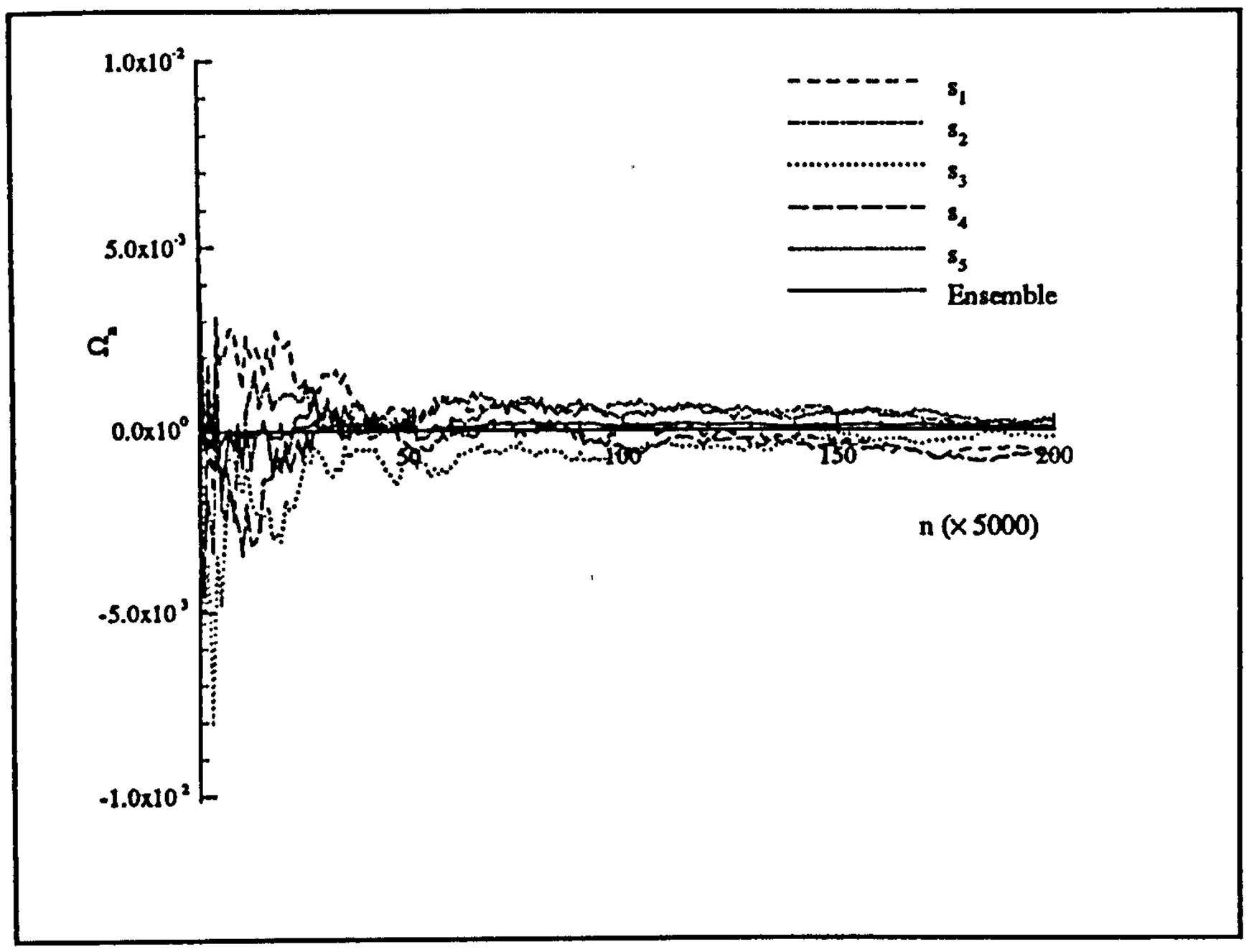

Figure 2.12 : Behaviour of Ergodic Sequence Ω_n

CHAPTER 3

Experimental Validation of Diffusion Coefficient Calculation

3.1 Introduction

In order to investigate the accuracy of the calculation of the diffusion coefficients of the particles, presented above, it is necessary to compare the performance of the models against available experimental data. However, relatively little reliable experimental data exists which can be used for comparison. Ideally an experiment would provide data on the dispersion of a range of particles in a stationary, homogeneous and isotropic flow of infinite extent; this being consistent with the approximations used in the model. The use of this type of flow would therefore enable the test of the model under optimal conditions. While such flows are not found in nature, as homogeneous flow are generally non-stationary and stationary flows are generally non-homogeneous, decaying grid generated turbulence provides a good approximation. The decay characteristics of this type of turbulence are well known and through the application of suitable temporal and spatial scaling it can be treated as quasi-stationary. Also corrections can be made to account for the inhomogeneity found in the mean flow direction and it can be considered isotropic, in planes perpendicular to the mean flow, thus allowing the application of a one-dimensional model.

Three experimental investigations have been chosen for comparison, all of which use a form of decaying grid-generated turbulence. Firstly the well known experiment of Snyder and Lumley (1971) (S&L) which is considered as the definitive experiment in this area; secondly the experiment of Wells and Stock (1983) (W&S) in which the extra effect of crossing trajectories was considered and finally the numerical experiment of Elghobashi and Truesdell (1992) (E&T), which has been mentioned in the preceding chapter.

These experiments will be discussed below and comparisons made between the various types of model derived in chapter 2 and the given experimental data.

3.2 Data of Snyder and Lumley

This experiment is considered to be the definitive work on the dispersion of particles in simple flow situations, and thus is used extensively in the literature as a test of models. This experiment together with the numerical simulation of the same flow performed by E&T, which is discussed later in this chapter, constitute the two main test-cases for the validation of the model derived above.

The experimental apparatus used by S&L consisted of a vertically orientated turbulent channel flow in a test section 16 ft (4.88 m) in length and 16 in (40 cm) square. The turbulence was generated from a 20 ft/sec (6.55 m/s) flow through a grid with a mesh length of 1 in (2.54 cm), which gave a grid Reynolds number of approximately 10,000. The flow conditions where chosen in order to allow direct comparison with the early work of Kennedy (1965).

The flow is non-homogenous since its intensity changes by a factor of 5/2 during the initial period of decay, Batchelor (1953). As this decay is rather slow it is possible to consider the flow as self-similar with just a change in scales with downstream distance. As a result scaling can be applied to obtain a homogenous and stationary flow. Thus the turbulence could be treated as a homogeneous flow with properties equivalent to the those measured at an arbitrary scaling point. This point was taken to be 73 mesh (x/M) lengths downstream. The corrections were made by (i) compensating for velocity fluctuations by normalising by the r.m.s fluctuation observed at the point in question at the time of observation and (ii) compensating for the increasing length scale by dividing separations used in the experiment by their central location

The particles used in the experiment were chosen to span a large range of relaxation times and particle diameters, ranging from a particle which would be expected to closely follow the flow field, a hollow glass bead, to one which would exhibit large inertial effects, a solid copper particle. The relevant particle characteristics can be found in table 3.1.

The particles were injected at the grid and their radial positions were measured at 10 downstream locations, spaced logarithmically starting at 43 mesh lengths downstream and ending at 171 mesh lengths. Particle radial displacements were measured from

photographs taken at each location. The particles were released individually to avoid any particle- particle effects. Furthermore the negligible loading of particles meant that the turbulent flow field was unperturbed by the presence of the particles. Thus the statistics of the flow field can be taken to be the same for all particle types and equivalent to the single phase flow field.

Particle	Diameter (μm)	Density (kg/m^3)	Time Constant (msecs)	Terminal Velocity (m/s)	Crossing Time l_L/u_t (secs)
Hollow Glass	46.5	260	1.7	1.67×10^{-2}	1.055
Solid Glass	87.0	2500	45.0	$44.2.\times10^{-2}$	3.99×10^{-2}
Corn	87.0	1000	20.0	19.8×10^{-2}	8.90×10^{-2}
Copper	46.5	8900	49.0	48.3×10^{-2}	3.65×10^{-2}

Table 3.1 : Particle Data for Snyder and Lumley

Downstream Location (x/M)	Intensity u'/U (%)	Intensity v'/U (%)	Dissipation (m^3/s^3)	Integral Length scale (m)
41	3.1	3.0	0.543	2.8×10^{-2}
64	2.2	2.2	0.161	3.0×10^{-2}
73	2.0	2.0	0.116	3.1×10^{-2}
107	1.6	1.6	0.048	3.7×10^{-2}
138	1.4	1.4	0.027	4.2×10^{-2}
171	1.2	1.3	0.017	4.6×10^{-2}

Table 3.2 : Flow Data for Snyder and Lumley.

In order to model this experiment an appropriate choice of turbulence scales is required. Since the downstream position chosen as the reference point in the scaling analysis was 73 mesh lengths from the grid, this was chosen as the point from which to take the

turbulent characteristics. As a result the calculations are based on a homogeneous, stationary, isotropic flow with characteristic flow properties equivalent to those found at this downstream location. The flow characteristics measured by Snyder and Lumley are given in table 3.2

The experimental values for the turbulent kinetic energy, obtained from the turbulent intensity, and the turbulent dissipation were used as outlined in the previous chapter to obtain the turbulent length, velocity and hence time scales used in the calculations.

3.2.1 Discussion of Snyder & Lumley Results

The measured radial dispersion of the particle is of main interest here. The results are presented in the form of scaled mean square radial displacement curves plotted against time. The displacement curves thus correspond to the dispersion of a range of particles in stationary, homogeneous and isotropic turbulence. The channel was also considered to be of sufficient diameter for the effect of the walls not to influence the measured dispersions. This enables a direct comparison between the given experimental data and the models presented in the previous chapter.

The particles used can be considered to capture the range of important effects. The heavier particles, the solid glass and copper, show large effects of both inertia and crossing trajectories. The corn pollen is an intermediate particle in that though it exhibits both of these effects they do not dominate the interaction between the particle and the eddy. Finally the hollow glass particles were chosen to represent a fluid point. Accordingly the effects of both inertia and crossing trajectories were considered minimal for this particle. The data presented for the hollow glass particle is generally accepted to be up to 40 % in error. This error was noted by the authors themselves and is ascribed to poor sampling within the experiment. Comparison with the fluid point calculation of E&T clearly shows this discrepancy. The numerical experiment of E&T enabled the results for a fluid point to be calculated directly. Use of these two experiments, both conducted under similar conditions, allows for the cross checking of results.

Another measurement of interest is that of the two point Lagrangian autocorrelation

functions. These results are also presented in corrected form allowing simple comparison with the calculation. The results quoted by S&L predict that the correlation functions of the heavier particles decay more quickly than those for the lighter particles. The authors propose that the effect of crossing trajectories is the reason for this anti-intuitive result in that this effect is of more importance than the effect of inertia, which would tend to suggest the opposite trend.

The comparison of the particle mean square displacement curves for five of the models discussed in the previous chapter will now be presented. First the results from the original model of HHD are compared with the data of S&L. This model is then extended to include the effect of crossing trajectories, by the simple inclusion of an additional interaction time scale. Next the vector model of chapter 2 is compared with the data. The modification to allow for the particle convection time is then applied. Finally the integrals of the autocorrelation functions themselves are considered.

3.2.2 HHD Models

The first model used for comparison with the experimental data of S&L is the modified form (i.e. dependent on turbulence characteristics) of the original model of HHD. The results are shown in figure 3.1. The result for the original model, without any effect of crossing trajectories, using ensemble averages can be seen to greatly over-predict the dispersion of the majority of particle types. This becomes more obvious as the particle mass increases. This is to be expected since the influence of crossing effects becomes more pronounced the more inertial the particle.

The prediction obtained using ensemble averages with the extra timescale to take account of cross-trajectory effects is shown in figure 3.2. Introducing this simple form of crossing effect can be seen to significantly enhance the accuracy of the calculation. While this simple model can be seen to give results comparable to the full vector model (figure 3.3) it fails to contain the correct physical description of the interaction process between particle and eddy in the presence of crossing trajectories.

The original model of HHD can be seen to be in error in its assumption of the lack

of influence of gravitational effects. The version of the original model presented here is a much modified version of the original model. The use of ensemble averages greatly increases the accuracy of the prediction over the use of time averaging (see previous chapter). This accuracy is further improved by the inclusion of a simplified crossing time scale. Though the results in figure 3.2 can be seen to predict the dispersion well the lack of physical consistency in the model used leads to a preference for the more complete vector model.

3.2.3 Vector Model - No Convection

Here the results for the vector model are presented. This model contains the extra effect of gravity over the model of HHD. The gravitational effects are intrinsically incorporated in the derivation of the model, unlike the simple inclusion of a crossing time scale used above.

The results for this model can be seen in figure 3.3. The accuracy of the results varies as the particle relaxation time changes. The best fit can be observed for the dispersion of the heavier particles, represented by the solid glass and copper. These particles show the largest crossing trajectory effects as well as the largest inertial effects. Both can be seen to be captured accurately by the model. The fit of these two particles is very good for all times considered, with errors typically less than 15%. The accuracy of the fit in the short time region, where the diffusion approximation loses validity, is due to the effects discussed in the previous chapter. Though the particles have a relatively long relaxation time, and hence remain in the initial quadratic interaction region for a greater time than the lighter particles, the gradient of the final curves is less. As a result the effect of this large quadratic region is much less noticeable and much better approximated by an assumption of a constant gradient.

The intermediate particle, the corn pollen, is less well predicted, as a result of the increased importance of the initial quadratic interaction region. Overall the degree of fit gradually degrades as the particle relaxation time becomes shorter and the change of gradient from the initial quadratic region to the long time behaviour becomes more pronounced.

Finally the hollow glass particle, which is the lightest particle considered is very

poorly described. As discussed above the results of Snyder and Lumley for this particle are considered to be up to 40 % in error and the calculations for the hollow glass particles are only presented for the sake of completeness

These results imply that the vector model, while a great improvement over the initial model proposed by HHD, encounters problems in accurately representing the lighter particles as the simple diffusion approximation loses validity in the short time region.

3.2.4 Vector Model - With Convection

The effect of the introduction of the proposed convection time on the ability of the vector model to correctly predict the given experimental data can be seen in figure 3.4.

The introduction of the convection time approximation can be seen to have only a small corrective effect on the dispersion curves for the heavier particles. This small improvement brings both the calculated curves for solid glass and copper more closely into line with the experimental results. The small correction is as expected as the relationship for the convection time is inversely proportional to the relaxation time of the particle. The relative difference between the calculations and measurements lies well within the quoted experimental error (~15%) for all times.

In addition the use of the convection time markedly increases the accuracy of fit of the intermediate particle. Introducing a delay in allowing the particle to disperse brings the calculated dispersion curve more into line with the experimental data. The fit using this model can be considered to be very good. Again the calculated curve lies within the experimental error (~12%). The fit between the model and measurements degrades at long time. The experimental results show slight curvature implying that the effect of crossing becomes more noticeable. This in turn implies that the scaling used to approximate a stationary flow begins to lose accuracy at the longest times measured. As the calculation is conducted using constant flow characteristics the gradient of the dispersion curve remains constant throughout. Even with this curvature the discrepancy between the two curves remains within the experimental error.

The dispersion of the hollow glass particle is most affected by the introduction of this

convection time. Again the experimental results are such that no comparison can be drawn and the hollow glass calculation is only presented for completeness.

3.2.5 Integration of Autocorrelation Function

Finally the results obtained from a continuous integral of the numerically obtained particle autocorrelation functions is presented in figure 3.5. The use of this method of calculation allows the quadratic effects at small times to be fully captured.

The heavier particles are again predicted well for all times. The quadratic effects which are captured by this method are shown to be small for these types of particles, as mentioned previously.

The intermediate particle shows an acceptable level of fit to the experimental data. The initial quadratic region is noticeable at short time in the calculated curve. The effect of this quadratic behaviour is insufficient to correctly delay the onset of the constant gradient portion of the curve, this leads to an over-prediction of the particle dispersion. This implies that the correlation time calculated for this particle is too small. This correlation time can be seen in figure 3.6, which shows the numerically calculated autocorrelation functions used to obtain the dispersion curves shown in figure 3.5, together with those of S&L. The calculated curves lie well within the range of experimental error, except the fluid point , which is as expected.

The curve for the hollow glass particle shows a significant quadratic region for short time, as would be expected. Again this curve is only presented for completeness.

3.3 Data of Wells and Stock

The second experiment considered was that of Wells and Stock (1983). The aim of this experiment was to isolate the effects of particle inertia and crossing velocity on the dispersion of particles. In order to accomplish this a potential field, given by a uniform electrical field was set up between two parallel plates in a horizontally orientated wind

tunnel. The potential field had sufficient strength to obtain free-fall velocities up to four times that due to gravity and, by reversing the polarity, allowed the gravitational field to be off-set.

The flow field used was a grid generated channel flow similar to that of S&L, selected with the intention of allowing comparison between the two studies. Therefore the grid spacing, size and shape together with the mean flow velocity were set equal to those used by S&L. The wind tunnel consisted of two glass plates for the vertical walls, to enable access for laser Doppler equipment, and two electrically isolated aluminium plate for the horizontal walls, which enabled application of the required potential field. The maximum natural free-fall distance for the larger particles was calculated to be approximately 10 cm. A doubling of the terminal velocity was originally required and therefore the channel height was set to 20 cm throughout the length of the test section. Consequently, when the crossing velocities were increased to four times the terminal velocity only the first half of the test section could be used. The important flow data is presented in table 3.3

To enable the effects of inertia to be investigated the particles used were chosen to have differing relaxation times. The relevant particle characteristics are given in table 3.4. An important consideration in the choice of particles was that they exhibited a narrow size distribution as the charge they can carry is a function of the square of their diameter. This was required to ensure all particles used had a similar charge and therefore behaved similarly in the applied electric field.

x/M	15	30	45	60	75	90
u'/U (%)	4.81	2.93	2.24	1.92	1.61	1.47
v'/U (%)	4.76	2.93	2.23	1.91	1.60	1.49
ϵ (m^2/s^3)	6.17	0.625	0.221	0.112	0.067	0.045
k (m^2/s^2)	1.5×10^{-1}	5.52×10^{-2}	3.23×10^{-2}	2.37×10^{-2}	1.67×10^{-2}	1.39×10^{-2}

Table 3.3 : Flow Data for Wells and Stock

The particles are assumed to be introduced at the grid. The particle concentration is assumed dilute therefore no particle-particle or particle-turbulent effects are considered.

Also this implies that no co-operative charge effects exist between the particles.

Parameter	5 μm Glass Sphere	57 μm Glass Sphere
Particle Diameter (μm)	5 ± 1	57 ± 6
Density (kg/m^3)	2475	2420
Relaxation Time, τ_p (msecs)	0.192	24.4
Terminal Velocity (m/s)	1.88×10^{-3}	0.23

Table 3.4 : Particle Characteristics for Wells and Stock

A laser doppler anemometry (LDA) system was used for the particle dispersion measurements. The measurement locations were situated every 10 mesh lengths between 20 x/M and 100 x/M inclusively.

Again the modelling of this experiment requires the assumption of constant turbulent characteristics. Due to the use of a similar flow field to that proposed by S&L the same turbulent properties were chosen for this calculation as for that of S&L.

3.3.1 Discussion of Wells and Stock Results

Conceptually this experiment is of great use. Unfortunately, the accuracy of the results obtained is in question. A critical discussion of the results is given below.

The 5 μm glass particle has a relatively small relaxation time. It therefore would be expected to closely follow the turbulent fluctuations in the case of zero crossing time (i.e. the applied electric field offsets gravity exactly) and therefore to approximate a fluid point. Within the current model the dispersion of a fluid point can be calculated analytically. Given a specified flow field, it is thus possible to calculate the fluid point dispersion analytically. Assuming, in the first instance, that the flow characteristics are the same as those given by S&L this calculation can be performed. The dispersion curves given in the work of W&S are dependent on downstream distance, rather than time. Making the assumption that the particles are convected downstream with the mean flow velocity, a valid assumption for the

5 µm glass particles , it is a straightforward calculation to convert this downstream distance to a time.

Following the analytical form given in the previous chapter for the dispersion of a fluid point, i.e.

$$\langle y^2 \rangle = 2\Gamma_{fp} t = 2(\tfrac{1}{2} u_e^2 t_L) t = u_e^2 t_L t \qquad (3.1)$$

and using the flow data from S&L, this results in a dispersion of more than twice that observed in the experiment of W&S.

Using equation (3.1) it is possible to invert the relationship to obtain the scales required to fit the experimental measured dispersion. This leads to

$$u_e^2 t_L = \frac{\langle y^2 \rangle}{t} \qquad (3.2)$$

At least one of the values on the LHS of equation (3.2) needs to be specified. Choosing to specify the velocity scale, since this is measured in the experiment, and assuming its value at the mid-point of the measurement region, that is 45 x/M, we can calculate the value required for the Lagrangian time scale and hence the eddy length scale.

This calculation results in a length scale of 3.956×10^{-3} m compared to a length scale obtained by applying the k-ϵ relationship (see previous chapter) to the turbulence characteristics measured at this flow point of 1.066×10^{-2} m. This implies that in order obtain the measured dispersion curves the turbulence length scale needs to be reduced by almost a factor of three, assuming the given velocity scale.

Another inconsistency with the given dispersion data arises out of the similarity of the magnitude of the dispersion of both particle types. The dispersion of the 57 µm glass particle is measured as being virtually identical to that of the 5 µm particle for the case of zero gravity. This implies that no inertial effects are present to distinguish the two particle types.

Yet further inconsistencies can be found by considering the dispersion of the 57 µm particle. The variation in the particle's crossing velocity is quoted as varying from 0 to 1.216

m/s. This corresponds to an increase of the potential field experienced by the particle from 0 to 7.2 g. The increase in the crossing trajectory effect exhibited by the particle over this range of accelerations would be expected to be extremely large. For example the time taken for the particle to fall across an eddy would vary from ∞ (zero fall velocity) to approximately 10% of the eddy lifetime. This would imply a large variation in the observed dispersion of the particle. The experimental data does not reflect this and the particle dispersion varies only by a factor of approximately two.

To highlight these inconsistencies the experimental data for the 57 μm glass particle is compared to the vector model, below. The convection time is not included as it has been shown in the previous section to only be important for particles with a low relaxation time and hence a large change in gradient between the initial quadratic region and the constant long time behaviour. This can be assumed not to be the case in the dispersion of the 57 μm glass particles, especially when a large potential field is applied.

3.3.2 Vector Model Comparison

The comparison of the calculated mean square displacements of the 57 μm glass particle with the experimental results can be seen in figure 3.7. The assumed turbulence field is that used for the S&L calculation. If the k-ϵ model formulation is applied to the flow data of W&S, and the turbulence is taken to be constant at the values given at 45 x/M downstream from the grid the calculated length scale is virtually identical to that found in S&L and the velocity scale is slightly higher. The use of the velocity scale of S&L will thus tend to under-predict the dispersion of the particles slightly.

Even with this proviso the dispersion of the larger glass particle for low crossing velocities is shown to be much greater than that measured in the experiment, as expected from the above discussion. Also it can be seen that the variation in the particles dispersion, as the effect of the crossing trajectory effect is increased, is much greater in the calculations than in the experiment. This fact also follows from the above discussion.

These results for the 57 μm particle lend support to the above arguments and again cast doubt on the validity of the experimental results.

3.3.3 Convection Time Comparison

Since the lighter, 5 μm, glass particles have a significantly smaller relaxation time than the heavier particles it was decided to include the convection time formulation in the calculation of the dispersion of particles of this type.

The results of the calculation can be seen in figure 3.8. Clearly the increase in the crossing velocity of the particles from 0 to 0.2365 m/s, which corresponds to an increase in the potential field from 0 to 127.5 g, has a more obvious effect in reducing the calculated dispersion of the particles than that found in the experiment.

Also the dispersion of the particle when a zero crossing velocity is applied can be seen to be much greater than that found in the experiment as expected from the above arguments.

These problems have been encountered by other authors, Sommerfeld (1993).

3.4 Data of Elghobashi and Truesdell

This work is a numerical experiment based closely on the original experiment of Snyder and Lumley. The calculation consisted of solving the single phase flow field for the grid generated turbulent channel flow of Snyder and Lumley using direct numerical simulation and then tracking a large number of particles through the flow.

The main rationale for considering this work together with that of Snyder and Lumley was the fact that this calculation enabled the consideration of the dispersion of a fluid particle. As mentioned above the results for the particle chosen by Snyder and Lumley to represent a fluid point, the hollow glass bead, are generally considered to be in error. A knowledge of the behaviour of a fluid point is extremely important in the development of the dispersion model. This data has been used previously in the calculation of the relationship between Eulerian and Lagrangian scales, as outlined in chapter 2.

Consequently the only comparisons drawn with this experiment are those concerning the dispersion of the fluid point. The calculations performed, by E&T, for the other particle types considered in the work of Snyder and Lumley agree closely with the experiments and,

therefore, are not directly considered here (see figures 3.1-3.5).

The numerical experiment consisted of a direct numerical simulation (DNS) of the flow field used by S&L. This entails solution of the full time-dependent Navier-Stokes equations together with continuity. This has the advantage that no closure model is required and the flow field properties are known at all points in the flow domain. To accomplish this a sufficiently fine computational grid must be applied to enable the calculation of all relevant scales up to and including the dissipative range. In the work of E&T the flow field was solved in a cubic computational domain of unit size with periodic boundary conditions. This domain was considered to move with a constant velocity equal to the mean stream velocity, thus, reducing the calculation to consideration of only instantaneous fluctuating velocities.

The initial random velocity field was chosen to be isotropic and periodic in space with a divergence free continuity equation. The resolution (96^3 grid cells) was such that all wavenumbers up to $k_{min}=2\pi$ were captured. The specification of the turbulent spectra was such that the ratio of the wavenumber of peak energy, k_p, to the above minimum wavenumber, k_{min} was 6. This led to a micro scale, λ_0, of approximately 4.5×10^{-3} m and a root mean square velocity, u_0, of approximately 8.8×10^{-2} m/s. The initial microscale Reynolds number, R_{λ_0} was therefore 25.

The behaviour of the particles in the flow was calculated by numerically tracking a statistically significant number of particles, 22^3, through the flow field. The tracking was accomplished using the full particle equation of motion (equation (2.3)) including all force terms on the RHS. Again no form of modelling of the interaction between the particle and the flow was required as the instantaneous flow properties are known at all points within the flow field. Small inaccuracies could still be found in the calculation since only one way coupling effects were considered. While this is consistent with the experimental data of S&L it fails to take into account the influence of the particle on its local flow field. This discrepancy occurs because the requirement the no-slip condition on the particle surface disturbs the local flow field. This effect though present can be seen to be small (E&T figure 10a) from the extremely good fit between the numerical and physical experiment for particle types considered.

3.4.1 Discussion of Elghobashi and Truesdell Results

DNS suffers from constraints on the Reynolds number of the calculated flow, due to the power of current computers. Therefore appropriate scaling of various quantities is needed to allow comparison with the experimental data of S&L. The microscale Reynolds number obtained in the numerical experiment decayed from an initial value of ~25 to 15.9 through the calculation. The corresponding value of R_λ found in the experiment of S&L was approximately 48.5 throughout the test section. It is therefore necessary to apply scaling procedures to the resulting DNS data to allow comparison with the experiment. This is accomplished through ensuring that the ratio of particle response time and eddy decay time are equivalent. Similarly the gravitational force must be scaled so that its effect relative to the fluid acceleration is consistent. Scaling was applied at the first measured particle dispersion position (i.e. 68.4 x/M).

It follows from the above discussion that the results obtained by E&T could not be compared directly with either the experimental data of S&L, or the calculations presented here. In order to be able to compare the results appropriate re-dimensionalisation with the relevant scales is needed. The results of E&T for the mean square displacement of the fluid point are quoted with a non-dimensional mean square displacement. The time used is dimensional since the time scaling is incorporated directly into the calculation through the scaling of the particle charateristics . The comparison of results with the experimental data is given here in dimensional form. The experimental data of E&T was re-normalised with the integral length scale of S&L.

The results presented by E&T for the non-dimensional mean square displacement of the particles give an accurate representation for all particle types, except the hollow glass (fluid point) as expected, when compared to the experimental results of S&L. Therefore, the only results considered here are those for a fluid point, which have been used extensively in the previous chapter and complement the original data of S&L.

3.4.2 HHD Model

The results shown in figure 3.9 for the HHD model can be seen to be identical with those obtained from the vector calculation (see figure 3.10). This is to be expected as the HHD model is the limiting case of the Vector model in the case of small particles (see Appendix I). No crossing trajectories are considered here since their effect on the fluid point is negligible. The curve given for this model can be seen to over-predict the dispersion of the fluid point significantly. Though the gradient is similar to the quoted experimental data the lack of fit in the initial quadratic region affects that in the constant diffusion region, as before.

3.4.3 Vector Model - No Convection

The results for the vector model with no convection, figure 3.10, are identical to those found from the HHD model, above, as expected. The inability of both of these types of model to correctly predict the initial interaction region leads to large discrepancy between the calculated dispersion and the experimental data for all times downstream. This level of fit is unacceptable and the model needs further refinement.

3.4.4 Vector Model - With Convection

The effect of the introduction of the convection time approximation can be seen in figure 3.11. The use of this approach to model the initial interaction period can be seen to enhance the prediction of the fluid point dispersion. Though this model gives a much improved fit over the previous two the dispersion in the initial region is still over-predicted. This is due to the underestimation of the duration of the initial quadratic region. Discussion of this effect is deferred to the following section

3.4.5 Integration of Autocorrelation Function.

The mean square displacement of the fluid point arising from the integration of the autocorrelation function is shown in figure 3.12. The agreement between this analytical form and the convection corrected vector model (also plotted) can be seen to be excellent. Both calculations exhibit the same gradient as the curve of E&T at long times. This implies that the fluid point diffusion coefficient is consistent between the two calculations. The quadratic region however shows poor agreement.

The results of E&T exhibit a much longer quadratic region than those of the present work. This implies that the correlation time of the E&T fluid point is much longer. Because the fluid point characteristics are specified analytically in the framework of the model presented here, it is possible to obtain this correlation time exactly. From the form of the turbulence model employed it follows directly that the correlation time for the fluid point is given by the eddy decay time, t_d. This time is set equal to the Lagrangian time scale, extensively discussed above. In the work of E&T the correlation time is of the order of three time this value.

The time scaling used in the DNS experiment of E&T was performed to ensure consistency between the particle relaxation times and gravitational effects found in the original work of S&L. This form of scaling is clearly not applicable to the fluid point, since it has a zero relaxation time and a zero relative terminal velocity. Therefore, it follows from the ratio of the Reynolds numbers found in the two experiments (~1/3) that the integral time scale found in the DNS data will be of the order of three times that in the experiment of S&L, which explains the discrepancy between the two correlation times is shown in figure 3.12.

3.5 Conclusions

The above calculations show that the vector model gives a good fit to experimental data throughout the range of particle types considered. The error between all the predicted dispersion curves and those measured falls within the experimental error (approximately 10-

15%). The introduction of a convection time formulation is especially important for the correct calculation of the dispersion of light particles which exhibit a small relaxation time. When this added effect is incorporated into the calculation the fit between the calculations and the experimental data of both S&L and E&T can be taken to be good. Though the modified form of the HHD model using ensemble averaging and including a crossing time scale gives results of similar accuracy to the vector model for heavy particles, it provides a poor description of the intermediate particles and the latter model intrinsically incorporates the underlying physical processes in a more systematic manner and therefore is preferred here.

The data of Wells and Stock has been shown to contain inconsistencies between the measurements of the particle dispersions and the turbulent scales of the flow field. Further the measured effect of increasing the applied electric field, which in turn increases the crossing effects for the particles, was much smaller than expected from the calculations. This discrepancy leads to an inability to correctly predict the experimental results, and has been noted by other authors.

The vector model is used throughout the remainder of this work as a basis for the calculation of particle diffusion coefficients. It should be noted that no convection time is implemented in the test-case calculations, presented later. Due to the types of particle, the inlet conditions and flow fields considered, the influence of this effect is considered negligible.

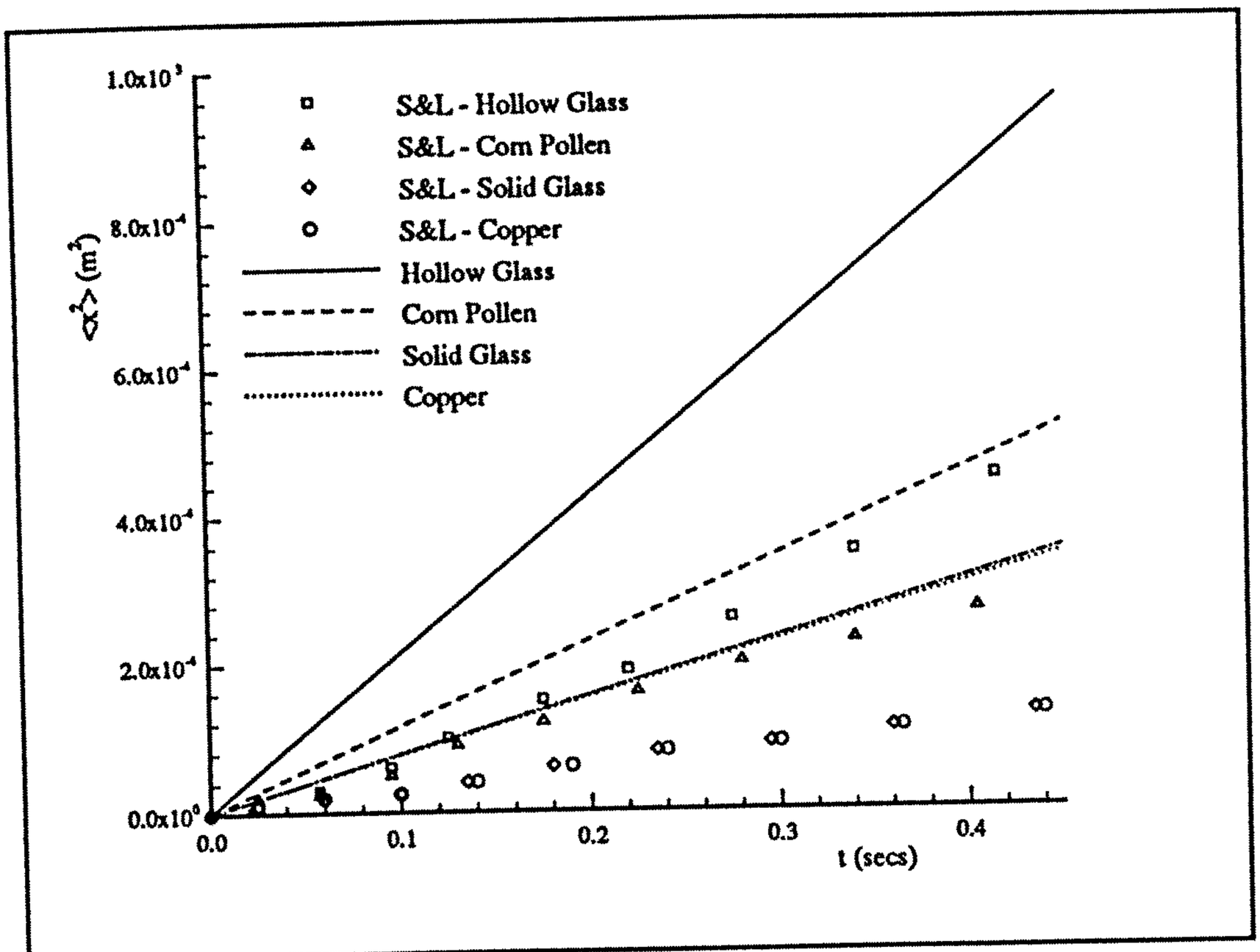

Figure 3.1 : Comparison of HHD Model - No Crossing, With S&L Data

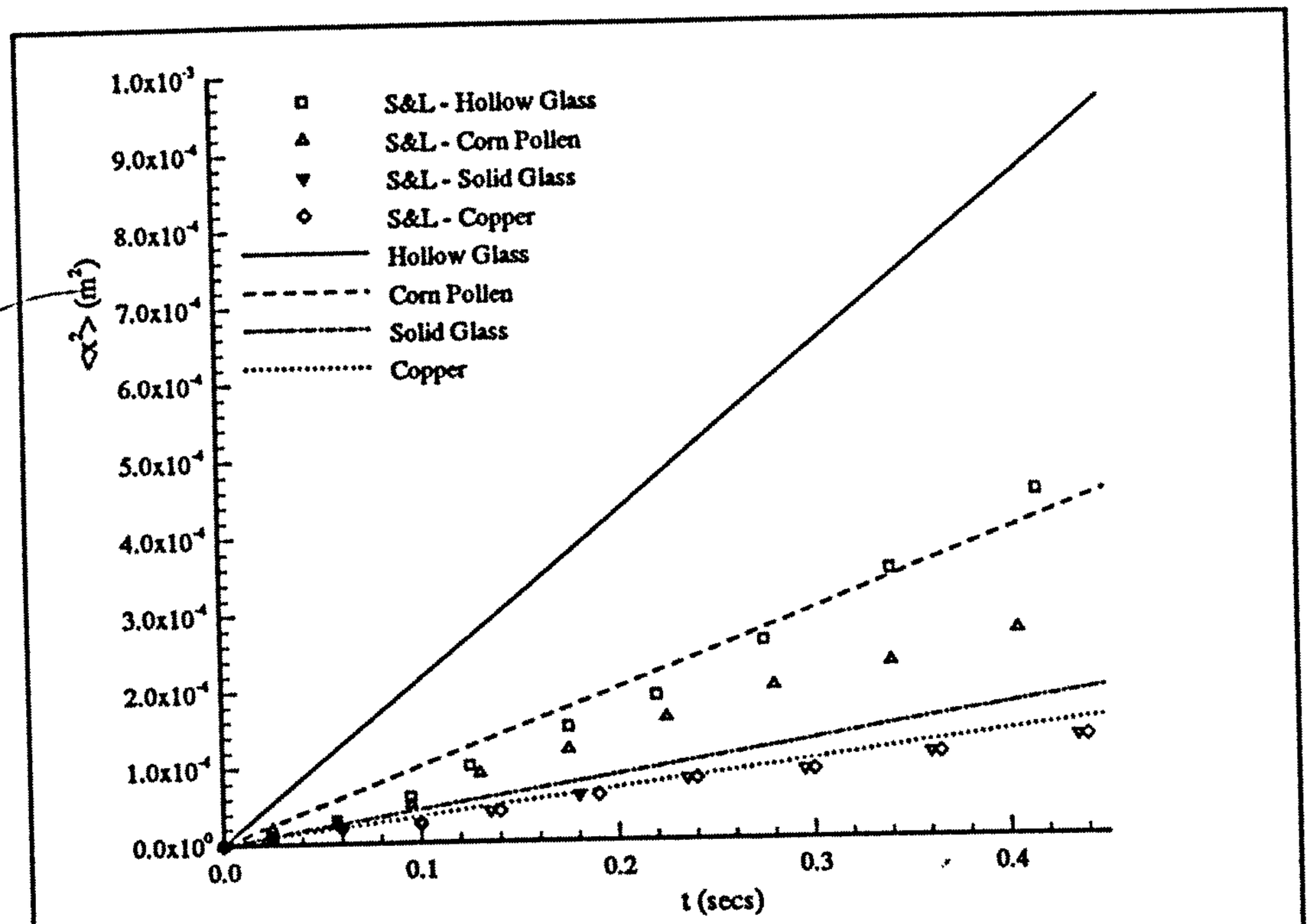

Figure 3.2 : Comparison of HHD Model - With Crossing, With S&L Data

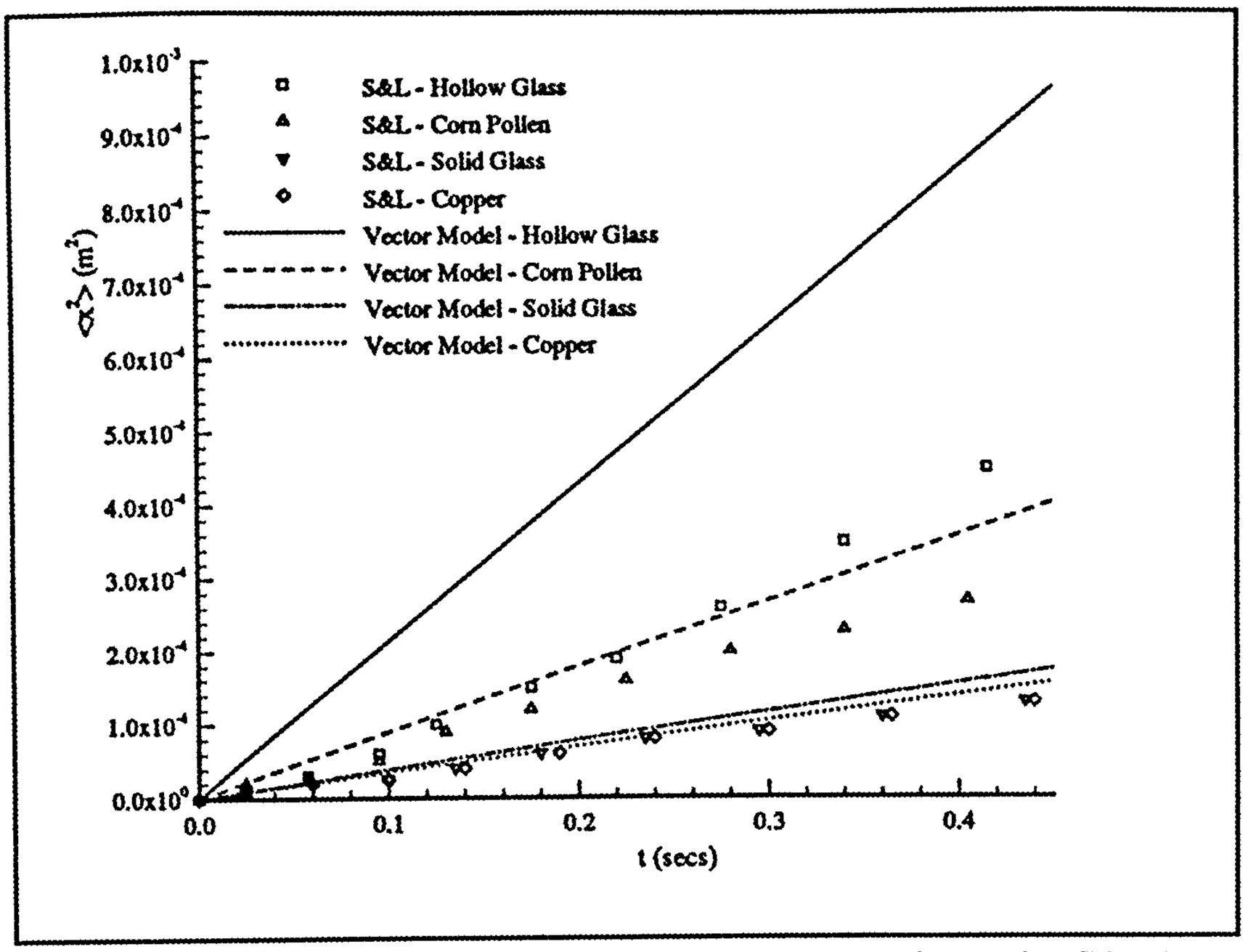

Figure 3.3 : Comparison of Vector Model - No Convection, with S&L Data

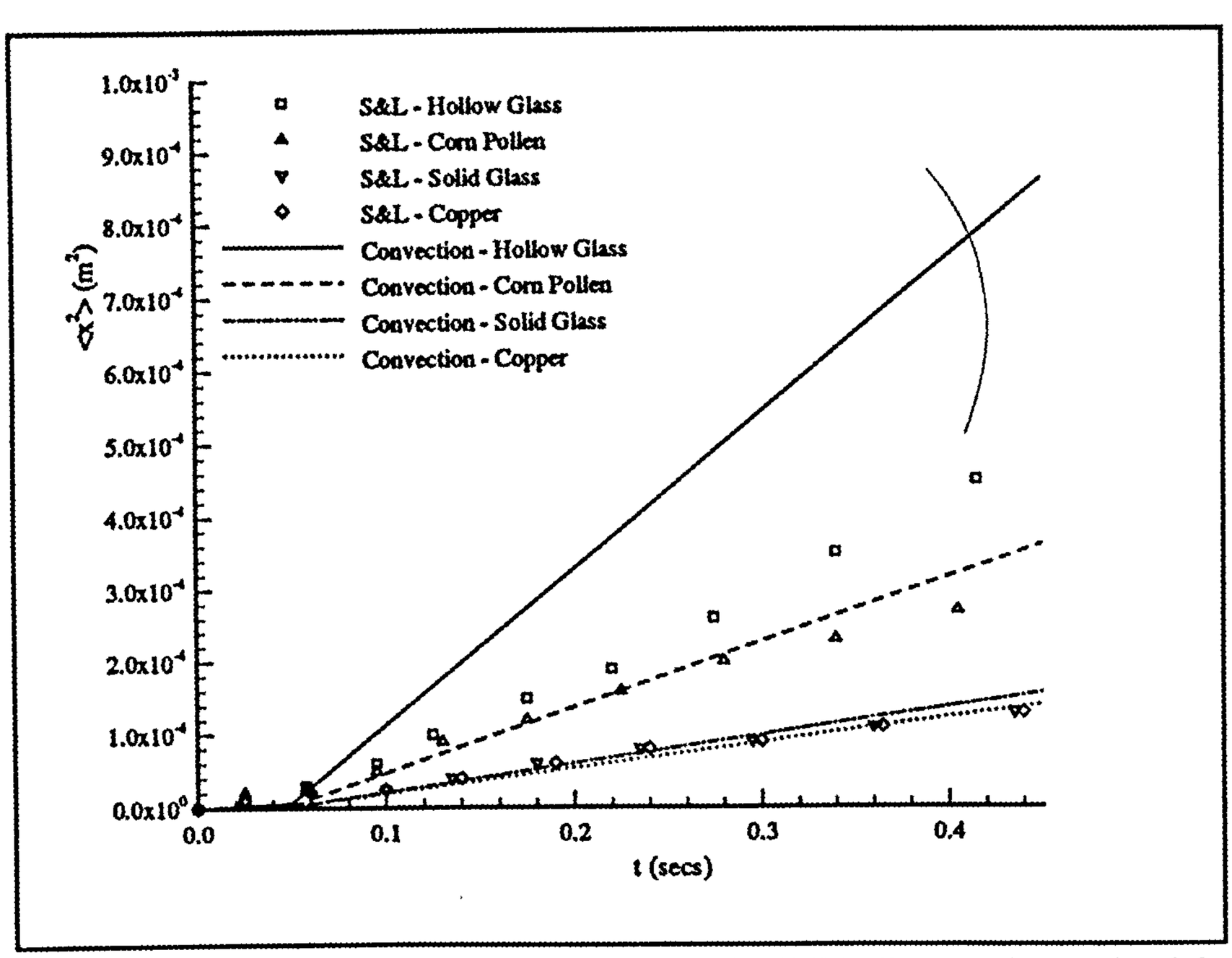

Figure 3.4 : Comparison of Vector Model - With Convection, with S&L Data

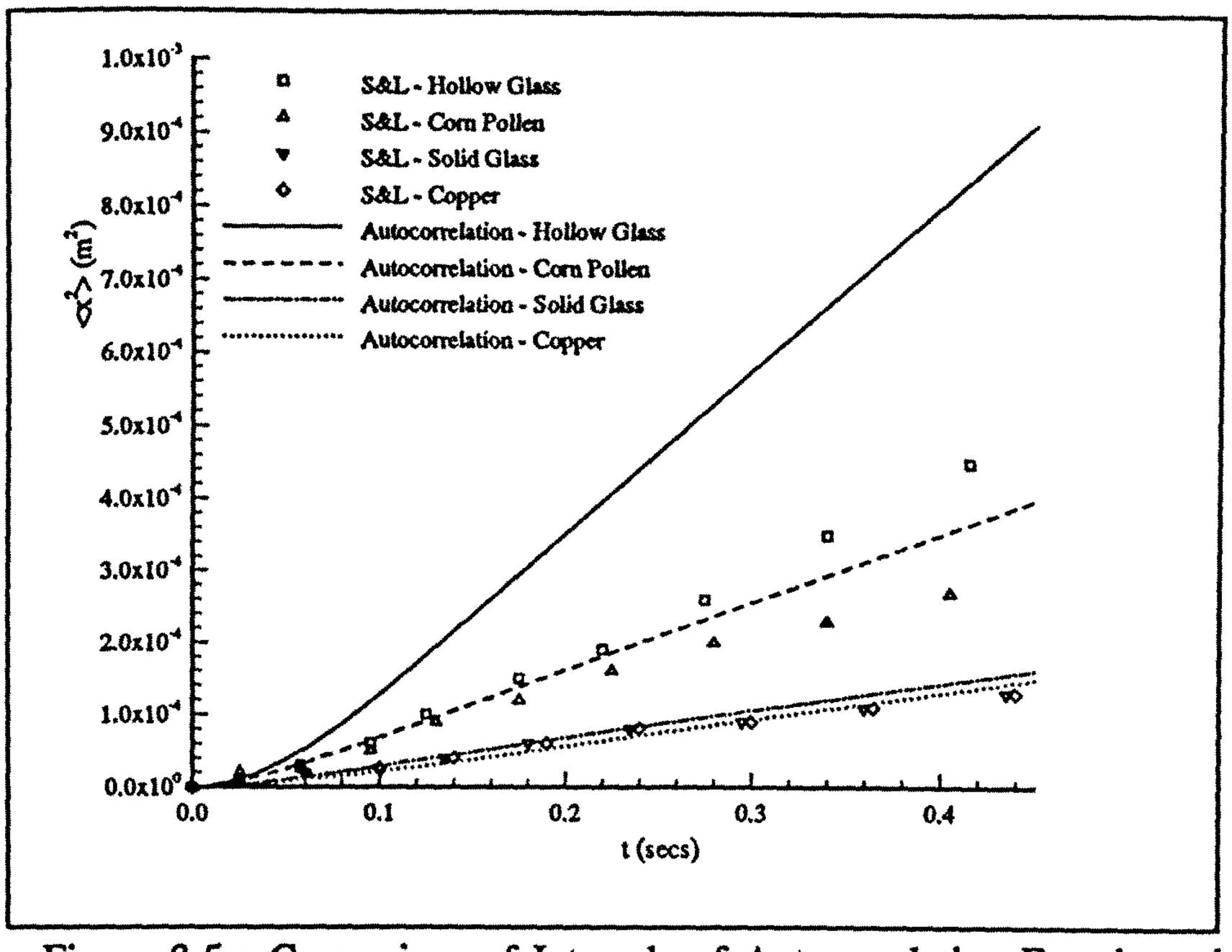

Figure 3.5 : Comparison of Integral of Autocorrelation Function with S&L Data

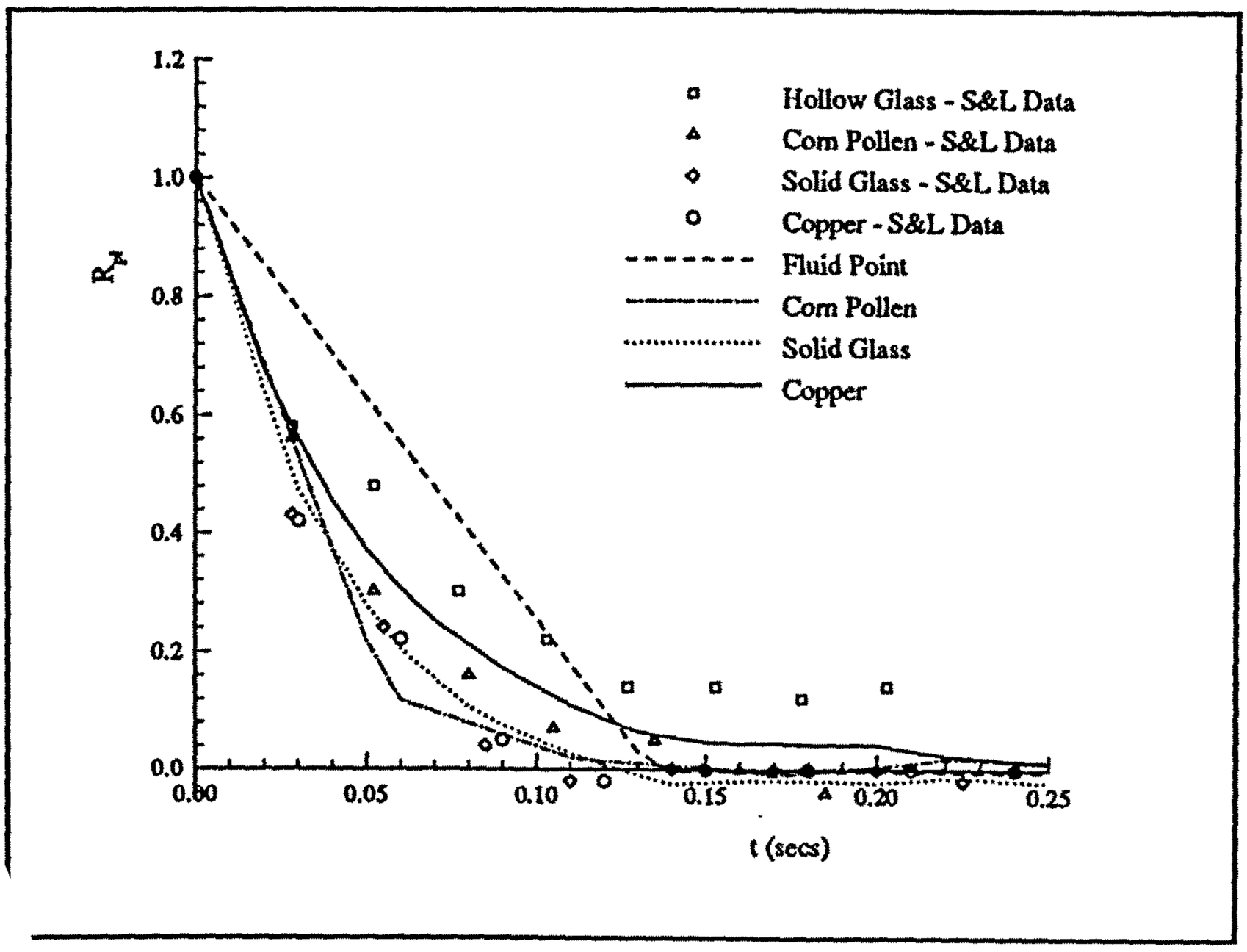

Figure 3.6 : Normalised Autocorrelation Functions

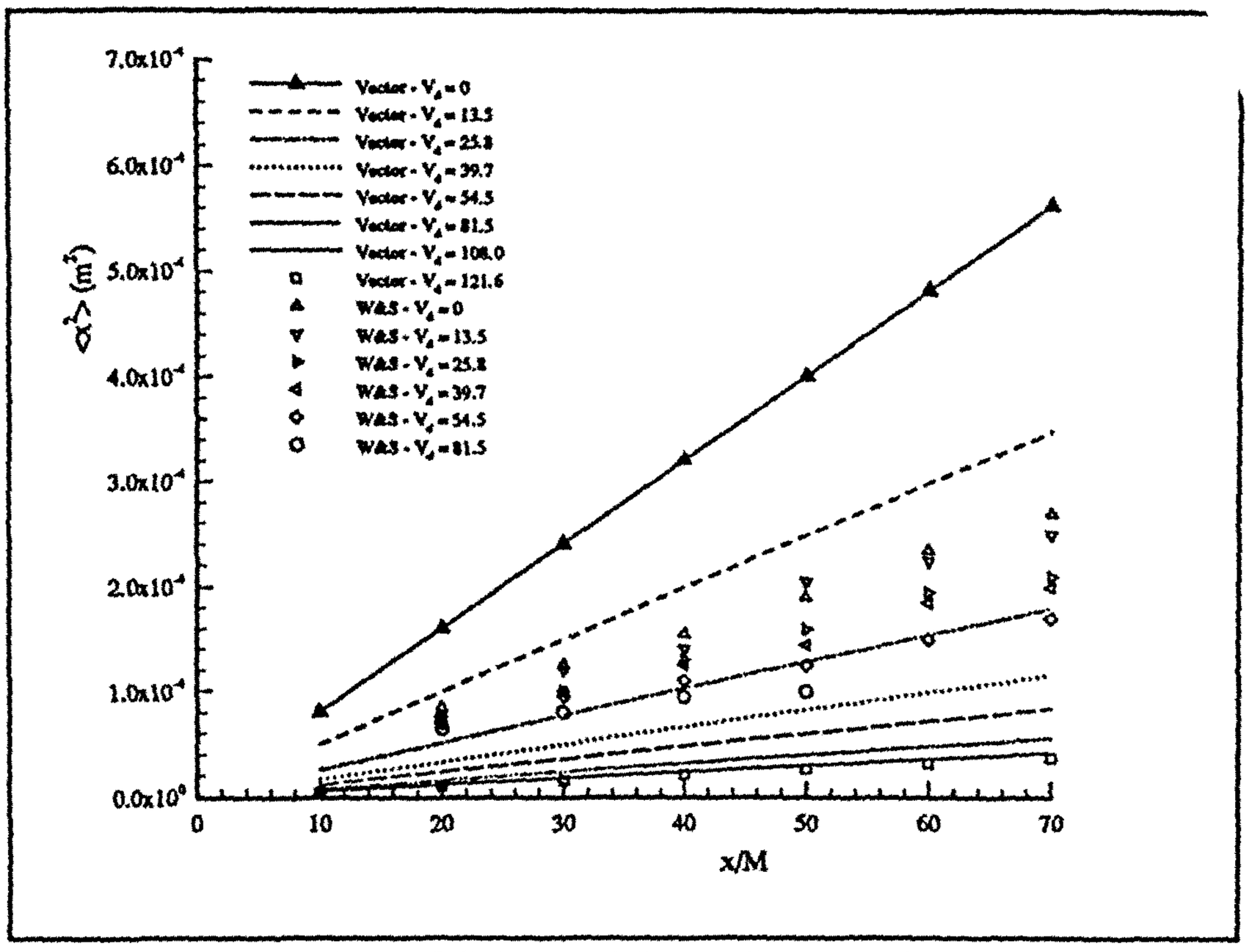

Figure 3.7 : Comparison of Calculated 57μm Glass Particle with W&S Data for a Range of Drift Velocities, v_d (m/s).

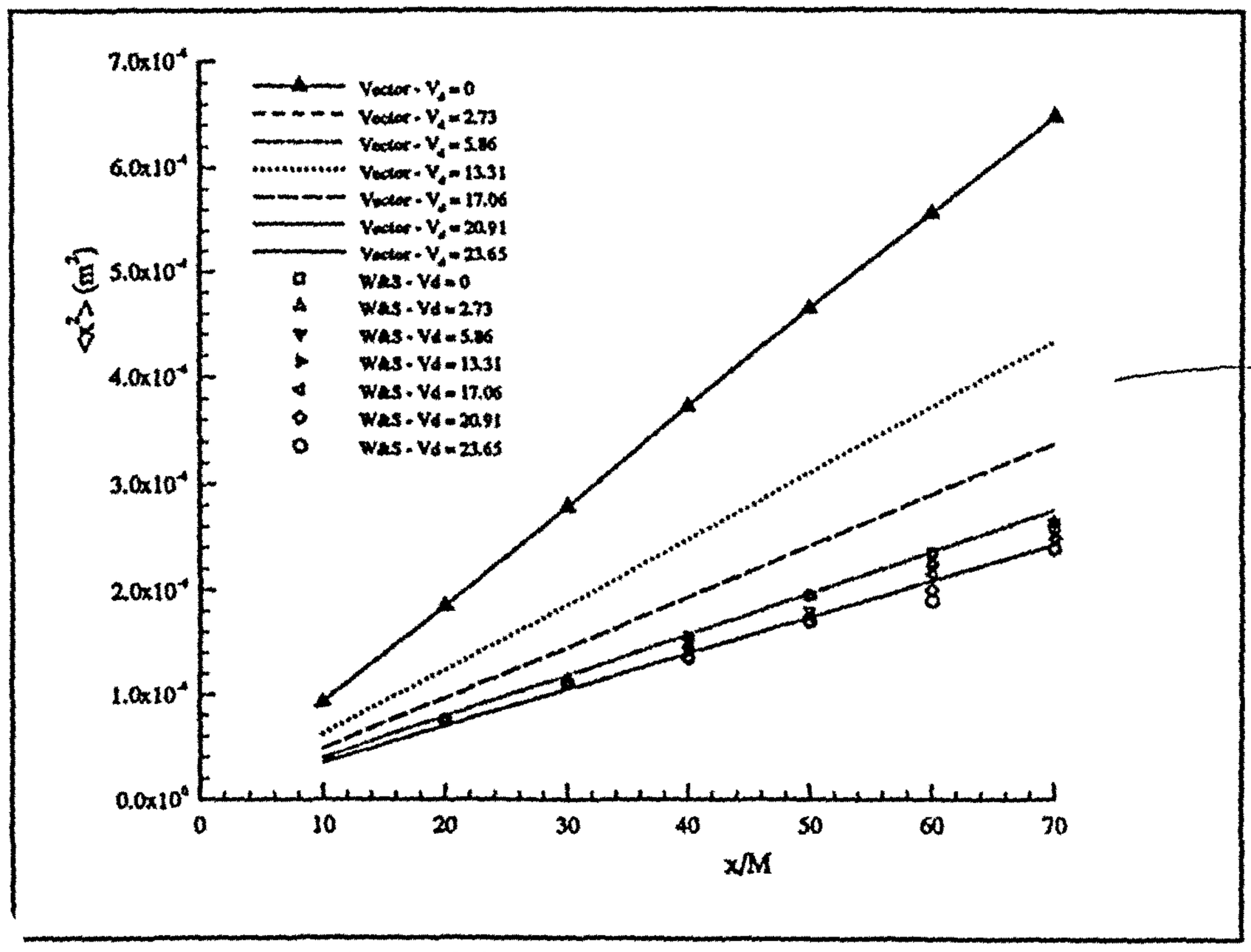

'igure 3.8 : Comparison of Calculated 5μm Glass Particle with W&S Data ' a Range of Drift Velocities, v_d (m/s).

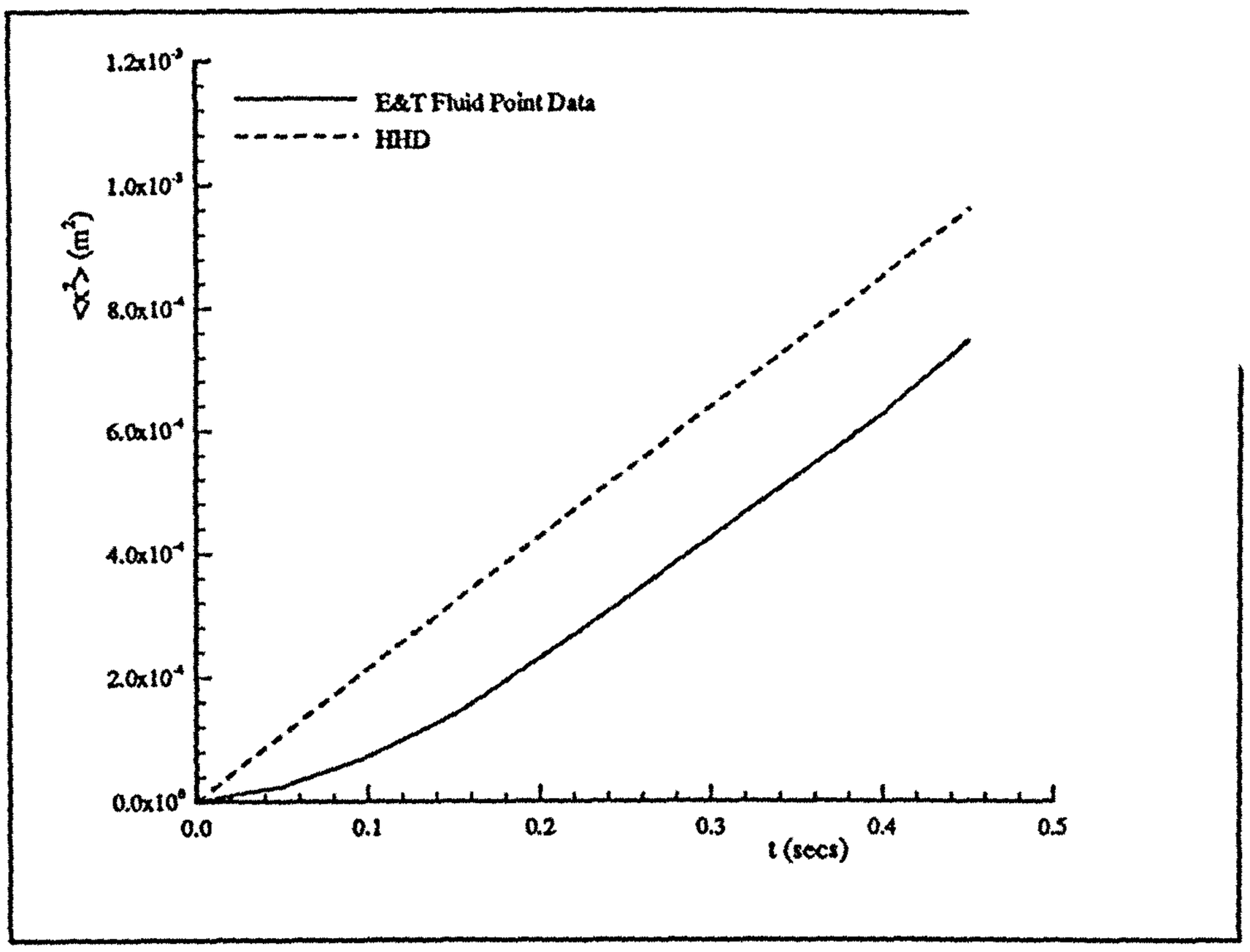

Figure 3.9 : Comparison of HHD Model with E&T Fluid Point

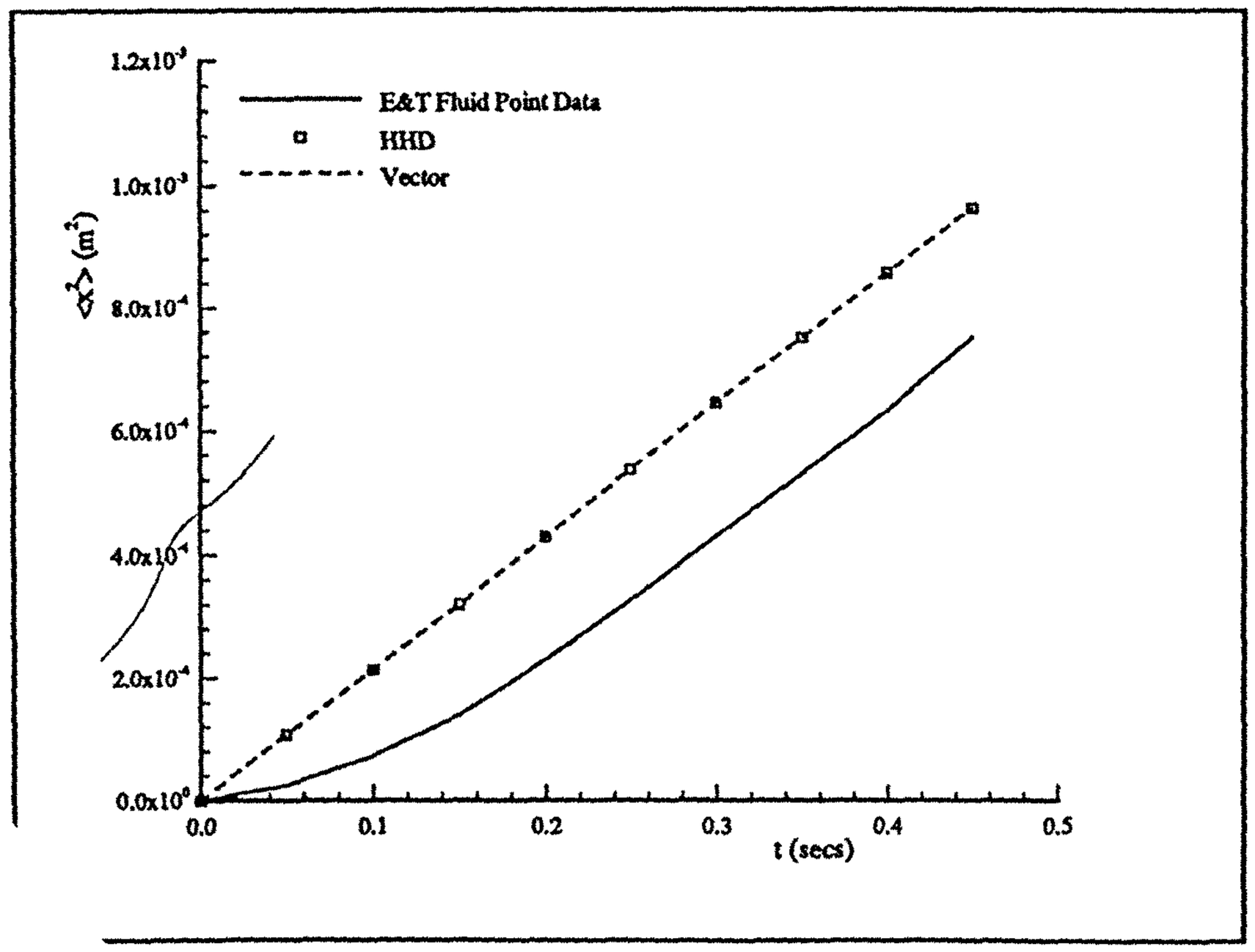

3.10 : Comparison of Vector Model - No Convection, with E&T
int

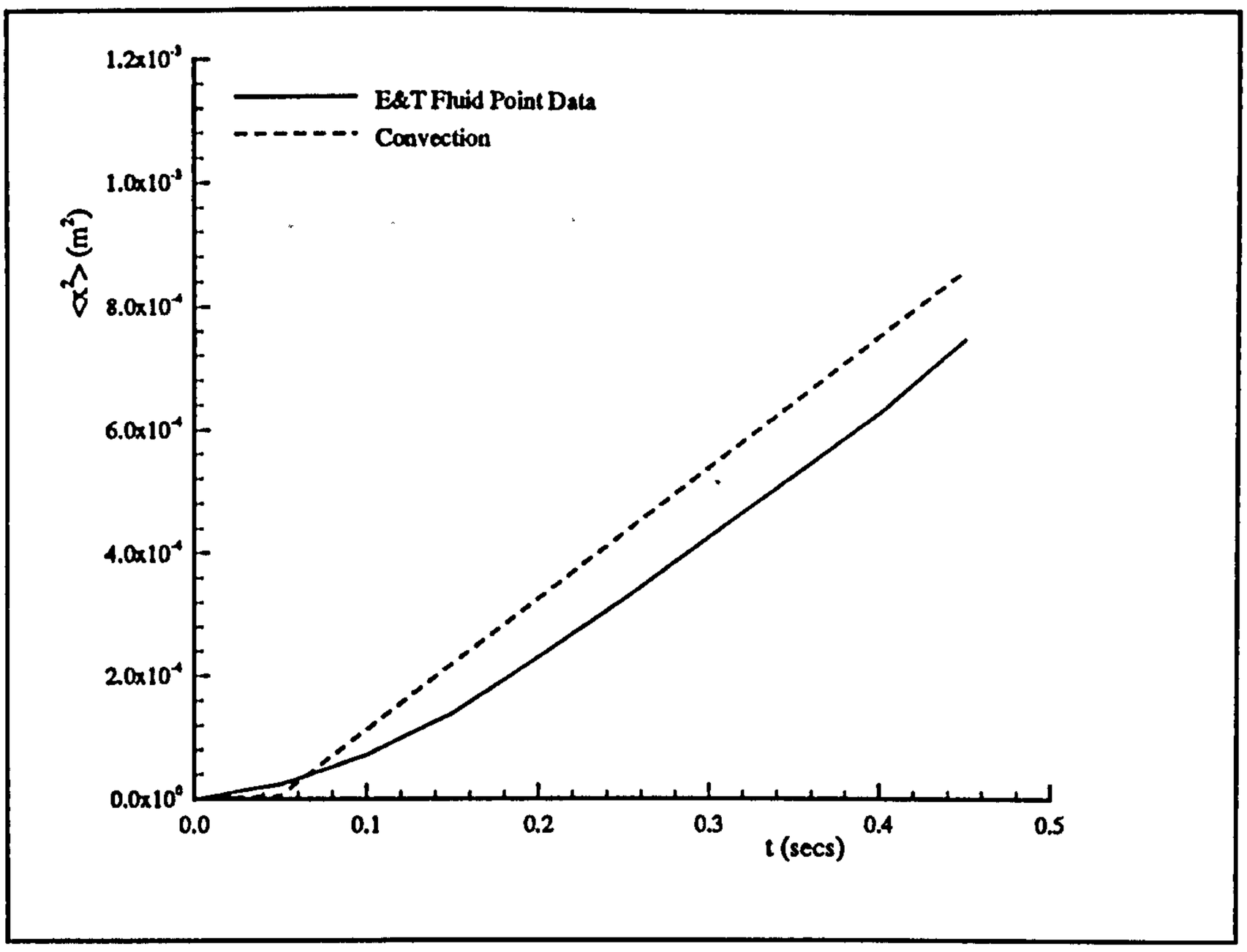

Figure 3.11 : Comparison of Vector Model - With Convection, with E&T Fluid Point

Figure 3.12 : Comparison of Integral of Autocorrelation Function with E&T Fluid Point, Showing Corresponding Correlation Times.

CHAPTER 4

Single Phase Calculation

4.1 Introduction

In order to model the behaviour of a dilutely dispersed second phase, in a turbulent fluid, it is necessary to be able to specify the behaviour of the carrier phase. Experimental investigation can provide the some of the required data but tends to be expensive. Also the measurement of some quantities of interest can be extremely difficult. Though experiments remain of great importance in the investigation of flow phenomena much use is made of analytical and numerical methods.

Equations to represent fluid flow have been known since the turn of the century, the well known to Navier-Stokes equations, but due to their highly coupled, non-linear nature analytical solutions are only possible in the most trivial of cases. Though numerical methods have become widely available with the advent of affordable and powerful computers only recently has it been possible to solve these equations at sufficiently small scales to simulate turbulence, and this using the most powerful computers and considering only simple, low Reynolds number flows.

Because of the problems encountered when attempting to solve the equations for fluid flow exactly, various approximation techniques have been developed. Foremost amongst these is that proposed by Osborn Reynolds.

This chapter provides a basic overview of the derivation of the equations of fluid flow together with their transformation into mean equations following the method of Reynolds. The turbulence closure problem is then discussed together with the required boundary conditions for the solution of the resultant equations. A simple numerical solution scheme is then presented based heavily on the work of Patankar (1980) Finally this numerical algorithm is applied to a simple pipe flow and compared to the data of Laufer (1954).

The work presented in this chapter is by no means a comprehensive discussion of the

field of computational fluid dynamics and as such contains little or no reference to many of the current discretisation and solution methods found in the literature. No mention is made of direct numerical simulation (DNS) or large eddy simulation (LES) or even higher order quadrature schemes. One of the main goals in the use of the solution procedure discussed below is that it can be run, in an acceptable amount of time, on a desktop personal computer. Another major aim was to develop a solution algorithm which was directly applicable to the solution of the second phase conservation equations presented in the following chapter. The straightforward pressure-correction code chosen fulfils both of the above goals as well as being well tested and accepted within the literature.

4.2 Conservation Equations

To be able to describe the flow situations required it is necessary to develop conservation equations for the important variables. Derived here are the conservation equations for mass, often called the continuity equation, and momentum. Using these equations as a base it is possible to develop a general form of differential equation applicable to most variables of interest. This general form has the added advantage of enabling direct application of many of the results developed in this chapter to the calculation of the Eulerian description of the second phase. This second phase calculation is discussed in detail in the following chapter.

Firstly the mass conservation equation will be developed. This is then extended to the required momentum equations and those of Navier and Stokes.

4.2.1 Mass Conservation

Consider the fluid volume, V with surface area S, given in figure 4.1. Also let ρ represent the mass per unit volume of the fluid. The mass flux through a small area dS_j with a normal in the x_j coordinate direction is hence given as $\rho u_j dS_j$. The total mass transfer through the surface of the volume is then given by

$$\int_s \rho u_j dS_j \tag{4.1}$$

Also the rate of change of mass, per unit time, in the volume V is given by

$$\frac{\partial}{\partial t}\int_V \rho \, dV$$

Assuming ρ is continuous and differentiable over a fixed V we get

$$\frac{\partial}{\partial t}\int_V \rho \, dV = \int_V \frac{\partial \rho}{\partial t} dV \tag{4.2}$$

It follows that the rate of change of the mass in volume V is given by the summation of (4.1) and (4.2)

$$\int_V \frac{\partial \rho}{\partial t} dV + \int_s \rho u_j dS_j$$

Applying Greens Theorem to convert the surface integral to a volume integral, we get

$$\int_V \frac{\partial \rho}{\partial t} dV + \int_s \rho u_j dS_j = \int_V \left\{ \frac{\partial \rho}{\partial t} + \frac{\partial}{\partial x_j}(\rho u_j) \right\} dV$$

Letting the volume become arbitrarily small this becomes

$$\frac{\partial \rho}{\partial t} + \frac{\partial}{\partial x_j}(\rho u_j) = S_\rho \tag{4.3}$$

The term on the RHS of (4.3) is used to represent other processes which could influence the

mass conservation principle. Internal sources or sinks need to be considered in reactive flows where mass can be destroyed or created within the flow due to chemical reaction. In the case of non-reactive flows this source term can be set equal to zero to give the standard form of the single phase continuity equation.

$$\frac{\partial \rho}{\partial t} + \frac{\partial}{\partial x_j}(\rho u_j) = 0 \qquad (4.4)$$

4.2.2 Momentum Conservation

The unsteady and convection terms for the momentum conservation equations can be derived in a similar manner to those in the continuity equation, above. It can be seen from figure 4.2 that in addition to these two terms an extra term arises due to the shear and normal stresses experienced by the surface of the volume, V. This results in the term

$$\int_S \sigma_{ij} dS_j$$

For a Newtonian fluid there exists a linear relationship between the stress and deformation tensors (i.e. the symmetrical part of the spatial variations)

$$\frac{\partial}{\partial x_j} u_i = \frac{1}{2}\left(\frac{\partial u_i}{\partial x_j} + \frac{\partial u_j}{\partial x_i}\right) + \frac{1}{2}\left(\frac{\partial u_i}{\partial x_j} - \frac{\partial u_j}{\partial x_i}\right) = \frac{1}{2} D_{ij} + \frac{1}{2} \Omega_k E_{ijk}$$

where E_{ijk} is the alternating third order tensor. Therefore the shear experienced by a Newtonian fluid is

$$\sigma_{ij} = \mu D_{ij}$$

where μ is defined as the dynamic viscosity. This leads to

$$\sigma_{ij} = p\,\delta_{ij} - \lambda\,\delta_{ij}\frac{\partial u_k}{\partial x_k} - \mu\left(\frac{\partial u_i}{\partial x_j} + \frac{\partial u_j}{\partial x_i}\right)$$

where p is the hydrostatic pressure force and $\lambda = \frac{2}{3}\mu$ is assumed. Thus representing momentum by ρu_i we have for the conservation of momentum

$$\int_V \frac{\partial}{\partial t}(\rho u_i)\,dV + \int_S (\rho u_i u_j)\,dS_j + \int_S \sigma_{ij}\,dS_j$$

Again using Green's theorem and assuming a small control volume we obtain

$$\frac{\partial}{\partial t}(\rho u_i) + \frac{\partial}{\partial x_j}(\rho u_i u_j) + \frac{\partial}{\partial x_j}\left\{p\delta_{ij} - \lambda\delta_{ij}\frac{\partial u_k}{\partial x_k} - \mu\left(\frac{\partial u_i}{\partial x_j} + \frac{\partial u_j}{\partial x_i}\right)\right\} = S_{\rho u}$$

$$\frac{\partial}{\partial t}(\rho u_i) + \frac{\partial}{\partial x_j}(\rho u_i u_j) = -\frac{\partial p}{\partial x_j} + \frac{\partial}{\partial x_j}\left(\lambda\delta_{ij}\frac{\partial u_k}{\partial x_k}\right) + \frac{\partial}{\partial x_j}\left(\mu\left(\frac{\partial u_i}{\partial x_j} + \frac{\partial u_j}{\partial x_i}\right)\right) + S_{\rho u} \quad (4.5)$$

The term $S_{\rho u}$ on the RHS of (4.5) again is used to represent the influence of other effects on the conservation of momentum. Setting this source term equal to $-\rho g$, the force due to an external gravitational field, leads to the well known Navier-Stokes equations.

For the case of an incompressible flow where density is constant and $\frac{\partial u_k}{\partial x_k} = 0$ we get

$$\rho\frac{\partial}{\partial t}(u_i) + \rho\frac{\partial}{\partial x_j}(u_i u_j) = -\frac{\partial p}{\partial x_j} + \frac{\partial}{\partial x_j}\mu\left(\frac{\partial u_i}{\partial x_j} + \frac{\partial u_j}{\partial x_i}\right) + S_{\rho u} \quad (4.6)$$

This equation can be written in a slightly more usable form, since

$$\frac{\partial}{\partial x_j}\left(\mu\left(\frac{\partial u_i}{\partial x_j} + \frac{\partial u_j}{\partial x_i}\right)\right) = \mu\left(\frac{\partial^2 u_i}{\partial x_j \partial x_j} + \frac{\partial^2 u_j}{\partial x_j \partial x_i}\right) + \quad (4.7)$$

$$\left(\frac{\partial u_i}{\partial x_j} + \frac{\partial u_j}{\partial x_i}\right)\frac{\partial \mu}{\partial x_j} = \frac{\partial}{\partial x_j}\left(\mu\frac{\partial u_i}{\partial x_j}\right) + \frac{\partial u_j}{\partial x_i}\frac{\partial \mu}{\partial x_j}$$

Hence, (4.6) can be written as

$$\frac{\partial}{\partial t}(\rho u_i) + \frac{\partial}{\partial x_j}(\rho u_i u_j) = -\frac{\partial p}{\partial x_j} + \frac{\partial}{\partial x_j}\left(\mu \frac{\partial u_i}{\partial x_j}\right) + \frac{\partial u_j}{\partial x_i}\frac{\partial \mu}{\partial x_j} + S_{\rho u}$$

Taking the second viscous term on the RHS into the source term, we get

$$\frac{\partial}{\partial t}(\rho u_i) + \frac{\partial}{\partial x_j}(\rho u_i u_j) = -\frac{\partial p}{\partial x_j} + \frac{\partial}{\partial x_j}\left(\mu \frac{\partial u_i}{\partial x_j}\right) + S_{\rho u} \tag{4.8}$$

which is the final form for the conservation of momentum equation for incompressible flow. This form is also assumed valid for compressible flow at low Mach numbers where the density can be assumed constant.

4.2.3 Generalised Form

Equations (4.4) and (4.8) can be considered to be special cases of a generalised form of differential equation for an unsteady, convection-diffusion process

$$\frac{\partial}{\partial t}(\rho \phi_i) + \frac{\partial}{\partial x_j}(\rho u_j \phi_i) = \frac{\partial}{\partial x_j}\left(\Gamma_\phi \frac{\partial \phi_i}{\partial x_j}\right) + S_\phi \tag{4.9}$$

where Γ_ϕ represents the diffusion coefficient of the general variable ϕ and S_ϕ is used to represent the source terms for the variable ϕ. The use of this type of generalised equation allows the straightforward development of solution algorithms. This is discussed in more detail later in this chapter.

4.3 Reynolds Averaged Equations

The conservation equations derived in the previous section are based on the instantaneous values of the dependent variables. In order to solve these equations it is desirable to reduce them into equations for the mean properties. This is accomplished by the use of Reynolds decomposition and averaging.

The process of decomposition assumes that the instantaneous value is formed from

a superposition of the mean and fluctuating components. Hence for a general variable ϕ we get

$$\phi = \Phi + \phi'$$

where Φ represents the mean component and ϕ' the fluctuating component. The mean of the fluctuating component is zero.

Introducing this form of decomposition and applying Reynolds averaging to the resulting equations leads to equations for the conservation of the mean properties.

The standard properties for Reynolds averaging can be expressed as

$$\begin{gathered}
\overline{a} = \overline{A + a'} = \overline{A} + \overline{a'} = A \\
\overline{AB} = \overline{A}\,\overline{B} = AB \\
\overline{Ab'} = \overline{A}\,\overline{b'} = A\overline{b'} = 0 \\
\overline{ab} = \overline{(A+a')(B+b')} = \overline{AB} + \overline{Ab'} + \overline{Ba'} = \overline{AB} + \overline{a'b'} = AB + \overline{a'b'}
\end{gathered} \tag{4.10}$$

where

$$a = A + a' \qquad \& \qquad b = B + b'$$

This decomposition and averaging is now applied to the continuity, (4.4) and momentum, (4.8) equations developed above.

4.3.1 Continuity Equation

The instantaneous mass conservation, or continuity equation, given in (4.4) is now considered. Introducing the decomposition of the dependent variables

$$\rho = P + \rho' \quad , \quad u = U + u'$$

we have

$$\frac{\partial \overline{(P+\rho')}}{\partial t} + \frac{\partial \overline{(P+\rho')(U_j+u_j')}}{\partial x_j} = 0$$

Using the properties (4.10) we obtain

$$\frac{\partial P}{\partial t} + \frac{\partial}{\partial x_j}(P U_j + \overline{\rho' u_j'}) = 0$$

For incompressible flows we have no density fluctuations. Setting the density equal to ρ we get

$$\frac{\partial \rho}{\partial t} + \frac{\partial}{\partial x_j}\rho U_j = 0 \qquad (4.12)$$

since the fluctuating term is zero.

4.3.2 Momentum Equation

The instantaneous momentum equations (4.8) are now considered. Assuming incompressible flow, hence a constant density, a zero source term and introducing the velocity decomposition form (4.11) together with

$$p = P + p'$$

and averaging we get

$$\rho \frac{\partial \overline{(U_j + u_j')}}{\partial t} + \rho \frac{\partial \overline{(U_i + u_i')(U_j + u_j')}}{\partial x_j} = -\frac{\partial \overline{(P + p')}}{\partial x_j} + \frac{\partial}{\partial x_j}\left(\mu \frac{\partial \overline{(U_i + u_i')}}{\partial x_j} \right)$$

Again applying the properties (4.10) this reduces to

$$\rho \frac{\partial U_j}{\partial t} + \rho \frac{\partial}{\partial x_j}(U_i U_j + \overline{u_i' u_j'}) = -\frac{\partial P}{\partial x_j} + \frac{\partial}{\partial x_j}\left(\mu \frac{\partial U_i}{\partial x_j} \right) \qquad (4.13)$$

The use of this Reynolds decomposition and averaging procedure leads to the inclusion of an extra term in (4.13) over the laminar viscous form of the Navier-Stokes equations. This term has the form of a mean stress and hence is known as the Reynolds stress tensor

$$\rho \frac{\partial}{\partial x_j}(\overline{u_i' u_j'})$$

Inclusion of this term leads to the classical closure problem. This problem is discussed in the next section

4.4 Turbulent Closure

The presence of the Reynolds stress terms in (4.13) imply that the set of equations defined by (4.12) and (4.13) contains more unknowns than equations. To calculate the required Reynolds stress terms it would be necessary to average for the next order in equation (4.13). This would in itself introduce a triple correlation term leading to a similar problem. Therefore a solution is not possible without further approximation. In order to address this problem various forms of closure hypothesis have been proposed.

Two types of model exist. Firstly those which use a so-called turbulent viscosity concept to approximate the additional stress terms of (4.13) and secondly those models which develop equations to describe the transport of the stresses themselves.

These two types of model are briefly discussed below and a preference is declared for a model based on the idea of an eddy viscosity. A comprehensive review of closure models can be found in Nallasamy (1987).

4.4.1 Turbulent Viscosity Model

This form of modelling treats the Reynolds stress terms found in (4.13) as additional viscous stresses of the form

$$\textit{Reynolds Stress} = \mu_T \left(\frac{\partial U_i}{\partial x_j} + \frac{\partial U_j}{\partial x_i} \right)$$

where μ_T is an additional viscosity due to turbulence. Substituting for the Reynolds stresses in (4.13) we get

$$\rho \frac{\partial U_i}{\partial t} + \rho \frac{\partial}{\partial x_j}(U_i U_j) = -\frac{\partial P}{\partial x_j} + \frac{\partial}{\partial x_j}\left((\mu + \mu_T) \frac{\partial U_i}{\partial x_j} \right) \qquad (4.14)$$

Again assuming the gradient of turbulent viscosity term is zero. This results in an equation which is of exactly the same form as the original momentum equation (4.8) with the simple addition of the extra viscosity term.

The variations between the models of this type arise from the method used to obtain the turbulent viscosity.

The simplest form of this type of model arises from mixing length arguments, Prandtl (1926). A dimensional analysis reveals that μ_T divided by the density, ρ has the dimensions of length multiplied by velocity. This implies that μ_T is a function of the density, a representative length scale and the local flow velocity. Using the expression for the turbulent shear stress as a model it can be postulated

$$\mu_T = \rho C_\mu l^2 \left(\frac{\partial U_i}{\partial x_j} + \frac{\partial U_j}{\partial x_i} \right)$$

where C_μ is a model constant and l the representative length scale. Both of these quantities needed to be specified. This is accomplished by consideration of experimental data for simple flows. This type of model is called a zero-equation model since no transport equations need to be solved to obtain the value of μ_T.

The next type of model is the one-equation model. In this form of model an equation for the turbulent kinetic energy, k, is derived based on the generalised form (4.9), Abbott and Basco (1989).

$$\frac{\partial k}{\partial t} + U_j \frac{\partial k}{\partial x_j} - \frac{\partial}{\partial x_j}\left(\frac{\mu_T}{\rho \sigma_k} \frac{\partial k}{\partial x_j} \right) = \frac{\mu_T}{\rho} \left(\frac{\partial U_i}{\partial x_j} + \frac{\partial U_j}{\partial x_i} \right) \frac{\partial U_i}{\partial x_j} - \epsilon \qquad (4.15)$$

This transport equation for k is then solved, the value of ϵ being specified empirically. The turbulent viscosity is obtained from

$$\mu_T = \rho c_\mu k^{\frac{1}{2}} l$$

Again this type of model requires the specification of the mixing length, l together with the various constants found in (4.15)

The final model of this type introduces a second transport equation whose dependent variable is a function of the representative length scale. The most commonly used equation is that of the turbulent dissipation, ϵ, which has the form, again from Abbott and Basco (1989).

$$\frac{\partial \epsilon}{\partial t} + U_j \frac{\partial \epsilon}{\partial x_j} - \frac{\partial}{\partial x_j}\left(\frac{\mu_T}{\rho \sigma_\epsilon} \frac{\partial \epsilon}{\partial x_j} \right) = C_{1\epsilon} \frac{\epsilon}{k} \frac{\mu_T}{\rho} \left(\frac{\partial U_i}{\partial x_j} + \frac{\partial U_j}{\partial x_i} \right) \frac{\partial U_i}{\partial x_j} - C_{2\epsilon} \frac{\epsilon^2}{k} \qquad (4.16)$$

Again the coefficients in both equation (4.15) and (4.16) need to be specified. The turbulent viscosity is given by

$$\mu_T = C_\mu \rho \frac{k^2}{\epsilon}$$

This is the standard two-equation model, first derived by Launder and Spalding (1974), and is used extensively throughout the literature, and is used in this work.

The main benefit of these types of models is their simple form and ease of computation. Conversely, the requirement to specify either a turbulent length scale, or the model constants in the two-equation model, implies the dependence of fitting experimental data and a possible lack of universality.

One of the main drawbacks of these models is that the use of an eddy viscosity leads to the assumption of isotropic turbulence, as a result of the scalar variables used in its definition. Consequently this type of model is generally inappropriate to situations where the flow is strongly anisotropic, though extensions to anisotropy can be found in the literature through the specification of a multi-dimensional turbulent viscosity. Only the isotropic form of equations (4.15) and (4.16) is considered in this work.

4.4.2 Stress Models

The second main type of turbulent model is concerned with modelling the Reynolds

stress terms, found in (4.13), explicitly. This allows the two, or three coordinate directions to be treated independently thus allowing for anisotropic effects. These models assume two main type, namely algebraic stress models and the more complicated Reynolds stress models. The transport equations take the form, Launder (1989)

$$\frac{\partial}{\partial x_k}(\rho U_k \overline{u_i' u_j'}) = -\rho\left(\overline{u_j' u_k'}\frac{\partial U_i}{\partial x_k} + \overline{u_i' u_k'}\frac{\partial U_j}{\partial x_k}\right)$$

$$+ \overline{(u_j f_i + u_i f_j)}$$

$$+ p\left(\frac{\partial u_i}{\partial x_j} + \frac{\partial u_j}{\partial x_i}\right)$$

$$+ \frac{\partial}{\partial x_k}\left(\rho \overline{u_i' u_j' u_k'} + \overline{p u_i}\delta_{jk} + \overline{p u_j'}\delta_{ik} - \mu\frac{\partial \overline{u_i' u_j'}}{\partial x_k}\right)$$

$$+ 2\mu\overline{\frac{\partial u_i}{\partial x_k}\frac{\partial u_j}{\partial x_k}}$$

where f_i represents a fluctuating density.

In the algebraic stress models algebraic transport equations are developed to represent the above equation. The Reynolds stress terms can be seen to have four components, in two dimensions, together with two components of the scalar flux. This implies that at least six equations need to be solved (ten in three dimensions) in order to predict the stress terms. The large computation overhead is reduced, in this method, by the use of algebraic, rather than differential, equations to model the transport equations.

Reynolds stress models, conversely retain the differential form, given above, for the transport equations for the Reynolds stresses, which adds considerably to the expense of the computation but has the advantage of reducing the number of approximations required to obtain a turbulence closure.

4.4.3 Choice of Turbulent Closure Model

In order to model a turbulent flow field a choice of turbulence model from those presented above is required. This choice presents a common problem since no firm guidelines exist to recommend the optimal approach. Due to both its simplicity of implementation, widespread use in the literature and its ready application to the second phase calculation, outlined in chapters 2 and 5, the standard k-ϵ model has been chosen.

This model requires the solution of equations (4.15) and (4.16) to obtain both a value for the turbulent viscosity and the distribution of kinetic energy and dissipation within the flow. These distributions are required for the calculation of the representative scales of the flow field to enable the computation of the particle diffusion coefficient, as outlined in chapter 2. The ease of translation of the properties of the single phase calculation into a form suitable for the calculation of the second phase was a major consideration in the choice of this turbulence model. Also the equations (4.15) and (4.16) can be seen to conform to the generalised ϕ equation (4.9). This allows the solution of these equations to be implemented within the CFD algorithm used, without extensive modification.

As mentioned above this type of turbulence model has two main drawbacks, namely the assumption of isotropy and the requirement to fit the model constants to experimental data.

The assumption of isotropy is also made in the derivation of the Lagrangian model for the second phase. The diffusion model used to close the second phase conservation equations also entails an isotropic assumption. Consequently the use of an isotropic flow field is consistent within the calculation. The use of an anisotropic turbulence model would therefore require the use of a similarly anisotropic model for the second phase. It should be noted that it is possible to extend the diffusion approximation, used for the second phase, to anisotropic flows. It is important to keep this intrinsic isotropic approximation in mind when applying both the single phase code , presented in this chapter, and the solution of the second phase equations, discussed in chapter 5.

The fitting of the model coefficients requires further discussion. A well recognised problem with the k-ϵ turbulence model is its inability to predict the behaviour of both a

round jet and a plane jet using the same specification of the model constants. This implies that universal values for these constants do not exist and they in fact vary from flow field to flow field. This variation in the values of these constants again needs to be born in mind when using this form of turbulence model. The standard values assumed for the constants in (4.15) and (4.16) are

$$\begin{aligned} C_{\mu} &= 0.09 \\ C_{1\varepsilon} &= 1.44 \\ C_{2\varepsilon} &= 1.92 \\ \sigma_{k} &= 1.00 \\ \sigma_{\varepsilon} &= 1.30 \end{aligned} \tag{4.17}$$

One benefit of these constants is that they can be used as parameters to enable a closer fit between the computation an any given flow field, where the object is to test a model for the behaviour of a dispersed second phase given an acceptably accurate description of the flow field of the carrier phase.

4.5 Boundary Conditions

In order to be able to solve the equations derived above, it is necessary to specify the boundary conditions for the calculation. Five types of boundary condition are considered here namely: inflow and outflow boundaries; periodic boundaries; planes of symmetry and solid boundaries. The first four conditions are treated with reference to the generalised variable, ϕ as given by (4.9). The final boundary, that of the solid wall is treated separately due to the need to introduce boundary layer approximations.

4.5.1 Inlet Boundaries

An inlet boundary allows the specification of either the calculated variable or its flux at a known position in the flow. These conditions are often the only known values for the flow variables and are of great importance in obtaining the correct solution.

There are, in general, two methods of specifying the inlet boundary condition. Firstly the value of the required variable ϕ may be known. In this case the implementation of this boundary condition is straightforward since this value of ϕ is applied at the corresponding edge of the calculation domain. Secondly the flux of the variable ϕ may be known. This leads to the need to construct an extra equation to solve for this boundary. It should be noted that in general this type of boundary condition is parabolic. The use of an elliptic inlet boundary is avoided in this work as it can lead to complications in the solution method due to the presence of recirculation at the boundary. This is discussed further below.

4.5.2 Outflow Boundaries

An outflow boundary is defined as a boundary where the fluid leaves the domain. Specification of this boundary condition is not necessary if it is ensured to be parabolic, in the same manner as the inlet condition above. Care must be taken in the placement of outlet boundaries that limit their behaviour to be parabolic. Incorrect placement of this type of boundary can lead to convergence problems in numerical solution algorithms.

4.5.3 Planes of Symmetry

A useful tool in reducing the cost of the flow field calculation is the use of symmetry properties. This can reduce the calculation region into two or more domains which are identical in nature. A good example of this is a simple pipe flow which exhibits a line of symmetry, the pipe centre-line. Care must be taken in the use of lines or planes of symmetry to ensure that the flow field is indeed symmetric. While the flow is symmetric in a mean sense, symmetry may be broken in instantaneous turbulent realisations.

The implementation of this symmetry condition is straightforward. By definition there cannot be any transfer of ϕ across the boundary. This implies that the velocity normal to the boundary is zero. Also the diffusion of ϕ at the boundary must be set equal to zero. Finally zero gradients must also be observed at the boundary itself. Applying these constraints it follows that the boundary thus described can be treated as a line of symmetry,

and a can lead to a large computational saving.

The use of this type of boundary condition in horizontally orientated flows requires caution. The presence of gravity in a direction normal to the symmetry boundary can lead to problems. This is especially true when considering either dense fluid flow or two phase flow.

4.5.4 Periodic Boundaries

Periodic boundaries represent another method of increasing computational efficiency. The use of these boundary conditions allows a small calculation region to embody the characteristics of a much larger domain. Implementing periodic boundaries entails setting up a pair of boundaries which are cyclic in nature. This means that the outlet conditions from one boundary are used as the inlet conditions of its corresponding partner. A good example of the use of this type of boundary is the calculation of the flow in pipe of infinite length. Repeated solution of the problem of a pipe of a finite length periodically resetting the inlet conditions to those at the downstream boundary, would result in a fully developed pipe profile throughout the calculation domain. This solution would be virtually independent of the initial profile assumed at inlet.

4.5.5 Solid Boundaries

Solid boundaries, be they stationary or moving, are found in virtually all physical systems. The correct implementation of this type of boundary in the calculation is therefore of great importance. A requirement of this type of boundary is the no slip assumption. This requires that the fluid velocity parallel to the wall is equal to that of the wall at the surface, zero in the case of stationary walls. Also, assuming a non-porous wall, the normal velocity at the wall is again equal to that of the boundary.

In the case of turbulent flows the presence of a boundary layer between the wall and the mean flow requires special treatment. Because of the large velocity gradients present in this boundary layer many calculation points would be required to correctly capture this

region. This would add appreciably to the cost of calculation. In order to avoid this problem empirical equations have been developed which relate the fluid velocity, and other properties, to the distance from the wall. The relationship has a logarithmic dependence, which arises from the assumption that the eddy viscosity varies linearly with distance from the wall within the boundary layer. This leads to the commonly used 'logarithmic law of the wall' for the fluid velocity. The equation relating the fluid velocity parallel to the wall to its normal distance is therefore of the form, Rodi (1984)

$$\frac{U_{res}}{u_\tau} = \frac{1}{\kappa}\ln(y^+E) \tag{4.18}$$

where U_{res} is the resultant velocity parallel to the wall, u_τ is the resultant friction velocity, y^+ is the non-dimensional distance from the wall given by $y^+ = yu_\tau/\nu$, κ is the von Kármán constant and E is a roughness parameter. This law is assumed to be valid for the region $30 < y^+ < 100$ though it is generally applied to the whole of the boundary layer.

Expressions for the specification of the values of both the turbulent kinetic energy and dissipation are also required for the use of one or two equation turbulence models. It is assumed that in the region of validity of (4.18) the Reynolds stresses are nearly constant. Assuming zero diffusion and hence local equilibrium together with the shear stresses being approximately equal to those at the wall we have for the kinetic energy

$$\frac{k}{u_\tau^2} = \frac{1}{\sqrt{C_\mu}} \tag{4.19}$$

where C_μ is defined above. An appropriate boundary condition for the dissipation can be obtained from

$$\epsilon = u_\tau^2\frac{\partial U}{\partial y} \quad \rightarrow \quad \epsilon = \frac{u_\tau^3}{\kappa y} \tag{4.20}$$

Rough walls can be accounted in the value of the roughness parameter, E which in turn influences the friction velocity u_τ.

4.6 Solution Procedure

To be able to make use of the description of a single phase flow field described by the above discussion it is necessary to prescribe a method of solution for equations (4.12) and (4.14) together with the correct boundary and initial conditions. Though analytical solution would be preferable, due to the highly coupled and non-linear nature of (4.12) and (4.14) this approach is not possible except in the simplest, trivial cases. This lack of analytical solution method necessitates the use of numerical methods.

The numerical solution method chosen for this work draws heavily on that of Patankar and Spalding (1970), (1972a), (1972b), (1974a), (1974b), (1978) and is in fact a direct implementation of the SIMPLER algorithm outlined in the book of Patankar (1980) "Numerical Heat and Mass Transfer". This is a semi-implicit pressure correction code based on a staggerd grid implementation. Though the method developed for the solution of the required conservation equations is relatively simple in derivation it has been chosen for its robustness of form and ease of application to the Eulerian conservation equation used to represent the second phase, see the following chapters.

Only two-dimensional steady situations are considered in this work, though the implementation remains valid for both three-dimensional and unsteady flows. Consequently only brief mention is made of the treatment of time dependent cases. The equations considered in the following sections are presented in Cartesian form, in one or two dimensions, though the algorithm also remains valid for all curvi-linear coordinate systems with only the need for geometrical considerations.

The method is designed to solve the generalised differential equation (4.9) with the specification of the diffusion coefficient and source term depending on the variable under consideration. As briefly mentioned previously, all of the equations discussed in this chapter can be cast into this generalised form. The correct specification of the diffusion coefficient and source term for the continuity and momentum equations, together with those required for the k-ϵ turbulent closure model can be found in table 4.1. Special consideration needs to be given to the solution of the momentum equations due to the presence of the pressure gradient term. This leads both to the need for a staggered grid and the use of pressure

correction. Both of these special problems are discussed below.

Equation	Diffusion Coefficient, Γ_ϕ	Source Terms, S_ϕ
Continuity	0	0
Momentum	μ_T	$-\frac{\partial p}{\partial x_j} + S_{pu}$
Kinetic Energy	$\frac{\mu_T}{\rho \sigma_k}$	$\frac{\mu_T}{\rho}\left(\frac{\partial U_i}{\partial x_j}+\frac{\partial U_j}{\partial x_i}\right)\frac{\partial U_i}{\partial x_j} - \epsilon$
Dissipation	$\frac{\mu_T}{\rho \sigma_\epsilon}$	$C_{1\epsilon}\frac{\epsilon}{k}\frac{\mu_T}{\rho}\left(\frac{\partial U_i}{\partial x_j}+\frac{\partial U_j}{\partial x_i}\right)\frac{\partial U_i}{\partial x_j} - C_{2\epsilon}\frac{\epsilon^2}{k}$

Table 4.1 : Diffusion Coefficients and Source Terms

A more detailed description of the model can be found in the book of Patankar (1980).

4.6.1 Numerical Solution

The numerical solution of these continuous differential equations requires their reduction into a set of linear algebraic equations whose solution at a finite number of calculation points can be taken to represent the continuum solution for the flow. This introduces the idea of a numerical solution grid consisting of these specific solution locations. Another set of assumptions needs to be made to represent the behaviour of the variables between the grid points.

Various methods exist to obtain these algebraic equations and the profiles between the grid points. Some of the most common methods are briefly discussed below.

4.6.2 Discretisation

One of the simplest discretisation procedures used for deriving the required algebraic equations is that of a truncated Taylor series expansion. This allows approximation of the derivatives found in the differential equations.

Considering a straightforward one-dimensional case, see figure 4.3, and truncating the sequence after the quadratic term

$$\phi_1 = \phi_2 - \Delta x\left(\frac{d\phi}{dx}\right)_2 + \frac{1}{2}(\Delta x)^2\left(\frac{d^2\phi}{dx^2}\right)_2 - \ldots.$$

and

$$\phi_3 = \phi_2 - \Delta x\left(\frac{d\phi}{dx}\right)_2 + \frac{1}{2}(\Delta x)^2\left(\frac{d^2\phi}{dx^2}\right)_2 - \ldots.$$

We get after adding and subtracting the two above equations

$$\left(\frac{d\phi}{dx}\right)_2 = \frac{\phi_3 - \phi_1}{2\,\Delta x}$$

and

$$\left(\frac{d^2\phi}{dx^2}\right)_2 = \frac{\phi_1 + \phi_3 - 2\,\phi_2}{(\Delta x)^2}$$

Substitution of these equations, for the differential terms, into equation (4.9) leads to the required finite-difference equation.

Though this method is straightforward it contains an intrinsic assumption that the profile of the dependent variable has the form of a polynomial. This can lead to problems when considering variables with an exponential distribution.

The second main method considered here is the method of weighted residuals, see Finlayson (1972).

Considering the differential operator

$$L(\phi) = 0 \tag{4.21}$$

which has the assumed solution

$$\tilde{\phi} = a_0 + a_1 x + a_2 x^2 + \ldots + a_n x^n \tag{4.22}$$

Substituting this approximate solution into the differential equation (4.21) leads to a residual

$$L(\tilde{\phi}) = R$$

Minimizing this residual is accomplished by the introduction of weighting functions of the form

$$\int W R \, dx = 0$$

where the integral is performed over the domain of interest. By choosing a sufficiently large number of weighting functions,W, enough equations can be generated to allow solution of the parameters a_1 to a_n in equation (4.22).

Different classes of this method exist depending on what functional form is chosen for the weighting functions. A discretisation method of this type is used in this work. This approach, again following Patankar (1980), is termed the control-volume formulation and is discussed in more detail below.

4.6.3 The Control-Volume Formulation.

As mentioned in the introduction to this chapter the numerical method used in this work follows closely the SIMPLER algorithm discussed in great detail by Patankar. The

disritisation method presented here is that recommended by Patankar and as such will only be presented in outline.

A simplified one-dimensional case is presented here for convenience. Also initially the unsteady term is omitted and only the convection and diffusion terms of the general ϕ equation are considered.

The control volume formulation consists of integrating the differential equation (4.9) over a control volume of size $\Delta x \Delta y$, see figure 4.4

$$\int_s^n \int_e^w \rho u \frac{\partial \phi}{\partial x} dx\, dy + \int_s^n \int_e^w \rho v \frac{\partial \phi}{\partial y} dx\, dy -$$

$$\int_s^n \int_e^w \frac{\partial}{\partial x}\left(\Gamma \frac{\partial \phi}{\partial x}\right) dx\, dy - \int_s^n \int_e^w \frac{\partial}{\partial y}\left(\Gamma \frac{\partial \phi}{\partial y}\right) dx\, dy = \int_s^n \int_e^w S_\phi dx\, dy$$

$$\int_s^n \{(\rho u \phi)_e - (\rho u \phi)_w\} dy + \int_s^n \rho v \frac{\partial \phi}{\partial y} \Delta x\, dy -$$

$$\int_s^n \left\{\left(\Gamma \frac{\partial \phi}{\partial x}\right)_e - \left(\Gamma \frac{\partial \phi}{\partial x}\right)_w\right\} dy - \int_s^n \left\{\frac{\partial}{\partial y}\left(\Gamma \frac{\partial \phi}{\partial y} \Delta x\right)\right\} dy = \int_s^n S_\phi \Delta x\, dy$$

This leads to

$$\{(\rho u \phi)_e - (\rho u \phi)_w\} \Delta y + \{(\rho v \phi)_s - (\rho v \phi)_n\} \Delta x -$$

$$\left\{\left(\Gamma \frac{\partial \phi}{\partial x}\right)_e - \left(\Gamma \frac{\partial \phi}{\partial x}\right)_w\right\} \Delta y - \left\{\left(\Gamma \frac{\partial \phi}{\partial y}\right)_s - \left(\Gamma \frac{\partial \phi}{\partial y}\right)_n\right\} \Delta x = S_\phi \Delta x \Delta y$$

In order to further simplify this equation assumptions have to be made about the profile of the variable, ϕ, between the grid points. This leads to an expression both for the values of the variable ϕ at the control volume interfaces, represented by the lower case letters, and the differential terms. This results in an equation of the form

$$a_P\phi_P = a_E\phi_E + a_W\phi_W + a_S\phi_S + a_N\phi_N + b \qquad (4.23)$$

where the expressions for the coefficients a_P, a_E, a_W, a_N, a_S depend on the profile assumption made.

As mentioned previously many forms of profile are available in the literature. A selection of simple cases is given below and their problems outlined. The choice made for the form of this profile assumption is again at the recommendation of Patankar and is presented below.

The most obvious choice of profile to both obtain the values of ϕ at the control volume interfaces and to represent the differential terms in (4.9) is that of central differencing, briefly discussed in the Taylor series derivation above, which leads to the following expressions

$$\phi_e = \frac{1}{2}(\phi_E + \phi_P) \qquad \& \qquad \phi_w = \frac{1}{2}(\phi_P + \phi_W) \qquad (4.24)$$

The pre-multiplier of 1/2 arises from an assumption that the control volume interface lies halfway between grid points; this is made without and loss of generality. The differential terms can thus be prescribed by

$$\left(\Gamma\frac{\partial\phi}{\partial x}\right)_e = \frac{\Gamma_e(\phi_E - \phi_P)}{(\delta x)_e} \qquad \& \qquad \left(\Gamma\frac{\partial\phi}{\partial x}\right)_w = \frac{\Gamma_w(\phi_P - \phi_W)}{(\delta x)_w} \qquad (4.25)$$

Similar equations arise for the corresponding terms in the y direction.

Though this formulation is intuitive and straightforward to implement, it has been shown to suffer from some important problems. It quite possible for this profile assumption to lead to physically unrealistic solutions. For example problems can occur when the convective terms in the discritised equation become greater in magnitude than twice the diffusive terms, which is the case for large Peclet numbers. This can lead to negative values of the coefficients in equation (4.23) which, in turn, can effect the stability of the solution procedure.

Another straightforward method is that of upwind-differencing. This was first

proposed by Courant, Isaacson and Rees (1952) and consists of assuming that the value of ϕ in the upstream grid point dominates over the whole control volume.

$$\begin{aligned} \phi_e &= \phi_P \qquad \rho u > 0 \\ \phi_e &= \phi_E \qquad \rho u < 0 \end{aligned} \tag{4.26}$$

The other neighbouring values of ϕ are treated similarly.

The approach implies an intrinsic parabolic assumption about the nature of the flow field. Another problem with this profile is that for large Peclet numbers the diffusion is overestimated, since the diffusion term is calculated from a linear $\phi \sim x$ profile.

The stated drawbacks of the above methods have lead to the development of various hybrid forms which capture the correct profile for a large range of Peclet numbers. One of these methods is proposed by Patankar, the power-law scheme, and is used throughout this work, and is given below.

Making the substitution

$$F \equiv \rho u \qquad \& \qquad D \equiv \frac{\Gamma}{\delta x} \quad \rightarrow \quad P \equiv \frac{F}{D} \tag{4.27}$$

we can represent the power-law scheme by

$$\begin{aligned} \frac{a_E}{D_e} &= -P_e && P_e < 10 \\ \frac{a_E}{D_e} &= (1+1P_e)^5 P_e && -10 \le P_e < 0 \\ \frac{a_e}{D_e} &= (1\ 0.1P_e)^5 && 0 \le P_e \le 10 \\ \frac{a_e}{D_e} &= 0 && P_e > 0 \end{aligned} \tag{4.28}$$

The final discritised equation for two dimensions is thus:

$$a_P \phi_P = a_E \phi_E + a_W \phi_W + a_S \phi_S + a_N \phi_N + b$$

with

$$a_E = D_e A(|P_e|) + \|-F_e, 0\|$$
$$a_W = D_w A(|P_w|) + \|F_w, 0\|$$
$$a_N = D_n A(|P_n|) + \|-F_n, 0\|$$
$$a_S = D_s A(|P_s|) + \|F_s, 0\|$$
$$a_P = a_E + a_W + a_N + a_S + a_P^{\circ} - S_p \Delta x \Delta y$$
$$b = S_c \Delta x \Delta y + a_P^{\circ} \phi_P^{\circ}$$

where the superscript o denoted values from the previous interation, S_c and S_p are the constant and variable dependent parts of the source term and $\|$ corresponds to the greater of the two values inside. The function A(|P|) depends on the profile scheme chosen. The various form of A(|P|) which correspond to the schemes discussed above are given in table 4.2. Throughout this work the power-law scheme is used as recommended by Patankar.

Scheme	Form of A(|P|)
Central Differencing	$1 - 0.5\|P\|$
Upwind Differencing	1
Power Law	$\|0, (1 - 0.1\|P\|)^5\|$

Table 4.2 : Forms of A(|P|)

The above derivation has dealt with a two dimensional steady case of the general differential equation. It can be seen that the extension of this work to a three dimensional steady case is relatively straightforward. So far the influence of the unsteady, time dependent term has been ignored. Though throughout this work only steady state solutions of the flow field are required. Thus only a brief mention of the discretisation of the unsteady term will be made for completeness.

Discretisation of the unsteady term of equation (4.9) is very similar to the treatment of the convection and diffusion terms discussed above. In a similar manner to that used for the convection and diffusion expressions the inclusion of a time dependence involves the integration of each of the terms of (4.9) over a given time step which results in a discritised equation representing the variation of ϕ with time. It is useful to note that the unsteady term

exhibits a solely one-way, parabolic, behaviour. Since all calculations used in the current work are steady in nature this discussion of the treatment of the unsteady term will be left here. A further discussion of the handling of the unsteady term can be found in the book of Patankar.

4.6.4 Pressure Coupling

The above solution procedure for the general variable ϕ is only possible with the knowledge of a given flow field. Since it is exactly this flow field whose solution is required, this implies the need for a pre-knowledge of the solution before calculation. Due to the fact that the momentum and continuity equations are special cases of the general differential equation it is possible to apply the above solution procedure to the flow field itself.

The main difficulty in implementation lies in the specification of the pressure field within the fluid. The pressure gradient appears as a source term in the momentum equations. Indeed given a pressure field solving the momentum equations for the flow field represents no real difficulty. In order to avoid this problem the continuity equation is used as an indirect method for calculation of this unknown pressure term.

Unfortunately this implementation is further complicated by the fact that if the pressure gradient terms are discritised using the above methods the value at the solution node depends on the values at alternate, not adjacent, grid nodes, as can be seen by considering the pressure gradient at point P

$$p_w - p_e = \frac{p_W - p_E}{2}$$

again assuming the control volume faces lie at the mid-points between cells, without any loss of generality. As a result a checkerboard pressure pattern can act like a uniform pressure field. A pressure field of this form is clearly unrealistic.

A similar problem arises in the discretisation of the continuity equation (4.12). Again using a piece-wise linear profile and the assumption of a mid-way control volume interface, we get

$$u_E - u_w = 0$$

which also implies that a similar distribution of velocity to that of the pressure, would satisfy the continuity equation. A velocity filed of this nature could not be expected to accurately represent a realistic flow field. In order to avoid these problems a staggered grid is introduced and is discussed below.

4.6.5 The Staggered Grid

The use of a staggered grid, where the velocities are solved at a point displaced from the other variables, was first proposed by Harlow and Welch (1965). This forms the commonly used method for avoiding the problems mentioned above. The basic idea underlying this method is that the velocity components are calculated on the faces of the control volumes, as shown graphically in figure 4.5. Figure 4.5 shows these velocities calculated on a interface lying mid-way between grid points. This mid-way location is not necessary and is only used for clarity of presentation.

Using a staggered grid, of this type, means that no interpolation is required for the velocity components at the control volume face since they are calculated directly. The main benefit of this method, however, is that the discretisation of the continuity equation in this new displaced grid, requires that the needed differences depend upon adjacent values. This removes the possibility of a wavy, unrealistic velocity field satisfying the continuity equation. Consequently this is also true for the pressure field which now uses pressure gradients from adjacent grid points, again removing the likelihood of unrealistic pressure fields.

Use of a staggered grid of this form means that the solution procedure for the momentum equations differs slightly in form from the solution of the other variables, ϕ. Since the only difference between the two grids is a matter of geometry the solution of the momentum equations requires only a suitable interpolation method to transfer quantities between the two calculation grids.

4.6.6 The Pressure Equation

At this point a slightly different formulation is used than that implemented in the standard SIMPLE algorithm. In the standard form a pressure-correction equation is used to iteratively solve the correct pressure field by updating a guessed initial pressure distribution through the introduction of a corrective pressure term obtained from the calculated velocity field.

A refinement to this method, also due to Patankar, is the so-called SIMPLER algorithm. In this method the pressure-correction equation is simply used to correct the velocity field and the pressure is calculated from an explicit equation for the pressure.

It is possible to write equation (4.23) for the momentum equation in the form

$$u_e = \frac{\sum a_{nb} u_{nb} + b}{a_e} + d_e(p_P - p_E) \tag{4.30}$$

where a_{nb} and u_{nb} represent the values of a and u at the neighbouring grid points. The pressure source term is presented explicitly on the RHS of (4.30). The basis of the method is the assumption of a so-called pseudo-velocity, $\hat{u}_e$ defined by

$$\hat{u}_e = \frac{\sum a_{nb} u_{nb} + b}{a_e} \tag{4.31}$$

which contains no pressure term. Thus from (4.30) we get equations of the form

$$u_e = \hat{u}_e + d_e(p_P - p_E) \qquad \& \qquad v_n = \hat{v}_n + d_n(p_P - p_N) \qquad etc.$$

Thus an explicit equation for the pressure is developed

$$a_P p_P = a_E p_E + a_W p_W + a_N p_N + a_S u_S + b$$

where

$$a_E = \rho_e d_e \Delta y$$
$$a_W = \rho_w d_w \Delta y$$
$$a_N = \rho_n d_n \Delta x$$
$$a_S = \rho_s d_s \Delta x$$
$$a_P = a_E + a_W + a_N + a_S$$

and

$$b = \{(\rho \hat{u})_e - (\rho \hat{u})_w\}\Delta y + \{(\rho \hat{v})_s - (\rho \hat{v})_n\}\Delta x$$

The use of this more explicit definition of the pressure equation leads to the solution procedure described below.

4.6.7 Solution Methods

Applying the above discretisation procedure to the conservation equations given in section 4.2 leads to a set of coupled nonlinear algebraic equations whose solution describes the flow at a set of discrete points. Due to the nonlinear character of these equations it is generally necessary to use a iterative solution procedure. This implies that given an initial guess for the solution of the dependent variable, ϕ, approximate values for the coefficients in equation (4.23) are obtained. Use of these coefficients then leads to an improved solution for ϕ. Repetition of this procedure is performed until the change in solution is small enough to satisfy some given convergence criterion.

The choice of solution method can be considered to be independent of the discretisation procedure used. Two relatively straightfroward and commonly used solution methods are briefly discussed below. Again the recommendations of Patankar are followed.

The simplest method available to accomplish this iterative solution of a set of algebraic equations is the Gauss-Seidel point by point method. This method has two main drawbacks. Firstly since it considers the computation grid on a cell by cell basis it can be slow to compute. Secondly it does not always converge. A useful measure of the likelihood

of the convergence of the Gauss-Seidel method is the well-known Scarborough criterion. This was developed by Scarborough (1958) and represents a sufficient, though not necessary, condition for the convergence of this solution method. Casting this criterion in terms of the discritised equation (4.23) it states

$$\frac{\sum |a_{nb}|}{|a_p|} \quad \begin{array}{ll} \leq 1 & \textit{for all equations} \\ < 1 & \textit{for at least one equation} \end{array}$$

where a_{nb} represent the coefficients for the neighbouring grid points a_E, a_W, a_N, a_S etc. It is useful to adopt this criterion as a foundation of the solution procedure used since it guarantees convergence by at least on iterative method.

As mentioned above the basic Gauss-Seidel method though attractive is slow in convergence as the transmission of the boundary information into the interior of the calculation domain proceeds only one cell per iteration. A more useful solution procedure is one which combines the direct tri-diagonal matrix algorithm (TDMA) with the above Gauss-Seidel method. This allows simultaneous solution along a grid line which greatly increases the rate of transfer of boundary conditions into the interior of the calculation region. Implementation of this method is accomplished by sweeping the solution line through the flow field along one coordinate direction followed by a sweep in the other coordinate direction. This is the method recommended by Patankar and implemented in the code used here.

4.6.8 The Solution Algorithm

Presented below is a step-by-step outline of the solution algorithm which constitutes that given by Patankar as the SIMPLER algorithm.

(i) Begin with an initial guess of the velocity field.

(ii) Calculate the coefficients for the momentum equations and hence calculate the pseudo-velocities.

(iii) Calculate the coefficients for the pressure equation and solve to find the pressure

field.

(iv) Treat the calculated pressure field as p^* and use this to obtain the values of the velocities, u^* etc.

(v) Calculate the mass source, b and solve the equation for the pressure correction equation p'.

(vi) Use p' to correct the velocities but not the pressure.

(vii) Solve any other ϕ equations required (such as temperature, mass fraction etc.)

(viii) Return to step (ii) and repeat until convergence.

The above sections give a basic overview of the SIMPLE and hence SIMPLER algorithm of Patankar. This is by no means complete and for a further explanation of this work the book of Patankar (1980) is recommended.

4.7 Validation Calculations

In order to test the above calculation procedure validation computations were performed in a simple flow. The flow was chosen to enable similar validation of the second phase code, discussed below, using a similar flow field.

Validation of this code is performed on a simple turbulent pipe flow. The well-known turbulent pipe flow data of Laufer (1954) is used. Two flow velocities, and hence pipe Reynolds numbers are considered which both lie within the range of flow situations covered in this work. The data of Laufer is based on the flow in a brass pipe of length 5 m and internal diameter 0.247 m. The two flow speeds used correspond to maximum mean flow velocities of ~ 3 m/s and ~ 30 m/s, and give Reynolds numbers based on this velocity and the pipe diameter of ~ 50,000 and 500,000 respectively. The pipe walls are considered smooth.

All calculations and measurements are presented for fully developed flow. The flow in a pipe can be considered fully developed after a critical entry distance given by (Hinze (1975)) as:

$$\left(\frac{x}{D}\right)_{critical} \geq \frac{10^5}{Re_D} \tag{4.24}$$

where the Reynolds number is that given above.

The calculation was conducted in axi-symmetric coordinates with a line of symmetry at the pipe centre-line. In order to further reduce the calculation domain periodic boundary conditions were applied at the pipe inflow and outflow, this led to the calculation of a fully developed flow without the need to satisfy (4.24). The computational grid cells were concentrated near the wall to enable the boundary layer to be well captured. A section of the computational grid is shown in figure 4.6.

Figure 4.7 shows the calculated velocity profile for the lower Reynolds number flow. The calculated curve consists of the profile at two locations (nominally 0.5 and 1.5 m from the upstream grid boundary). The coincidence of the curves shows that the calculation is converged and fully developed throughout the domain. The curves are compared to the experimental data of Laufer. The maximum error between the calculation and experimental data is approximately 5%. Since the experimental data was obtained by measurement of graphs and hence contain a large margin of error, the agreement can be considered to be excellent. Also plotted is the predicted profile from a standard power law which, though it shows good agreement with the experimental data it exhibits a non-zero gradient at the pipe centre-line which would lead to a discontinuity in gradient at this point.

Figure 4.8 shows a typical kinetic energy and dissipation profile for the same flow. As expected both show a peak at the boundary layer and decay to a relatively constant value in the core of the flow. Figure 4.9 shows a comparison between the calculated and measured non-dimensionalised fluctuating velocity for the case of Reynolds number equal to 500,000. The graphs agree qualitatively but exhibit an approximate 20% difference in magnitude. This is due to the isotropic assumption made in the calculations by the use of the k-ϵ turbulence model. The actual boundary is non-isotropic as can be seen in figure 4.10 (reproduced from Laufer).

This simple calculation of a turbulent pipe flow shows that the calculation procedure obtains good results. The choice of turbulence model, while assuming isotropic turbulence,

is shown to capture the wall boundary layer well. On this basis the above method is used to calculate the carrier phase flow field throughout the remainder of this work.

4.8 Conclusions

A straightforward method of calculating the turbulent flow field of a fluid has been presented. The method is based on the semi-implicit, pressure correction (SIMPLER) formalism of Patankar and is calculated on a staggered grid. The turbulent closure model chosen was the standard k-ϵ model of Launder and Spalding (1974). The isotropic nature of this closure model was shown to be consistent with the representation of the discrete phase. The method was also shown to be generally applicable to convection-diffusion equations, and, hence suitable for solution of a diffusion representation of a second phase.

The code was tested in the case of a simple fully developed pipe flow and shown to give good results.

This code is therefore used throughout the remainder of this work to obtain the carrier phase flow field required for the second phase. A discussion of the implementation of the above algorithm for the second phase conservation equations is given in the following chapter.

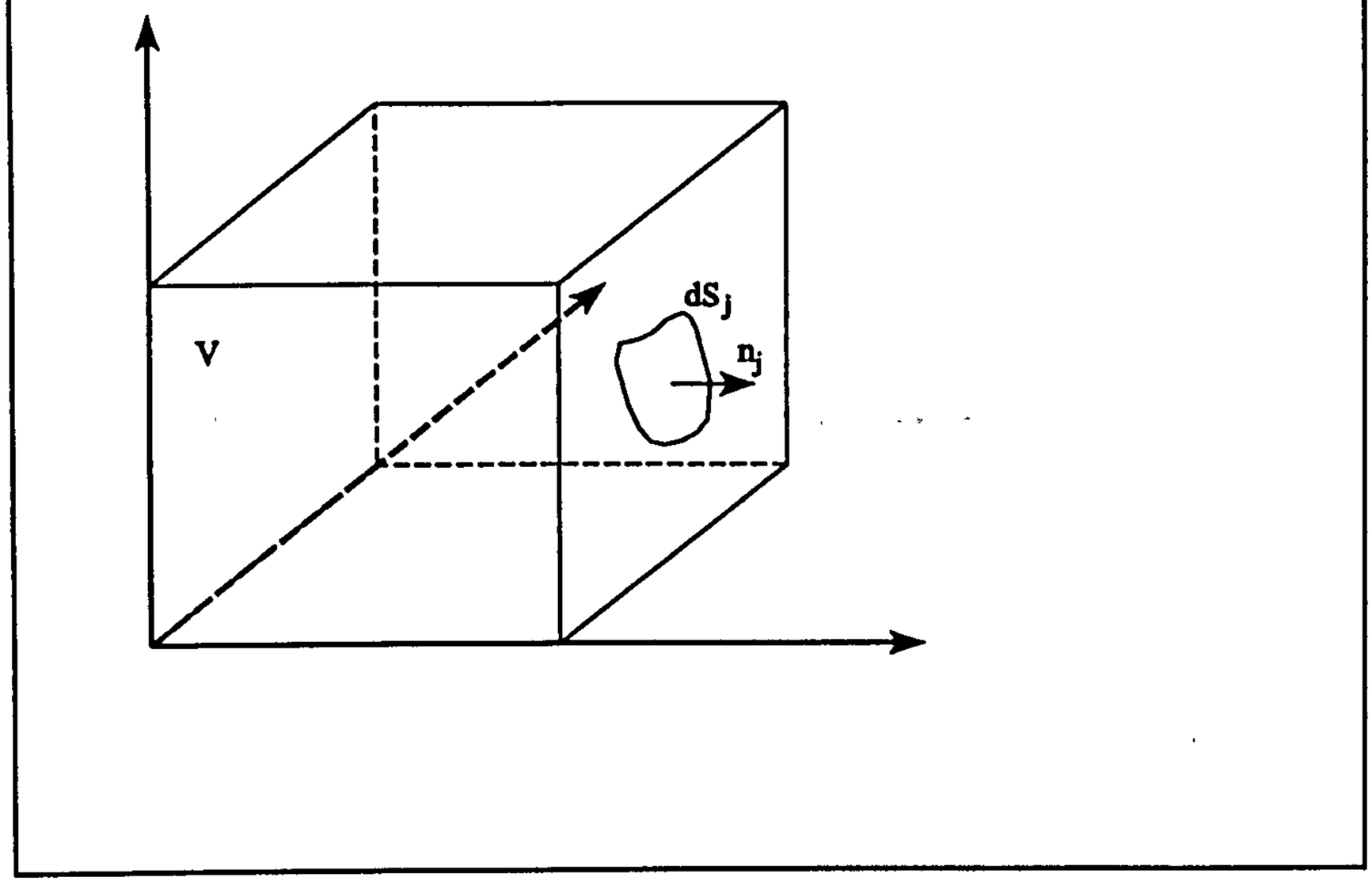

Figure 4.1 : Elementary Volume Flux

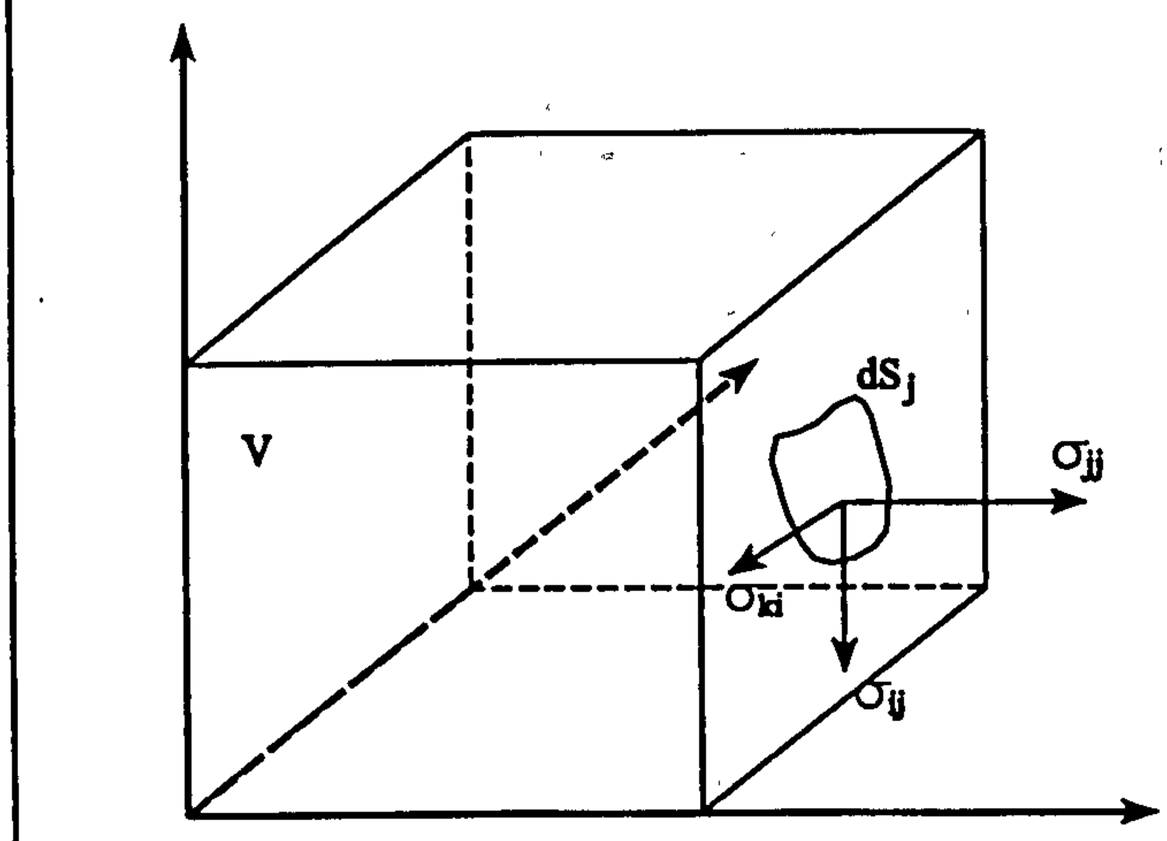

Figure 4.2 : Elementary Volume Stress

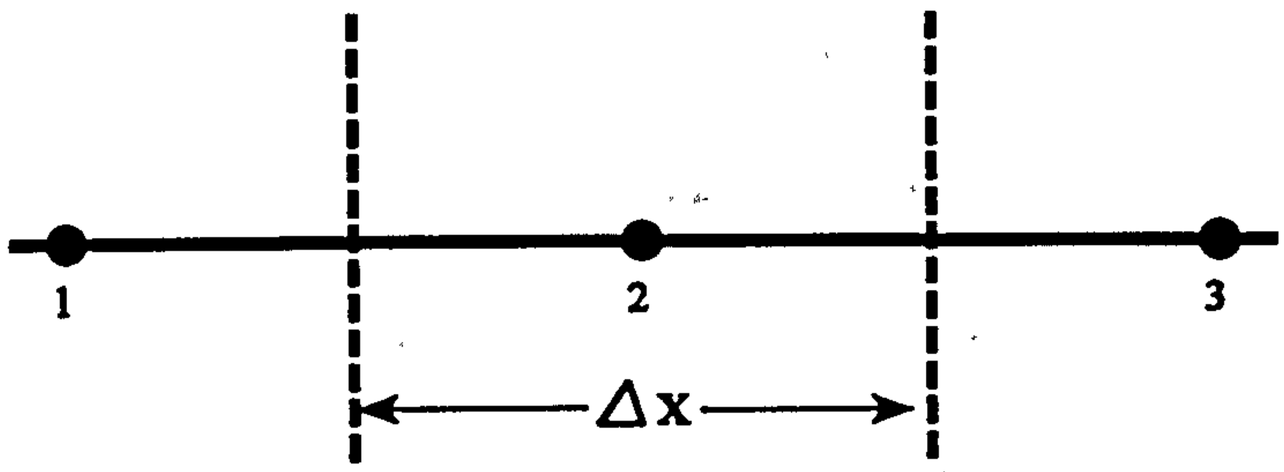

Figure 4.3: A Simple One-Dimensional Control Volume

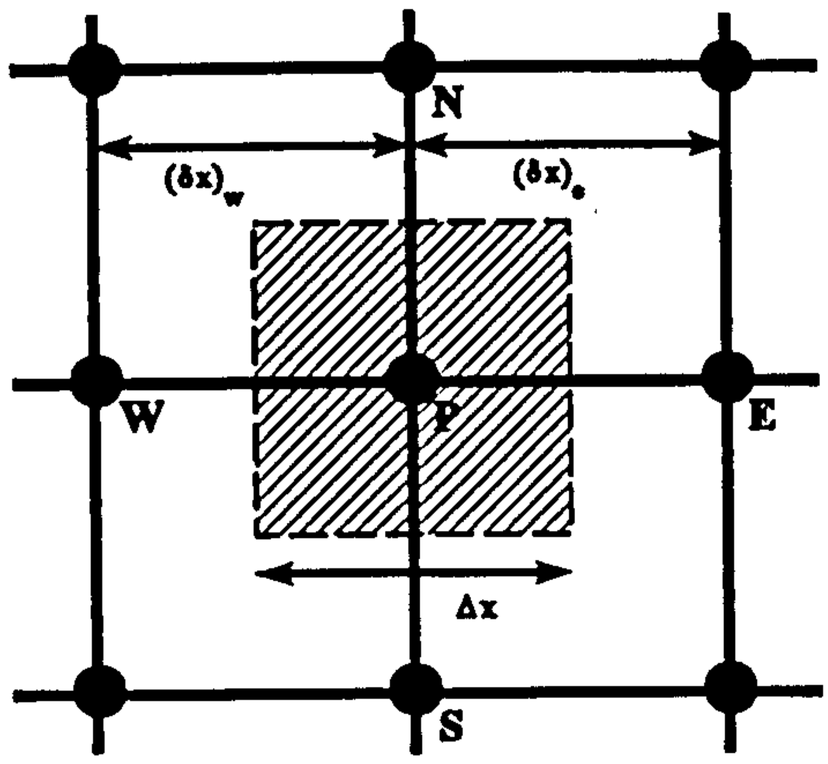

Figure 4.4: A Simple Two-Dimensional Control Volume

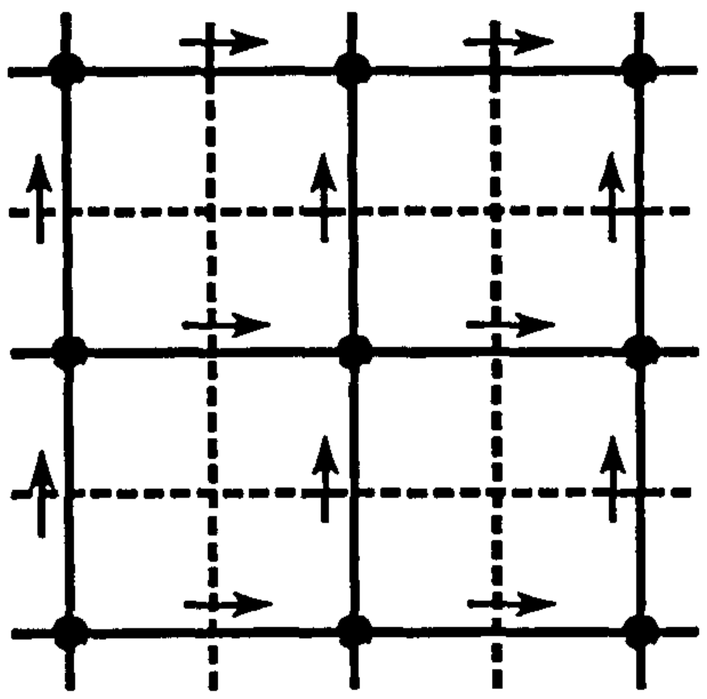

Figure 4.5: A Portion of the Staggered Grid

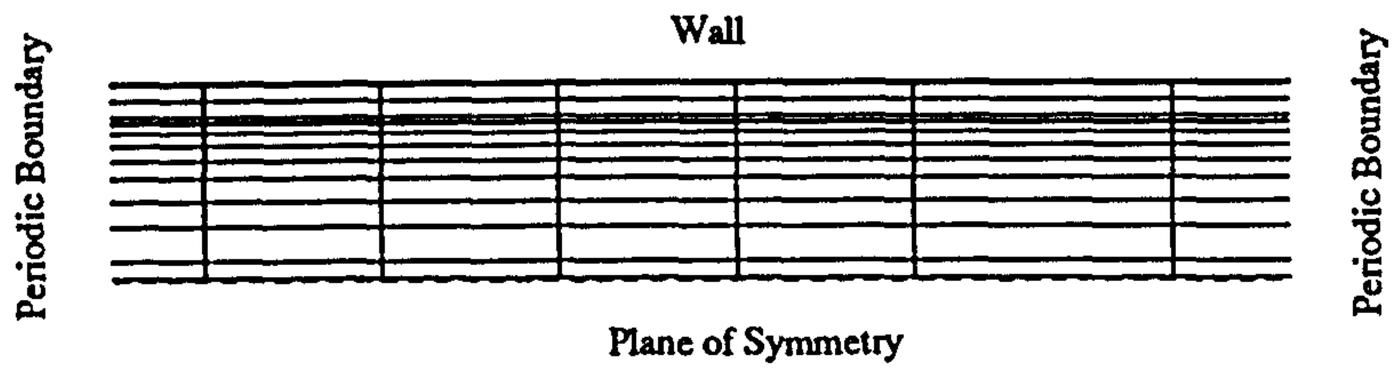

Figure 4.6: Calculation Grid for Pipe Flow

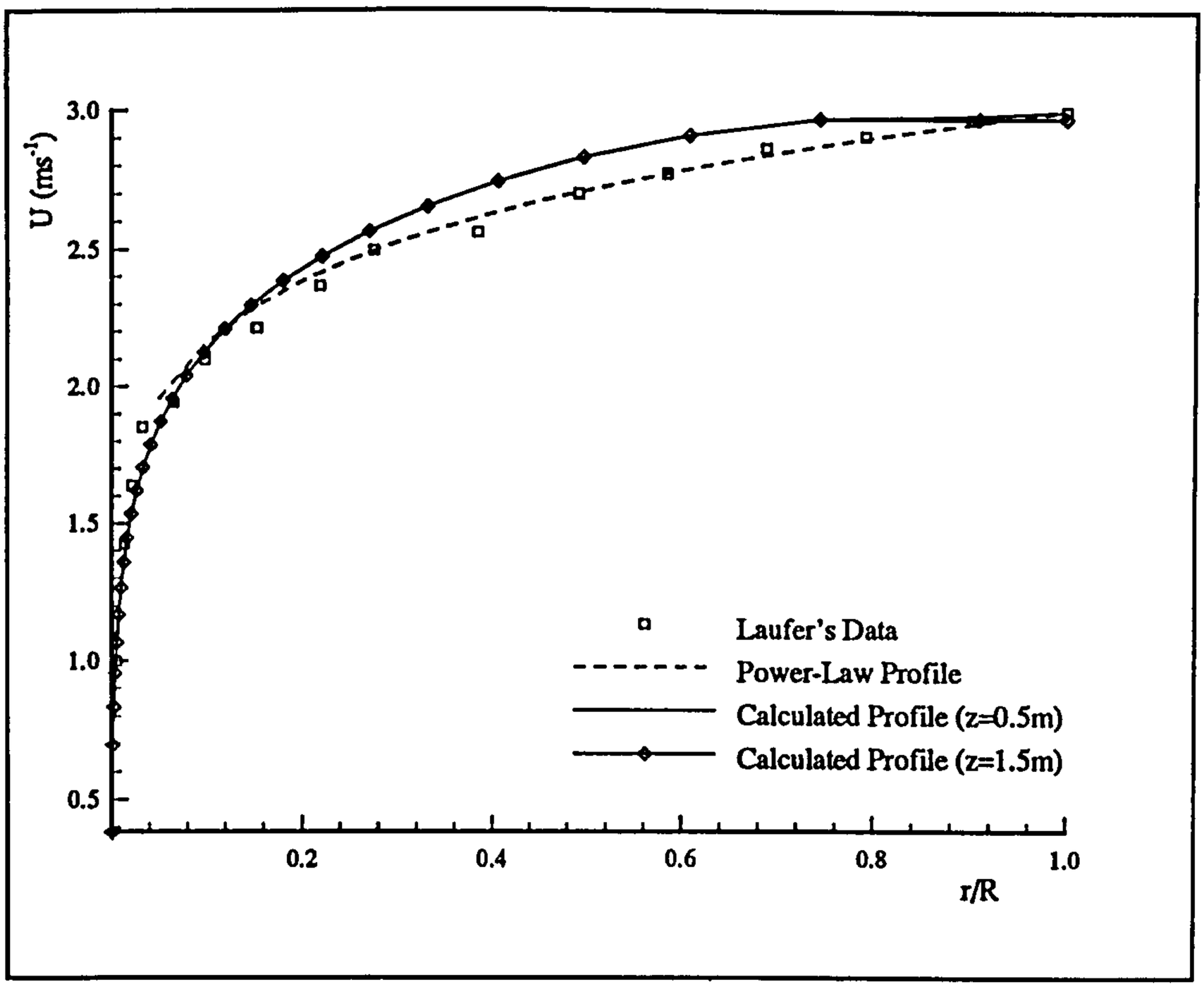

Figure 4.7: Comparison of Mean Velocity Profiles Across Pipe (Re_D=50,000)

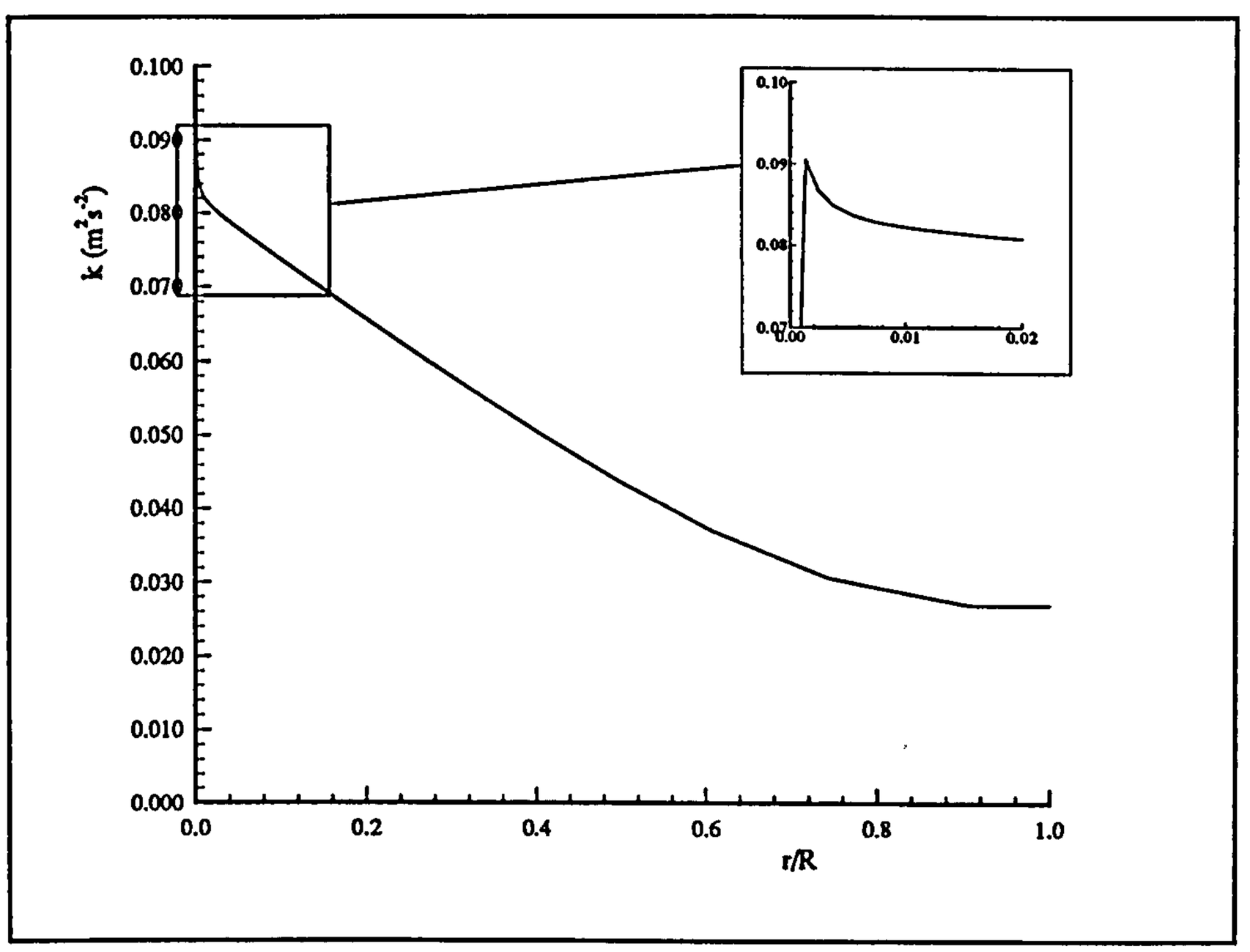

Figure 4.8(a): Calculated Kinetic Energy Profile Across Pipe (Re_D=50,000)

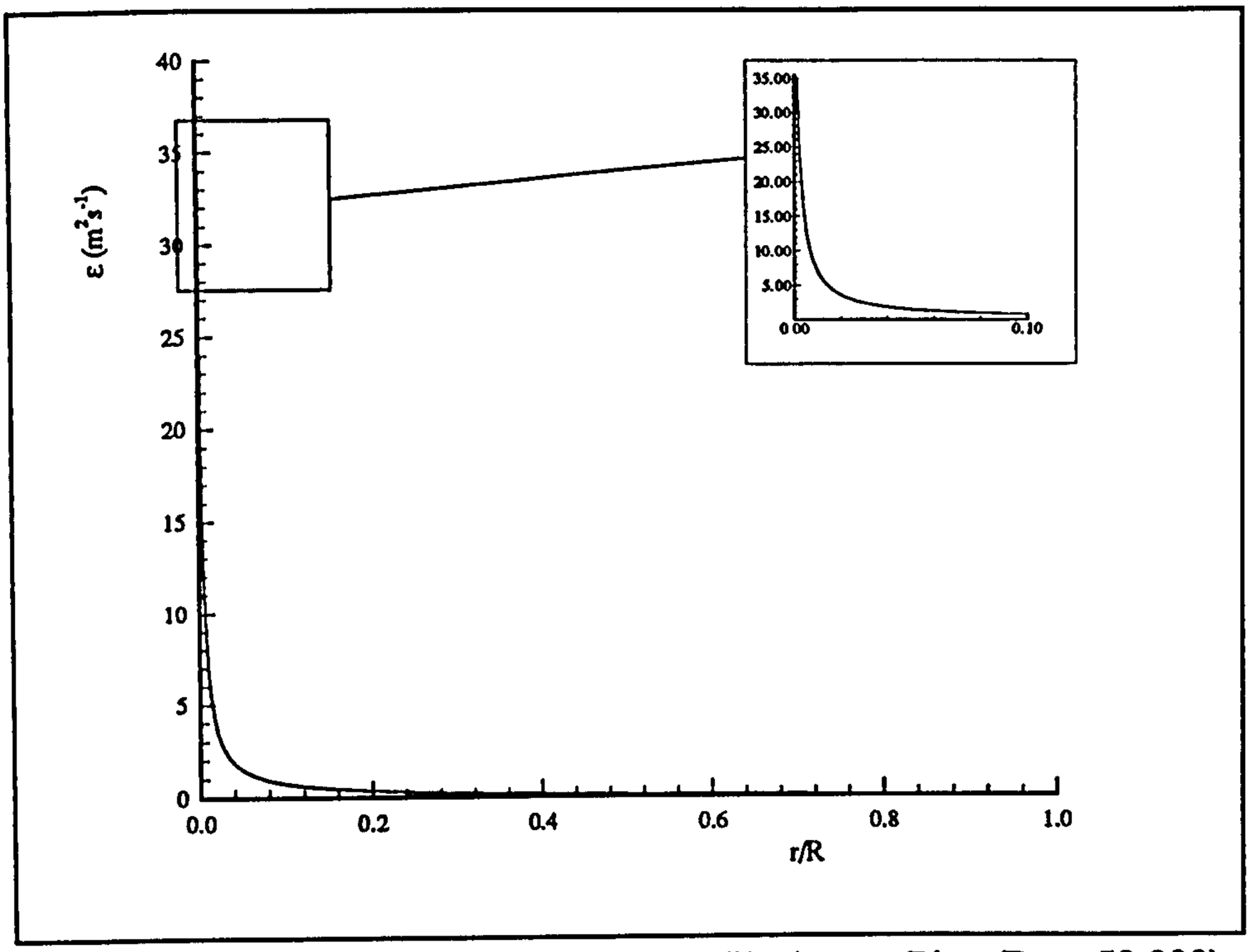

Figure 4.8(b): Calculated Dissipation Profile Across Pipe (Re_D=50,000)

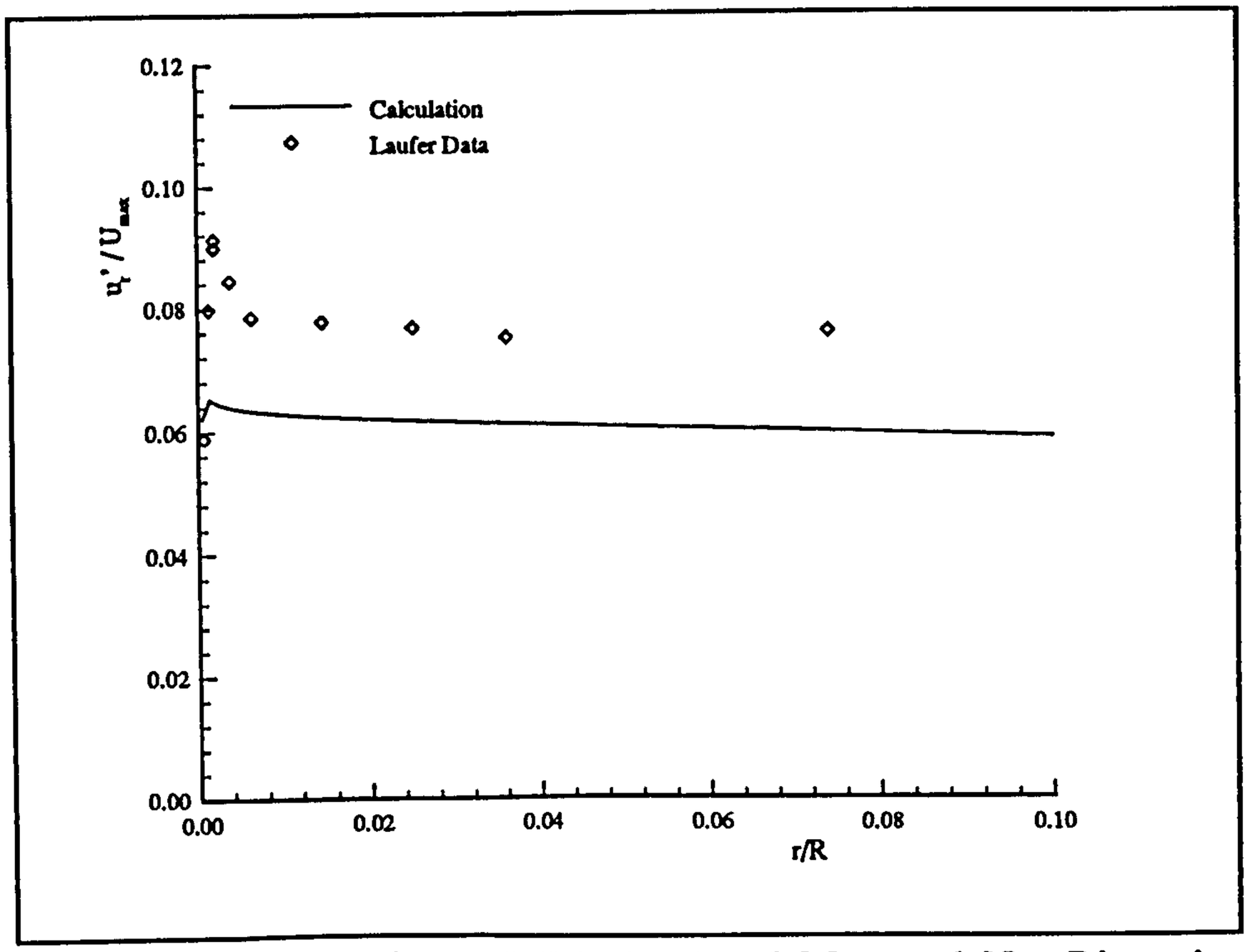

Figure 4.9: Comparison of Calculated and Measured Non-Dimensional Radial Fluctuating Velocity in the Boundary Layer (Re_D=500,000)

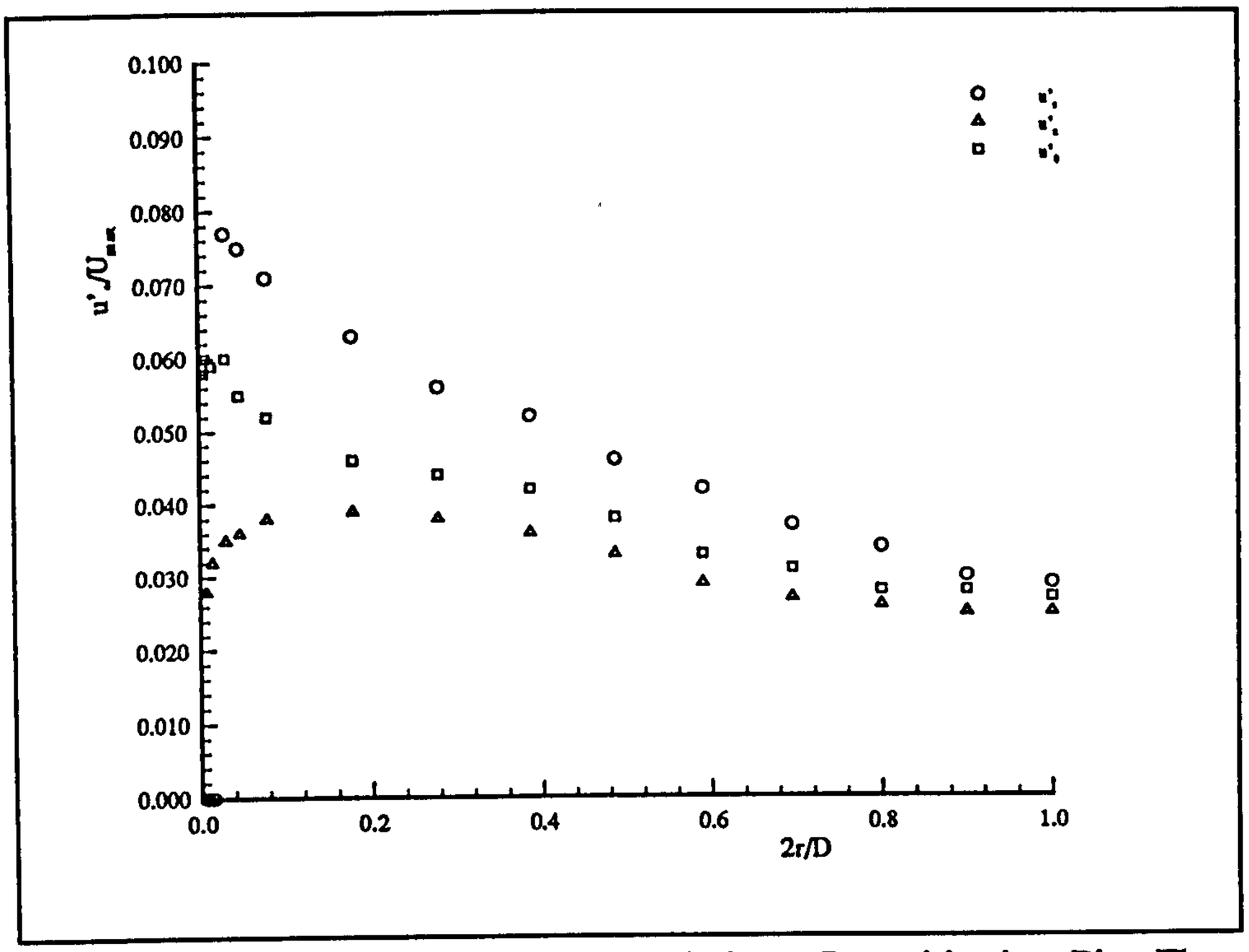

Figure 4.10 : Normalised Relative Turbulence Intensities in a Pipe Flow, $Re_D = 5\times10^5$, (from Laufer (1954))

CHAPTER 5

Eulerian Calculation for Second Phase

5.1 Introduction

In order to develop an Eulerian description of the second phase, representative conservation equations must be derived. In a similar fashion to the single phase discussion, in the previous chapter, the two equations required are those for mass and momentum conservation. These equations are obtained in a similar manner to those discussed previously. Intrinsic in this formulation is the assumption that the second phase can be represented by a continuum, which can lead to difficulties in the treatment of some of the resultant terms..

To avoid these problems various assumptions are made here when formulating the conservation equations for the second phase. Firstly the particle phase is assumed dilute and to consist of mono-dispersed, spherical particles. The use of this dilute assumption avoids the requirement of the modelling of particle-particle collisions. Considering only spherical particles makes the specification of the inter-phase forces more straightforward Further, the consideration of mono-dispersed particles is made in order to simplify the calculation. A discussion of the extension to poly-dispersed flows and particle-particle interaction can be found in a chapter 8. Secondly it is assumed that the average properties of both phases can be treated as continua. It is also assumed, for simplicity, that no phase changes occur within the flow and that both phases are Newtonian. The assumption of a continuum taken together with the first assumption of a dilute suspension, places a constraint on the ratio of the size of the smallest control volume used, generally based on the Kolmogorov microscale, and the size of the particle and the period of time over which averages are taken. The continuum representation assumes that a statistically significant number of particles exist within a control volume over a given time. Conversely the assumption of a dilute suspension places constraints on the distance between particles and hence on the volume they occupy. These problems have been discussed extensively in the literature by Reif (1965), Hinze (1975) and

Lumley (1978). It has been shown that modelling the flow in this manner is valid even in situations which do not strictly obey both of the above criteria, Chen and Wood (1983). Finally it is assumed that the effect of turbulent dispersion dominates over those of Brownian motion or molecular diffusion.

The equations of mass and momentum are derived below by applying the above assumptions, and are then Reynolds averaged to obtain equations for the mean mass and momentum transport of the second phase. During this averaging procedure extra terms arise containing the products of fluctuating quantities. As a result a closure model is required, in a similar manner to the previous chapter. The closure model used here is the diffusion approximation discussed in chapter 1.

The source terms arising from the assumption of a one-way coupled calculation, i.e. no influence of the particles on the carrier fluid is considered, are then derived, as are the required boundary conditions. The solution procedure of the resultant equations is then discussed with reference to the algorithm presented in the previous chapter.

Finally the importance of the method of the calculation of the particle properties required to specify the source terms in the second phase transport equations is noted and discussion is deferred to the following chapter.

5.2 Conservation Equations

The conservation equations used to describe the second phase can be derived in the same way, and have a similar form to, those used to represent the primary phase. With this in mind the derivation of the equations given below draws heavily from the results of the previous chapter.

The mass conservation principle can be obtained in an identical manner to that given above hence is not derived explicitly. The same is not true for the momentum equations due to the presence of the second phase stress terms. As mentioned in the above introduction the use of a continuum representation for the dilute second phase can lead to both conceptual and mathematical problems. These problems are dealt with below.

5.2.1 Mass Conservation

The principle of mass conservation for the second phase is similar to that used for the primary phase. Consequently, with reference to figure 5.1, it is possible to form the instantaneous mass conservation equation for the second phase directly, as

$$\frac{\partial}{\partial t}c + \frac{\partial}{\partial x_j}(c u_{p_j}) = S_{p_c} \tag{5.1}$$

where c is used to represent the mass concentration of the second phase per unit volume.

5.2.2 Momentum Conservation

As in the case of mass conservation the equation for the conservation of the second phase momentum is similar to that for the single phase case. Care must be taken in the expression of the stress forces experienced by the second phase, due to the above assumptions. These terms are discussed in detail below.

Consider figure 5.2 which depicts the stress tensor acting on the volume, V, as before. As in the single phase calculation this tensor can be defined in terms of a pressure force and a viscous force

$$\sigma_{p_{ij}} = p_p \delta_{ij} - \lambda_p \delta_{ij} \frac{\partial u_{p_k}}{\partial x_k} - \mu_p \left(\frac{\partial u_{p_i}}{\partial x_j} + \frac{\partial u_{p_j}}{\partial x_i} \right) \tag{5.2}$$

where the subscript p denotes properties of the particulate phase and F_e represents external effects. As before $\lambda_p = \frac{2}{3}\mu_p$. Expressing the final term in (5.2) in the form of a diffusion term we obtain

$$c\frac{\partial u_i}{\partial t} = \frac{\partial}{\partial x_j}\left\{ p_p \delta_{ij} - \lambda_p \delta_{ij} \frac{\partial u_{p_k}}{\partial x_k} - \mu_p \left(\frac{\partial u_{p_i}}{\partial x_j} + \frac{\partial u_{p_j}}{\partial x_i} \right) \right\} + F_e$$

As in the single phase case the gradient of the viscosity is assumed zero. Also assuming incompressibility of the particle which make up the second phase leads to

$$c\frac{\partial u_i}{\partial t} = p_p\delta_{ij} - \frac{\partial}{\partial x_j}\left(\mu_p\frac{\partial u_{p_i}}{\partial x_j}\right) + F_e \qquad (5.3)$$

Due to the assumption of a dilute suspension the viscosity of the second phase can be assumed to be negligible hence the second term in (5.3) can be set to zero.

As mentioned in the introduction the use of an Eulerian description to represent a dilute suspension can lead to conceptual problems. The existence of the remaining pressure term in (5.3) falls into this category. The assumption of a dilute concentration implies that the mean free path of the point representation of the particles, which make up the second phase, is sufficiently large that no particle-particle interactions occur. In addition the assumption of a one-way coupled calculation removes any mechanism by which pressure forces due to the action of a particular particle of the second phase can effect another member of the suspension.

From these considerations the pressure term can be set equal to zero in the framework of the current calculation. It should be noted however that it is not possible to neglect the influence of this term when either the suspension is sufficiently dense that particle-particle interactions occur or a two-way coupled calculation is made which allows 'communication' between distant members of the suspension through their effect on the carrier phase.

From the above discussion of the treatment of the second phase stress tensor it is possible to write down the momentum equation for the suspension by substitution of the second phase properties into the single phase momentum equation. Thus

$$\frac{\partial}{\partial t}(cu_{p_i}) + \frac{\partial}{\partial x_j}(cu_{p_i}u_{p_j}) = S_{cu_p} \qquad (5.4)$$

As in the mass conservation equation, above, c is used to represent the mass concentration of the second phase per unit volume. The source terms on the RHS of (5.4) result from the

action of the carrier flow field on the second phase, together with those arising from the action of external body forces. The specification of these forces is discussed in more detail in a later section.

5.2.3 Generalised Form

Again, in similar manner to the primary phase equations (5.1) and (5.4) can be cast into the generalised form (4.9)

$$\frac{\partial}{\partial t}\phi\rho + \frac{\partial}{\partial x_j}(\rho u_i \phi) = \frac{\partial}{\partial x_j}\left(\Gamma_\phi \frac{\partial \phi}{\partial x_j}\right) + S_\phi$$

It should be noted that in the implementation of the second phase equations the term ρ found in (4.9) should be replaced by the concentration, c as in the mass conservation equation, above, hence

$$\frac{\partial}{\partial t}\phi_p c + \frac{\partial}{\partial x_j}(c u_{p_i} \phi_p) = \frac{\partial}{\partial x_j}\left(\Gamma_{\phi_p} \frac{\partial \phi}{\partial x_j}\right) + S_{\phi_p} \qquad (5.5)$$

5.3 Reynolds Averaged Equations

Equations (5.1) and (5.4), together with correct specification of the source term in (5.4), are used to formulate an Eulerian description of the second phase. As in the previous chapter equations (5.2) and (5.5) are concerned with the instantaneous value of their respective dependent variable. In order to solve for the mean values for these equations it is necessary to apply a Reynolds decomposition, of the form

$$c = C + c' \qquad \& \qquad u_p = U_p + u_p' \qquad (5.6)$$

This decomposition together with a Reynolds averaging procedure leads to mean transport equation for the second phase.

Firstly consider the mass conservation equation (5.1). Applying the above decomposition (5.6) and the properties of the Reynolds average, as given in (4.10), we obtain

$$\frac{\partial}{\partial t}C + \frac{\partial}{\partial x_i}\left\{C U_{p_i} + \overline{c'u'_{p_i}}\right\} = 0 \tag{5.7}$$

as the mean mass transport equation for the second phase. As in the previous chapter the source term on the RHS of (5.7) has been set equal to zero. This again assumes that no mass is created or destroyed within the flow.

The decomposition (5.6) is also applied to the second phase momentum equation (5.4). This together with Reynolds averaging, also following (4.10), gives the mean transport equation for the second phase momentum, as

$$\begin{aligned} &\frac{\partial}{\partial t}\left\{C U_{p_i} + \overline{c'u'_{p_i}}\right\} + \\ &\frac{\partial}{\partial x_i}\left\{C U_{p_i} U_{p_j} + \overline{c'u'_{p_i}} U_{p_j} + \overline{c'u'_{p_j}} U_{p_i} + \overline{c'u'_{p_i} u'_{p_j}} + C\overline{u'_{p_i} u'_{p_j}}\right\} = \bar{F}_p \end{aligned} \tag{5.8}$$

The term $\bar{F}_p$ is used to represent the mean forces experienced by the second phase.

In a similar manner to the primary phase, the presence of the extra terms arising from the products of the fluctuating velocity and concentration components introduces the need for a closure model. This closure is accomplished through the use of a diffusion approximation, and is discussed below.

5.4 Closure Model

The equations (5.7) and (5.8) contain more unknowns than equations. This leads to a classical closure problem, though in addition to the extra terms in the momentum equation (5.8) found in the equivalent single phase calculation, the mass conservation equation (5.7) also includes a term dependent on the product of fluctuating quantities.

In order to model these terms a diffusion approximation is used. This assumes that

these correlation can be approximated by a diffusion process. This diffusion approximation is presented below.

5.4.1 The Diffusion Approximation

In order to model these correlation terms we make the assumption of a diffusion process for the transport of the required quantity. This is valid, since the velocity autocorrelation of the particle vanishes after a certain correlation time. An estimate of this time can be obtained from the convection time discussed in chapter 2. It follows, from the central limit theorem, that the sum of the particle velocities, and hence displacement, becomes uncorrelated and the distribution of the displacement becomes Gaussian in nature as time progresses, Papoulis (1984), also see figure 5.3 which depicts the convolution of the probability density, $f_i(x)$, of a sum of independent random variables, $x=x_1+..+x_n$. This Gaussian behaviour implies a diffusion like process is observed. It is therefore assumed that the discrete particles of the second phase respond to the turbulent fluctuations of the carrier gas in a similar fashion to that proposed by the kinetic theory of gases.

The theory of diffusion in isotropic substances, due to Fick (1855), gives the flux through a unit area of a surface as being proportional to the concentration gradient normal to the surface.

$$Flux = -\Gamma \frac{\partial C}{\partial x}$$

Thus, assuming a Ficks law of diffusion we get

$$\overline{c' u_{p_i}'} = -\Gamma_p \frac{\partial \bar{C}}{\partial x_i} \qquad (5.9)$$

where Γ_p is the diffusion coefficient for the second phase. As mentioned previously the assumption of isotropy has been made throughout this work hence Γ_p is represented by a scalar quantity. Repeated application of this assumption together with the assumption of a constant Γ_p leads to

$$\overline{c' u_{p_i}' u_{p_j}'} = \Gamma_p^2 \frac{\partial^2 \bar{C}}{\partial x_i \partial x_j} \tag{5.10}$$

Important consideration must also be given to the treatment of the product of fluctuating velocity components. It should be noted that though the off-diagonal correlation terms can be set equal to zero the diagonal terms are non-zero. This leads to the following expression for this product.

$$\overline{u_{p_i}' u_{p_j}'} = \delta_{ij} \overline{u'^2_{p_i}} \tag{5.11}$$

The use of equations (5.9), (5.10) and (5.11) allow the closure of equations (5.7) and (5.8).

5.4.2 Mean Transport Equations

Introducing this closure model into equations (5.7) and (5.8) leads to

$$\frac{\partial}{\partial t} C + \frac{\partial}{\partial x_i}(C U_{p_i}) = \frac{\partial}{\partial x_i}\left(\Gamma_p \frac{\partial C}{\partial x_i} \right) \tag{5.12}$$

and

$$\frac{\partial}{\partial t}(C U_{p_i}) + U_{p_j} \frac{\partial (C U_{p_i})}{\partial x_i} - \frac{\partial}{\partial x_i}\left(\Gamma_p \frac{\partial (C U_{p_i})}{\partial x_i} \right) = \overline{F_p} - \delta_{ij} \overline{u'^2_{p_i}} \frac{\partial C}{\partial x_i} \tag{5.13}$$

which constitute mean transport equations for mass and momentum. A more detailed derivation of these equations can be found in Appendix IV.

In order to solve these equations it is useful to cast them into the general form developed in the previous chapter. Since these equations are of a convection-diffusion type this generalisation is straightforward and only requires the specification of the correct forms of the diffusion coefficient and source terms.

The mass conservation equation (5.12) can be seen to consist of an unsteady term;

a convection term and, on the RHS, a diffusion term. This implies a simple expression for both the diffusion coefficient of Γ_p and a source term of zero. The zero source term arises out of the fact that mass is neither created or destroyed within the calculation domain. In the case of reactive flows or in the presence of mass sources and sinks the source term would be non-zero.

The momentum equation (5.13) is slightly more complicated in form than (5.12) due to the presence of terms $\bar{F}$ and $\delta_{ij}\overline{u_i'^2}\frac{\partial C}{\partial x_j}$. Because of the method used to define the general ϕ equation in chapter 4, it is possible to treat these terms simply as source terms. Again the diffusion coefficient is given by Γ_p.

This leads to two equations of the general form of (4.9) with the specification of the diffusion coefficient and source term as given in table 5.1.

	Mass Conservation	Momentum Conservation
Diffusion Coefficient	Γ_p	Γ_p
Source Terms	0	$\bar{F} - \delta_{ij}\overline{u_i'^2}\frac{\partial \bar{C}}{\partial x_j}$

Table 5.1 : Terms in Generalised ϕ Equation for Second Phase

In order to fully close these equation the term F needs to be specified together with appropriate boundary conditions.

5.5 External Forces

The term on the RHS of (5.13) has been used to represent the external forces experienced by the second phase. These forces fall into two main categories. Firstly those due to an external potential field, such as gravity and secondly those due to the interaction between the two phases.

Throughout the current work the only external force considered is that of gravity. This leads to the inclusion of the term, cast into the concentration form of (5.13)

$$F_g = gc \tag{5.14}$$

The only inter-phase force considered in this work is that of drag. The use of this simplified form of interaction has the same justification as given in chapter to in the derivation of the reduced particle equation of motion (2.4) neglecting the gravity term which is dealt with explicitly. For the flow situations considered in this work the other terms in the particle general equation of motion, (2.3) can be assumed to be small. The form of this drag term can be obtained directly from (2.4), giving the instantaneous form of F as

$$F = F_g + F_d = gc + A_i(u_{g_i} - u_{p_i})\,|u_{g_i} - u_{p_i}| \tag{5.15}$$

where A_i is the drag pre-multiplier as given in chapter 2.

This form of the force term concerns the instantaneous variable and hence must be Reynolds averaged in a similar manner to the conservation equations. This operation is straightforward and leads to

$$\bar{F} = g\bar{C} + A_i(U_{g_i} - U_{p_i})\,|U_{g_i} - U_{p_i}| \tag{5.16}$$

the products of fluctuating terms being neglected. With the specification of this force term it is now possible to solve the conservation equations for the second phase given an appropriate set of boundary conditions.

5.6 Boundary Conditions

For the correct solution of the mean transport equations (5.12) and (5.13) the boundary conditions for the flow must be specified. Specifying the inlet and outlet boundary conditions, together with those of a plane or line of symmetry and periodic boundaries can be accomplished in the same manner as outlined in the previous chapter. As for the primary phase, the treatment of a wall boundary condition requires more discussion.

5.6.1 Wall Boundaries

The interaction between the wall and the particles which make up the second phase is highly complex. The way in which an individual particle reacts in the near wall region and with the wall itself can lead to the development of complex wall interaction models, Sommerfeld (1990). In the current work a much simplified wall boundary condition is used. This takes the form of

$$\bar{C}_{wall} = \bar{C}_{node} - \gamma \bar{C}_{node} \qquad \& \qquad \bar{V}_{wall} = \bar{V}_{node} - 2\gamma \bar{V}_{node}$$

where the subscript node represents the first calculation point away from the wall and $\bar{V}$ represents the mean velocity normal to the wall. γ is a coefficient of proportionality, one corresponding to a fully reflective boundary and zero corresponding to a fully absorptive boundary. This type of boundary condition is straightforward to implement and allows the modelling of a large range of wall types.

5.7 Solution Procedure

To enable the specification of the mean properties of the second phase equations (5.12) and (5.13) must be solved, together with the appropriate boundary conditions. As for the primary phase the transport equations derived above are not analytically soluble for any but the most trivial cases. This again implies that a numerical solution approach is required.

The solution of these conservation equations can be accomplished in a similar manner to those of the previous chapter. Because of the ability to cast equations (5.12) and (5.13) into the generalised convection-diffusion form, (4.9), the same numerical procedure as used for the primary phase can be applied to the second. The calculation is simplified due to the lack of any second phase pressure field and there is no need to use a staggered grid.

Since the assumption that the second phase does not disturb the solution for the first phase (one-way coupling), as outlined in the introduction, it is possible to solve for the second phase in the form of a post-processed calculation. This uncoupled approach requires

the primary flow field, the particle diffusion coefficient and the particle mean square fluctuating velocity as initial conditions.

The primary flow field can be obtained either from the solution procedure outlined in the previous chapter, as done here, or by other numerical, analytical or experimental methods. In addition to the velocity field, for the primary phase, the length and velocity scales present in the flow need to be specified directly or indirectly through the use of equations of the form of (2.10).

In addition to the flow field characteristics the particle diffusion coefficient and mean square velocity need to be specified at every calculation point. This can either be accomplished by the use of a simulation technique, as outlined in chapter 2, or some form of empirical correlation.

The correct specification of these particle properties is of importance to the accurate calculation of the second phase characteristics and therefore is dealt with in more detail in the following chapter.

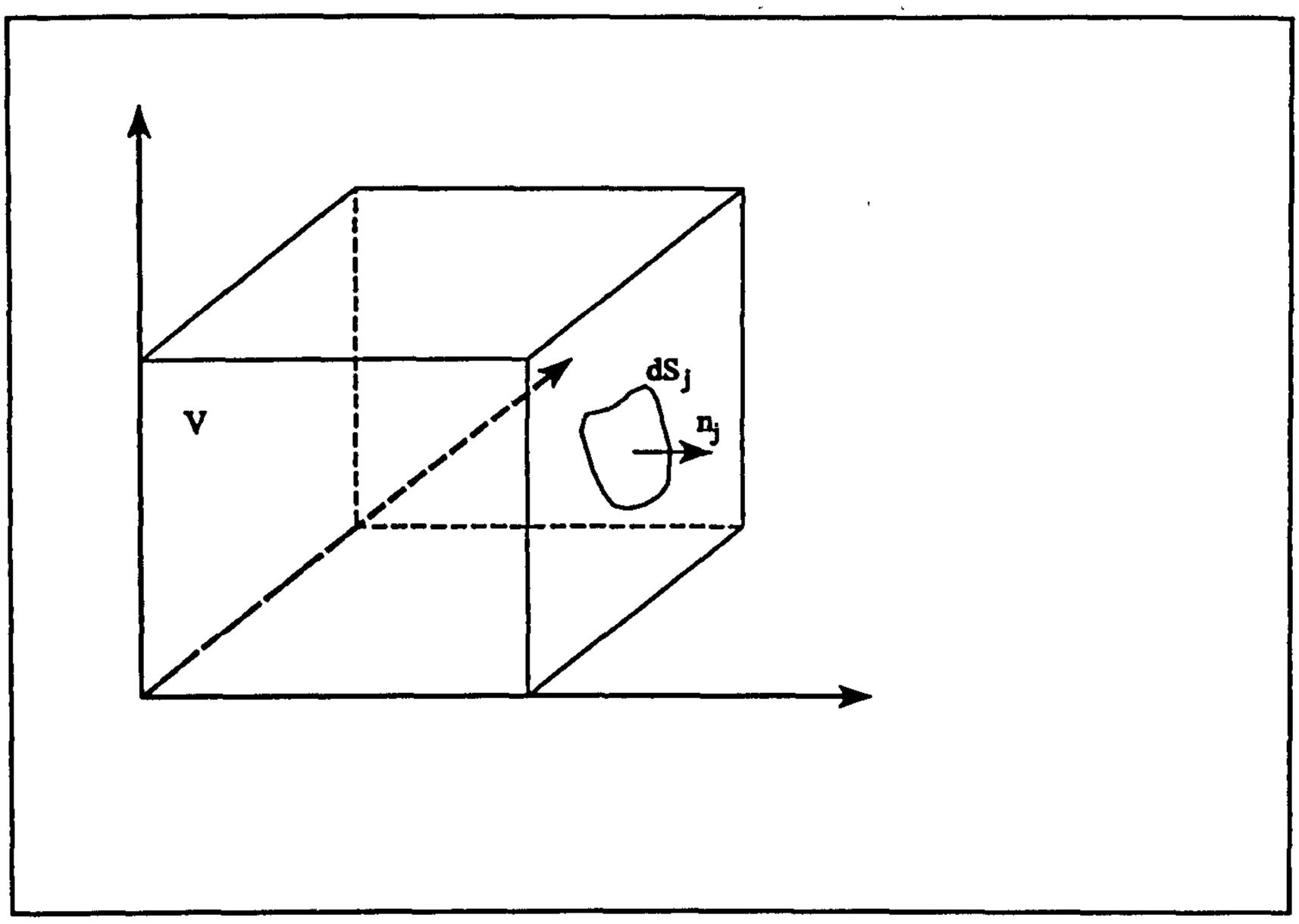

Figure 5.1 : Elementary Volume Flux for Second Phase

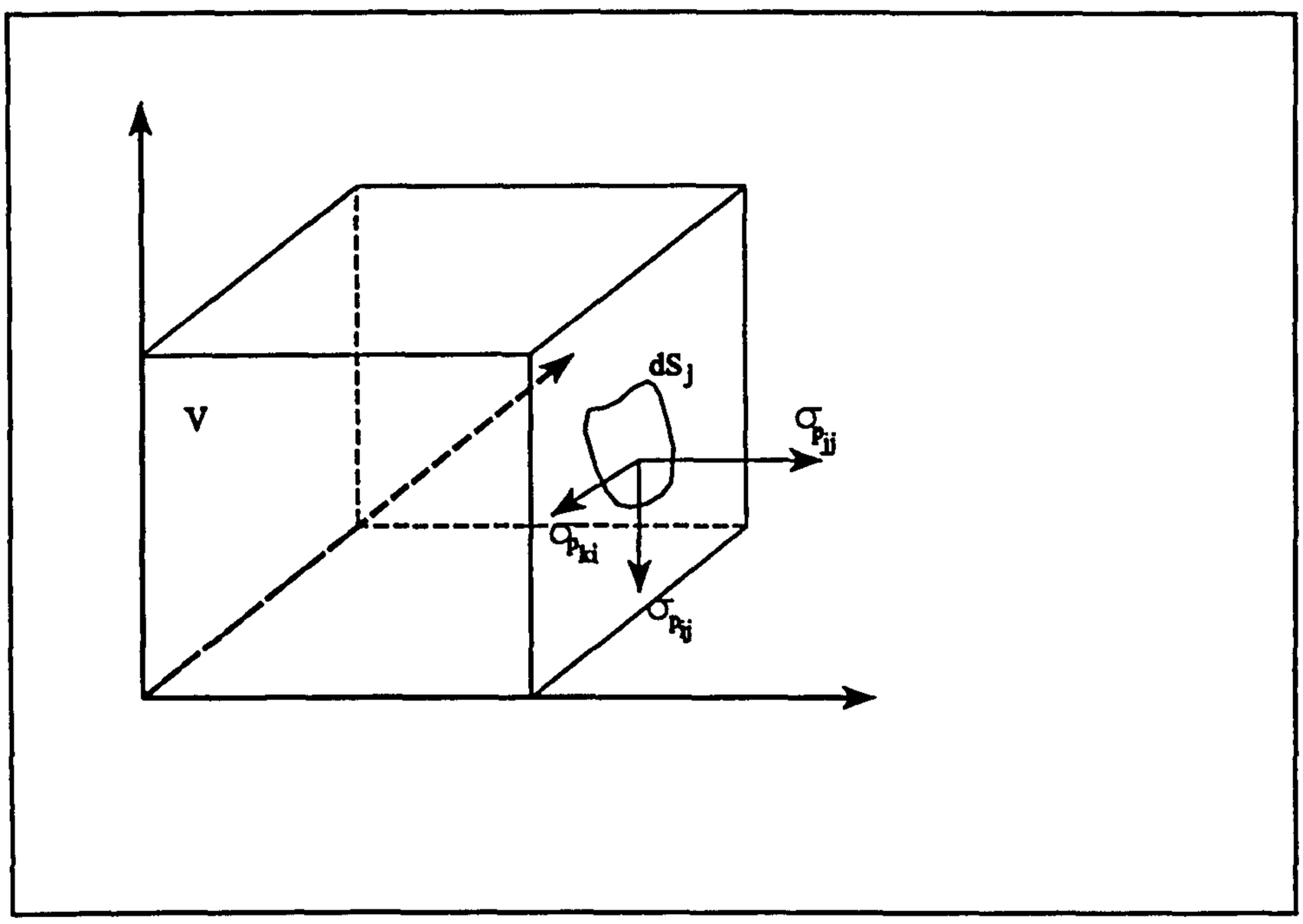

Figure 5.2 : Elementary Volume Stress for Second Phase

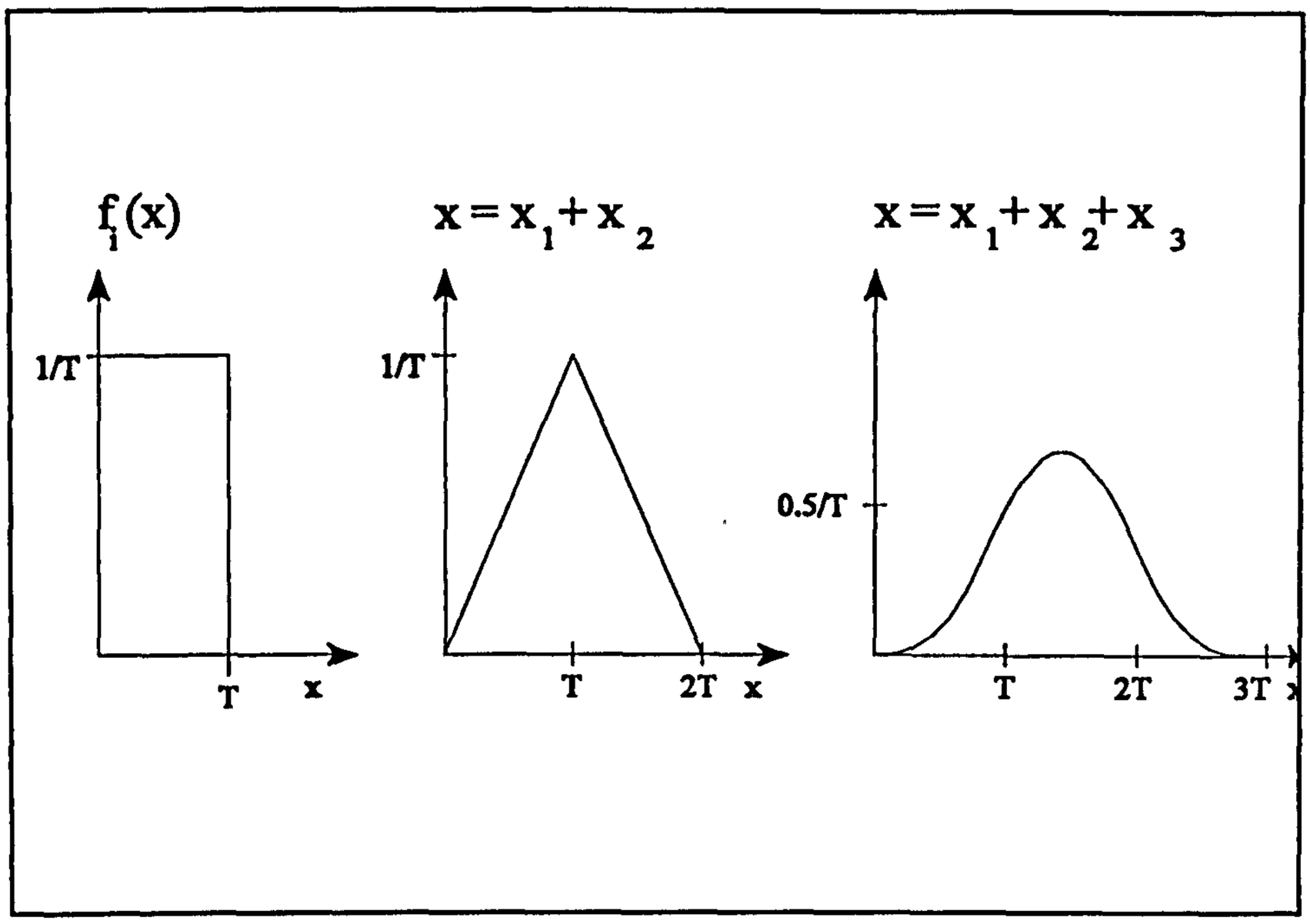

Figure 5.3 : Example of the Convolution of the Probability Density Function $f_i(x)$, Papoulis (1984), Showing the Rapid Approach to a Normal Distribution Characteristic of a Diffusion Process.

PAGE NUMBERING AS ORIGINAL

Chapter 6

Complete Calculation

6.1 Introduction

As described in the previous chapter, the work presented here is based on a post-processed calculation of the second phase flow field. This chapter contains a discussion of the solution method implemented in this work. Special attention is paid to the calculation of the particle diffusion coefficients. Use of the simulation method to calculate the particle diffusion coefficient at every point in the flow field would be the bulk of the calculation cost of the method. In this chapter various methods for reduction of this cost are discussed in detail. Use is made of the smoothness of the particle diffusion coefficient field within the flow to reduce the number of points which need to be calculated. The use of interpolation techniques, both in the reduction of the number of calculation points, and in the formation of a possible look-up table of particle diffusion coefficients, is described. Finally the application of the empirical correlation, developed in chapter 2, in order to reduce the cost of computation is investigated.

Special attention is paid to the importance of the concentration gradient driven source term found in the momentum equations for the second phase. The effect of this term on the particle dispersion becomes important when considering the use of the empirical correlation as its form prohibits the easy calculation of the required particle mean square fluctuating velocity. The correlation is such that knowledge of the mean particle-eddy interaction time, together with the particle diffusion coefficient, is required to obtain the particle's mean square fluctuating velocity. This time is not known a priori hence direct use of the correlation equation to obtain the required particle velocity is not possible.

6.2 Solution Algorithm

Equations (5.12) and (5.13) have been cast into the generalised form (4.9) and if the

expressions for both the diffusion coefficient and source term have been specified, it is possible, with the correct boundary and initial conditions, to solve these equations using the same basic method as outlined in chapter 4. The solution for the second phase by this method is more straightforward than that for the single phase due to the lack of a need for a staggered grid. As discussed above, the requirement for the use of a staggered grid arises out of problems which appear when solving for both the velocity and pressure at the same grid points. This problem does not arise in the solution of the second phase as no pressure coupling is required.

It is possible to solve equations (5.12) and (5.13) simultaneously with the flow field. As the calculation of the second phase is one-way coupled, the carrier phase flow field can be specified as an initial condition for the solution of the second phase equation. Throughout this work the carrier phase flow field is obtained by the solution of the pressure-correction code discussed in chapter 4.

In order to correctly model the behaviour of the second phase it is necessary to use an accurate solution for the carrier phase. It is possible to vary the coefficients of the k-ϵ turbulence model to obtain the best fit for a measured flow field, and also enables an implicit accommodation of the two way coupling effects of the dispersed phase on its carrier fluid.

The complete solution algorithm is outlined below.

(i) The first phase flow field is calculated using a form of the SIMPLER algorithm including a modified k-ϵ turbulence model. This results in the mean velocity field for the corresponding single phase flow field, together with the distribution of kinetic energy and dissipation within the calculation domain. This step can be repeated, modifying the coefficients in order to give a good fit to the measured flow field.

(ii) These distributions of k and ϵ are then converted into length, time and velocity scales, as outlined in chapter 2. A representative range of scales is then chosen for calculation of particle diffusion coefficients.

(iii) The particle diffusion coefficients corresponding to the chosen scales are obtained. These are then formed into a look-up table of for the calculated flow field. This calculation is also used to obtain a corresponding look-up table for the mean square fluctuating velocity of the particle, as required in the second phase momentum equation.

(iv) A modified SIMPLER algorithm is used to calculate the second phase flow field. A bi-cubic spline is fit to the diffusion coefficient look-up table to obtain the diffusion coefficient of the particles in each calculation cell based on the turbulent scales found in that cell.

A more detailed discussion of steps (iii) and (iv) can be found in the next section

6.3 Calculation of Particle Diffusion Coefficients

The calculation of the particle diffusion coefficient at all solution points in the flow field would be excessively expensive. It is therefore desirable to develop ways to reduce the cost of this calculation.

The diffusion coefficient can be shown to be smoothly varying. Considering the simplest case of the above chapters, dependence of the diffusion coefficient can be written as

$$\Gamma_p = f(\langle t_l \rangle, d_p, \frac{\rho_p}{\rho_g})$$

where $\langle t_l \rangle$ represents the mean particle-eddy interaction time. Using scaling arguments we can write

$$\Gamma_p = f(\frac{d_p^2}{\langle t_l \rangle}, \varrho) \qquad (6.1)$$

where ϱ represents the non-dimensional density ratio. It is clear from equation (6.1) that the diffusion coefficient is smooth if the particle diameter and the mean interaction time are smooth. We specify the former and, though the interaction time has discontinuous gradients at the interfaces between the various interaction time scales, these have little influence on the smoothness of the diffusion coefficient as figure 6.1 shows . It also follows from (6.1) that the strongest dependency of the particle diffusion coefficient is on the particle size.

Therefore, it is possible to reduce the number of calculations by considering only a representative range of parameters and using an interpolation approach. Figure 6.1 shows the variation of the diffusion coefficient, for a representative particle, with the range of turbulent scales found in the simple pipe flow considered below, and illustrates that the variation is indeed smooth. Thus, a significant reduction in the computational cost in the calculation can be realised.

Here, the range of both turbulent length and velocity scales present in the flow is approximated by the calculation of ten representative values, which leads to the calculation of one hundred diffusion coefficients. Intermediate values are then obtained from a bi-cubic spline interpolation algorithm. Since the dispersion distance is a function of the square root of the diffusion coefficient, the sensitivity of the dispersion to a small change in the diffusion coefficient is small. As a result, given the smoothness of the function, a slight extrapolation of values outside those spanned by the calculation would also be possible.

The above discussion together with the post-processed form of the calculation, allows the formation of a look-up table for the particle diffusion coefficient. The number of dimensions of this look-up table is a function of the required number of dependent variables. In the simplest case the table for a particle of given (constant) properties would require a look-up table of two-dimensions, namely the two dependent turbulent scales. As the flow situation considered becomes more complicated (e.g. the introduction of evaporation) the dimensions of the look-up table increase. The use of a pre-calculated look-up table enables the consideration of many flow regimes without the need for the expensive computation of the particle diffusion coefficient.

To be able to form this look-up table a method for calculation of the diffusion coefficient of the particles is required. It is possible to use either a simulation method, as

presented in chapter 2, or some form of empirical correlation.

The use of a simulation method, although allowing greater insight into the interaction processes between the two phases, is expensive. To achieve a statistically useful result a large number of particle-eddy interactions must be simulated. Also the lack of ergodicity in the interaction process requires the use of ensemble averages, which increases the required number of samples still further. It would therefore be desirable to avoid the need for simulation if possible.

In this work a simple empirical correlation has been developed to enable the rapid calculation of the required particle diffusion coefficient, see chapter 2. The use of the correlation reduces the cost of the calculation of the diffusion coefficient sufficiently to negate the need for a look-up table. As shown previously, the correlation is in very good agreement with the results of the simulation calculations.

While the correlation is useful for the diffusion coefficients, problems occur in the computation of the mean square fluctuating velocity of the particles, which is required for the calculation of a source term in the momentum conservation equation for the second phase. This velocity can be obtained from the simulation directly, but requires modelling if use is made of the correlation. This is discussed in the following section.

6.4 Mean Square Velocity Term

Examination of (5.13) shows the presence of the term

$$\overline{u_p'^2}\frac{\partial C}{\partial x_j} \tag{6.2}$$

for each velocity component, u_{pi}.

The presence of the source term (6.2) leads to complications in the use of empirical calculation methods for the characteristics of the particle. A simple empirical correlation for the diffusion coefficient of the particles is known, see above, but its form is such that the straightforward calculation of the mean square fluctuating velocity is not possible

Before discussing ways of modelling the term it is useful to investigate its importance

in the correct calculation of the behaviour of the second phase.

6.4.1 Importance of the Fluctuating Velocity Term

To investigate the effect of this extra source term on the calculated dispersion of the second phase, a simple pipe flow example similar to that discussed in the previous chapter was extended to the second phase. The flow was extended to a vertical pipe of radius 1 m and length 5 m and the flow velocity used was 10 m/s. The changes were made to the calculation used in the previous chapter to allow greater dispersion of the particles within the pipe before they encountered the walls, while still retaining a relatively higher Reynolds number (Re_D~130,000). The particles used to represent the second phase were introduced on the line of symmetry of the flow smeared across three computational cells to avoid large concentration gradients at the inlet. The particle characteristics chosen are given in table 6.1.

	Diameter (μm)	Density (kg/m^3)	Terminal Velocity (m/s)
Fluid Point	1.0	1.0	0.
Water	46.5	1000.0	6.1×10^{-2}
Copper	46.5	8900.0	4.8×10^{-1}

Table 6.1 : Particle Characteristics

The diffusion coefficient and mean square fluctuating velocity of the particle were obtained using the simulation method. It was then possible to solve for the second phase both including the source term and setting it equal to zero.

Figures 6.2(a)-(d) and 6.3(a)-(d) show a comparison of the calculated second phase concentration at four downstream locations for a range of particles both with and without this source term. The diffusion coefficients of the particle are calculated using the vector model of chapter 2 without convection. It is clear from all the graphs that the presence of this additional source term leads to no noticeable change in the calculated dispersion. Thus, the influence of this term on both the particle velocity and concentration distribution is small,

less than 1%. Due to this small dependence, the estimate of the mean square fluctuating velocity of the particles in the empirical correlation need only be approximate.

6.4.2 Empirical Correlation

The simplest way of calculating the particles mean square fluctuating velocity would be to invert the relationships (2.11), of the form

$$\Gamma_p = \frac{1}{2}\langle u_p^2 \rangle \langle t \rangle \quad \rightarrow \quad \langle u_p^2 \rangle = 2\frac{\Gamma_p}{\langle t \rangle} \tag{6.3}$$

To obtain the mean square fluctuating velocity of the particle from (6.3) it is necessary to know both the diffusion coefficient of the particle and the mean particle-eddy interaction time, <t>. Due to the form of the empirical correlation (2.18) the knowledge of one requires that of the other. It is therefore necessary to develop an equation for the mean particle-eddy interaction time.

The limited influence of this term on the calculation for the dispersion of the second phase, together with the problem outlined above lead to the development of a simple correlation for the particle mean fluctuating velocity. This velocity can be assumed to be inversely proportional to the particles relaxation time. Making this assumption and fitting one of the points from the simulation calculation it was decided to approximate this velocity from the following simple expression

$$\langle u_p'^2 \rangle = MIN\left(u_e^2, \frac{u_e^2}{\alpha u_t^2}\right) \tag{6.4}$$

Where α was chosen to be 30 and has dimensions of $m^{-2}s^2$. The degree of fit of (6.4) compared to the value calculated from the simulation is shown in figures 6.4 and 6.5. The fit is acceptable (approximately 10% error) for both types of particles. As any discrepancies

will be statistically reduced by the weak effect of the resultant source term on the concentration and velocity distributions of the particles, use of the correlation is possible.

6.5 Validation Calculation

The dispersion calculations for the particles, with properties given in table 6.1, in the turbulent pipe flow defined above are presented in figures 6.2-6.3. The calculations used the simulation method of chapter two to obtain both the particle diffusion coefficients and mean square fluctuating velocities. As mentioned previously this method is costly to compute and the use of a much simpler empirical correlation to obtain the required particle characteristics is preferred.

Figures 6.6(a)-(d) to 6.9(a)-(d) show a comparison of the dispersion of the range of particles considered using the empirical calculation procedure and the simulation method. Only the results for water and copper are presented as the simulation and correlation properties for the fluid point are identical (due to the form of the model). It can be seen that the difference in dispersion for both the copper and water particles is approximately 10%, and that the error is consistent whether or not the mean square particle fluctuating velocity source term is considered, as expected. The error implies that the dependence of the correlation on the turbulent characteristics is significant. This is not surprising since the premise of the correlation is that the errors in the fluctuating velocity term and the mean interaction time offset, see chapter 2. The relationship between these two quantities varies as the turbulence scales change leading to a breakdown of the mutual error offset.

Because the ~10% error between the correlation and the simulation results in figures 6.6-6.9 is acceptable, and is consistent with the level of agreement found in the diffusion coefficient calculations, the correlation method is used to calculation the diffusion coefficients of the particles throughout the remainder of this work. As a result there is a much reduced computational overhead. However, it would be advantageous, in the future to develop a more robust form of the correlation which minimises the observed dependence on the turbulent scales. This has not been attempted here.

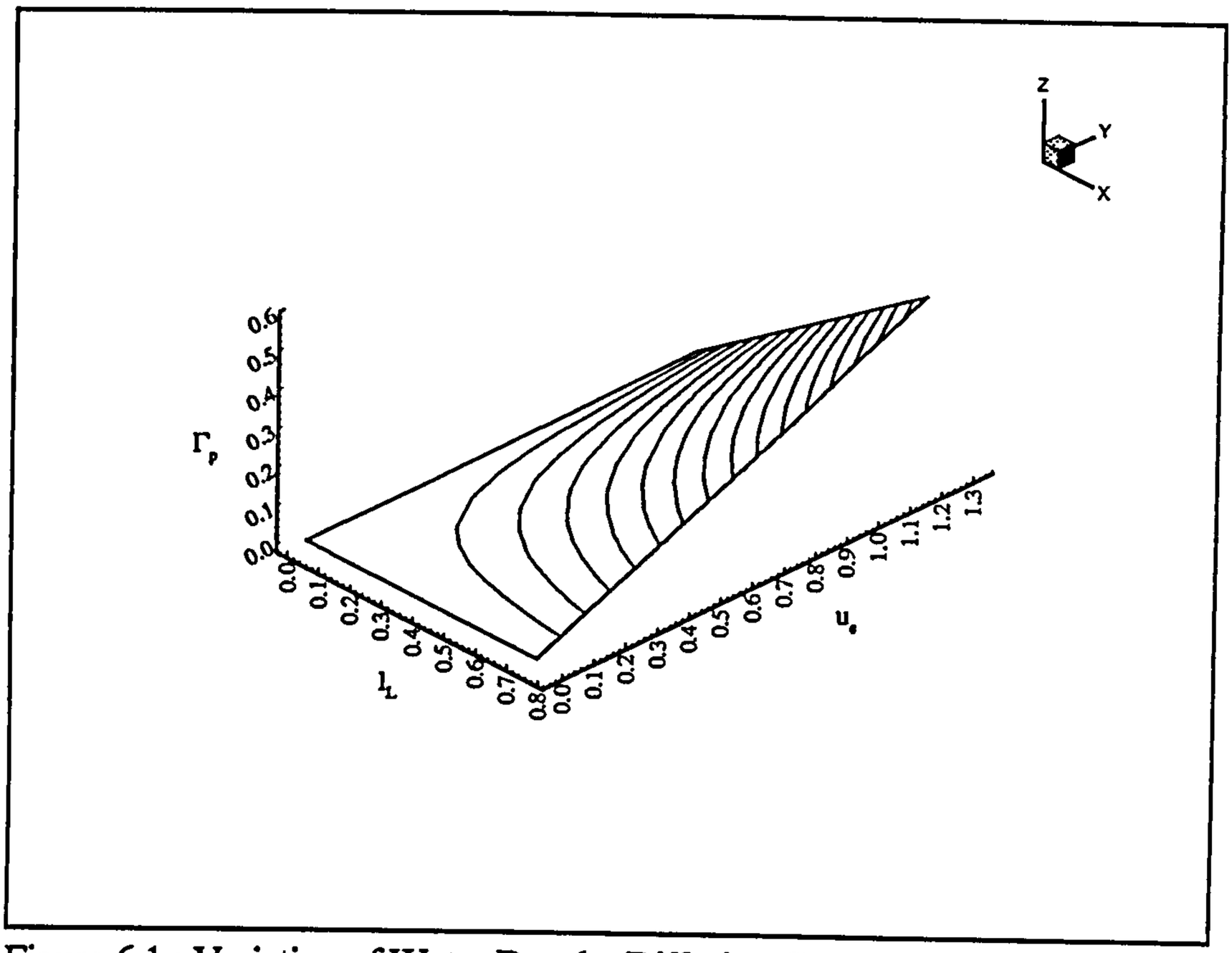

Figure 6.1 : Variation of Water Droplet Diffusion Coefficient With Turbulent Scales

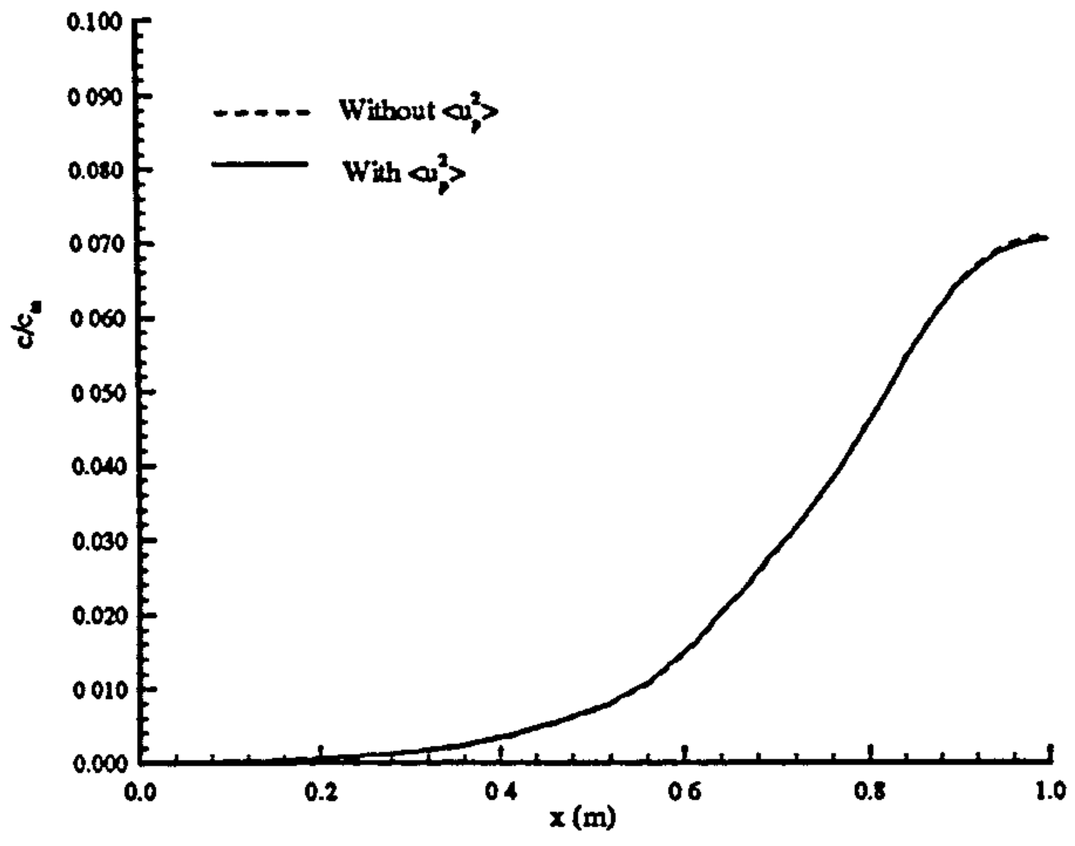

(a) 1m Downstream

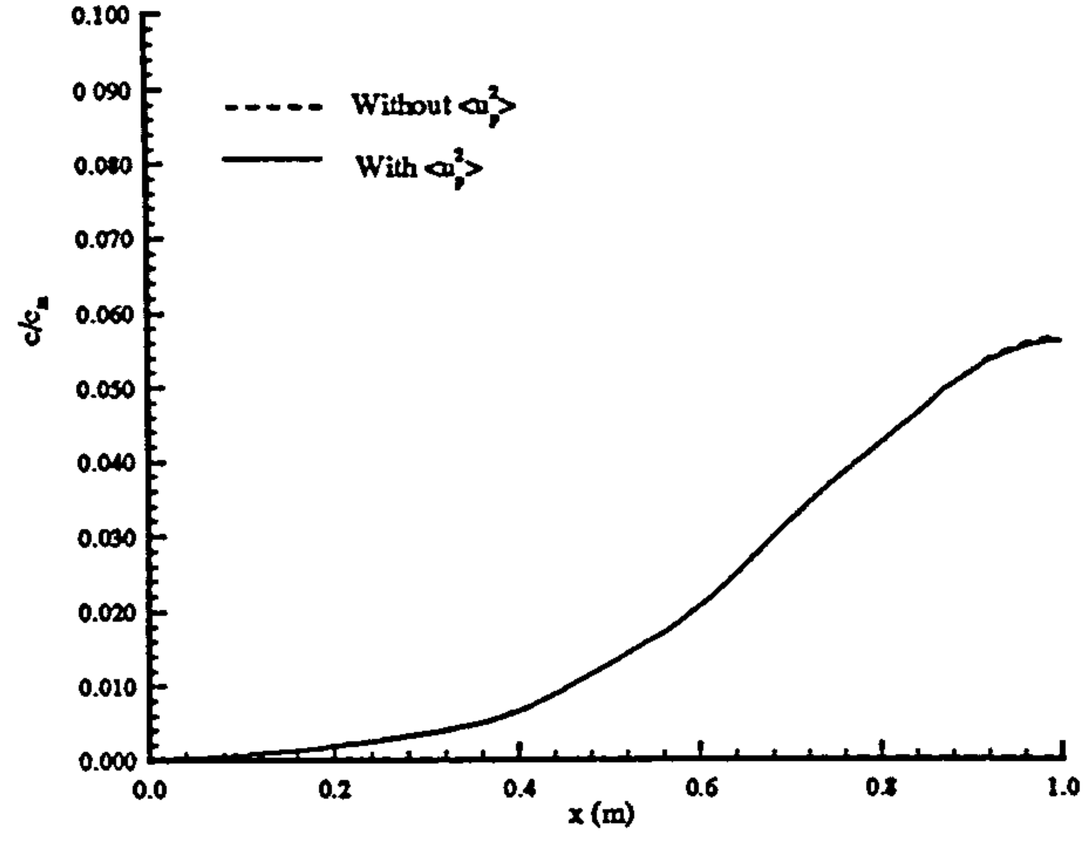

(b) 2m Downstream

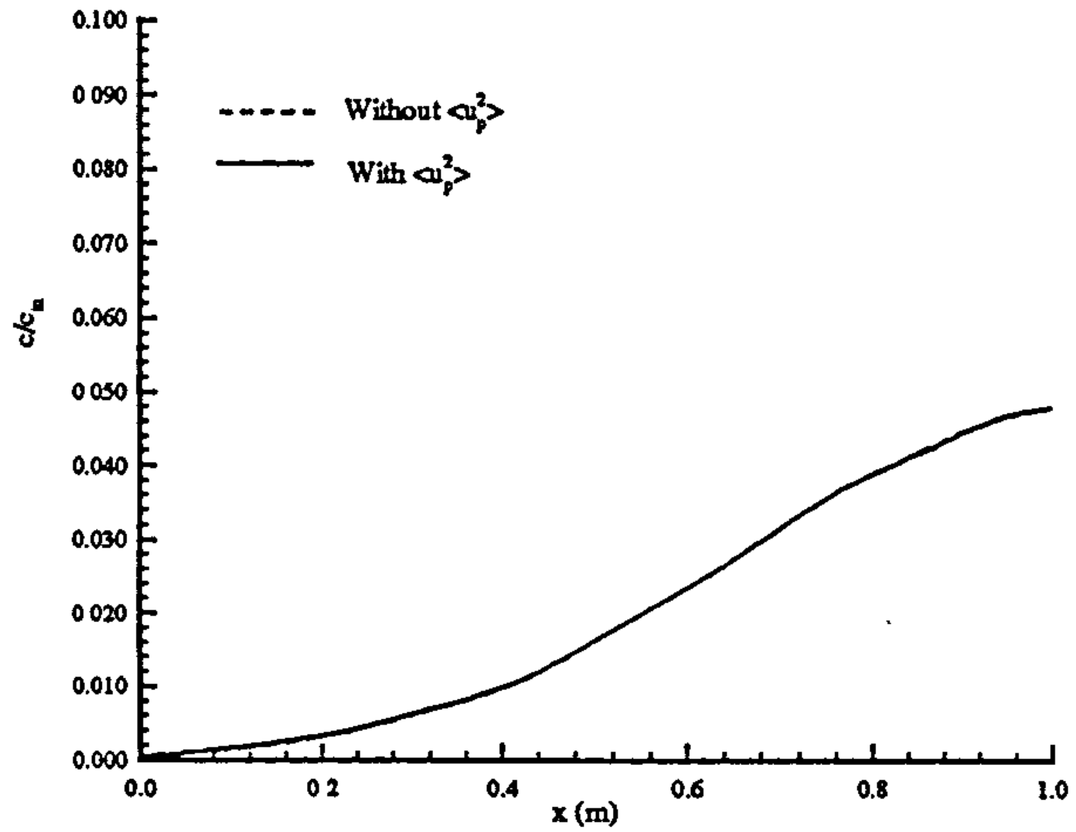

(c) 3m Downstream

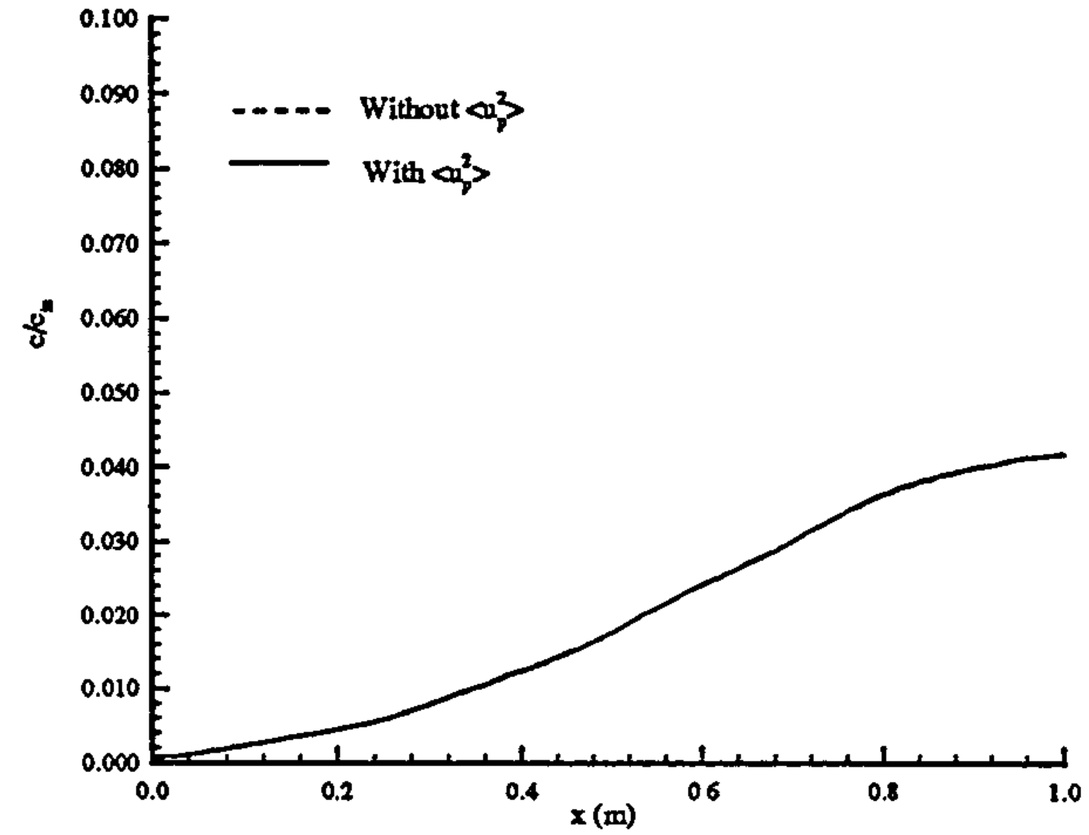

(d) 4m Downstream

Figure 6.2 : Concentration Profiles, Water, Using Simulation for Γ_p

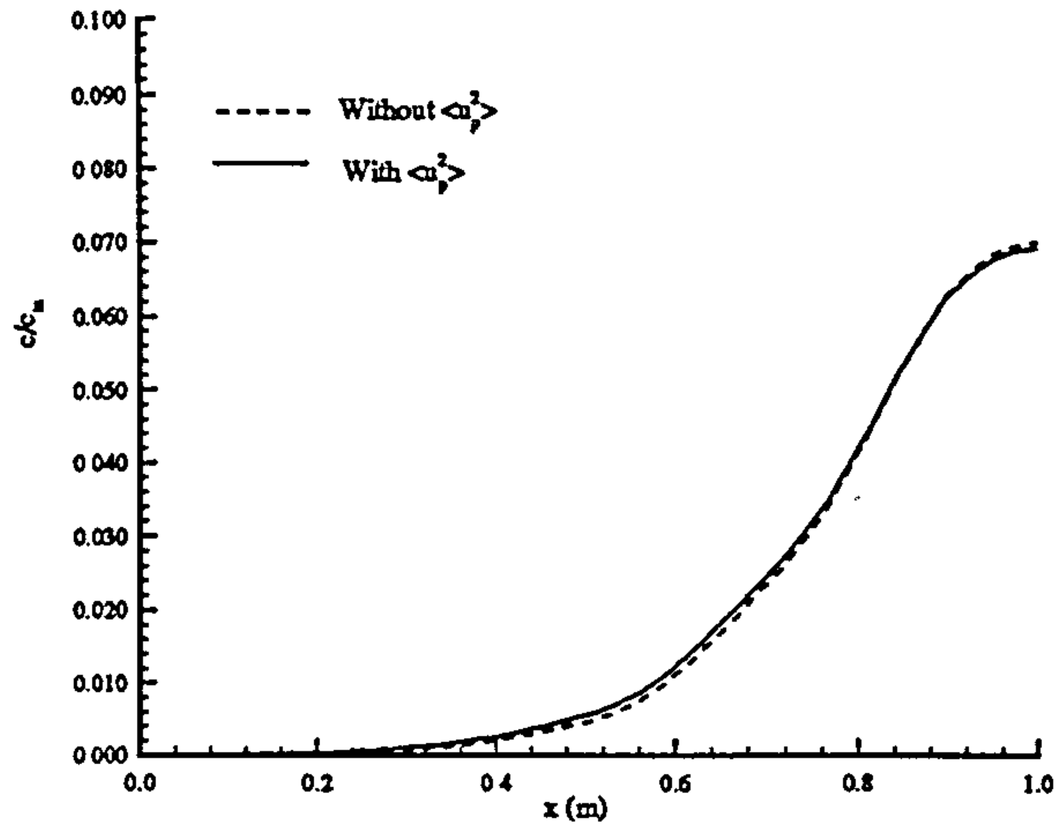

(a) 1m Downstream

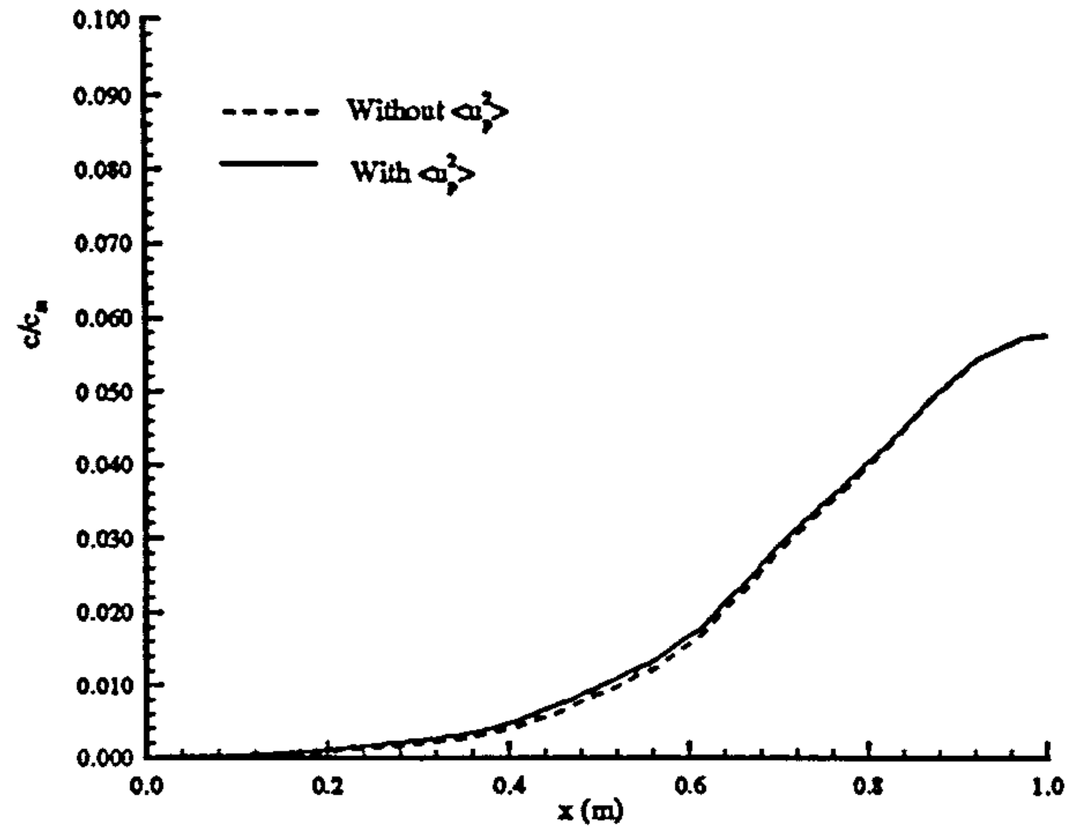

(b) 2m Downstream

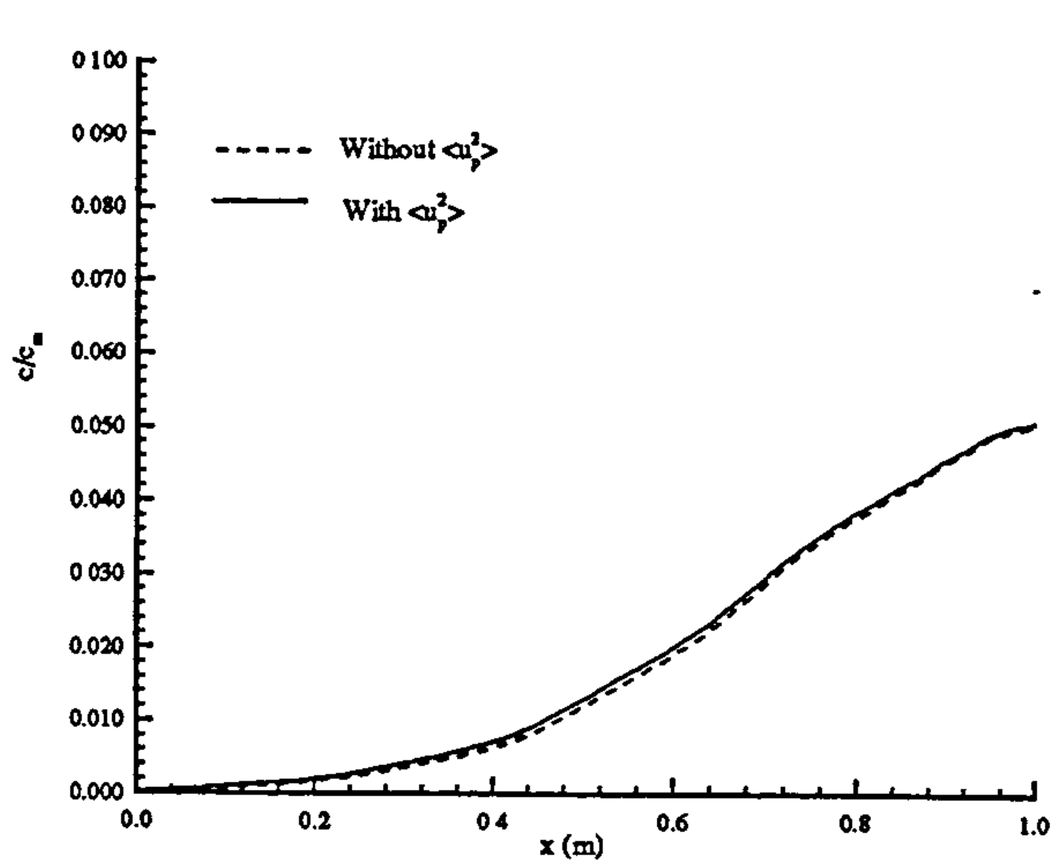

(c) 3m Downstream

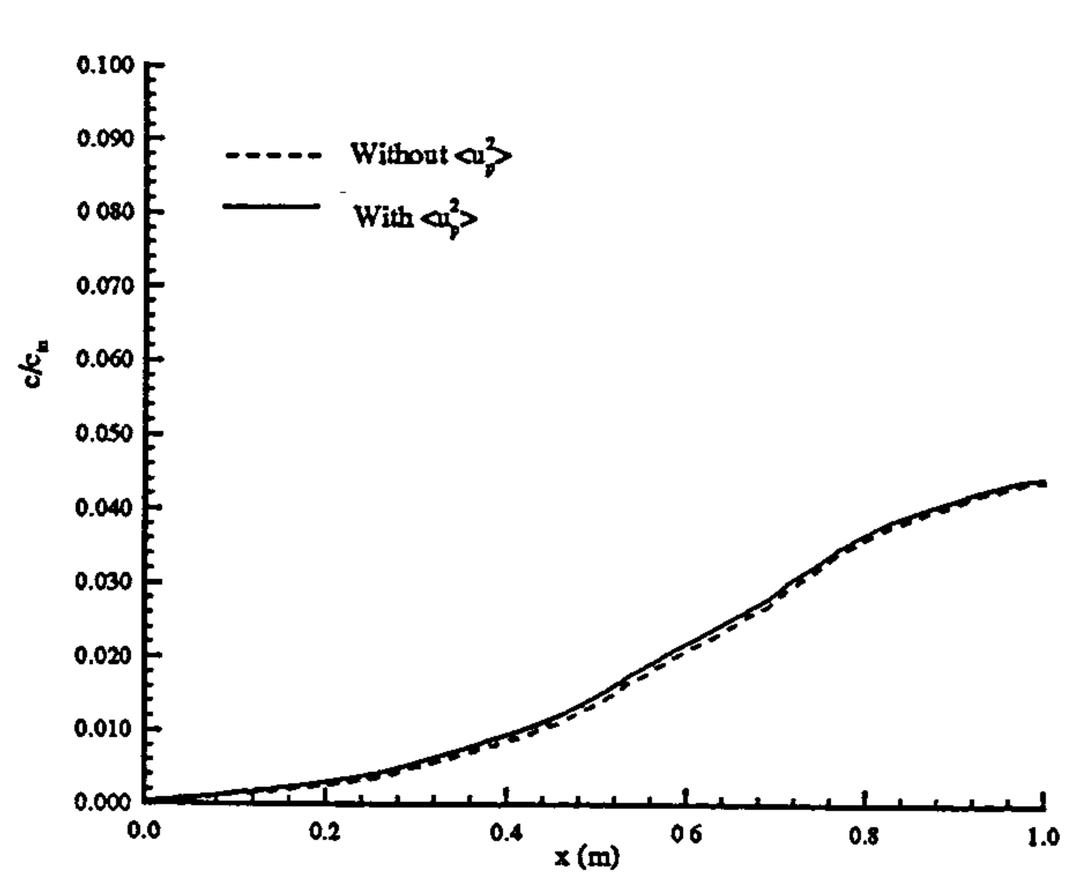

(d) 4m Downstream

Figure 6.3 : Concentration Profiles, Copper, Using Simulation for Γ_p

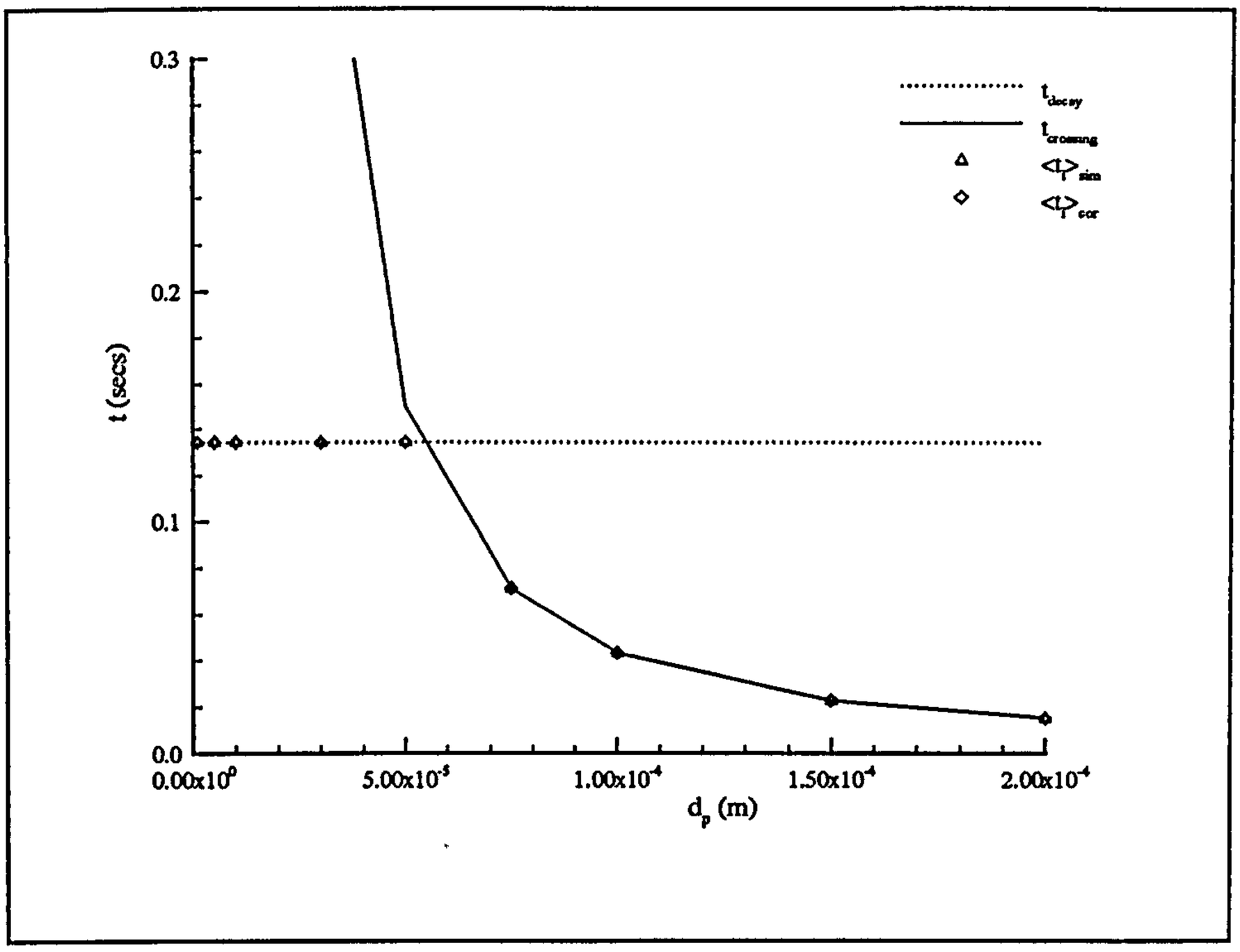

Figure 6.4 : Comparison of Interaction Time Scales, Water

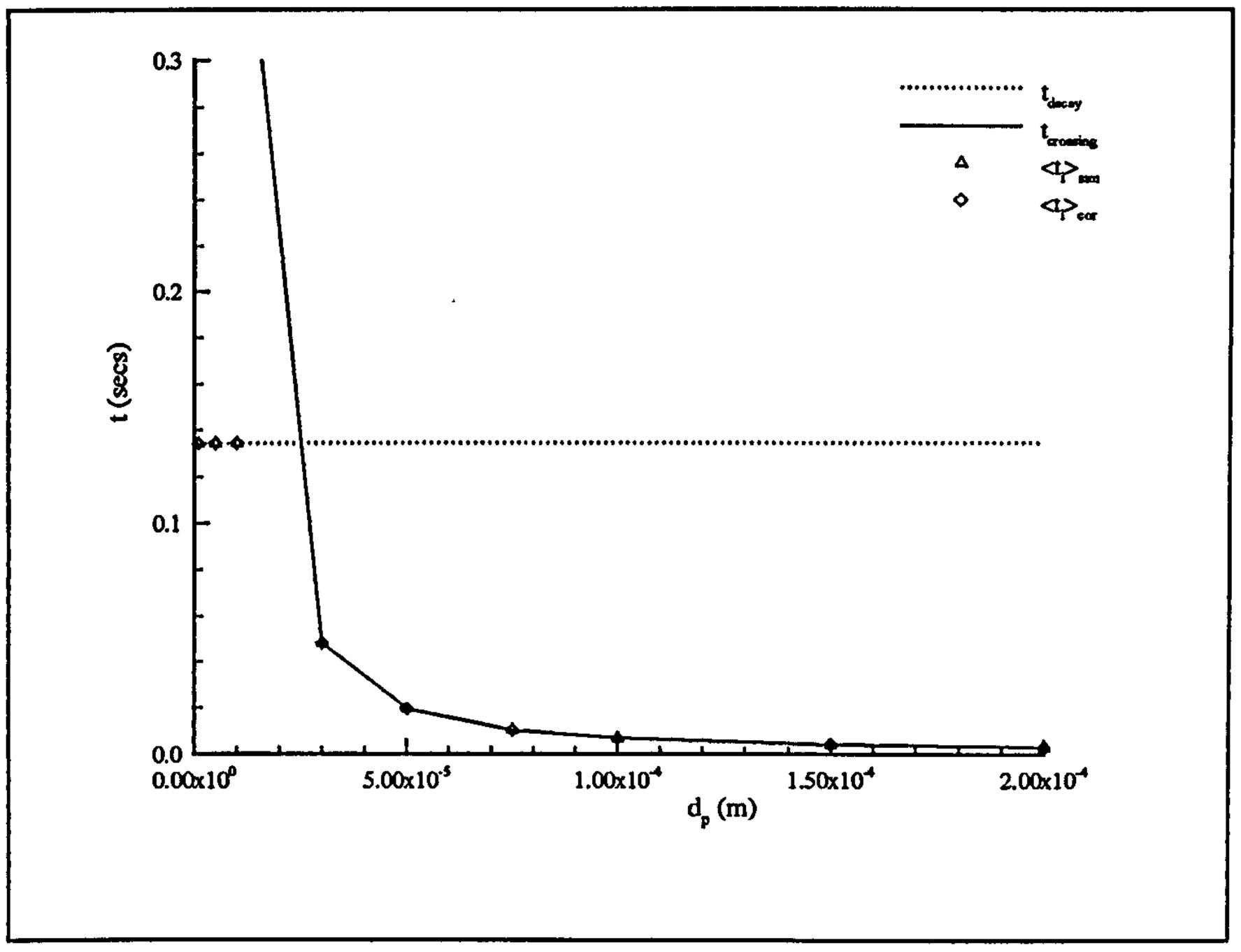

Figure 6.5 : Comparison of Interaction Time Scales, Copper

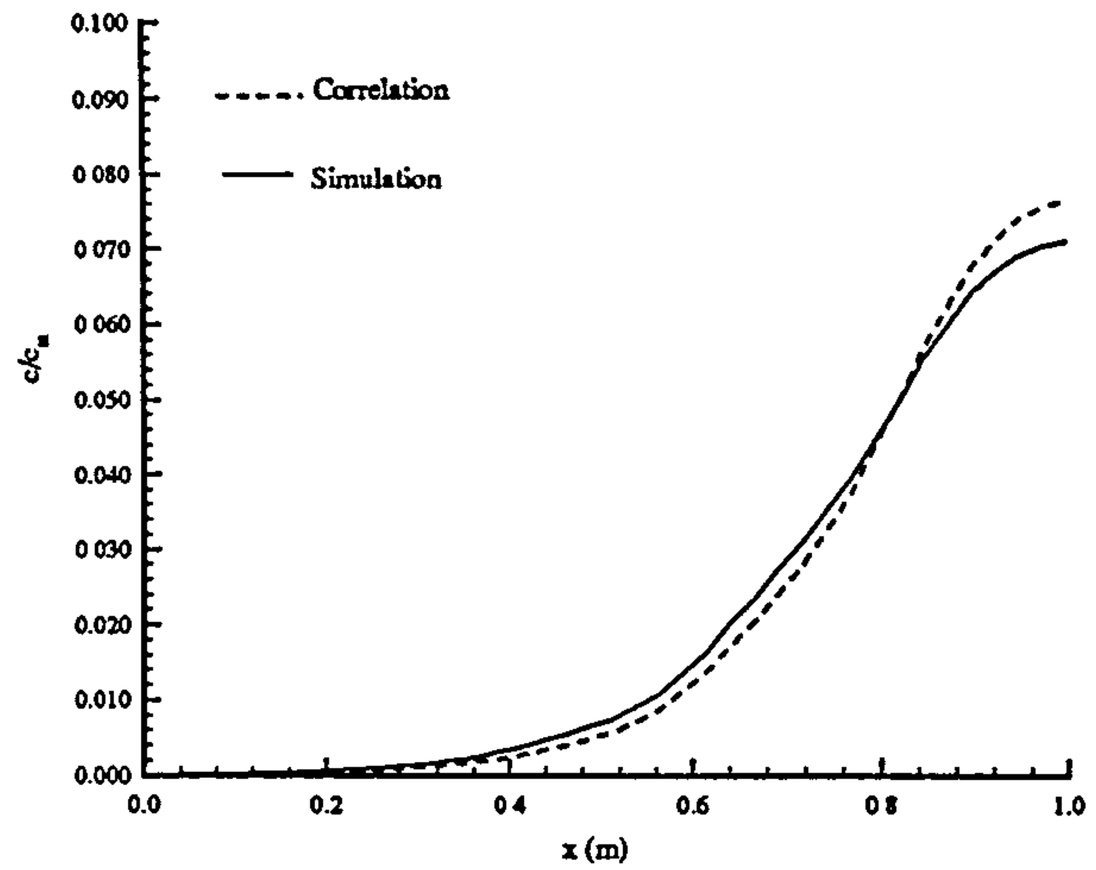

(a) 1m Downstream

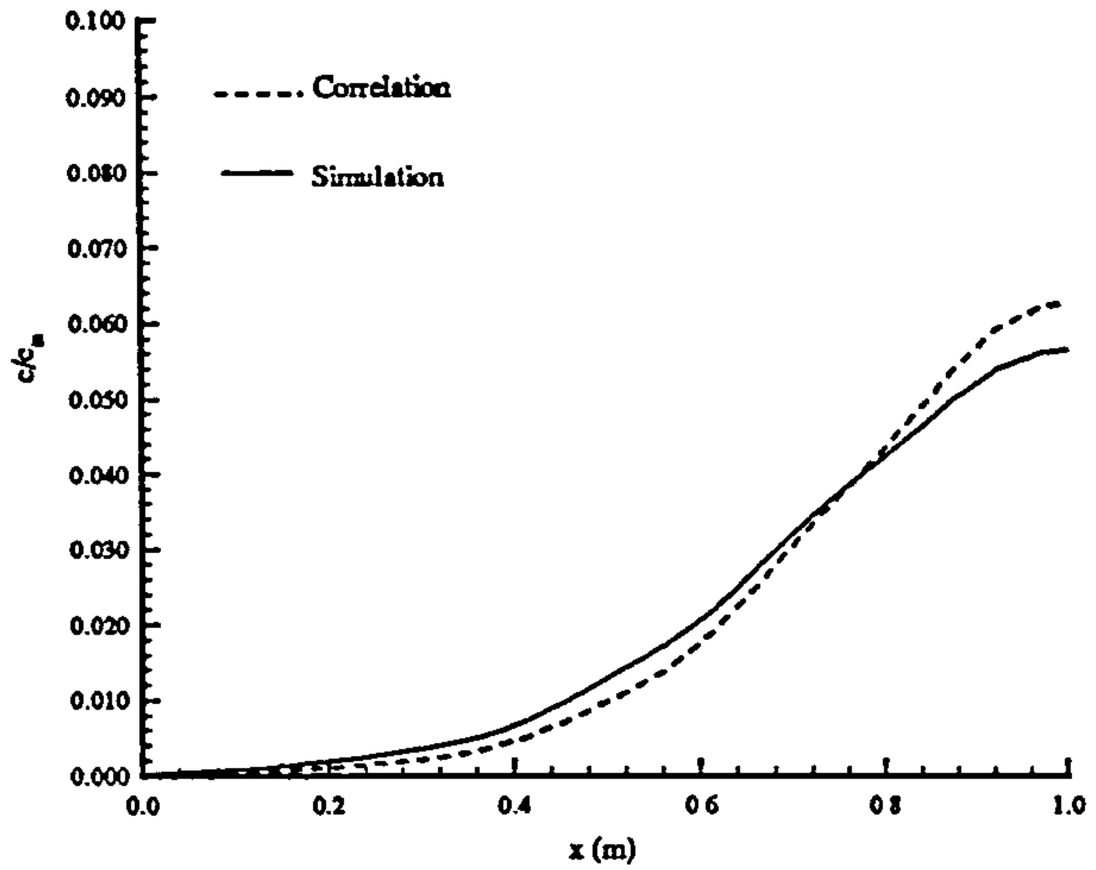

(b) 2m Downstream

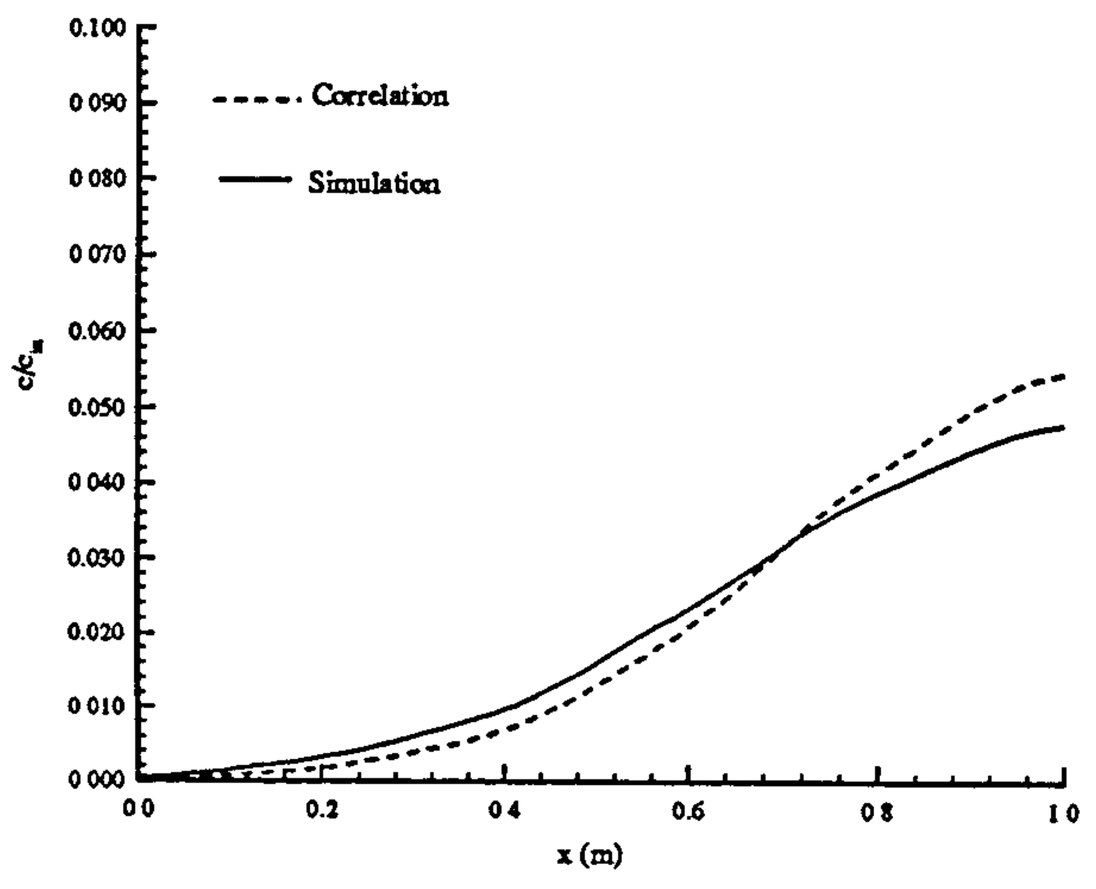

(c) 3m Downstream

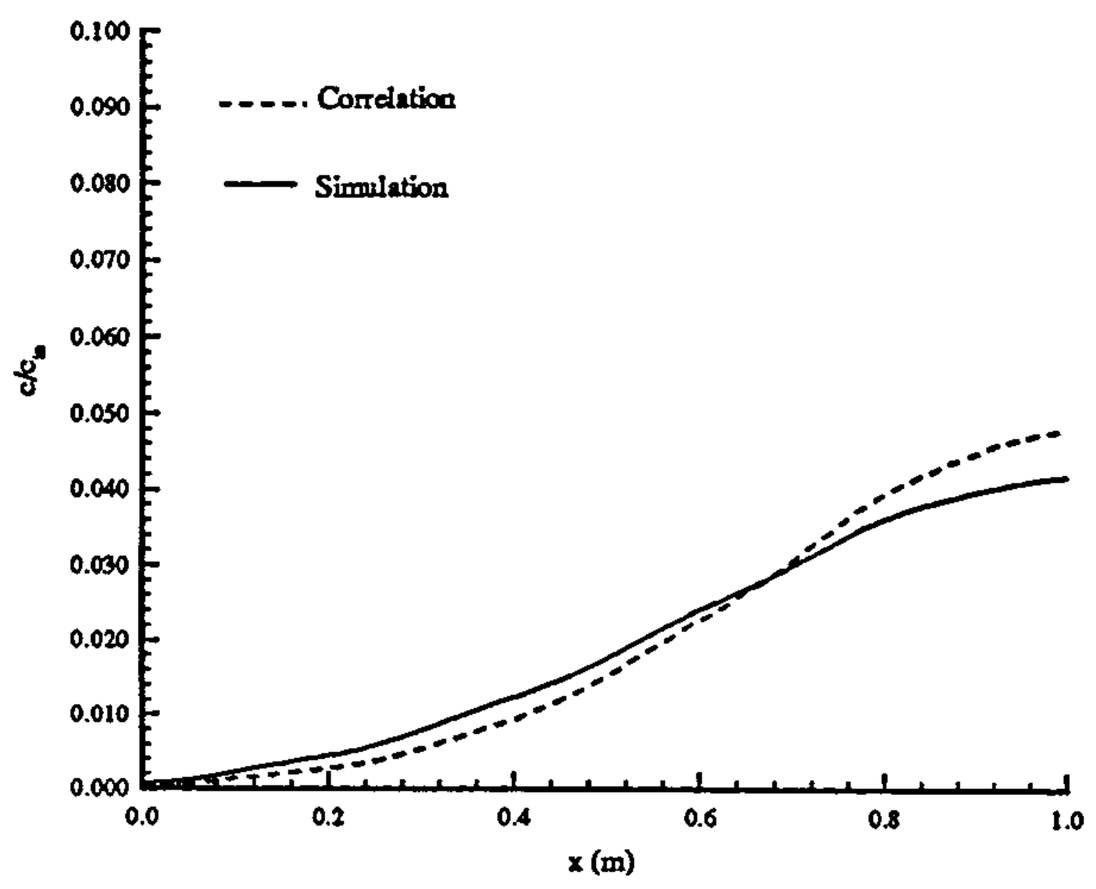

(d) 4m Downstream

Figure 6.6 : Comparison of Correlation and Simulation, Water, Without $\langle u_p^2 \rangle$

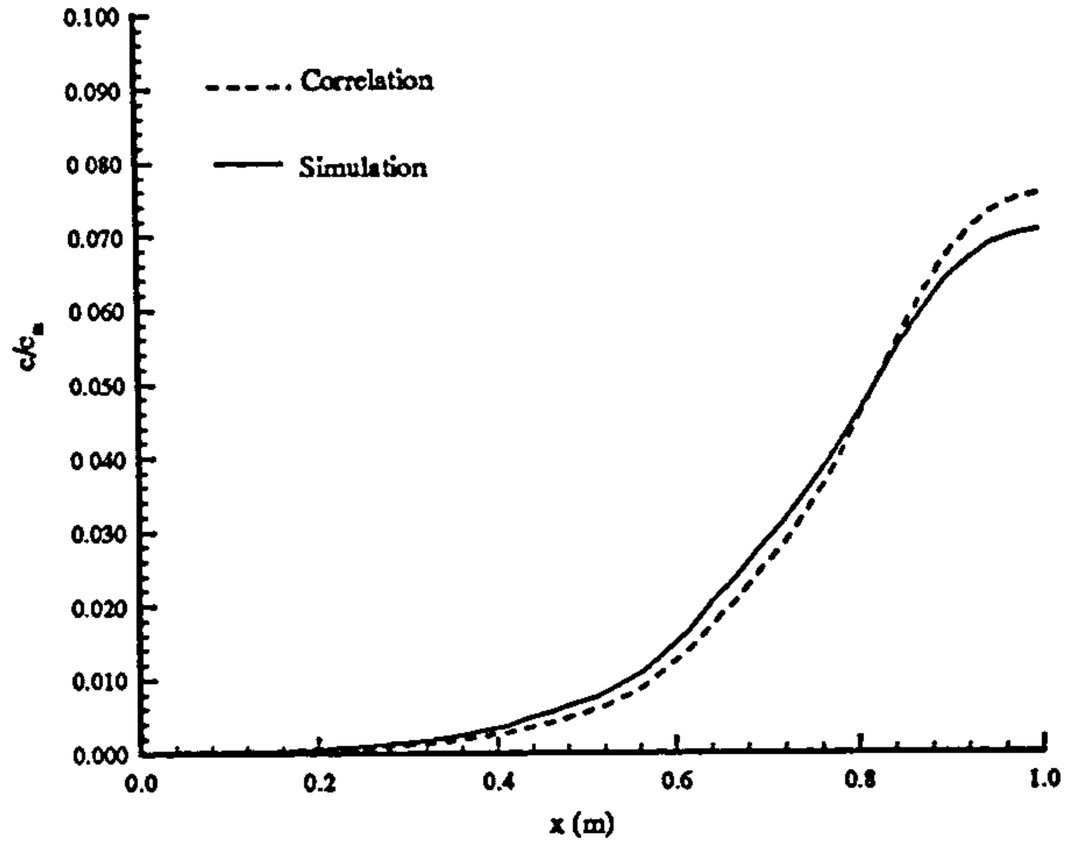

(a) 1m Downstream

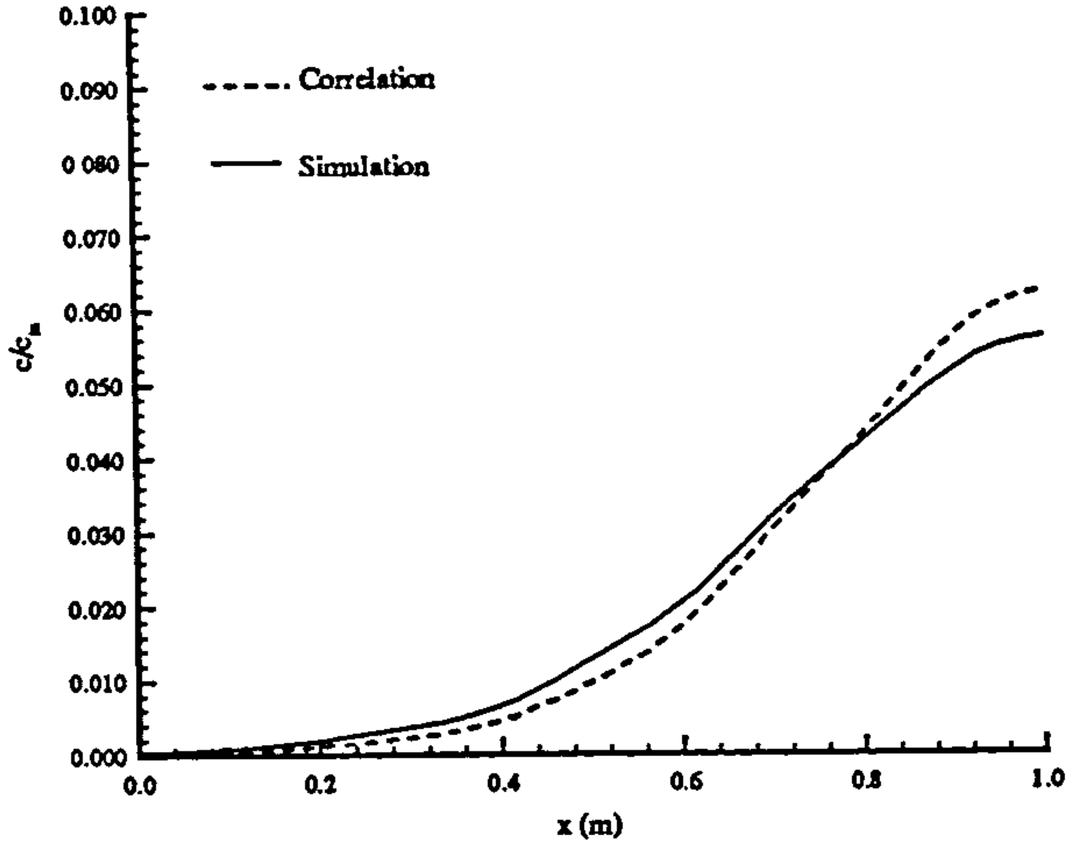

(b) 2m Downstream

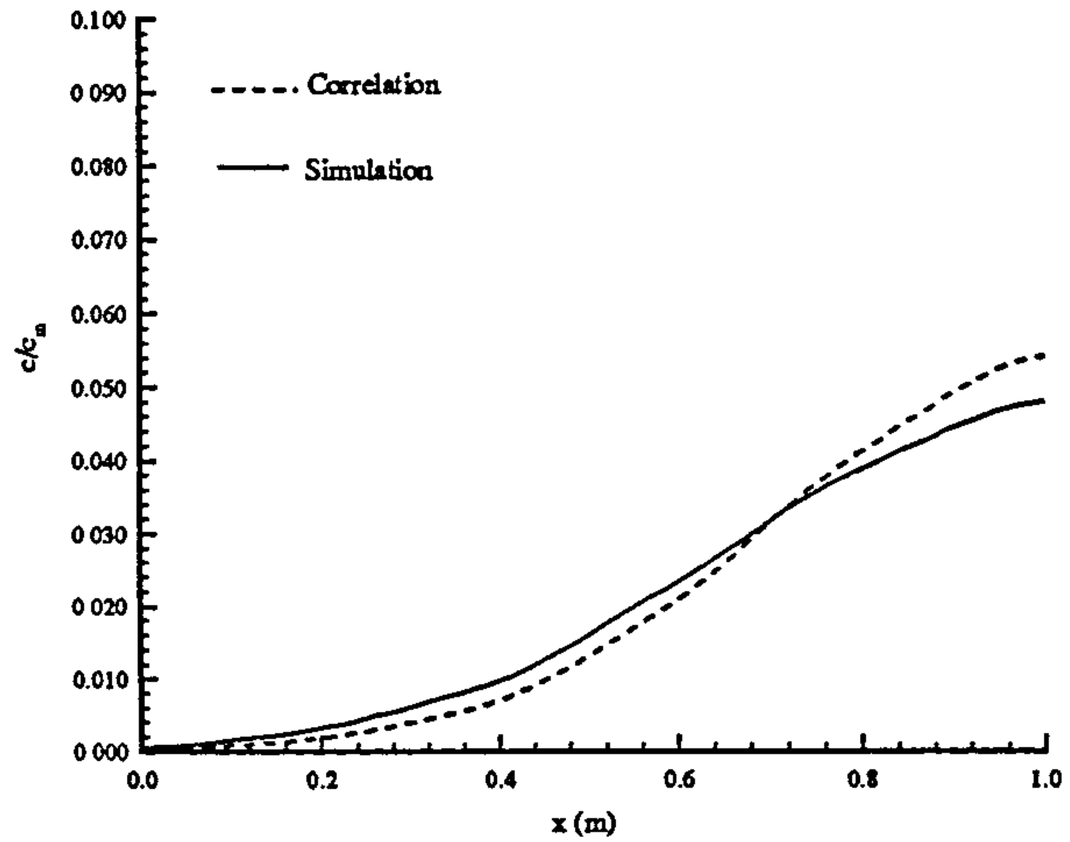

(c) 3m Downstream

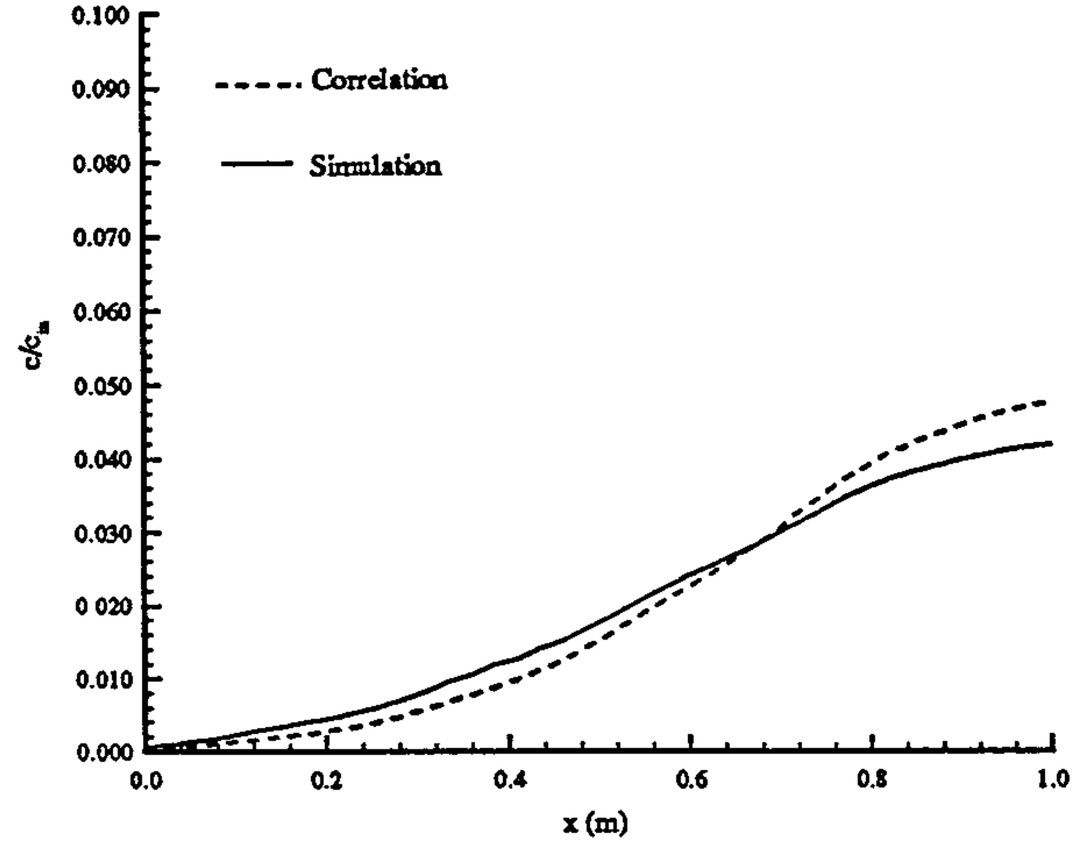

(d) 4m Downstream

Figure 6.7 : Comparison of Correlation and Simulation, Water, With $\langle u_p^2 \rangle$

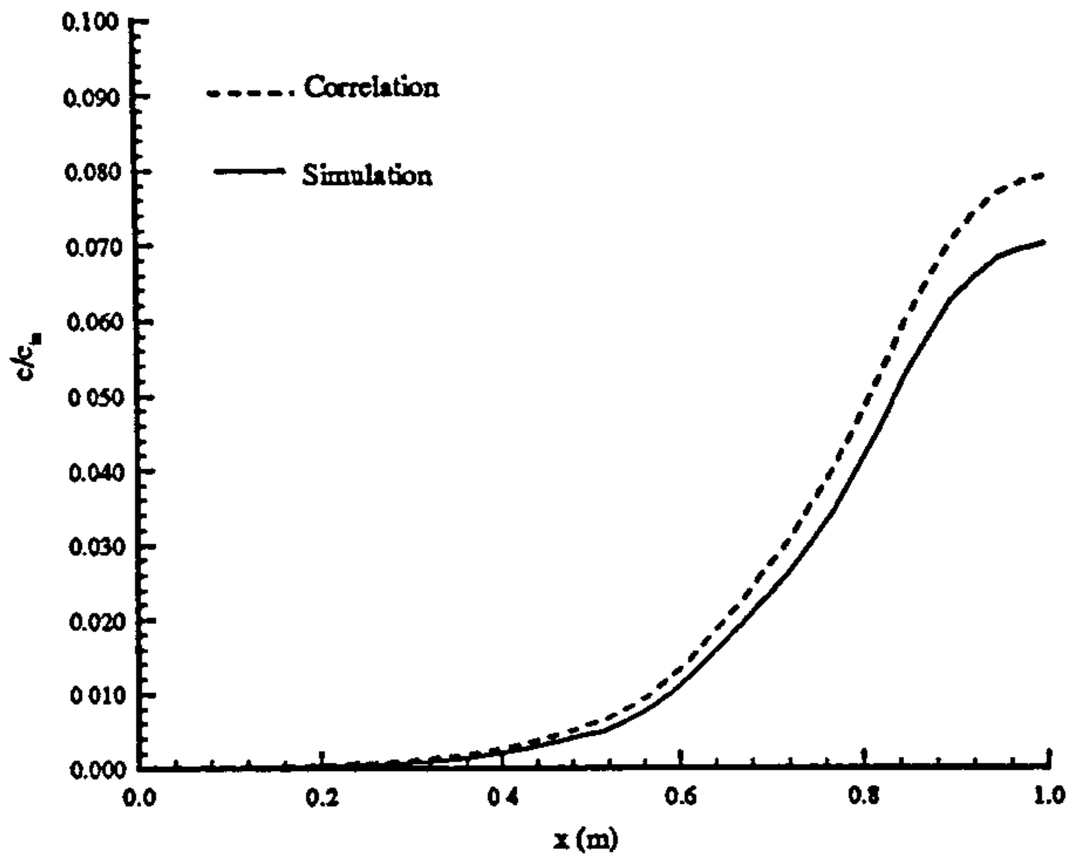

(a) 1m Downstream

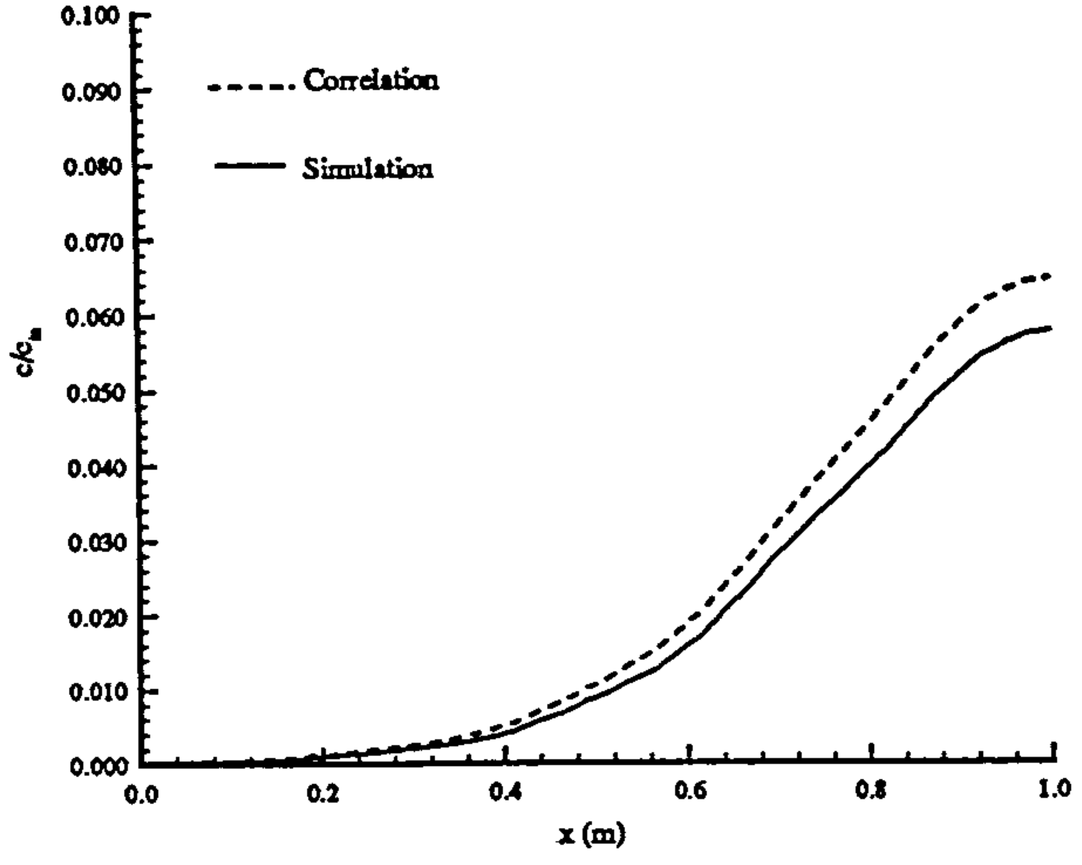

(b) 2m Downstream

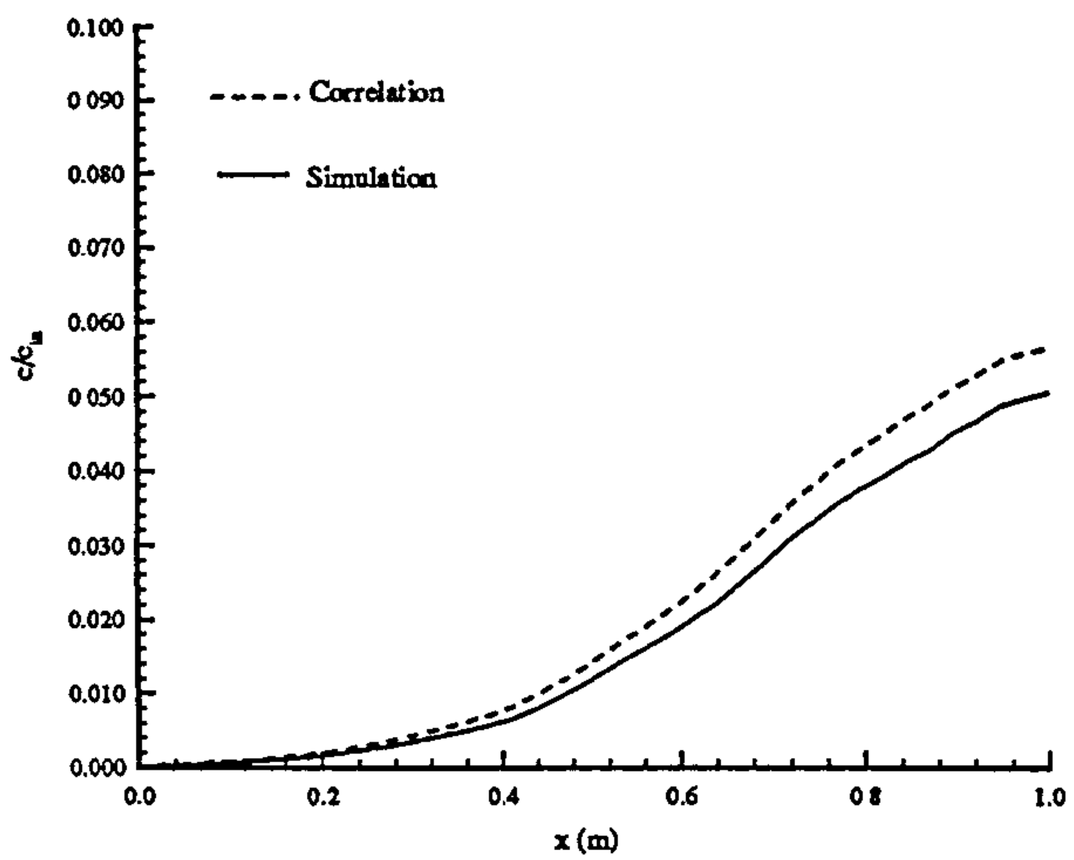

(c) 3m Downstream

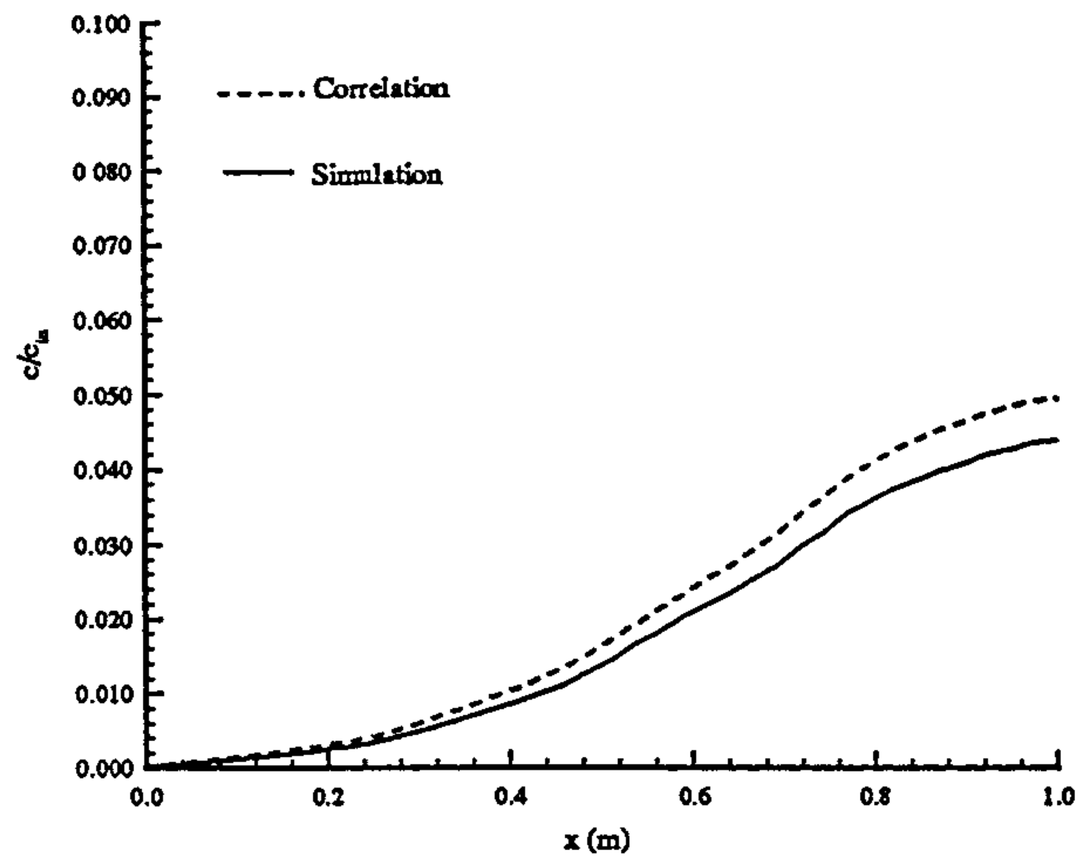

(d) 4m Downstream

Figure 6.8 : Comparison of Correlation and Simulation, Copper, Without $\langle u_p^2 \rangle$

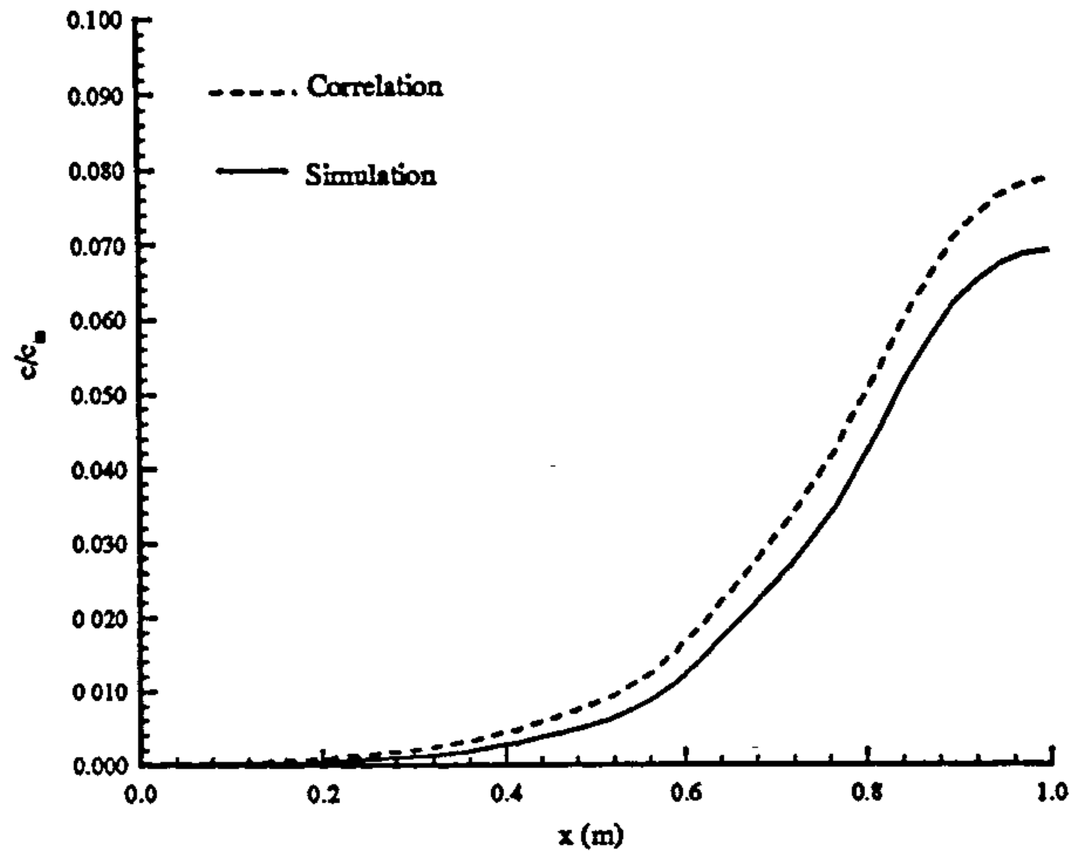

(a) 1m Downstream

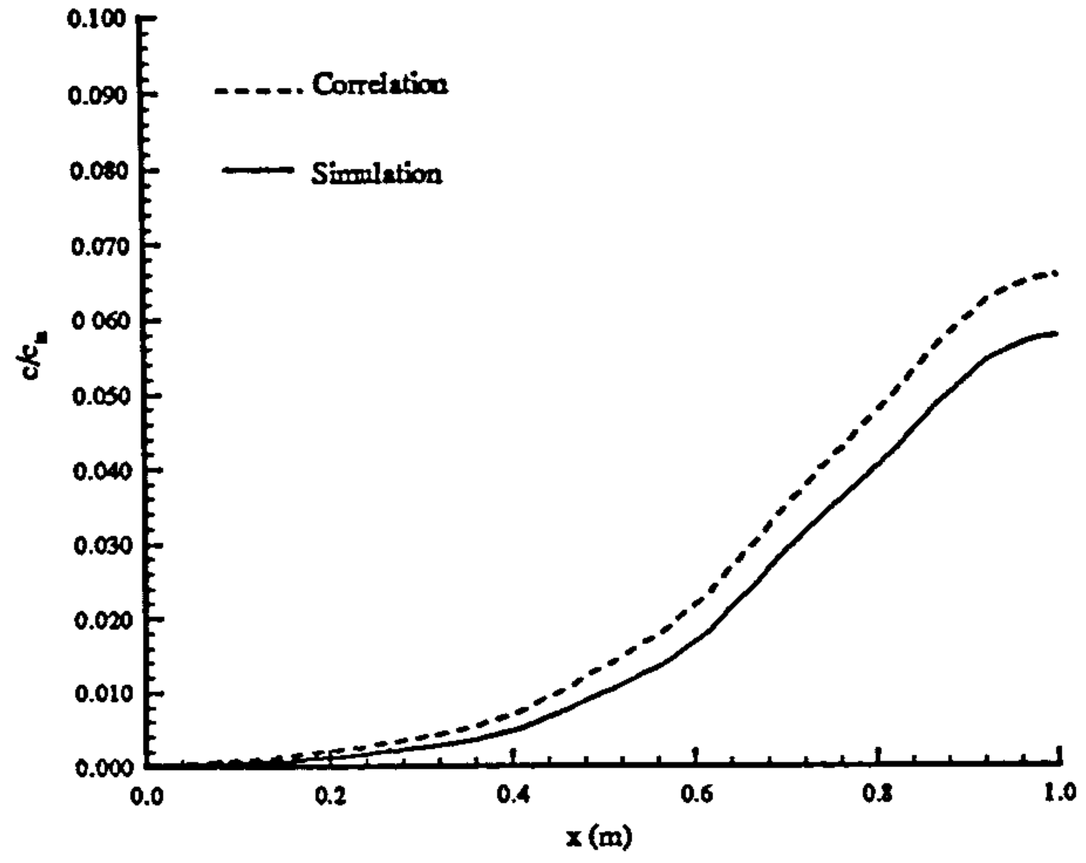

(b) 2m Downstream

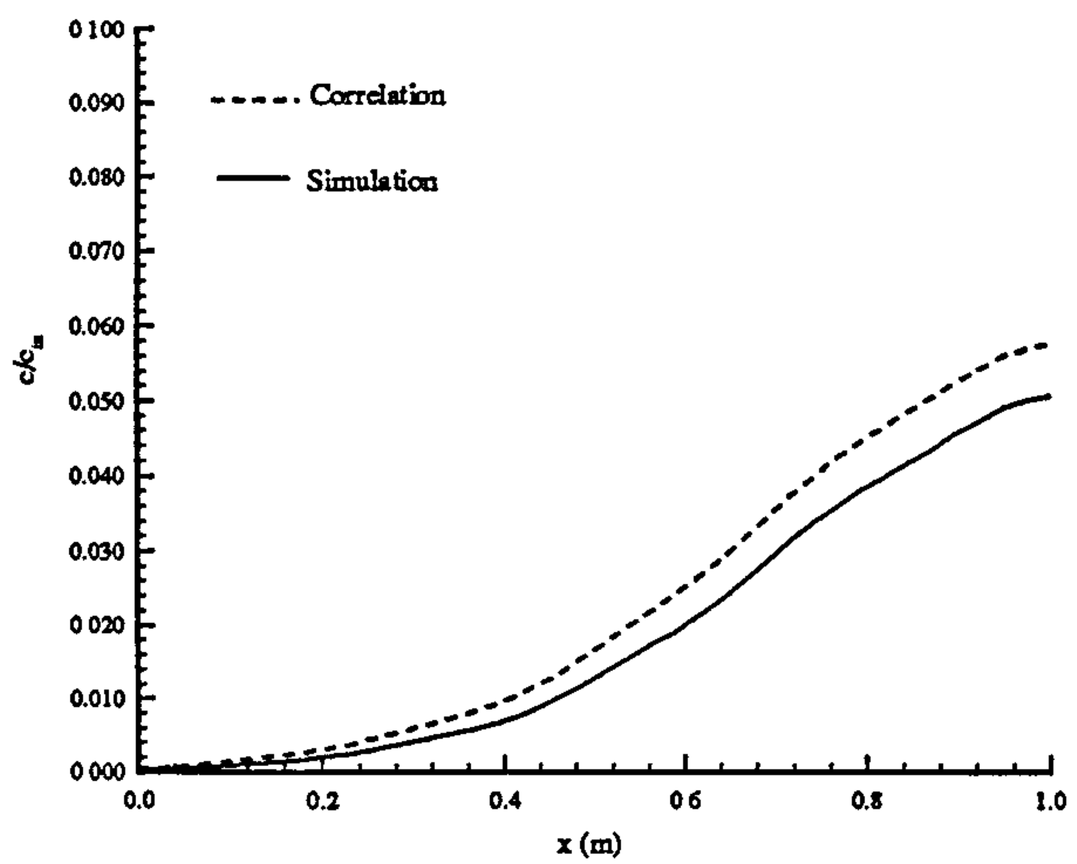

(c) 3m Downstream

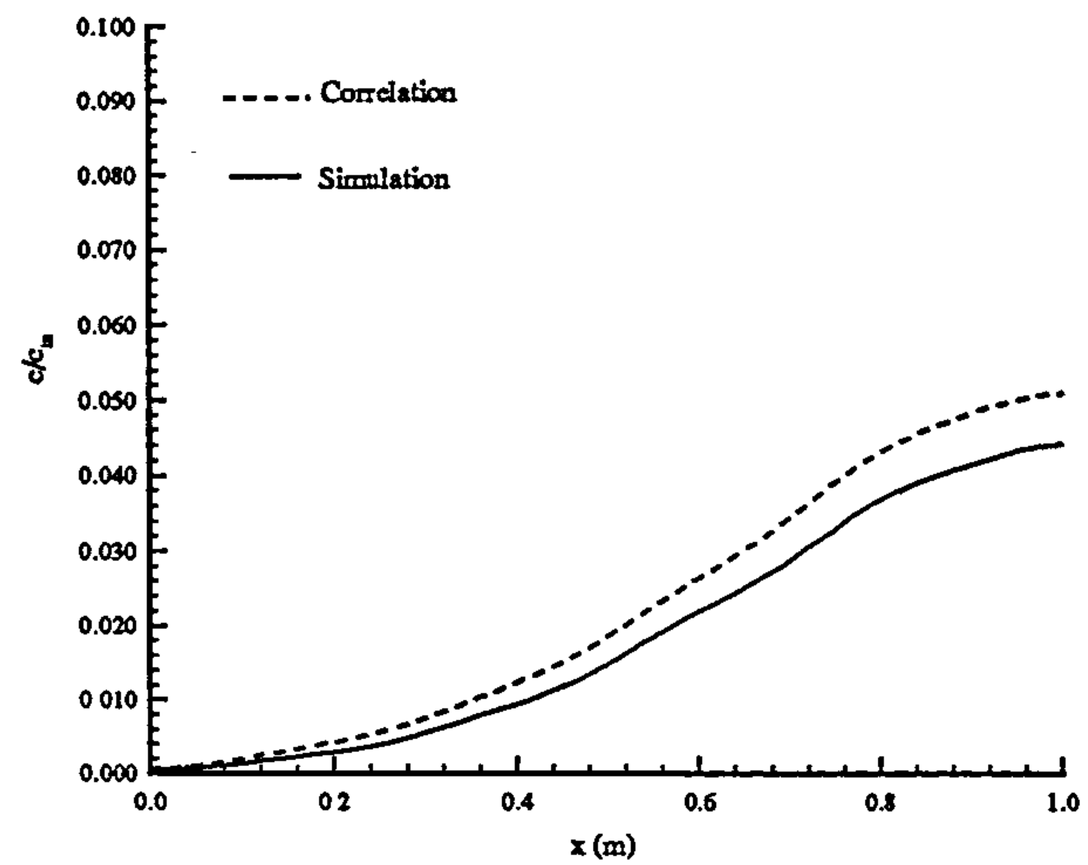

(d) 4m Downstream

Figure 6.9 : Comparison of Correlation and Simulation, Copper, With $\langle u_p^2 \rangle$

Chapter 7

Test-Case Calculations

7.1 Introduction

To evaluate the model developed in the previous chapters it is necessary to compare the calculations with available experimental data. To accomplish this two experimental test cases have been chosen for comparison.

The first case considered is that of a confined coaxial jet, Hishida and Maeda (1987), which was used as a comparative test case at the fifth workshop on Two Phase Flow Prediction at Erlangen, Germany in 1990 (proceedings (1990)), and enables comparisons to be drawn between not only the current model and the experimental data but also with a variety of prediction methods.

The second test case was that of particle dispersion in a horizontal wind-tunnel. The specific study considered is that of particle dispersion in homogeneous decaying grid turbulence with a uniform mean velocity, reported by Perkins, Vassilicos and Hunt (1994). This study also included a comparison of the experimental results and a range of Lagrangian based models, and again, this allows comparison with both the experimental data and the predictions.

The choice of test-cases was made on both the availability of the original experimental data and the previous comparisons with various models found in the literature. The selection enabled the evaluation of the current model in the frame of the other calculation methods. Due to the high flow speeds used and small measurement volume the first test-case contains only limited effects of diffusion as most transport of the particles is due to convection. The second test case, however, is much more demanding and, because of its horizontal orientation, allows a fuller investigation of crossing trajectory effects.

The two test case calculations are presented below.

7.2 Test-Case 1 - Confined Coaxial Jet

Test-case one is the experiment of Hishida and Maeda (1987) as used at the 5th workshop on Two Phase Flow Prediction.

7.2.1 Experimental Setup

The flow consisted of a vertical coaxial jet confined in a pipe of diameter 60 mm. The diameter of the internal tube was 13 mm. A schematic of the flow field is shown in figure 7.1. The inlet flow velocities for the two jets were an internal centre-line velocity of 30 m/s and an external velocity of 15 m/s. These relatively high velocities were chosen to avoid the presence of recirculation zones in the flow.

Measurement of both the single phase flow field and particle laden flow was accomplished by using a modified LDA system which allowed velocity measurements with particle size discrimination, Hishida et al (1984). The carrier phase flow field was established by introducing 1 μm alumina powder as trace particle into both inner and outer flow regions. The inlet velocity profiles for the first phase were shown to agree well with the 1/(6.6) th power law implying a fully developed inlet condition.

Two particle types were considered, their characteristics are given in table 7.1.

Particle	d_p (μm)	σ (μm)	ρ (kg/m^3)	τ_p (secs)	ϕ_p	M
Heavy Particle	64.4	9.5	2590	0.0328	1.4×10^{-4}	0.30
Light Particle	80.1	15.6	280	0.0055	1.4×10^{-4}	0.033

Table 7.1 : Particle Data from Hishida and Maeda

Measurements were taken at 4 downstream locations, 0, 65, 130, 260 mm from the jet orifice.

The use of two particle types of differing density and mass loading allowed

investigation of the effect of the particles on the turbulence in the carrier phase.

As this experiment was used for comparison at the workshop the conditions at the inlet are fully specified, which reduces errors in the final calculations arising from uncertainties in the inlet profiles.

7.2.2 Experimental Results.

The gas mean velocity distributions across the pipe were shown to have a Gaussian distribution. Introduction of the particles led to a reduction in the half width of the jet, compared with the single phase flow field at the same downstream location. The heavy particles were shown to have a larger velocity than the carrier phase downstream of the inlet, though the same situation was not observed for the lighter particles.

The velocity fluctuations of the continuous phase were reduced by the addition of the particles. This effect was more pronounced for the heavier particles. The Reynolds shear stresses were also shown to decrease with the addition of the particles. Again the reduction was larger for the heavier particles. Thus, the addition of the particles enhances isotropy in the carrier fluid.

An analysis of the data shows that the diffusive effects in the flow are low, due to the small amount of time the particles spend in the measurement region. Since the particles are injected with an axial velocity of approximately 28 m/s and the final measurement location is positioned only 260 mm downstream of the jet nozzle the time taken for the particles to leave the flow field is approximately 10 msces. This compares to a relaxation time of the heavy particles of 32.8 msecs thus the reaction of these particles to the turbulence is not observed in the measurement region. The corresponding relaxation time for the light particles is 5.5 msecs. Though this is less than the residence time within the measurement region the particle's reaction to the turbulent fluctuations and therefore radial diffusion will be small. Thus the test-case is most useful for validating that part of the model describing convective transport of the particles.

Therefore it would be possible to model the experiment using a simple tracking calculation where only convective effects are considered, as this approach should lead to

answers comparable to the more complex models, described below.

7.2.3 Comparative Models

The results of comparison between a large range of models and the above experimental data were reported at the fifth workshop on two-phase flows. Both Eulerian and Lagrangian methods were presented. Three specific models are considered here; two based on Lagrangian methods and one on Eulerian methods. The models were chosen since a virtually complete set of calculated data is available for both particle types, unlike many of the other models, and a detailed description of each model is available. An overview of the main characteristics of these models is given in table 7.2.

First the Lagrangian model due to Desjonqueres, Berlemont and Gouesbet (hereafter referred to as BERLEMONT) is discussed first. The model was based on the work of Berlemont et al (1990). The primary phase turbulence was modelled using a standard k-ϵ turbulence model for mean quantities and an algebraic second order closure scheme to obtain the fluctuating velocity correlations. Additional source terms arising from the particle modulation of the turbulence were included. Discrete particle behaviour was obtained by integration of the particle equation of motion for a statistically stationary sample. The required instantaneous flow field, at the particle location, was found from an Eulerian correlation which was modified to take account of crossing trajectories by the introduction of a correlation scale. This scale defined the distance within which a particle was correlated with its corresponding fluid particle (i.e. a fluid particle started with the same initial conditions as the particle). Once the particle deviated from its corresponding fluid particle by this length scale a new coincident fluid particle was defined. These fluid particle trajectories were obtained through the specification of the fluid point Lagrangian autocorrelation function. These autocorrelations were defined using a family of Frenkiel functions, Frenkiel (1948).

The Eulerian model considered here is due to Simonin (denoted by SIMONIN) based on the work of Simonin and Viollet (1989), (1990). The turbulence field of the continuous phase was predicted using a k-ϵ eddy viscosity model with additional terms to

account for the interaction between the two phases. A drift velocity was introduced arising from the correlation between the instantaneous distribution of the particles and the turbulent fluid motion to account for the dispersion effects arising from fluctuation in the momentum transfer term, and was taken to be proportional to the dispersion coefficient.

Finally the Lagrangian model of Wenneberg (denoted by WENNEBERG) was considered, based on the earlier work of the author, Wenneberg (1989). The code used to solve for the continuous phase allowed application of a wide range of discretisation schemes, skew upwind differencing was used for the test-case calculations. The code also allowed the use of either a k-ϵ or algebraic Reynolds stress (ASM) turbulence model. The test-case calculations were performed using a modified k-ϵ model, with additional source terms to account for two-way coupling effects. The particle turbulence interaction was performed using a discrete eddy model with the characteristic scales of the eddy obtained from the relations given by Shuen (1985). The particulate phase was modelled using Lagrangian tracking. The inertial interaction time was taken to be 0.3 times the turbulent time scale. The minimum of this time and the particle crossing time was taken as the particle-eddy interaction time. Each particle iteration step considered typically 1,000-2,000 particles. The particle calculations were performed every 10-15 carrier phase iterations to allow for the inclusion of two-way coupling effects.

Model	Modelling Approach	Turbulence Model	Two-Way Coupling
BERLEMONT	Lagrangian	Modified k-ϵ	Yes
SIMONIN	Eulerian	Modified k-ϵ	Yes
WENNEBERG	Lagrangian	Modified k-ϵ	Yes

Table 7.2 : Properties of Models used for Comparison.

7.2.4 Comparison between Models and Experiment

First the results of the models discussed above are presented and compared to the

experimental data for both the carrier fluid and each particle type. The results of the transport model are given in section 7.2.5 and measured against the experimental data and the best of the models outlined above, thus allowing direct comparison of the performance of the transport model with that of other models found in the literature.

Comparisons of the numerical predictions, from the above models, were made with the experimental data for three downstream locations; x/D = 5, 10 and 20 (corresponding to distances of 65, 130 and 260 mm from the jet nozzle). The results are plotted, where available, in figures 7.2-7.15. First comparison is drawn between the measured and predicted gas velocity profiles figures 7.2-7.5. The mean and fluctuating velocities are presented both axially and radially. Only the gas flow field for the heavy particles (case 1) is reproduced here, since this was the experimental flow field used throughout the current calculations, as this flow field is expected to exhibit greater effects of the particle on the turbulence than the case of lighter particles (case 2), both due to the greater particle loading and the increased particle density. Figures 7.6-7.10 present comparison of particle characteristics for the heavy particles. Both mean and fluctuating particle velocities are shown together with particle mass flux.

For the light particles only the particle characteristics are presented. The single phase flow field being very similar to that for case 1, as the difference lies well within the error observed in the flow field solution algorithms (see below). Again particle mean and fluctuating velocities together with particle mass flux are given, figures 7.11 to 7.15.

The results of the calculations compare favourably with the experimental data, giving an error of approximately 10% throughout, though significant discrepancies were found between the experiment and predictions for the particle mass flux calculations for both particle types. Overall agreement between the models was also good, again of the order of 10%. A more detailed discussion of the results is given below.

7.2.4.1 Gas Flow Field

Mean gas velocity profiles for case 1 (solid glass) are shown in figures 7.2-7.3. The calculated axial velocity profiles show a significant over-prediction of velocity, about 13%,

outside the jet core, though the core velocities are generally well predicted. As a result the jet spread rate was generally over-predicted. These differences could be due to variable flow rate in the experiment, which is often observed in axisymmetric flows. More pronounced discrepancies are found in the predictions for the mean radial gas velocities. The predictions all fail to capture the sharp changes in gradient measured in the experiment. It was proposed that the shape of the inlet nozzle used in the experiments induced a inward velocity on the flow resulting in a slower mixing of the two jets. This effect was not included in any of the models and would result in slowing the spread of the jet further explaining the differences in the mean axial velocity profiles. The gas axial velocity fluctuations, figure 7.4, show an example of the well-known deficiencies in the standard k-ϵ turbulence model. The velocities were slightly under-predicted in the core region of the primary jet and fail to capture the interface between the two jets. This error is consistent throughout the calculations and arises from the inability of the k-ϵ turbulence model to accurately capture the mixing layer. In general the agreement was surprisingly good. The radial velocity fluctuations of the carrier phase (figure 7.5) were in very good agreement, typically less than 10%, with the experiment for all of the prediction methods presented.

The gas flow field predicted by the models agrees with that measured to a satisfactory level (of the order of 10%) for all relevant flow characteristics apart from the axial fluctuating velocity. The discrepancies can be explained by a combination of un-modelled effect at the inlet and the use of the relatively simple k-ϵ turbulence model used by all the above authors.

7.2.4.2 Case 1 -Heavy Particles

Figures 7.6-7.10 show the results for the heavy particles (solid glass). The calculated mean axial particle velocities show a similar over-prediction to that observed for the gas phase, as above, and, similarly, results in a significant over-prediction of the jet spread. The discrepancies between the calculated and measured profiles, thus become greater further downstream. The observed error at the first measurement location is relatively small (~2%), which increases to ~15% at the second downstream location, at the final measurement point

the predicted profiles disagree markedly with those measured giving a difference of upto ~20%. However the centre-line prediction is good for all downstream locations. The higher predicted spread of the jet can further be seen in radial mean velocity plot (figure 7.7). Consequently, higher particle velocities were predicted in the region outside the jet core. Again the discrepancy between measured and predicted values increases further downstream, from ~1% at x/D=5, ~30% at x/D=10 up to ~40% at x/D=20.

Both of the plots for the fluctuating particle velocities (figures 7.8 and 7.9) show considerable error, up to ~30% in both cases. All of the presented models have difficulty in capturing the structure found in the experimental data. However, the agreement seen in figures 7.9 and 7.10 is significantly better than that observed at earlier workshops.

Calculated and measured mass-flux profiles are shown in figure 7.10. Experimental data is not available for the second downstream location (65 mm). Significant differences between the predicted and measured profiles are visible, as can large differences between the predictions of different models. The models of BERLEMONT and WENNEBERG significantly under-predict the measured value by up to ~30%. Conversely, the Eulerian model of SIMONIN matches the experimental data much more closely, though a slight under-prediction of the spread can be seen for the largest downstream distance.

Overall the presented models give a good account of the dispersion of the particles. Differences found in the gas phase calculations and measurements, which tend to an over-prediction of the spread of the jet, persist through the second phase calculation, as is to be expected. The mean behaviour of the heavy particle is well predicted but all the models fail to capture the structure found in the experiment for the particle fluctuating velocities.

7.2.4.3 Case 2 - Light Particles

The flow field calculations for this particle type are not presented here. The results are virtually identical to those given for above. It should be noted however that the predicted mean axial velocities show a slight improvement over those for case 1. This is probably due to the reduced influence of the particulate phase on the gas flow field and implies that the difficulty lies in the models used to calculate the effect of the two-way coupling on the

carrier phase.

The particle mean velocities are again very close to those measured though still slightly over-predicted (figures 7.11 and 7.12). The predicted mean axial velocities agree closely with those measured for all downstream locations leading to a maximum error at x/D=20 of only ~1%. The particle mean radial velocities again show a much larger difference than found in the axial direction. The agreement however is significantly improved over case 1.

The particle axial velocity fluctuations (figure 7.13) are again considerably under-predicted for the case of light particles with a similar error to that found in case 1. A similar discrepancy can be seen in the radial fluctuating velocities (figure 7.14).

The particle mass-flux calculations, figure 7.15, are shown to significantly over-predict the measured data. Experimental data is only available here for the last two measurement locations. All of the considered models show a large discrepancy (varying from ~40 to ~100%). Again the Eulerian model of SIMONIN is shown to give the closest agreement with the experimental data.

The mean behaviour of the particles for case 2 is again well captured, with agreement slightly better than for the heavy particle of case 1. Also the structure of the fluctuating particle velocities is better captured by all the models, which implies that the lighter particle react to the fluid fluctuations more so than the heavier particles. The particle mass-flux, however is poorly predicted. It is proposed in the proceedings of the workshop that this may be due to difficulties in measuring this quantity in the experiment, proceedings (1990).

The models discussed above predict the experimental results well, typically to an accuracy of ~10%. However, from figures 7.2-7.15 it is clear that the predictions of the Eulerian model of SIMONIN show the highest level of agreement with the experimental data. Therefore, this model has been chosen for comparison with the transport model in order to directly evaluate its performance against other modelling techniques. These calculations are thus shown in figures 7.16-7.24, together with the results of both the transport model and the experimental data.

The following section presents an evaluation of the predictions of the transport

model compared with both the experimental data and the predictions of SIMONIN. The transport model is shown to predict both the carrier phase flow field and the behaviour of both particle types to an accuracy comparable to that of SIMONIN.

7.2.5 Transport Model Calculations

The predicted profiles for both the gas phase (case 1 only) and both particle types are given in figures 7.16-7.24.

The flow field was calculated using the pressure correction code discussed in chapter 4. A k-ϵ turbulence model was used with the coefficients C1 and C2 chosen to allow best possible fit between the calculations and experiment. The chosen values were C1=2.5 and C2=2.55 compared to their standard values of C1=1.44 and C2=1.92. The use of the fitted coefficients allowed the effect of the particles on the gas phase to be included, to some extent, in the single phase calculation. Choice of these values of the coefficients was made to allow best possible fit with the measured flow field. The same flow field was used for both particle types, namely that of case 1.

The calculations for the second phase used the formalism outlined in chapter 5 and 6. The empirical correlation, equation (2.18), was used to compute the required diffusion coefficients of the particles.

First the gas flow field results are discussed, figures 7.16-7.18. Only the flow field for the case of heavy particles is calculated due to the close similarity between the two experimental flows, and the lack of a direct two-way coupling calculation, however the effects of the particles on the carrier fluid are included intrinsically through the specification of the coefficients in the k-ϵ turbulence model.

The results of the calculation for case 1 (heavy particles) are shown in figures 7.19-7.21. Only mean particle velocities are presented because the correlation used to compute the diffusion coefficients of the particles is unable to accurately describe the fluctuating particle velocities, see chapter 6.

Finally, figures 7.22-7.24 present the results of the calculations for the light particles. These results are discussed in more detail below.

7.2.5.1 Gas Flow Field

The comparisons between the calculated and measured flow fields are shown in figures 7.16-7.18. The plots for both mean axial and mean radial velocities are of comparable accuracy to those shown previously.

The resulting mean axial velocity profiles are shown in figure 7.16. The profile at x/M=5 downstream slightly under-predicts the centre-line velocity and over-predicts the velocity in the exterior region, both differences are of the order 2 m/s (~10%) . At x/M=10 the centre-line velocity is well captured but the exterior region remains over-predicted, again by ~10%. Finally at x/M=20 the centre-line velocity is over-predicted by about 2 m/s (~ 10%) and this error is consistent across the whole profile. The level of agreement between the two calculation procedures is acceptable and implies that the use of fitted values for C_1 and C_2 in the k-ϵ turbulence model closely approximate the results for the coupled calculation, as used by SIMONIN.

Figure 7.17 shows the mean radial velocity profiles. Initially the large peak velocity at the interface between the two jets is not well captured. This smoothing of the profiles is shown at all downstream locations. The results are comparable to those obtained in the model of SIMONIN. Both calculations are unable to capture the structure of the velocity profiles observed in the experiment, though the agreement between the models is again excellent. The discrepancies between the two calculations and the experimental data are probably due to an additional inwards radial velocity present in the experiment at inlet, as discussed above.

Figure 7.18 shows the predicted gas fluctuating velocity. Only the radial velocity is shown as the model used here is isotropic. The agreement between both calculations and the experiment is excellent for all downstream locations. The maximum observed difference between the calculations (which again agree well) and experiment is ~12% at the second measurement position. The accuracy of the calculation is especially important to the transport model as the correct prediction of the turbulent kinetic energy, together with the turbulent dissipation, is required to calculate the diffusion coefficients of the particles.

Overall the fit between the calculated and measured flow field is of a comparable accuracy to that achieved throughout the derivation of the model (~10%). Also the discrepancies found in both the mean and fluctuating gas velocity fields are comparable to the calculations discussed above. The agreement between the flow field calculations is expected due to the similar methods used, though the values of the coefficients C_1 and C_2 used in the turbulence model of SIMONIN are unsure.

7.2.5.2 Case 1 - Heavy Particles

First the calculation of the dispersion of the heavy particle is considered. Figures 7.19-7.21 show the calculated behaviour of the heavy glass particle. Again all the predictions show good agreement with the experiment and are comparable to those obtained from the other models

Figure 7.19 shows the particle mean axial velocity. The predictions are in good agreement with the measurements for all downstream locations. The calculated profile at x/M=5 is slightly more smeared than that measured, as a result of the inability of the carrier phase prediction to capture the shear accurately. The profile at x/M=10 slightly under-predicts the centre-line velocity by approximately 2 m/s (~10%) and this under-prediction is consistent across the jet. At x/M=20 the centre-line velocity is slightly over-predicted, again by approximately 2 m/s. Agreement improves as the radial coordinate increases leading to a slight under-prediction of the velocity at the extreme radial location. The predictions of both models disagree quite substantially for all given locations. The transport model is shown to more accurately capture the shape of the velocity profile than the model of SIMONIN, which tends to flatten out the profiles. Both models generally agree at the jet centre-line but the discrepancy becomes more pronounced the greater the radial position. The discrepancy arises from the variation in the predicted radial velocities of the particles, discussed below.

Calculated mean radial velocity profiles are shown in figure 7.20. The transport model again fails to capture the initial sharp peak in radial velocity, which leads to a predicted particle radial velocity which is too low. The agreement between the predicted and

measured profiles is therefore poor. The agreement improves downstream to the point at x/M=20 where the two profiles agree closely across the whole profile. The prediction of SIMONIN conversely captures the large velocity gradient well, though the predictions show a large degree of scatter in the exterior of the jet.

Figure 7.21 shows the calculated mass flux profiles. The poor agreement shown for the transport model is not surprising and follows from the poor account of the particle radial velocity profiles, which resulted in a poor description of the rate at which the jet spreads. The difference between the calculated and measured mass flux is of the order of ~20-~40%. The model of SIMONIN however captures the particle mass flux well, which as before arises from the ability of this model to correctly capture the steep radial velocity profile as shown in figure 7.20.

The inability of the calculation to correctly resolve the particle behaviour in the mixing layer leads to a much slower spreading of the jet in the calculation than found in the experiment. This in turn leads to an over-prediction of the particle mass flux. However, in general the predictions of the transport model are quite good.

7.2.5.3 Case 2 - Light Particles

The results of the calculation for the dispersion of light particles are presented here. Figures 7.22-7.24 show the comparison between the predicted and measured behaviour of the hollow glass particle. The same flow field is used as for the heavy particle case. The general agreement is slightly better than for the heavy particles, and is again comparable to the other models reviewed.

Figure 7.22 show the calculated and measured particle mean axial velocity. The discrepancy between the calculated and measured profiles is at most ~10% at x/M=10. The accuracy improves to ~5% for the last downstream location. No experimental data is available for x/M=5. Differences of up to ~15% can be seen between the two models. While the transport model under-predicts the measurements slightly at x/M=10 the model of SIMONIN gives an over-prediction. The shape and fit of the transport model curves are, in general, better than that shown by the other model.

Particle mean radial velocities are shown in figure 7.23. The fit for all locations is much better than obtained for the heavier particles which implies that the behaviour of the light particle is better captured by the transport model, again no experimental data is available for x/M=5. The shear region is still slightly smeared by the calculation but the predicted radial velocity is much enhanced. The model of SIMONIN greatly over-predicts the particle velocity at all locations.

Finally the particle mass flux profiles are given in figure 7.24. The initial profile is similar in form to that given for case 1. The predicted mass flux profiles for both models agree closely. The profiles, however, greatly over-predict the measured curves, experimental data is only available for the last two downstream locations. The discrepancy between the calculations and measurements is of the order of ~100%. Figure 7.15 shows that this difference is found in all the models considered.

Generally the velocity predictions for the light particle of case 2 agree better with the experimental data than is the case for case 1. However, this is not true for the mass flux profiles. All the models considered here greatly over-predict this quantity, and the consistency between the models points to either a potential error in the experimental data or an effect not considered in any model. Also, there is some doubt as to whether the initial profile supplied for the workshop calculations is as specified in the experiments or simply the application of a self similar profile to that found in case 1. This potential error in the inlet conditions would account for the observed discrepancy.

7.2.6 Discussion of Results

The results presented above for the prediction of particle behaviour in a confined coaxial jet are good for most of the calculated velocity profiles, though poor for the radial velocity profiles of case 1, and both the mass flux profiles. The results, however, are comparable to the other calculation methods presented at the two-phase flow workshop.

The calculated gas field gives a good approximation to that measured, through the varying of the turbulence model parameters to obtain the required flow field. Also, it can be seen from the comparison of figures 7.2, 7.3 and 7.6 and 7.7 that the assumption of a

single flow field for both particle types was valid.

Calculated axial velocity profiles, figures 7.16 and 7.19, were shown to give excellent agreement with those measured. The radial velocity profiles however failed to correctly capture the large particle velocities in the mixing region. The large gradients of radial velocity of the particles found in this shear region were significantly smoothed by the calculation method. The error was greater in the case of the heavier particles, since the effect of the fluctuating radial gas velocities, which dominates over transport by the mean radial velocity, is much smaller for this particle type than for the hollow glass particle due to inertia effects. The under-prediction of the particle radial velocity lead to a corresponding under-prediction of the jet spread rate.

The mass-flux calculations are consequently over-predicted. For the case of the light particles the observed error is systematic in all calculation methods. As a result it may be reasonable to speculate that the experimental measurements are in error and are systematically low. The difference between the calculated and measured profiles could also be further influenced by the unsure initial conditions.

In conclusion the calculations of the transport model presented here show comparable agreement with those models presented at the two-phase flow workshop. The three models chosen for comparison were shown to have the best performance of all the models presented at the workshop, (see proceedings(1990)). The transport model performs well in comparison.

As mentioned above, the small residence time of the particles in the measurement region implies that the dispersive effects experienced by the particles are small, and therefore the above comparisons do not test the model fully. This said the above test-case provides a useful test of the convective calculation contained in the model. The above results show that these convective effects are indeed well captured by the transport model.

The second test-case discussed below was specifically chosen to further investigate the effects of particle dispersion in the model.

7.3 Test-Case 2 - Horizontal Channel Flow

Test-case 2 consists of part of the work of Perkins, Vassilicos and Hunt (1994), which is concerned with the transport of aerosols through a Light Water Reactor (LWR) cooling system. To this end various properties of the processes involved are discussed.

The portion of the work of interest here is the experiment concerned with the dispersion of particles dropped vertically, under the influence of gravity, in a horizontal, grid generated, turbulent channel flow. An attempt was also made to investigate the effect on dispersion of the interaction of particles and the wall boundary layer, this being of interest in particle deposition.

Only the simple case of the particle transport by homogeneous, isotropic decaying turbulence is considered here.

Perkins et al also compared their experimental results with the predictions of various Lagrangian tracking models. Thus, it is possible to compare the present model not only with the test data, but also with the results of these models and hence to measure it against their performance, in a similar manner as before.

7.3.1 Experimental Setup

The experiments were performed in a horizontally orientated wind tunnel, as shown in figure 7.25. A suction tunnel with a cross-section of 0.45 m × 0.45 m and with a working length of approximately 2.13 m was used. Air was drawn through a large intake with a honeycomb flow straightener followed by a 9:1 contraction. The free-stream velocity, U_∞, could be varied between 1 and 12 m/s. Turbulence generating grids were introduced upstream of the working section with mesh spacing of 2.5 cm to 15.2 cm to select turbulence intensities over the range 2-15%.

Two types of particles were considered - hollow glass spheres and solid glass spheres, see table 7.3. Sieving was used to obtain particle nominal diameters of 131 μm with a standard deviation of approximately 6 μm.

Particles were discharged into the flow at a position 0.954 m downstream from the

grid, at varying heights, and collected in trays positioned on the floor of the wind tunnel. The trays spanned the width of the tunnel and had a square section of 15 mm. 32 trays were used, giving a measurement length of 0.48 m. Prevention of particle re-suspension and boundary layer change due to possible recirculation within the trays was avoided using a 3 mm porous aluminium honeycomb at the tray openings.

Particle	Diameter (μm)	Density (kg/m^3)	Terminal Vel. (m/s)
Hollow Glass	131±6	730	0.295
Solid Glass	131±6	2830	0.916

Table 7.3 : Particle Properties from Perkins et al

Fluid velocity measurements were obtained using LDA techniques. Particle seeding was performed using 0.6 μm to 2 μm oil droplets with a density of approximately 980 kg/m^3.

The particles were injected with a velocity equal to the mean flow velocity in the streamwise direction. The particle flow rate was kept small both to avoid particle-particle interactions and turbulence modulation due to the presence of the particles.

7.3.2 Gas Flow Field

All experiments were conducted using a grid of mesh length 2.54 cm and a blocking factor of 4.0. The decay of the turbulence energy was measured for 3 free-stream velocities (1,2, and 5 m/s). These measurements were compared with the empirical decay formula of Baines and Peterson (1951)

$$\left(\frac{u'}{U_\infty}\right)^{-2} = 52.1\left(\frac{x}{M} - 16\right) \qquad (7.1)$$

(where U_∞ is the freestream velocity) and shown to give good agreement.

Mean velocity profiles were measured at five downstream distances (x=0.915, 1.22, 1.524, 1.829 and 2.032 m) and three free-stream velocities (U_∞=1, 2 and 5 m/s). Growth of

the boundary layer was noted and shown to agree with empirical correlations. Fluctuating velocity profiles within the boundary layer were also measured and coefficients obtained for suitable empirical forms.

7.3.3 Deposition Experiments

Five deposition experiments were conducted for various particle types, release heights and free-stream velocities, see table 7.4. Particle concentration profiles were measured at the floor of the wind tunnel. The mass of particles collected in each tray was normalised by the total particle mass released and averaged over the width of the tray. For all of the following calculations the effect of the boundary layer on the particle dispersion is neglected. The implications of this simplification are discussed later.

Expt.	d_p (μm)	ρ_p (kg/m^3)	h_{rel} (m)	U_∞ (m/s)	u' (m/s)
D1	131	730	0.255	1.0	0.05
D2	131	730	0.125	2.0	0.1
D3	131	2830	0.4	1.0	0.05
D4	131	2830	0.32	2.0	0.1
D5	131	2830	0.1	5.0	0.25

Table 7.4 : Deposition Experiments

The deposition profiles measured in the experiment were compared with a range of Lagrangian models, namely those due to Hunt & Nalpanis (1985), Berlemont et al (1990) (see previous test-case), Ormancey & Martinon (1984) and Kallio & Reeks (1988). All the Lagrangian models used required the estimation of some parameters such as the integral time scale which could not be measured in the experiments. It was proposed that the estimation of the required parameter is intrinsic in the models and therefore that the ease of obtaining the required parameters should be considered as part of the assessment of the performance and suitability of the model.

In the implementation of the above models, for uniform homogeneous turbulence,

i.e. the case considered here, the integral length scale, L, was assumed equal to the mesh size and the turbulence intensity to be 5%. The integral time scale was thus estimated from L/u'. This led to an assumption of the typical eddy characteristics being equal to the integral scale. The number of particles tracked for each model during each experiment are given in table 7.5.

Model	D1	D2	D3	D4	D5
Hunt & Nalpanis	4000	7000	8000	10000	10000
Gouesbet et al	700	2000	8000	10000	10000
Ormancey & Martinon	4000	7000	8000	10000	10000
Kallio & Reeks	10000	10000	8000	10000	10000

Table 7.5 : Number of Particles Tracked per Experiment

The predicted deposition profiles, together with those from the experiment and transport model are plotted in figures 7.26-7.30. The results from the four Lagrangian models agree well with each other for experiments D1-D4. For D5 a larger spread is shown between the predicted results. The predictions disagree markedly with the measured deposition profile for experiment D1, fit the measured data poorly for experiments D2, D3, and D5 and agree very well for experiment D4.

The discrepancy between the simulations and experiments is greater for the lighter particles (expt. D1 and D2). Figures 7.26 and 7.27 show that the experimental data produced a much more smeared concentration profile with a much greater degree of asymmetry. It was proposed that these discrepancies could arise from the differences between the measured flow field and that used in the models. Further calculations were made using the measured flow field properties and the agreement between the simulations and the experiments was only slightly improved. It was also proposed that uncertainty over the initial conditions to apply to the particles in the experiment could lead to errors.

In the following section comparison is made between the current transport model and both the experimental measurements and the Lagrangian simulation results of Perkins

et al.

7.3.4 Flow Field Calculation

Due to the well-prescribed decay behaviour of a grid generated channel flow the flow field, together with the k and ϵ distributions, were modelled analytically.

The mean profiles given by Perkins et al, show a virtually constant mean flow velocity at the centre-line over the region of interest. Therefore, the flow was approximated by a constant mean velocity. The effect of the boundary layer on the particle dispersion is therefore neglected, and is consistent with the comparison calculations made by Perkins et al; the implications are discussed later.

The decay of grid generated turbulence has been investigated extensively in the literature Batchelor (1953), Townsend (1956), Snyder and Lumley (1971), among others. Many empirical correlations exist which relate fluctuating velocities to downstream distance. The one chosen here is due to Wells and Stock (1983) and is used to represent isotropic turbulence.

$$\frac{U_\infty^2}{u'^2} = 54.88\left(\frac{x}{M} - 7.989\right) \qquad (7.2)$$

Equation (7.2) is only valid for positions downstream of the virtual origin of decay, x_0. The distance of the onset of decay from the grid varies with Reynolds number. Wells and Stock give a curve (from Naudaskhar and Farsel (1970)) specifying this origin as a function of grid spacing and Reynolds number. The data was curve fitted to enable the calculation of x_0/M for the flows considered. The fluctuating velocities were assumed constant and equal to the turbulence intensity (5%) upstream of this point. Downstream of the decay point they were specified by (7.2). Again a uniform profile was assumed across the channel.

From the above assumptions of homogeneous turbulence and a constant velocity profile the turbulence-energy equation reduces to, Hinze (1975):

$$\frac{dk}{dt} = -\epsilon \tag{7.3}$$

making the transformation:

$$\frac{d}{dt} = U\frac{d}{dx} \tag{7.4}$$

gives

$$\epsilon = -U\frac{dk}{dx} \tag{7.5}$$

Equation (7.5) was used to calculate the dissipation field present in the flow. This together with

$$k = \frac{3}{2}u'^2 \tag{7.6}$$

allows the specification of the k and ϵ distributions required for the calculation of the diffusion coefficient of the particle.

7.3.5 Particle Dispersion Calculation

Using the flow field and k-ϵ distributions calculated above, the model described in chapters 5 and 6 was used to obtain the concentration profiles and velocity field for the second phase.

Figures 7.26 through 7.30 show the predicted deposition profiles for the above experiment. The calculated profiles are in fair agreement with the experimental data for all cases. The calculated locations of the peak concentration are generally well predicted for all cases, but, the spread of the profile is generally over-predicted.

Figure 7.26 shows the results for experiment D1. The predicted location of the peak concentration profile is well predicted as is the general shape of the deposition profile. The

predicted spread however is greater than that found in the experimental data. The predicted half-width of ~0.2 m compares to a measured half-width of ~0.15 m, leading to a difference of approximately 25%. The peak concentration (per metre), is approximately 40% higher, and is in better agreement with the experimental data than the Lagrangian models, which differ by up to 400%. Though they capture the position of the peak concentration well they exhibit a much narrower distribution.

Figure 7.27 shows the results for experiment D2. Again the location of the peak concentration is well captured as is the general shape of the profile. The width of the distribution is still over predicted (a half width of ~0.3 m for the calculation compared to ~0.2 m for the measurements, an error of ~50%). The predicted peak concentration is within 10% of that measured. The Lagrangian calculations still over-predicted the maximum value of concentration, by up to 40%, however, the width of the distribution is much closer to that of the experiment than for D1.

Results for D3 are given in figure 7.28. Both the location and magnitude of the peak deposition are again well predicted. The width of the distribution and its shape are also very similar to those measured. The half-width of the calculations is ~0.1 m which is very similar to the experimental half-height of ~0.08 m (~20% error). The difference in peak concentration is also small and of the order of 10%. Although the Lagrangian models again capture the location of the peak concentration well, poor agreement is shown for the magnitude, which is over-predicted by ~40%. The width of distribution predicted by these Lagrangian models is also narrower than that measured, as in the previous cases.

Figure 7.29 shows the results for case D4. The transport model again predicts the location of the peak concentration well but fails to capture both the correct magnitude and width. The predicted half-width of ~0.17 m compares to that measured of ~0.1 m (60% error). Similarly, the peak predicted concentration over-predicts that measured by ~12%. Conversely, the Lagrangian models under-predict the peak concentration by a similar amount (~12%). The Lagrangian models also predict the location of the peak and the half-width well. It should be noted that this is the case of optimal fit for the Lagrangian models.

Results for the final experiment, D5, are given in figure 7.30. All the calculations fail to predict the correct behaviour shown in the experiment. The transport model performs

best, though only the shape of the profile is predicted well. The location of the peak concentration is under-predicted by approximately 0.1 m. Also, the peak concentration is over-predicted by approximately 30%. In contrast to the Lagrangian models which under-predict the peak concentration by ~50% and the location of this peak by ~0.3 m.

Figures 7.26-.30 clearly show that the transport model performs better than the Lagrangian calculations, for all experiments. In general the location of the peak measured concentration is well predicted, as is the shape of the deposition profile. The half-width of the distribution is over-predicted for all cases, though the error throughout is relatively small. A possible reason for this is the presence of numerical dispersion due to the simple quadrature scheme implemented in the code. This possibility is discussed in the next section. The transport model is further shown to capture the magnitude of the peak concentration well with typically an error of less than 30%. Conversely, the Lagrangian models fail to capture this value for most cases and give an error of up to 400%.

7.3.6 Discussion of Results.

Overall the transport model can be seen to predict the measured deposition profiles much more accurately than the Lagrangian models reported by the Perkins et al. The ability of the transport model to correctly predict the location of the peak concentration shows that the inertial effects of the particles are well captured, as in the previous test-case. Over-prediction of the profile widths implies a possible error in the diffusive calculation. As mentioned above this may be due to numerical dispersion arising from the low order discretisation scheme used in the calculation.

The problem of numerical dispersion is present in many CFD approaches. The specific problems encountered in the SIMPLER algorithm, and its associated discretisation scheme, have been discussed by Patanker (1980). Numerical dispersion is can be considered a function of the incidence angle between the flow and the cell boundaries. An approximate expression for the corresponding false diffusion coefficient for two-dimensional situations developed by de Vahl Davis and Mallinson (1972) gives:

$$\Gamma_{false} = \frac{\rho U \Delta x \Delta y \sin 2\theta}{4(\Delta y \sin^3\theta + \Delta x \cos^3\theta)} \tag{7.7}$$

where U is the resultant velocity and θ is the angle made by the velocity vector with the coordinate direction. Because this numerical dispersion depends on the incidence angle between the second phase flow field and the computational grid the size of the effect will differ between the experiments D1-D5. It is also possible to reduce this effect by using a more refined grid, which also adds considerably to the calculation time.

In order to investigate the influence of this false dispersion on the calculations presented above it is useful to know the mean incidence angle between the second phase flow field and the calculation grid. A good estimate of this angle can be found by considering particle trajectories based on a straightforward ballistics calculation. Applying this simplification allows the incidence angle, θ, to be calculated from, see figure 7.31

$$\tan\theta = \frac{gt}{U_g} \tag{7.8}$$

where g is the gravitational acceleration, t is the time of flight and U_g is the mean downstream convection velocity (assumed equal to the gas velocity). Since we always require the minimum angle between the trajectory and the grid equation (7.8) becomes

$$\tan\theta = \begin{cases} \dfrac{gt}{U_g} & \dfrac{gt}{U_g} < 1 \\ \dfrac{U_g}{gt} & \dfrac{gt}{U_g} > 1 \end{cases}$$

The cut-off angle of $\pi/4$ occurs when $t = U_g/g$ hence

$$\theta = \begin{cases} \tan^{-1}\left(\dfrac{gt}{U_g}\right) & \dfrac{U_g}{g} \geq t > 0 \\ \tan^{-1}\left(\dfrac{U_g}{gt}\right) & T \geq t \geq \dfrac{U_g}{g} \end{cases} \tag{7.9}$$

where T is the time of flight needed for the particle to leave the calculation domain (due to gravity) and is given by

$$T = \sqrt{\frac{2h}{g}}$$

where h is the particle release height.

The mean incidence angle can thus be obtained by integrating (7.9) over time. This leads to

$$\bar{\theta} = \begin{cases} \dfrac{1}{T}\displaystyle\int_0^T \tan^{-1}(g\,t/U_g)\,dt & U_g/g \geq t \geq 0 \\ \dfrac{1}{T}\left\{\displaystyle\int_0^{U_g/g} \tan^{-1}(g\,t/U_g)\,dt + \int_{U_g/g}^{T} \tan^{-1}(U_g/g\,t)\,dt\right\} & T \geq t \geq U_g/g \end{cases} \qquad (7.10)$$

Performing this integration gives

$$\bar{\theta} = \begin{cases} \dfrac{1}{T}\left\{T\tan^{-1}(g\,T/U_g) - \dfrac{U_g}{2g}\ln\left|1+(g\,T/U_g)^2\right|\right\} & T \leq U_g/g \\ \dfrac{1}{T}\left\{T\tan^{-1}(U_g/g\,T) - \dfrac{1}{2}\ln\left|\dfrac{(U_g/g\,T)^2\,U_g}{2g}\ln|2| + \dfrac{1}{2}\ln\left|\dfrac{1}{2}\right|\right|\right\} & T \geq U_g/g \end{cases} \qquad (7.11)$$

Table 7.6 shows the results of applying (7.11) to the five experiments discussed above. Also shown is the mean particle diffusion coefficient used in the calculations, $\bar{\Gamma}_p$ the false diffusion, $\bar{\Gamma}_{false}$ obtained from (7.7) and the ratio of calculated to false diffusion coefficient. All calculation are for the grid size used in the calculations of 200×80 cells.

The data in table 7.6 shows that the influence of numerical dispersion is small for all cases except D2 where the ratio $\bar{\Gamma}_p/\bar{\Gamma}_{false}$ is less than one. Though this would result in a slight over-prediction of the profile half-width, the error would be small as the half-width depends on the square root of the diffusion coefficient. It can be concluded, therefore, that the numerical effects on the particle dispersion are modest.

Experiment	$\bar{\theta}$ (°)	$\bar{\Gamma}_p$	$\bar{\Gamma}_{false}$	$\bar{\Gamma}_p/\bar{\Gamma}_{false}$
D1	9.5	9.8×10^{-3}	5.56×10^{-4}	17.6
D2	37.7	3.87×10^{-2}	5.19×10^{-2}	0.75
D3	8.0	3.19×10^{-3}	4.69×10^{-4}	6.80
D4	32.1	1.26×10^{-2}	4.30×10^{-4}	29.30
D5	15.5	7.90×10^{-2}	4.70×10^{-3}	16.81

Table 7.6 : Influence of Numerical Dispersion on Perkins et al Calculations.

The implications of neglecting the boundary layer are now discussed. The use of a logarithmic velocity profile across the channel would have the effect of reducing the gas velocity near the wall. This would cause the peak deposition profiles to move closer to the release point, and would increase the spread of the jet slightly due to the increased residence time of the particles in the flow. The particle diffusion coefficient would also change due to the variation of both kinetic energy and dissipation in the boundary layer. However, the size of these effects on the above data would be expected to be small, the greatest influence being seen for the lighter particles (D1 and D2). In the case of D5, where the least influence would be expected, the time of flight of the particles is approximately 0.2 s which corresponds to only about twice the particle relaxation time. Therefore the particles response to the velocity gradient near the wall would be small. The maximum residence time of approximately 0.9 s is found in experiment D1 which is equivalent to roughly 30 times the particle relaxation time. Even in this case the largest change in velocity profile would occur in the final one or two particle response times. For example, assuming that the particle falls at a constant velocity the distance fallen by the particle in two response times is approximately 18 mm, which corresponds to ~90 wall units. From the data of Perkins et al it is shown that the mean streamwise velocity has only fallen to roughly 75% of the free-stream value at this point. Thus the velocity profile in the boundary layer can also only have a small effect on the particle dispersion.

It follows from the above discussion that the influence of neglecting the boundary

layer is small on both the convective and dispersive calculations within the transport model. The measured locations of the peak concentration are generally well captured implying that the convection calculation is accurate. Conversely, the observed over-prediction of the half-width of the distribution profiles implies a potential error in the diffusive calculation. However, it is possible that there exist un-modelled effects in the experiment arising from the influence of the collection trays on the local flow field, this, together with, the relatively coarse size of the collection trays and the lack of mass conservation due loss of particles not deposited in the collection region could explain the noticed discrepancies.

7.4 Conclusions

From the above work it can be seen that the transport model predicts the behaviour of dispersed two-phase flows well. The results in both of the test-cases considered show good agreement with the experimental data. The performance of the model has been shown to comparable to, or better than, other models, both Lagrangian and Eulerian, which have been applied to the same test-cases.

Both of the test-case calculations show that the accuracy of the predictions depends on the particle response time. The behaviour of those particles with a smaller response time is generally better predicted than that of particles which show significant inertial effects. This is clearly shown in test-case 1, where the heavy particles fail to respond correctly to the radial fluctuating velocities of the gas flow field and hence the radial velocities for the particles is significantly under-predicted. The same failure is not noticed for the light particles. This result is not surprising, as the mean radial gas velocity is small the only mechanism present in the model to allow radial transport of the particles is turbulent dispersion and, because of the short residence time of the particles in the measurement region this effect is negligible. This is turn implies that there is possibly a need to consider further source terms in the second phase momentum equations, in addition to the mean drag and gravity terms included here.

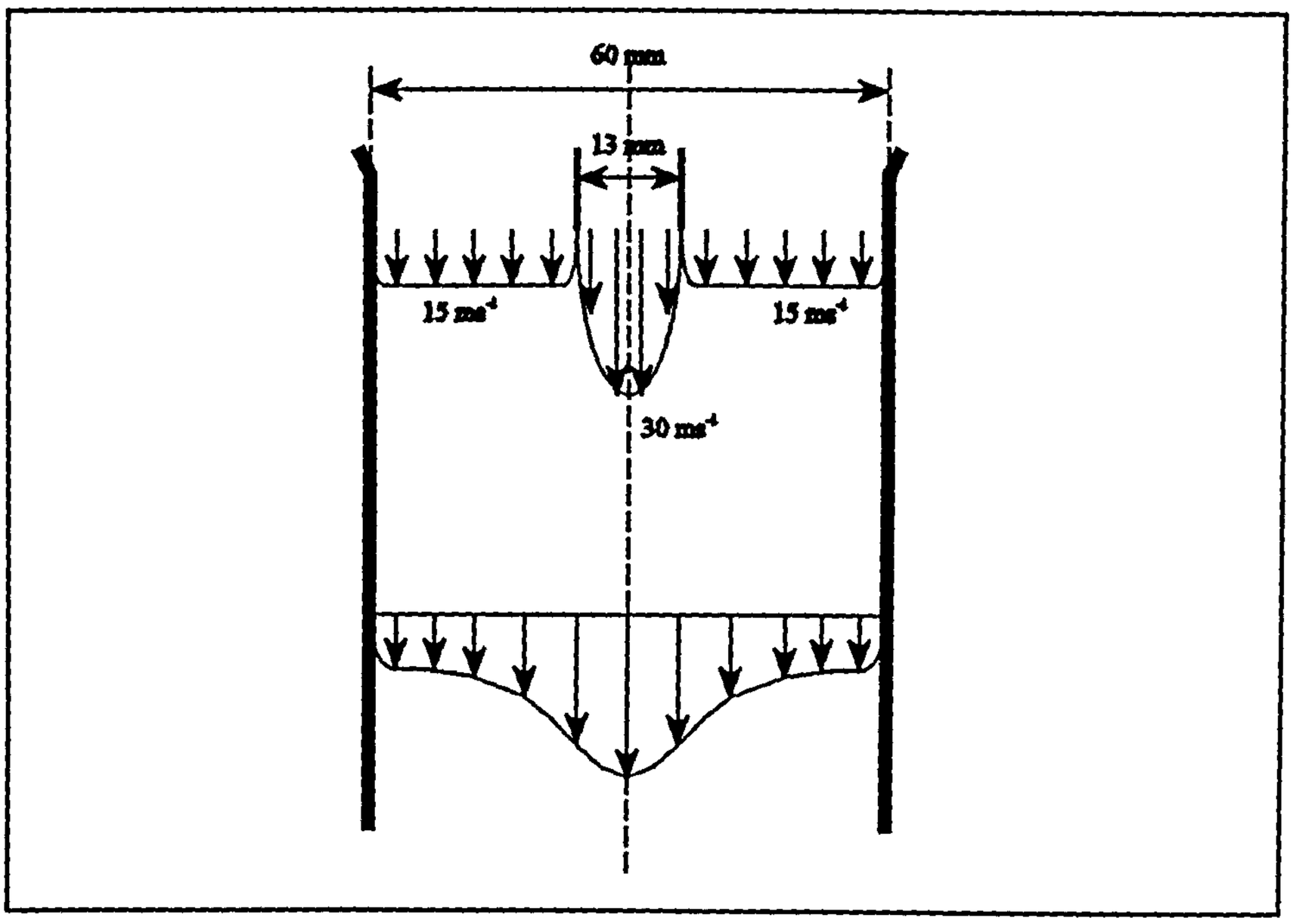

Figure 7.1 : Schematic of Hishida and Maeda Flow Field

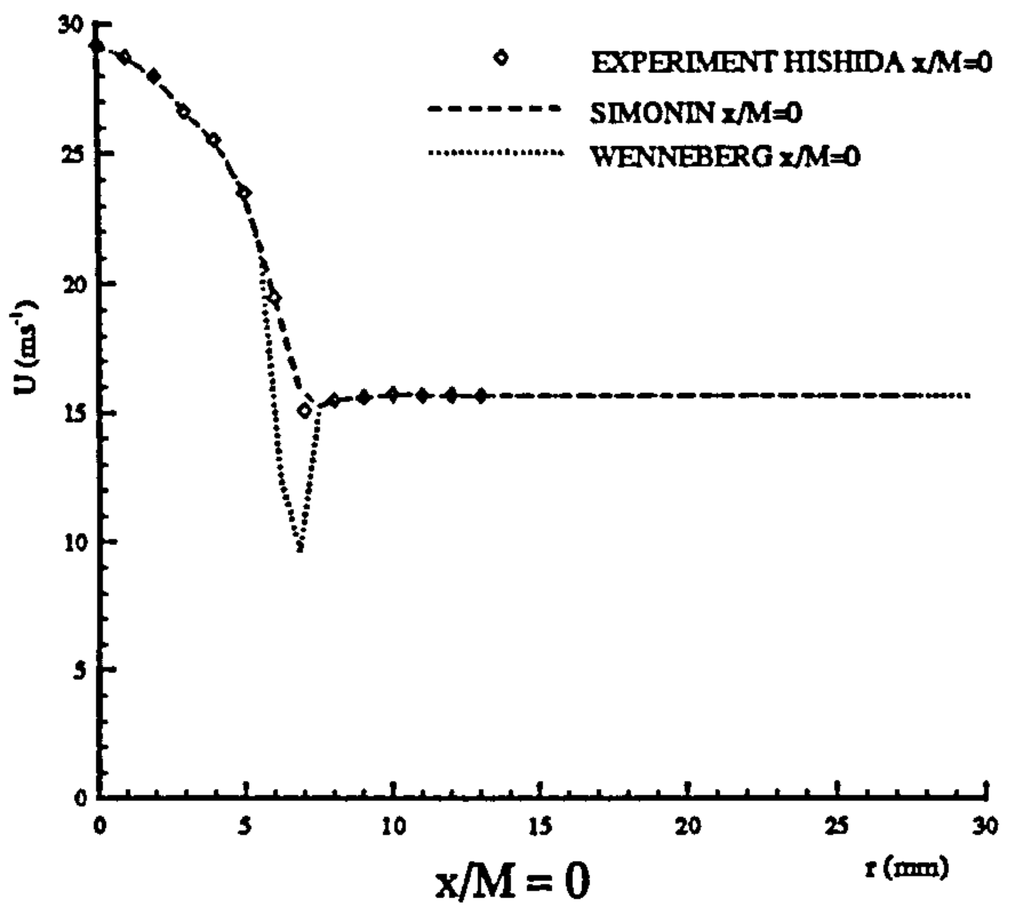

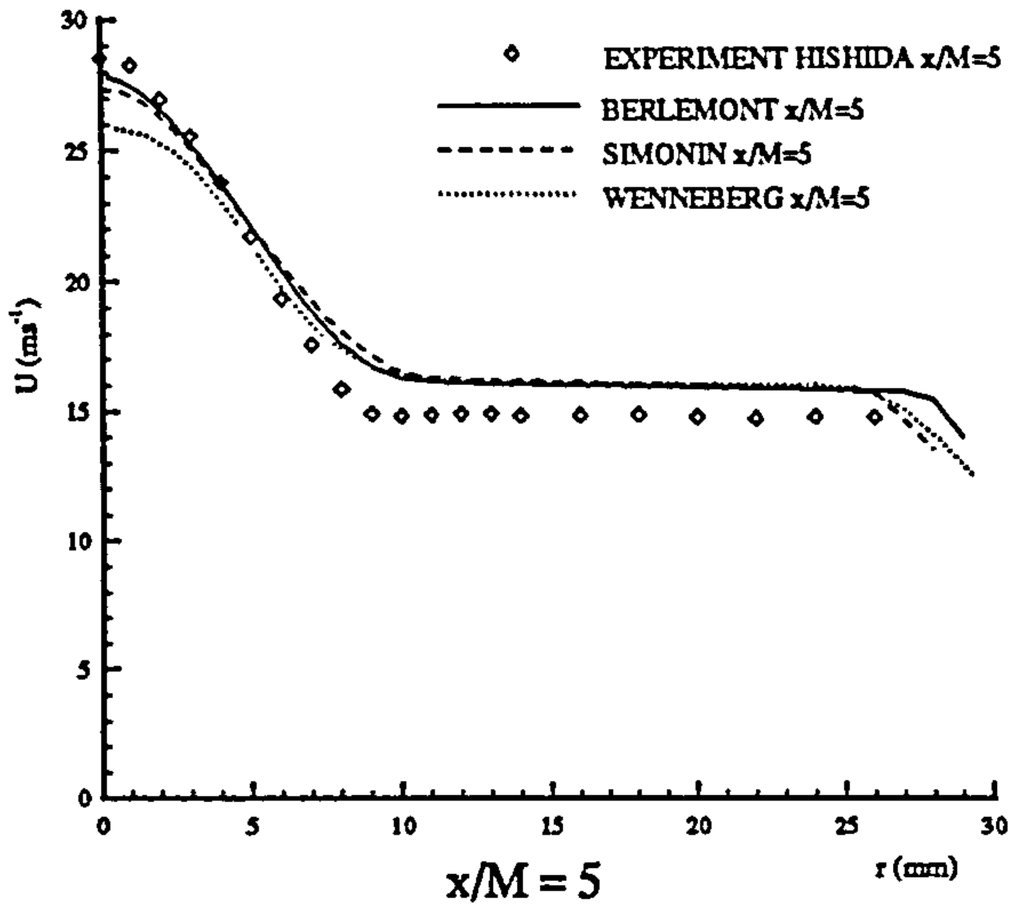

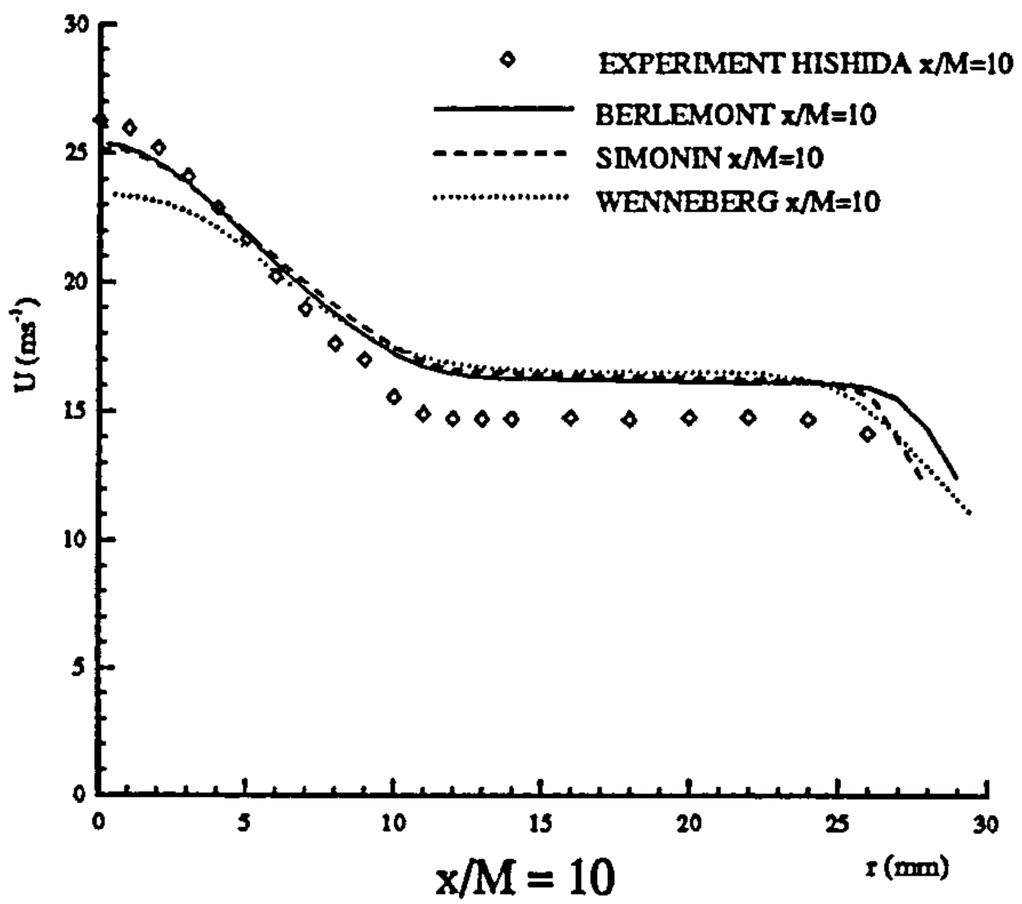

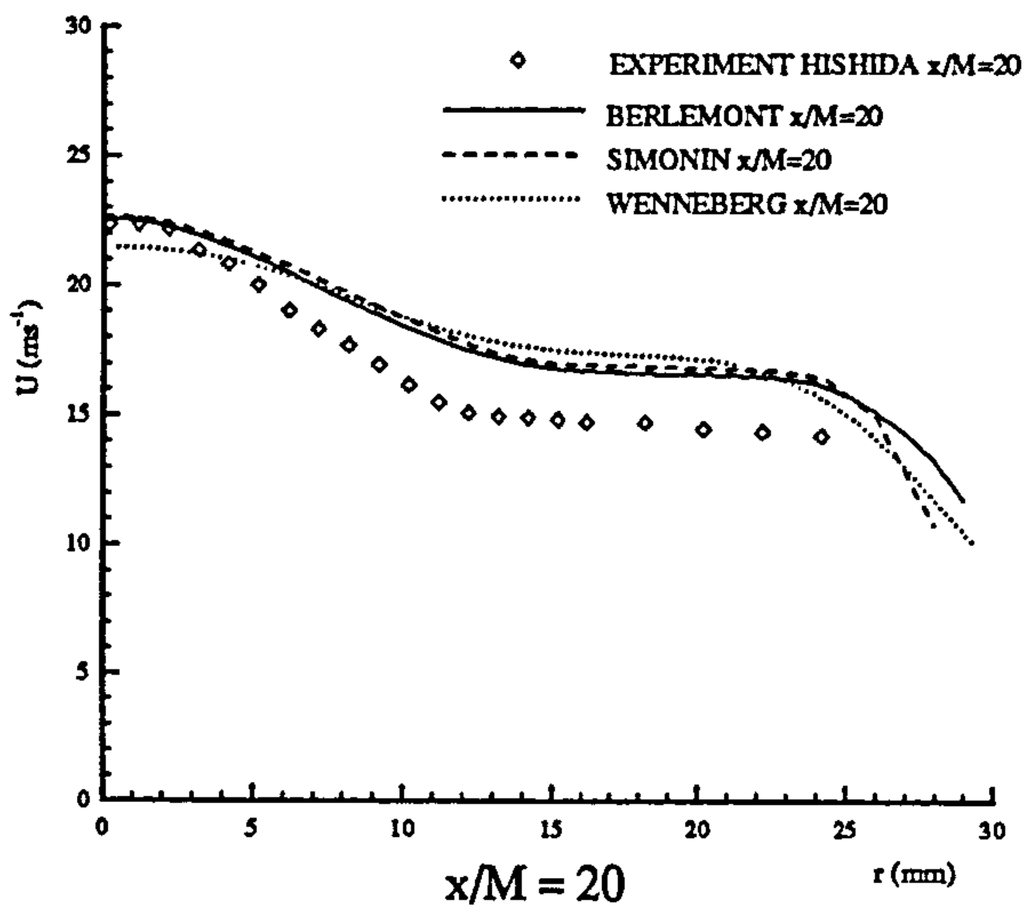

Figure 7.2 : Mean Axial Gas Velocity Profiles - Case 1 (Heavy Particles)

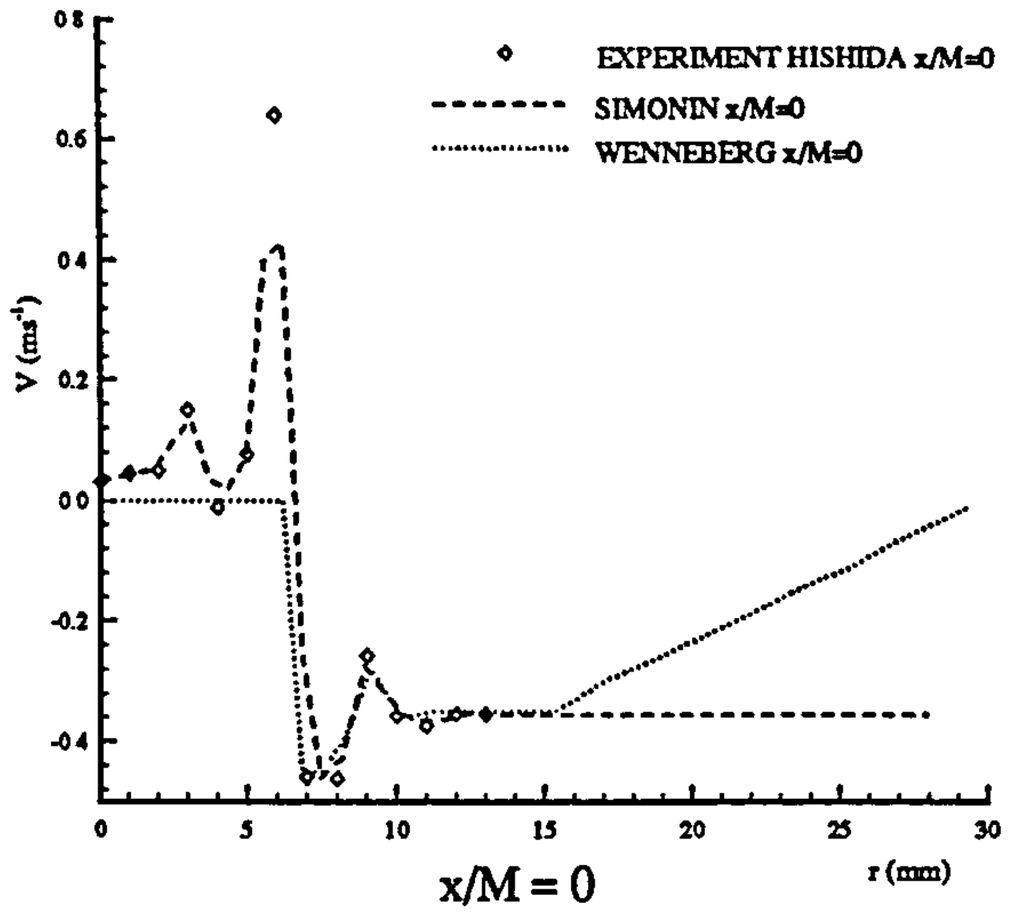

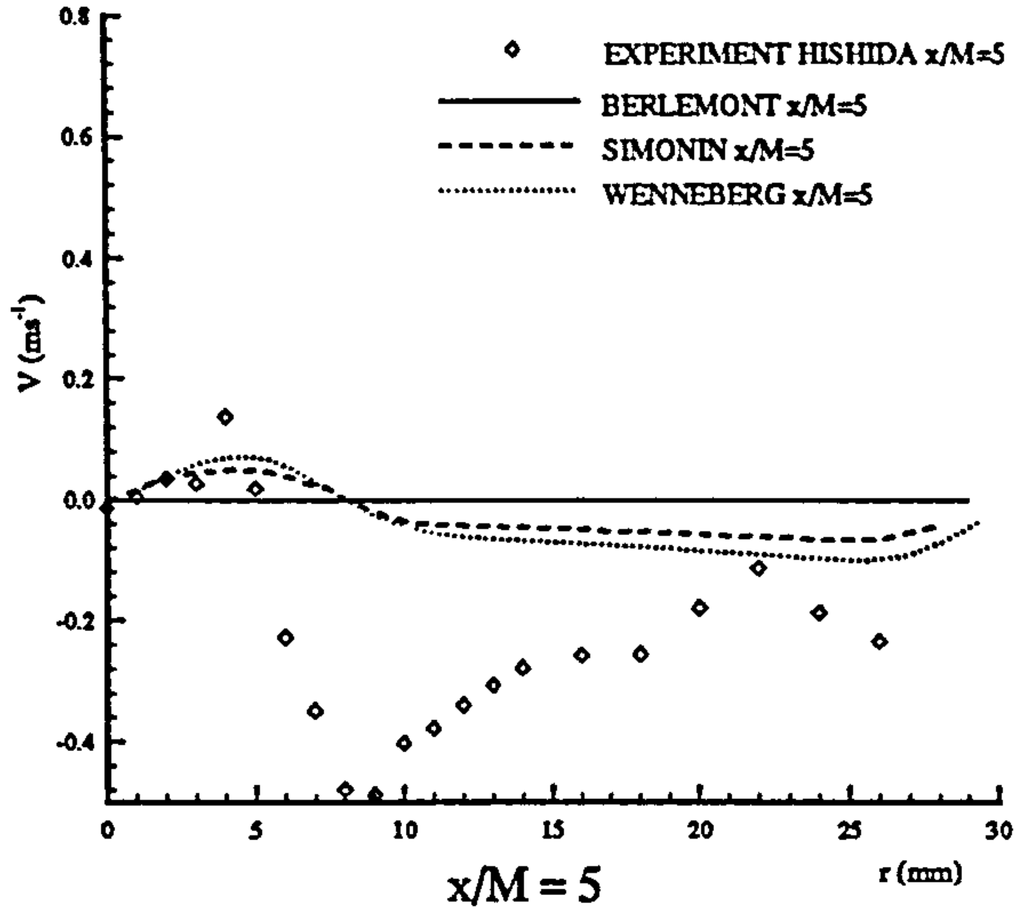

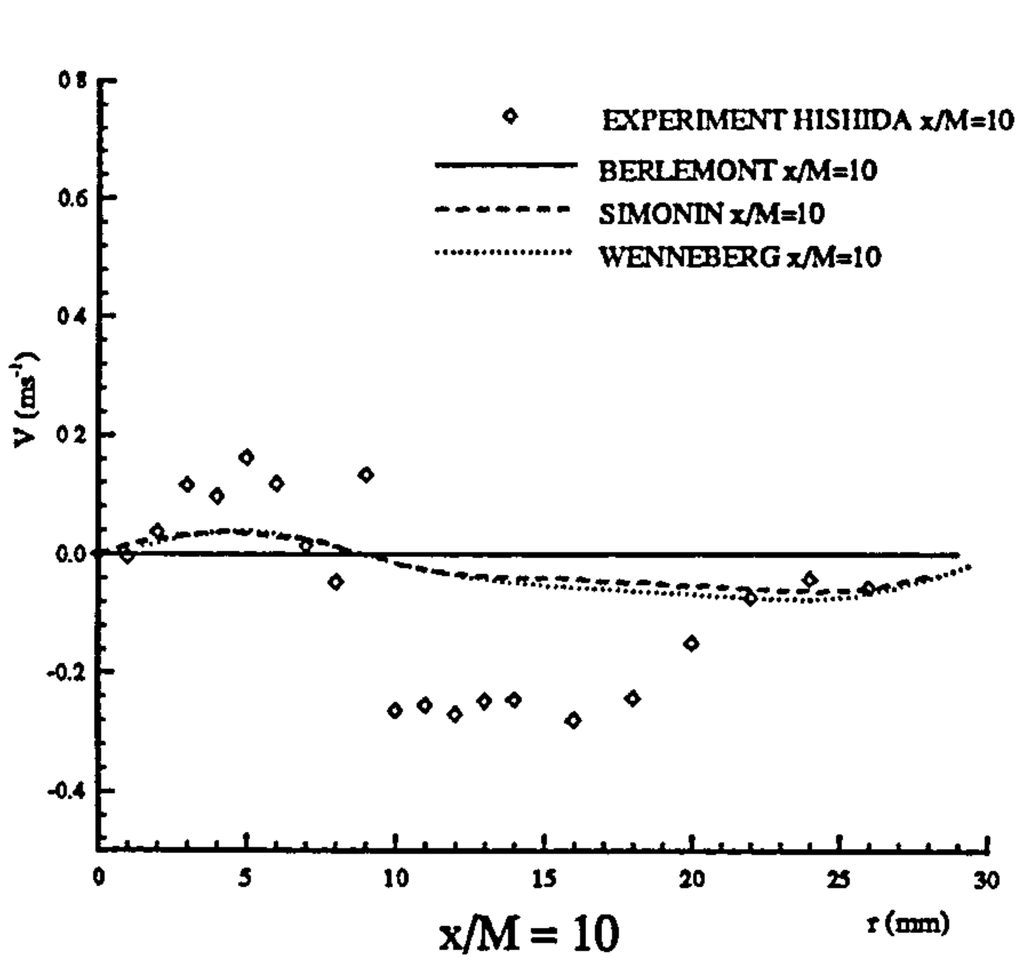

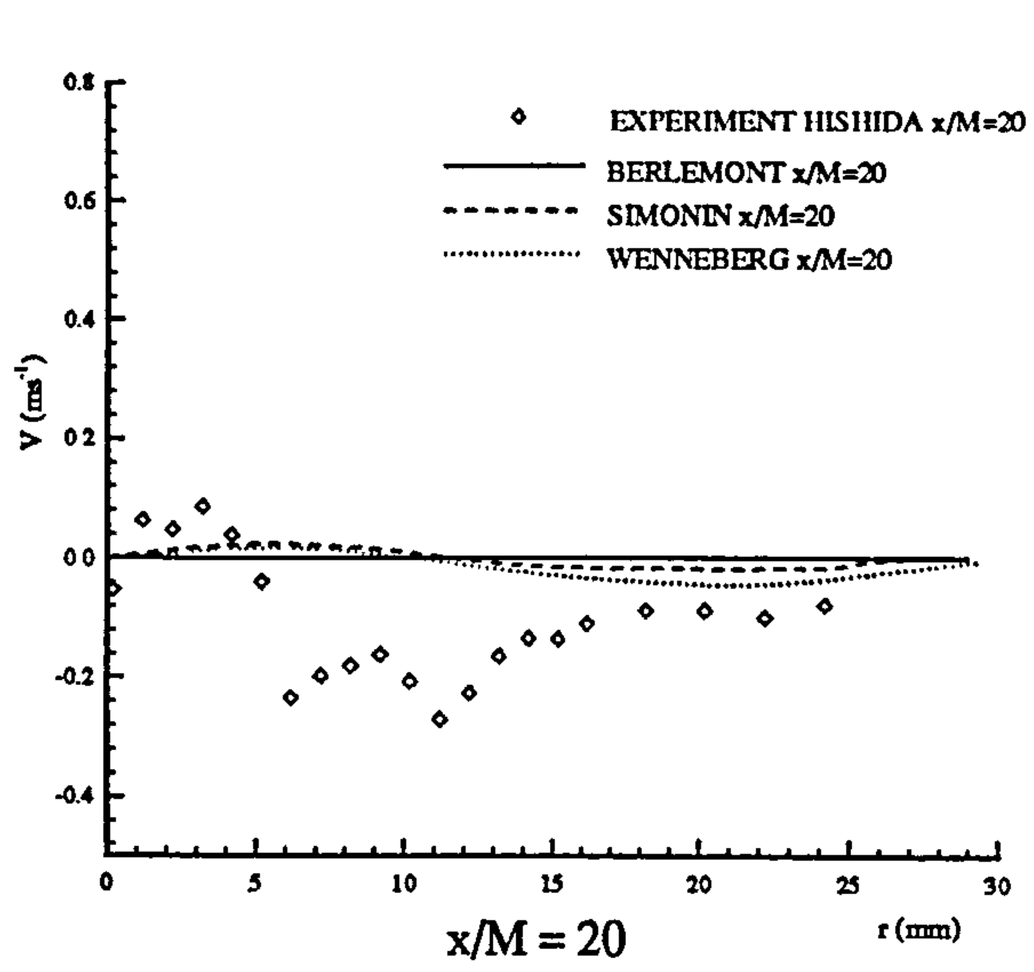

Figure 7.3 : Mean Radial Gas Velocity Profiles - Case 1 (Heavy Particles)

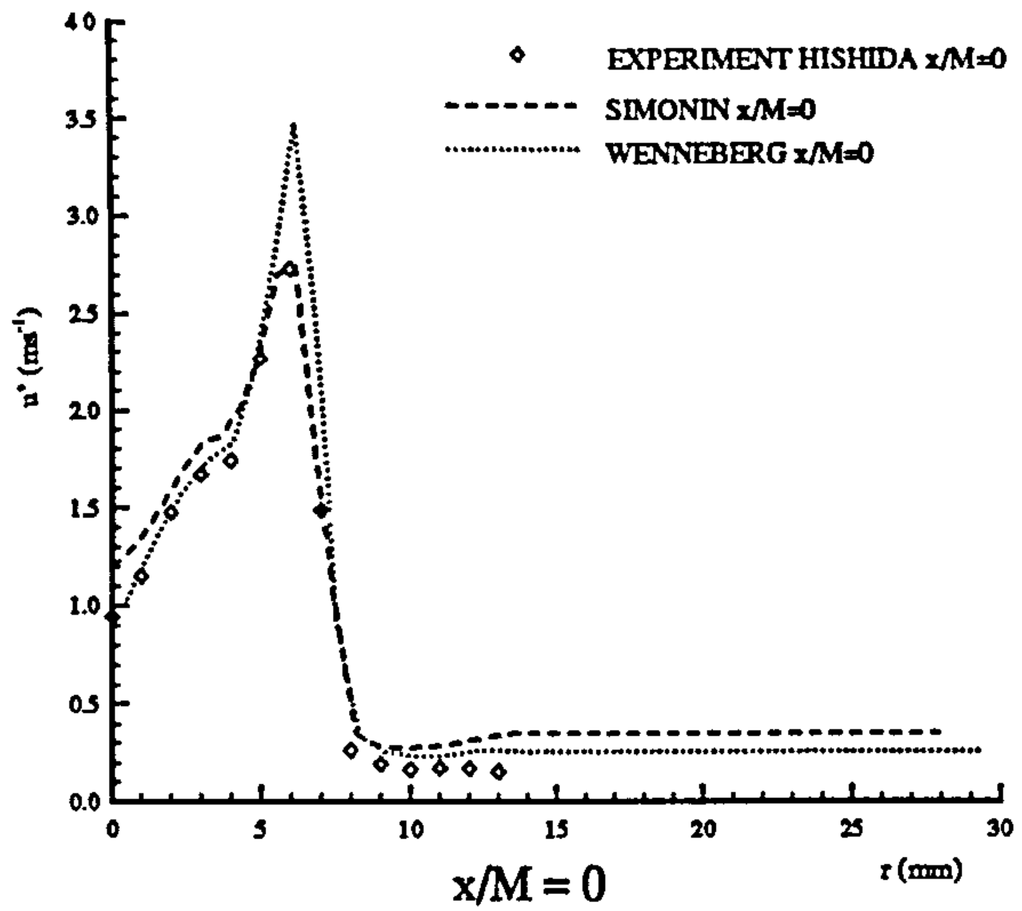

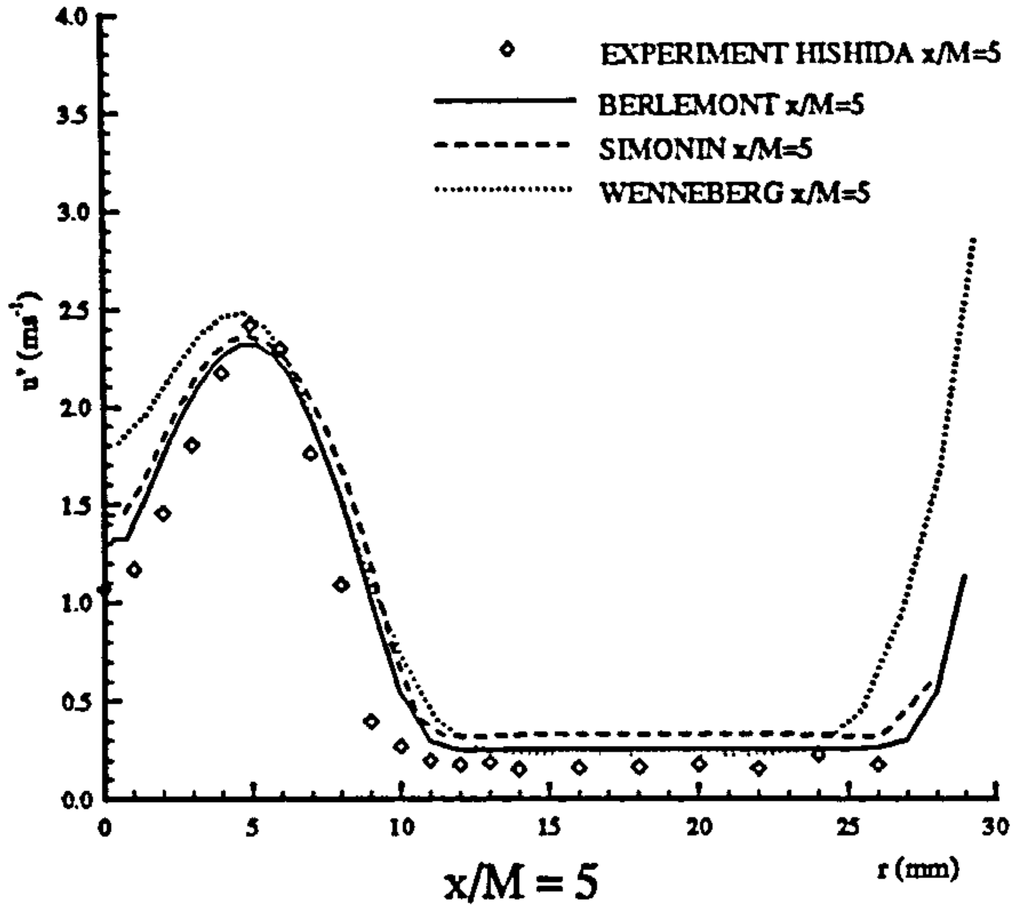

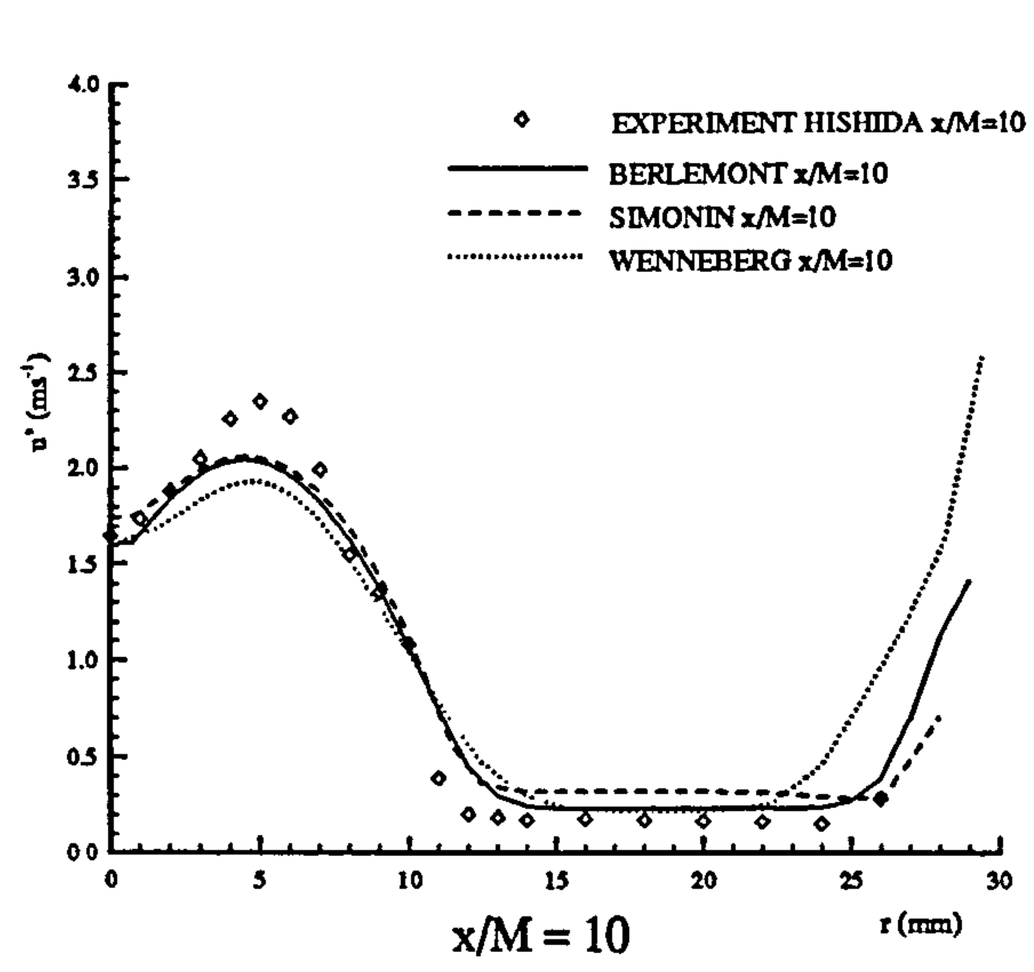

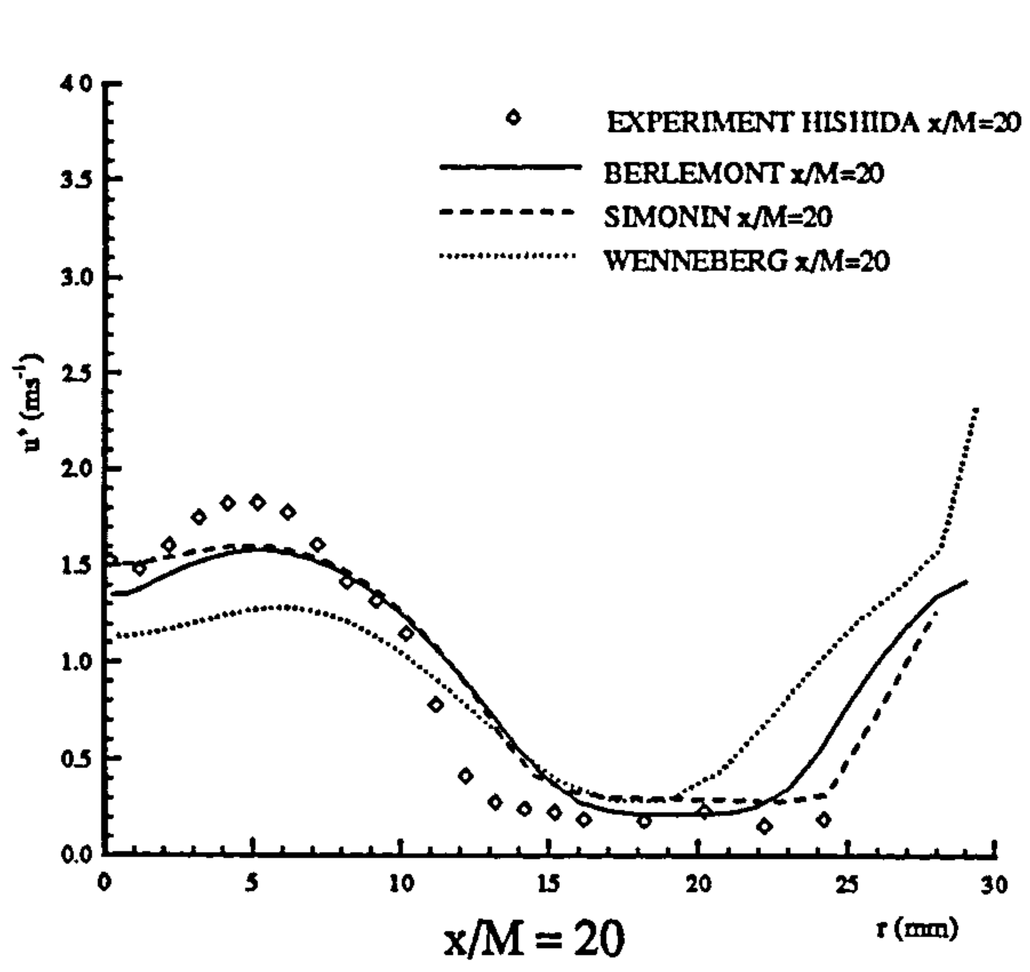

Figure 7.4 : Fluctuating Axial Gas Velocity Profiles - Case 1 (Heavy Particles)

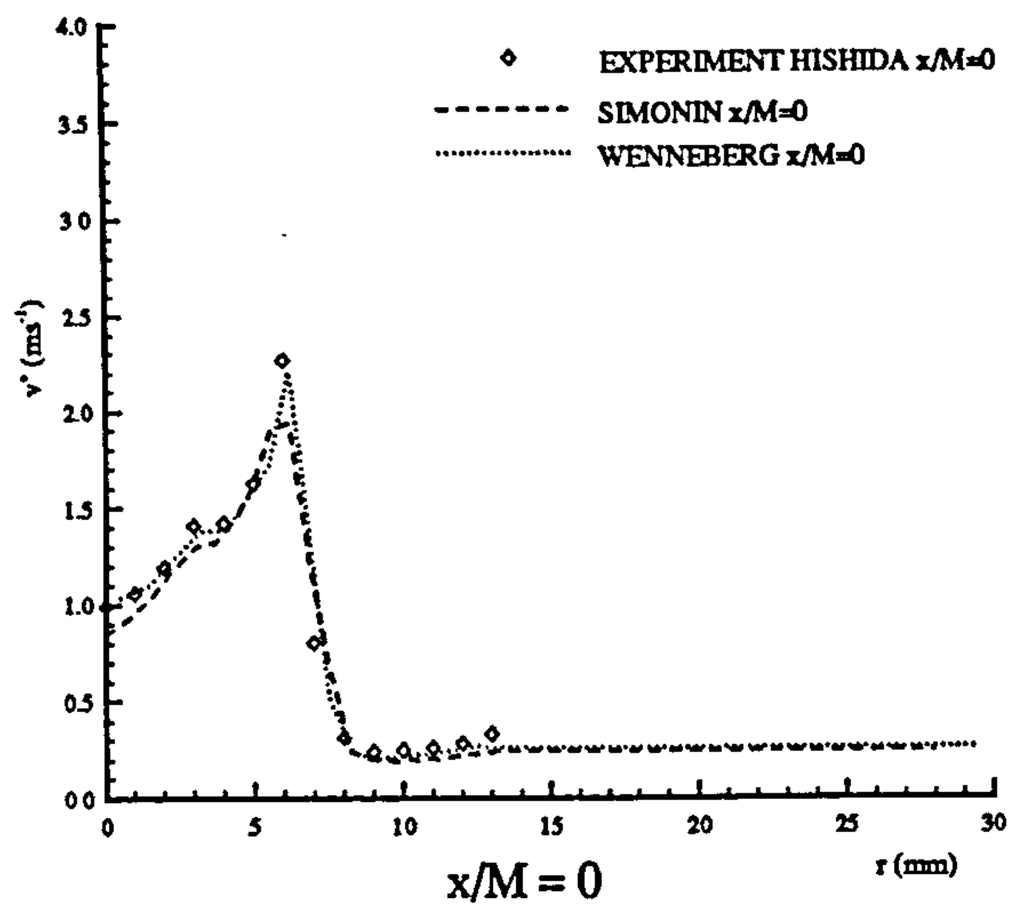

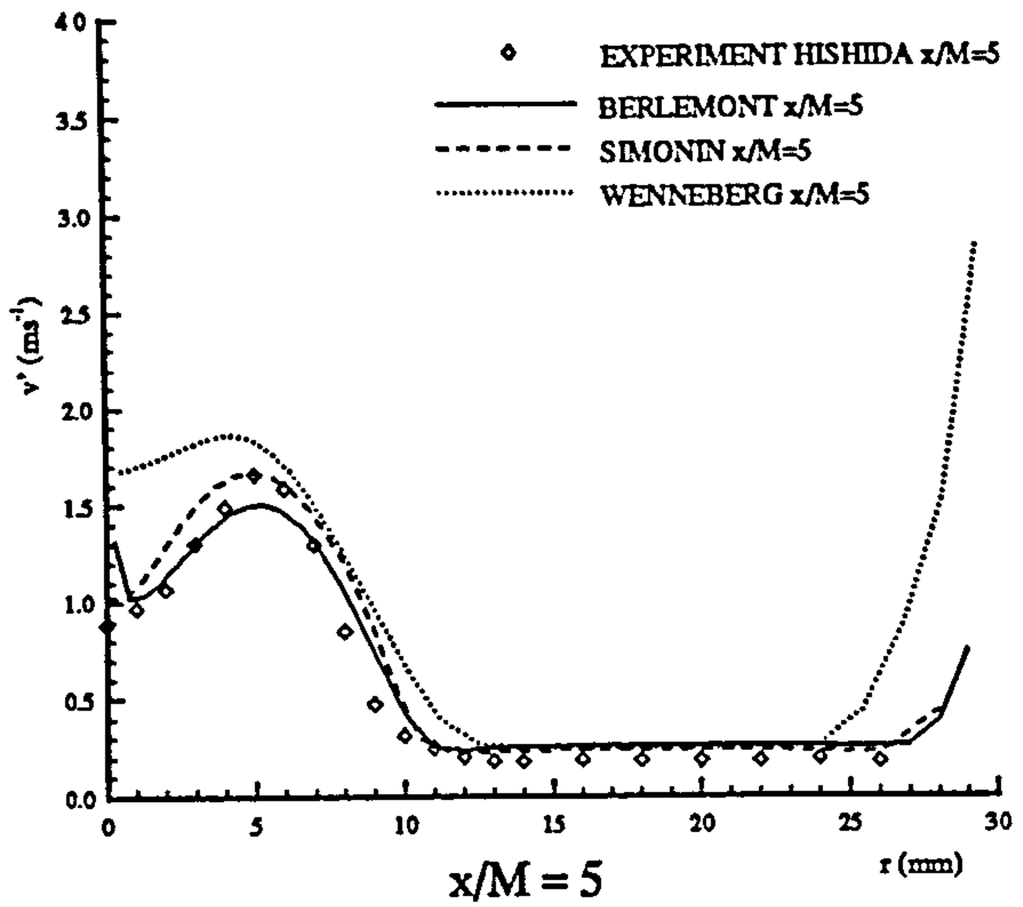

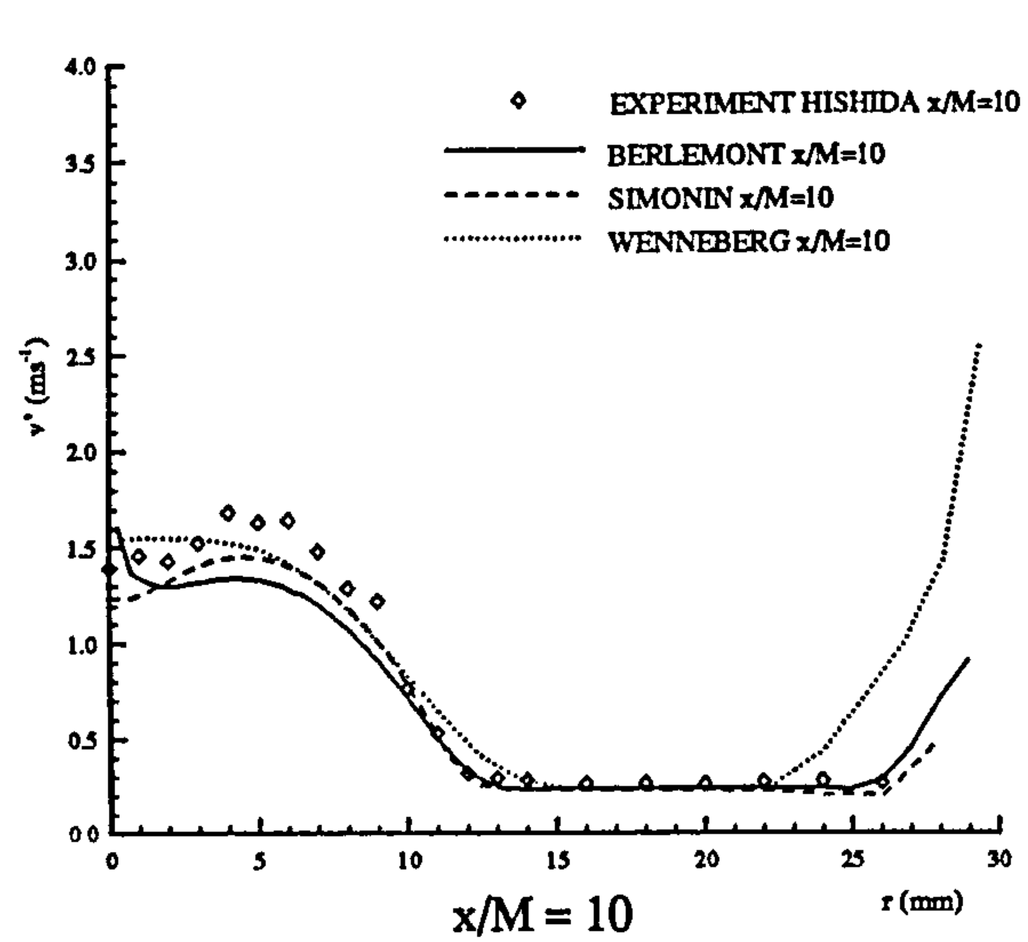

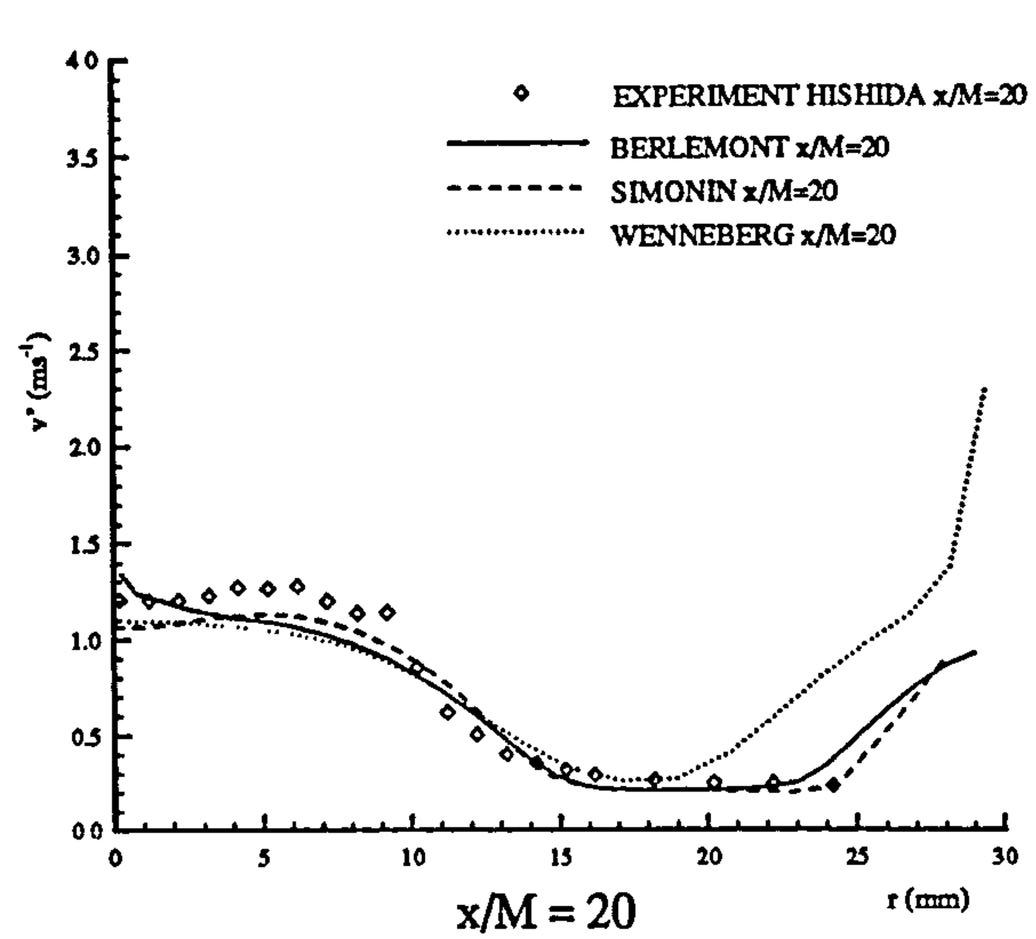

Figure 7.5 : Fluctuating Radial Gas Velocity Profiles - Case 1 (Heavy Particles)

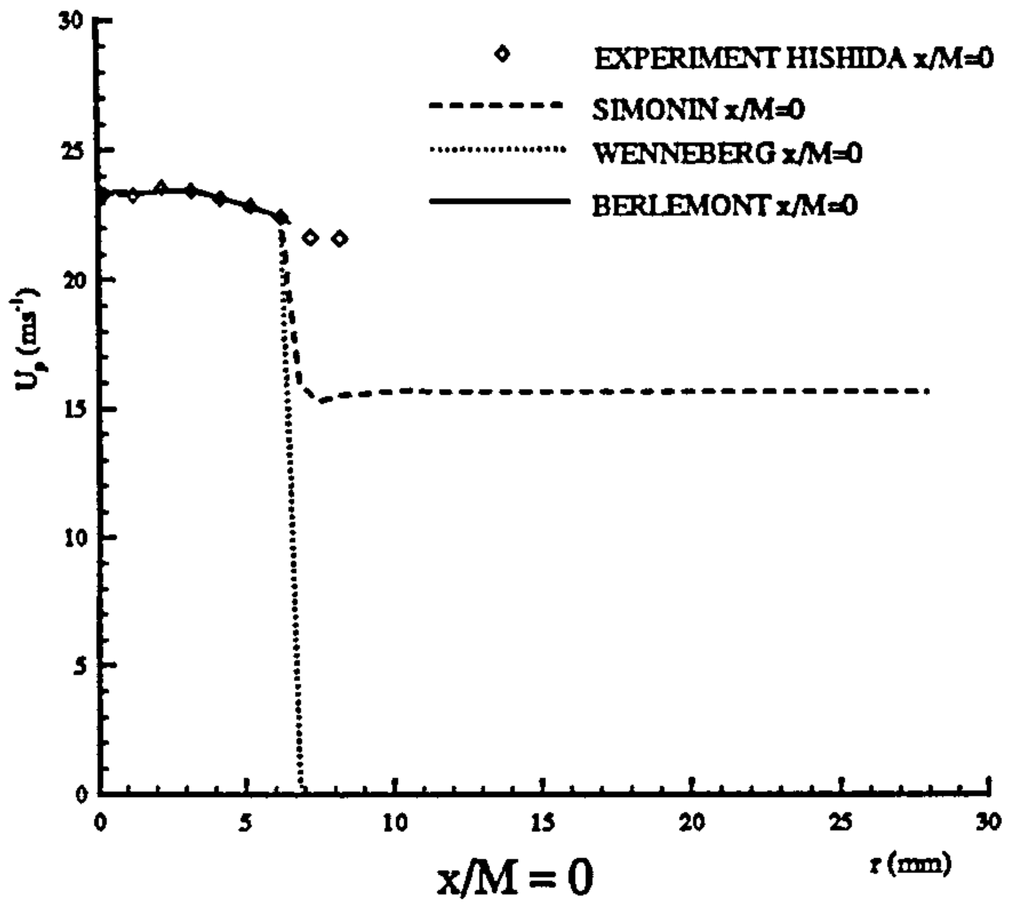

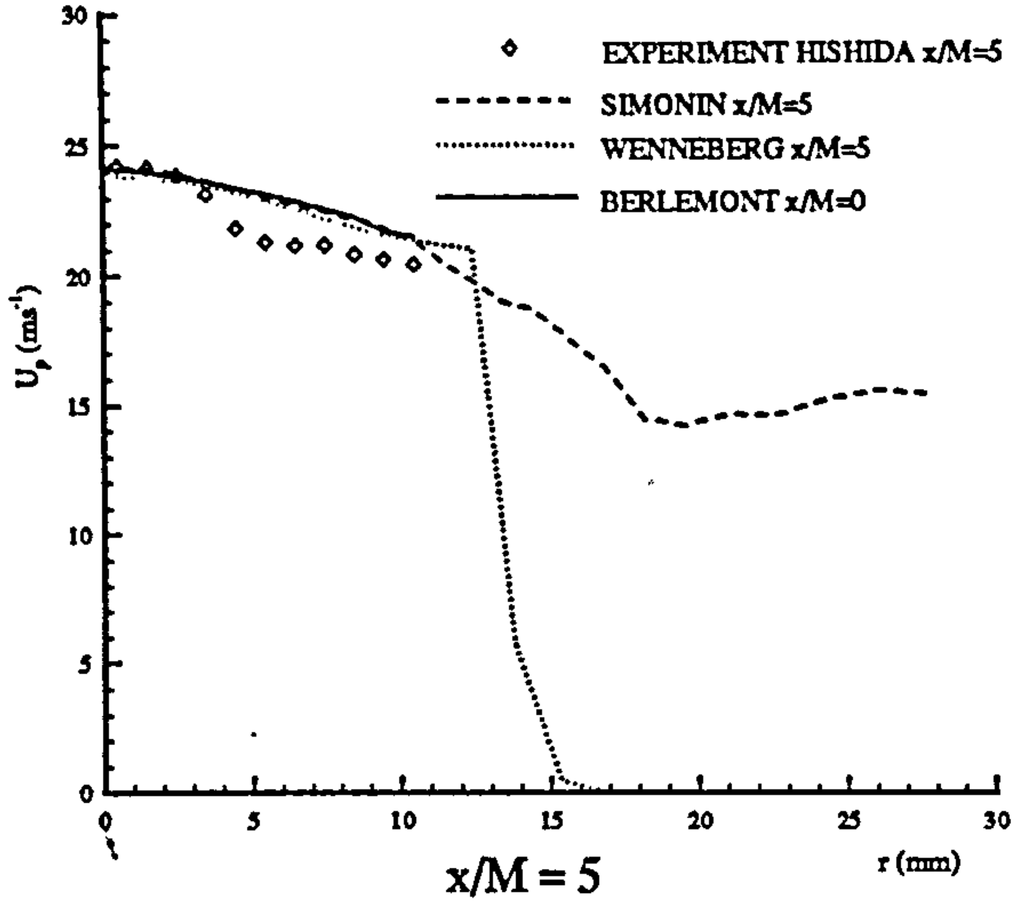

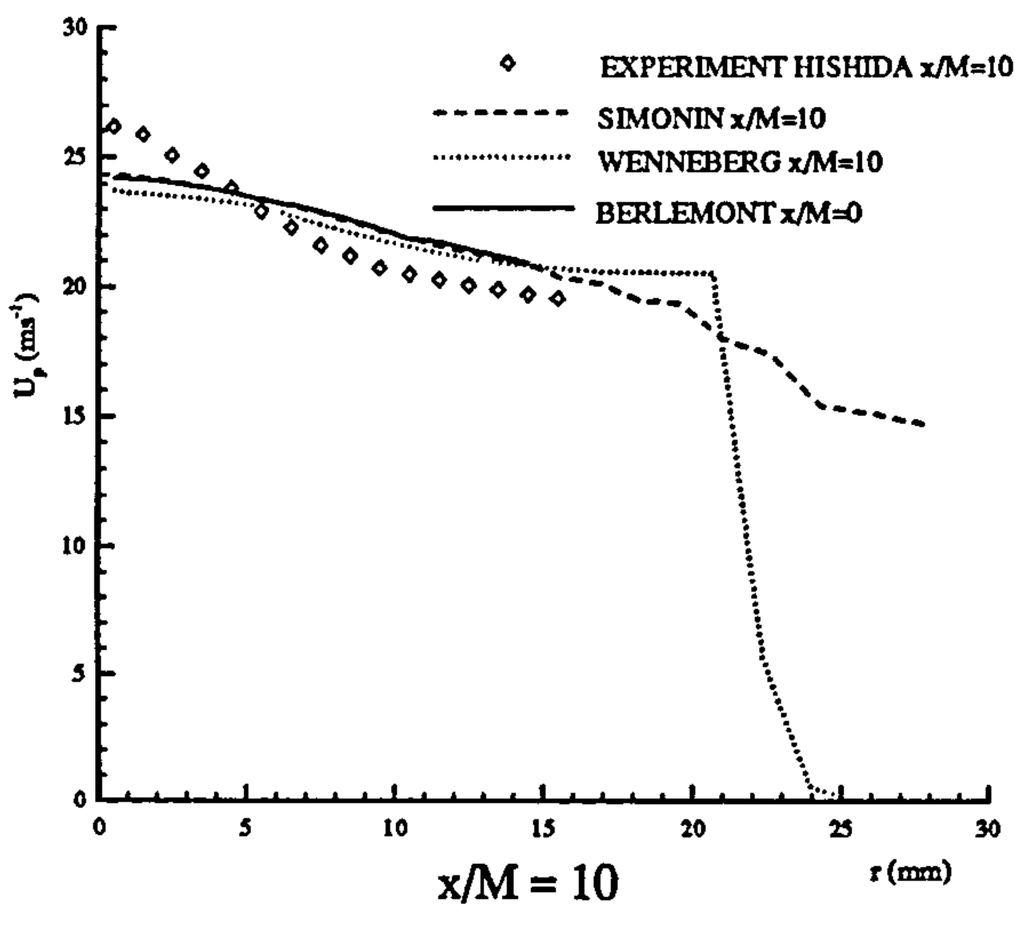

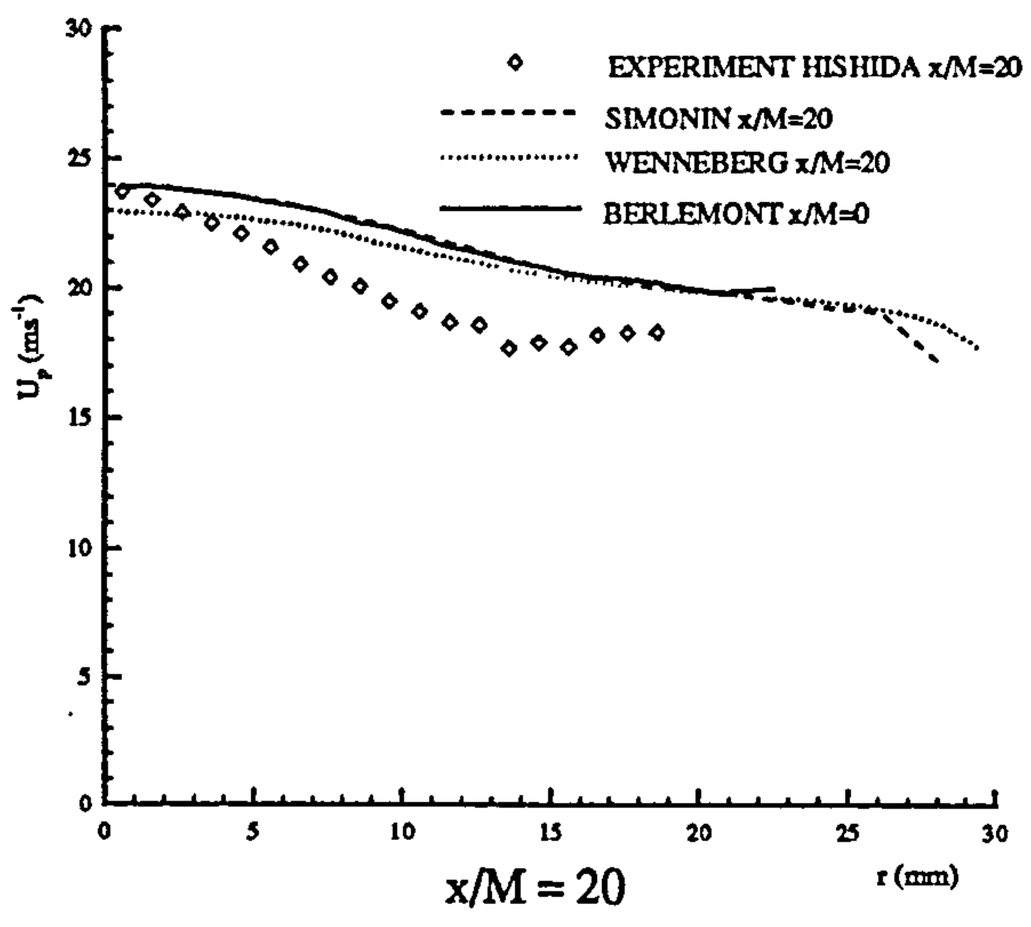

Figure 7.6 : Mean Axial Particle Velocity Profiles - Case 1 (Heavy Particles)

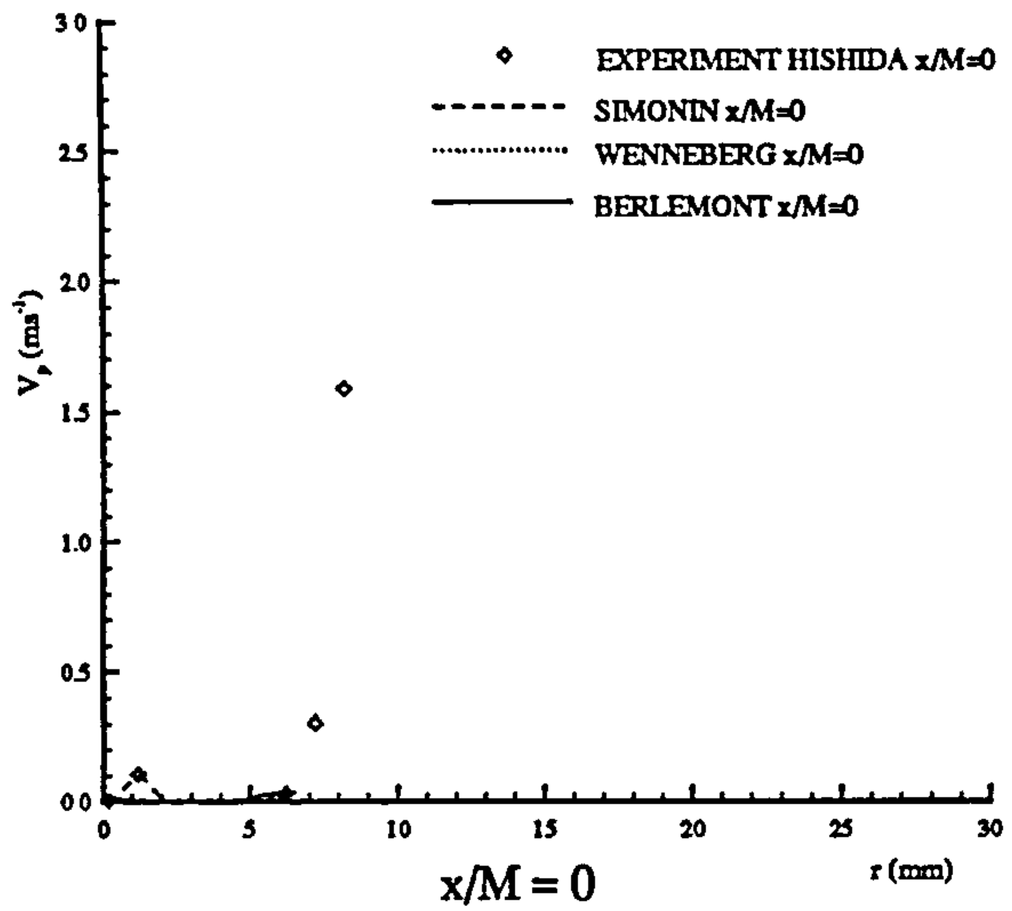

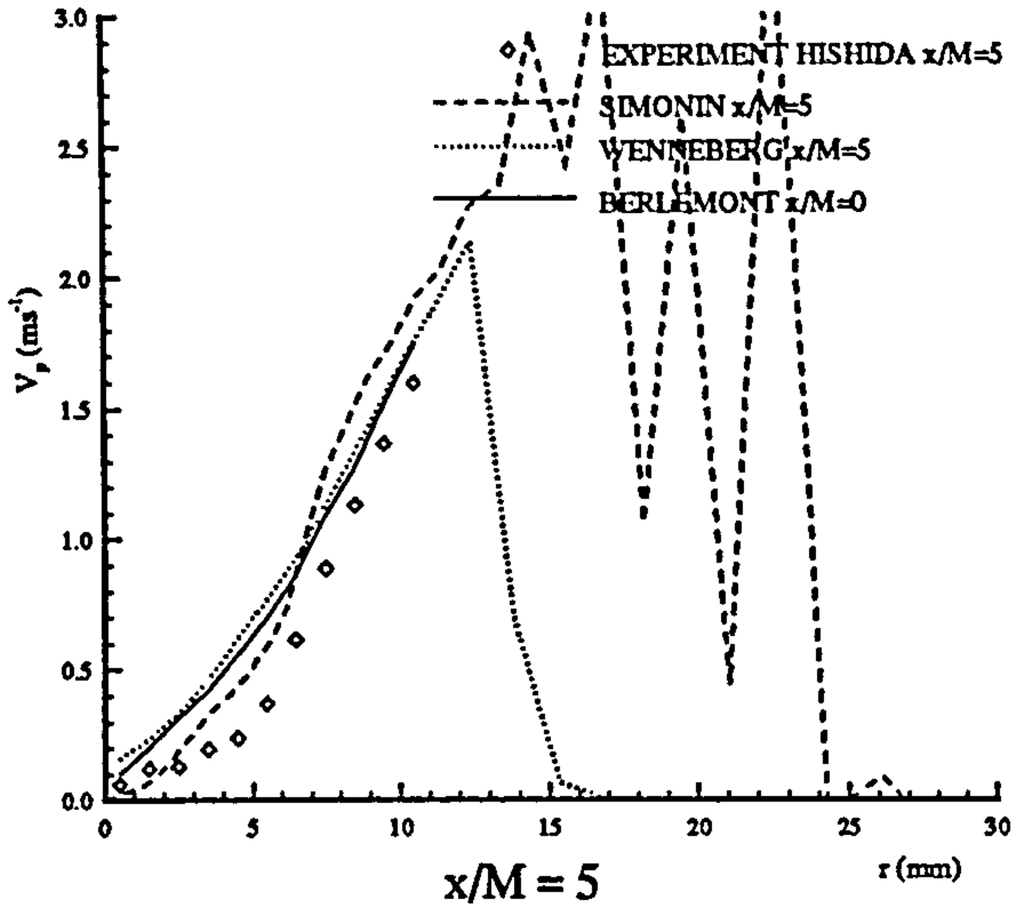

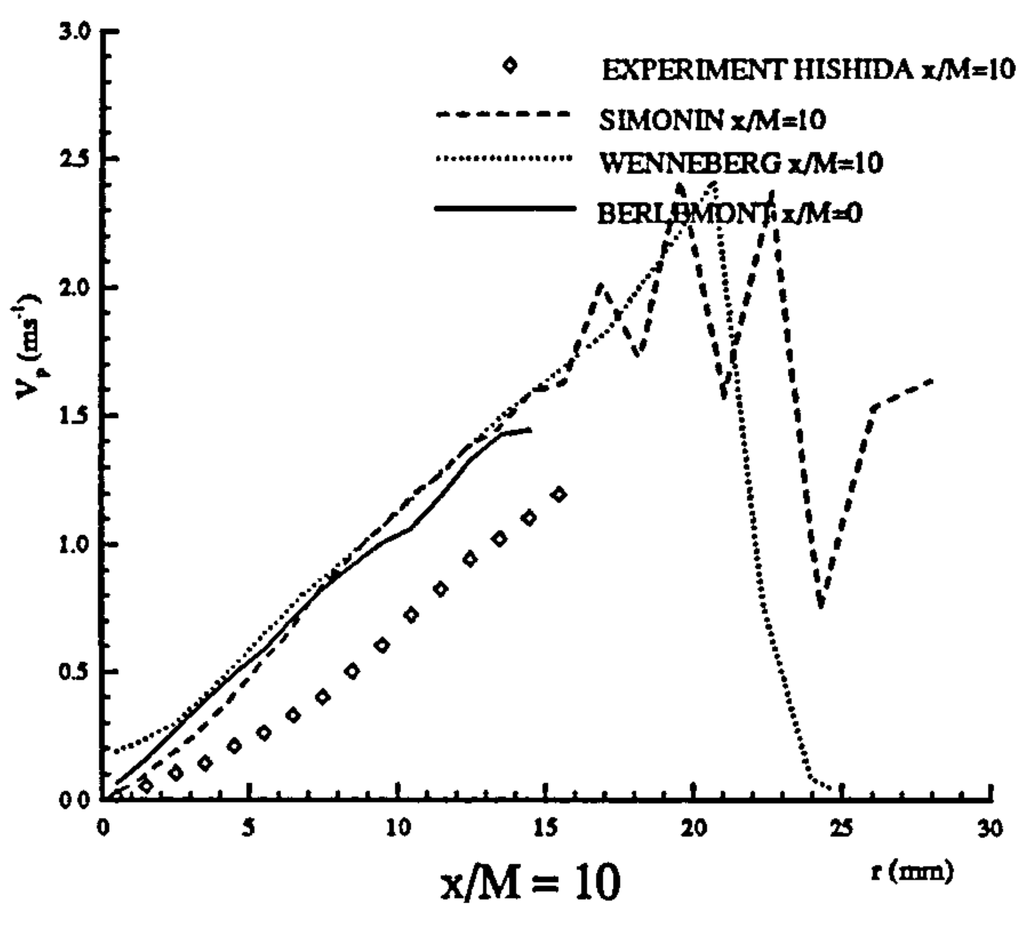

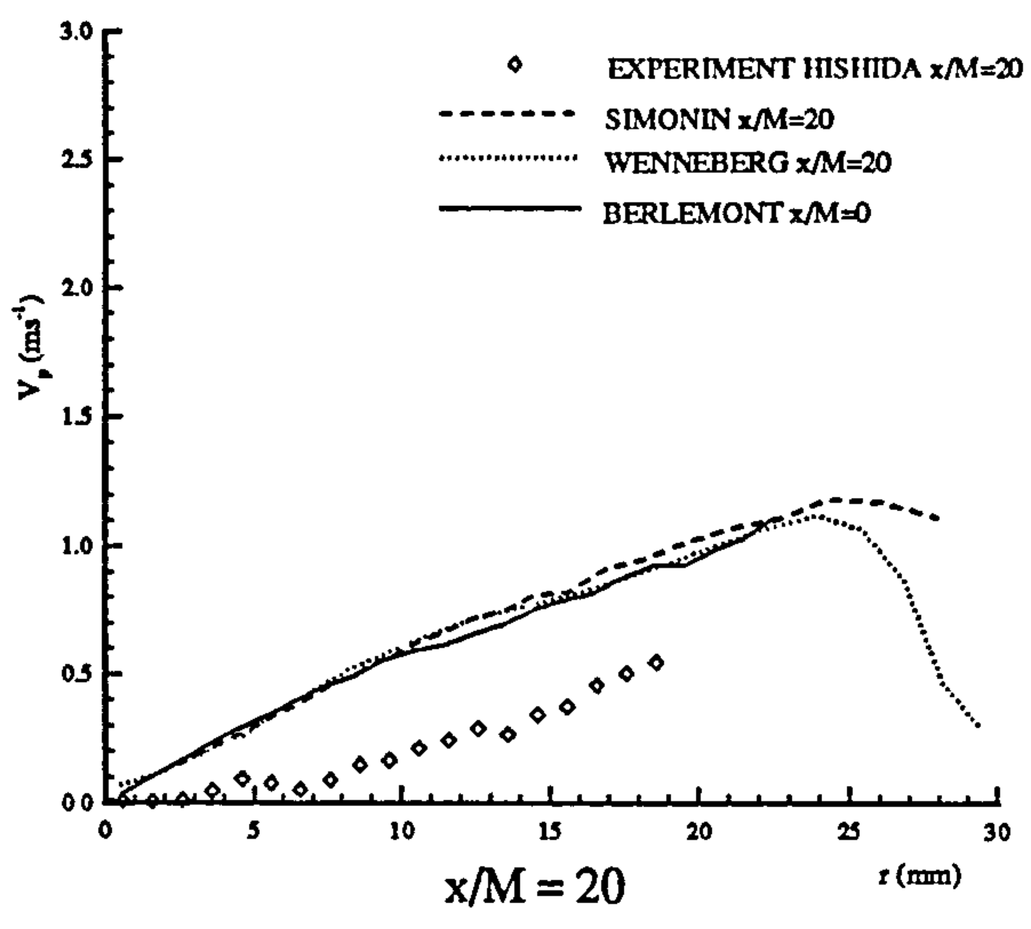

Figure 7.7 : Mean Radial Particle Velocity Profiles - Case 1 (Heavy Particles)

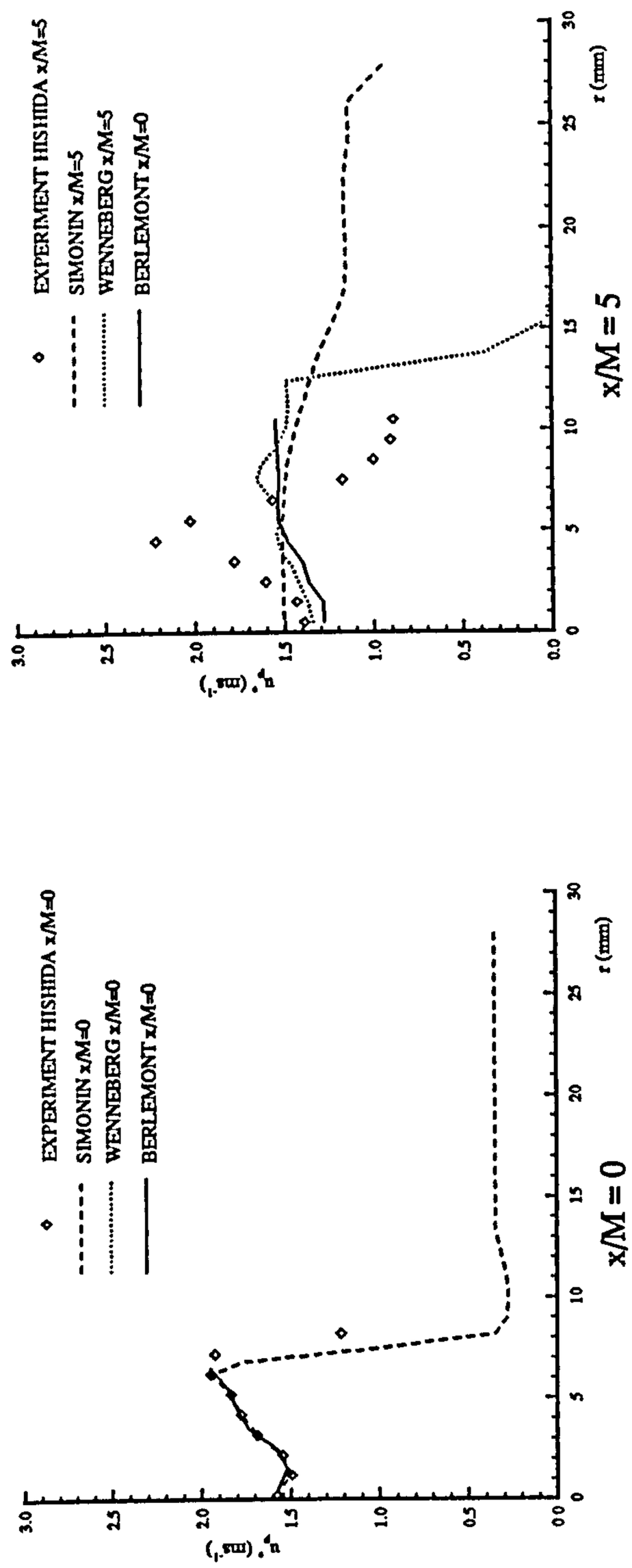

Figure 7.8 : Fluctuating Axial Particle Velocity Profiles - Case 1 (Heavy Particles)

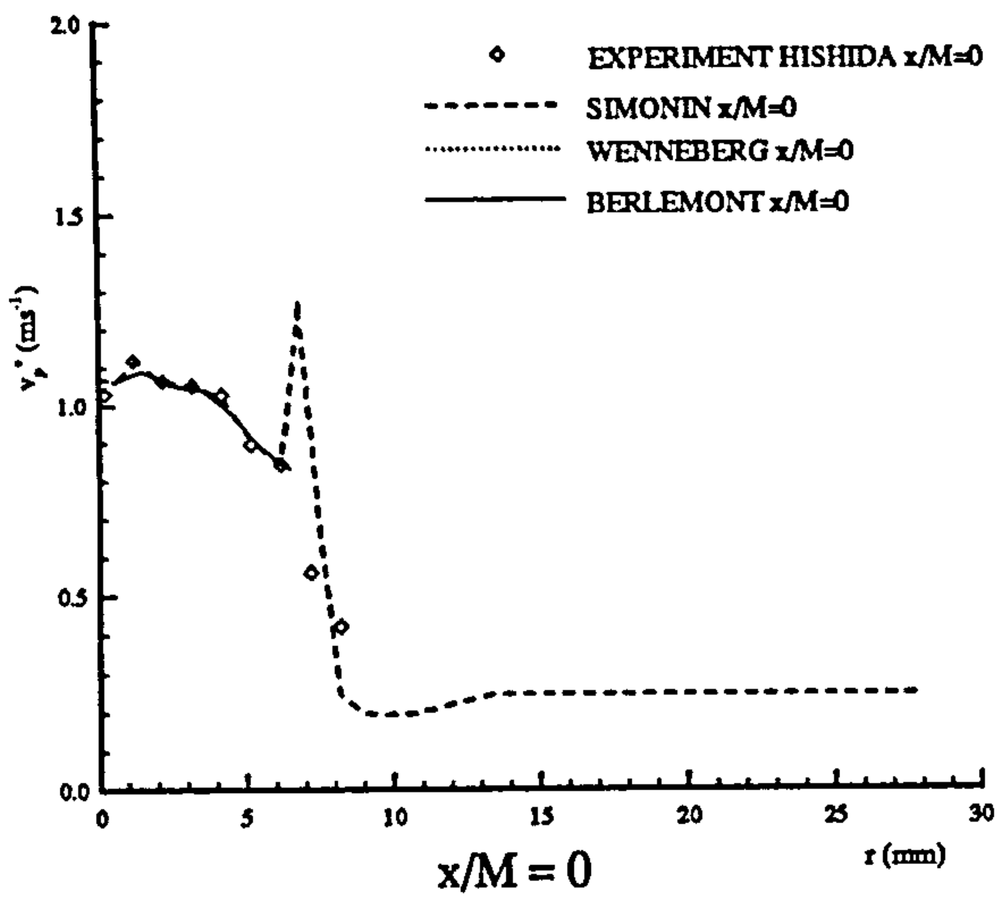

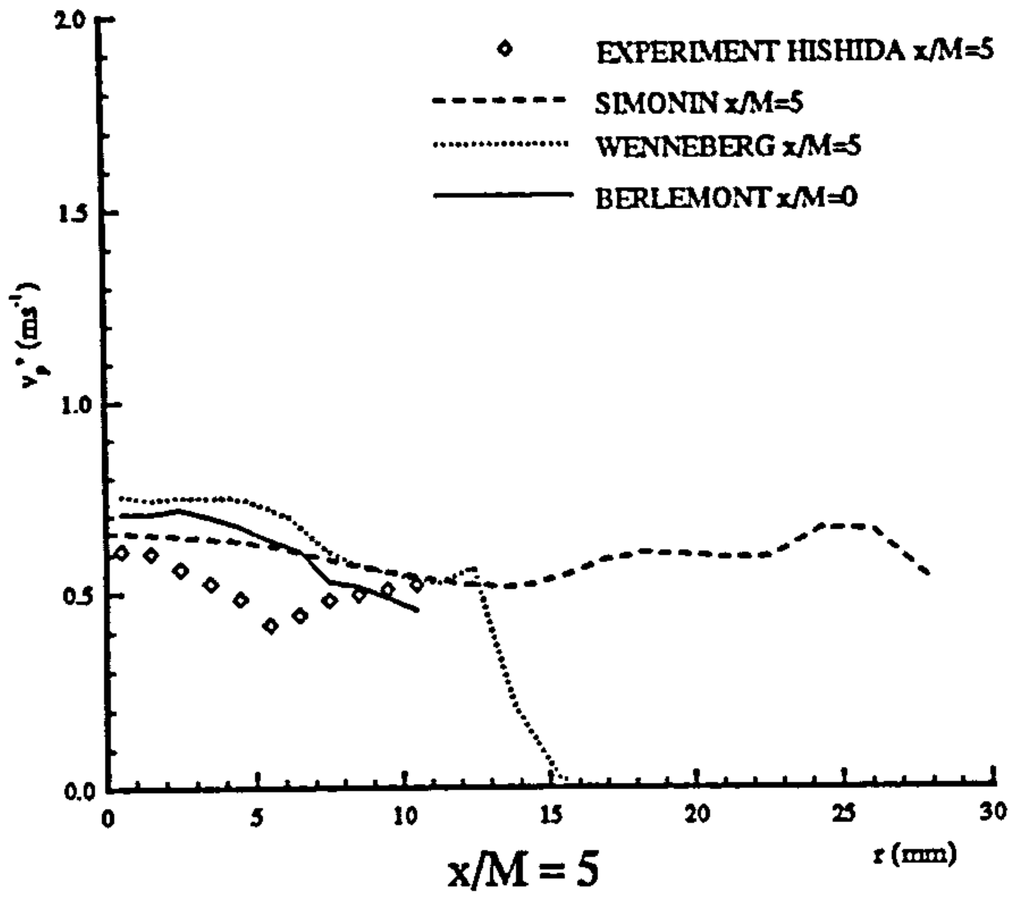

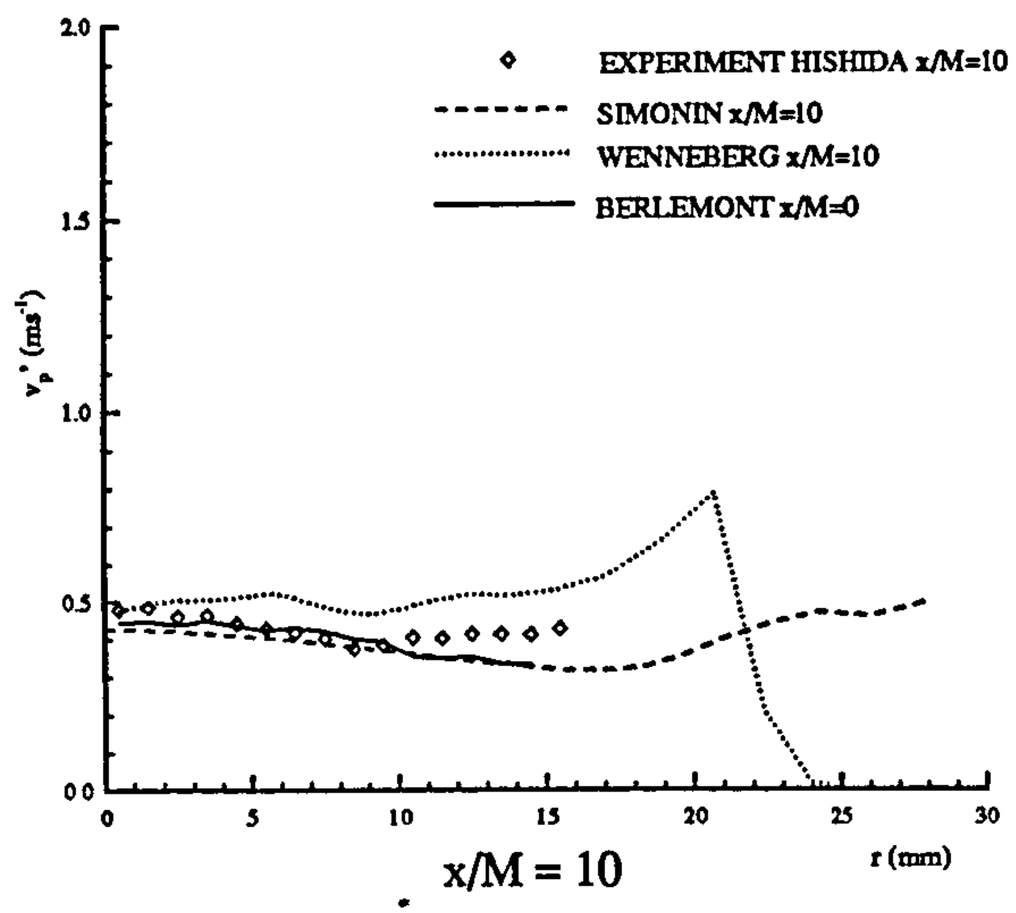

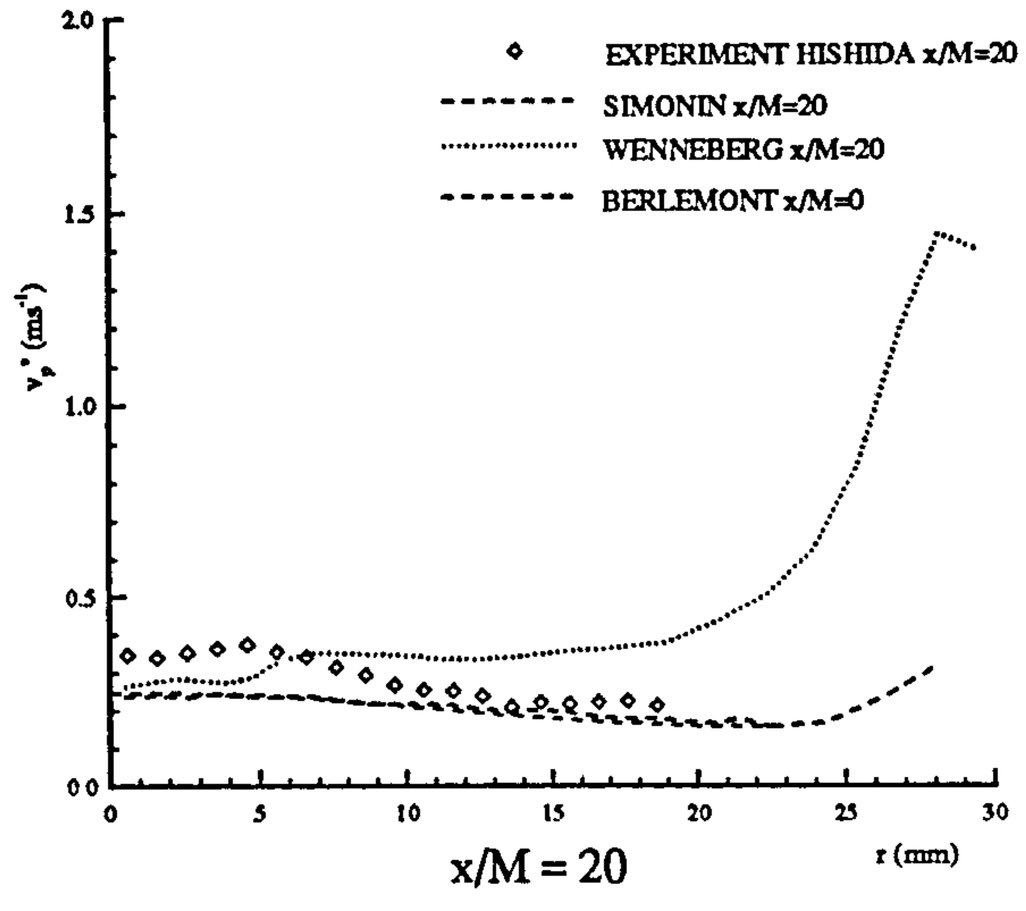

Figure 7.9 : Fluctuating Radial Particle Velocity Profiles - Case 1 (Heavy Particles)

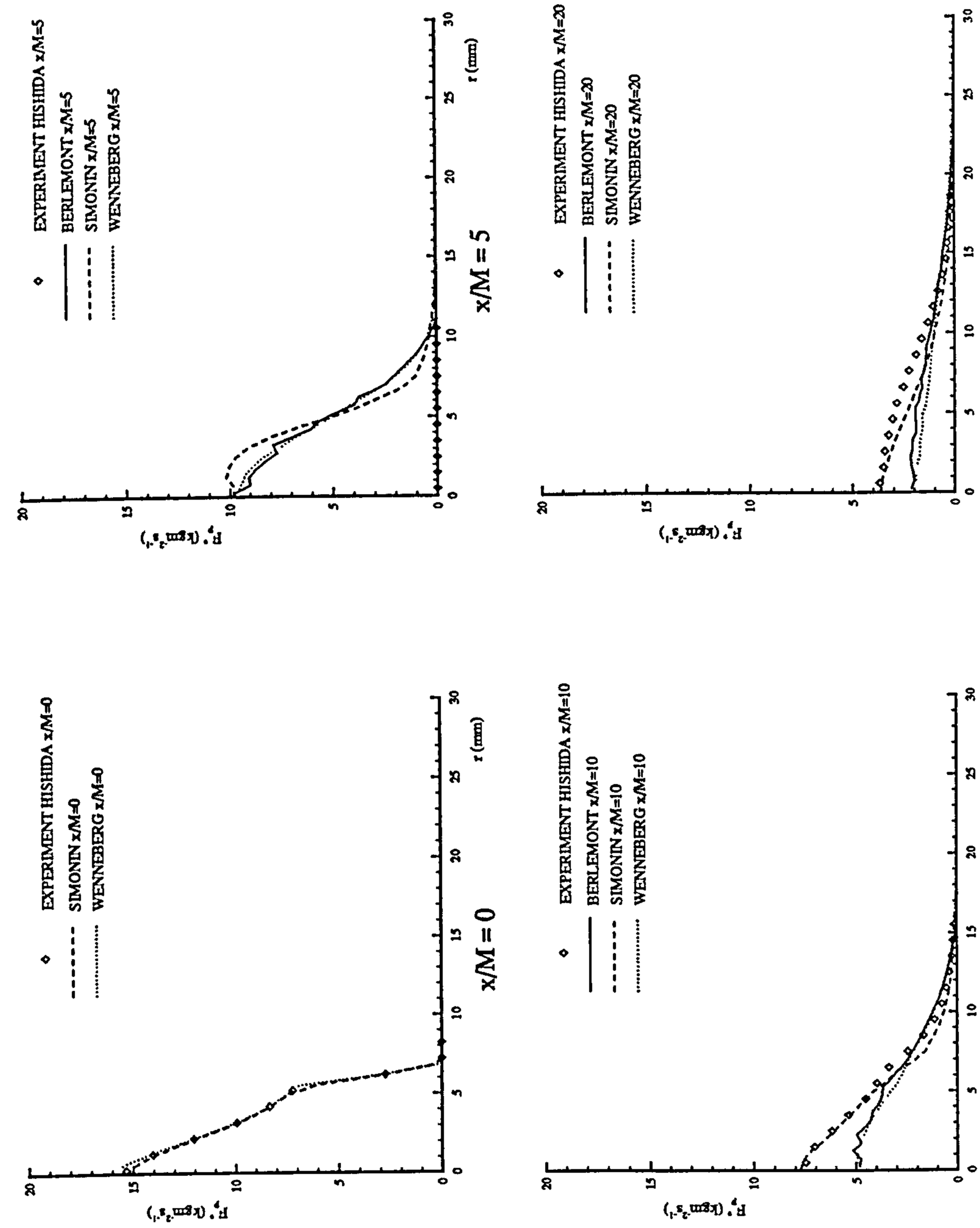

Figure 7.10 : Particle Mass Flux - Case 1 (Heavy Particles)

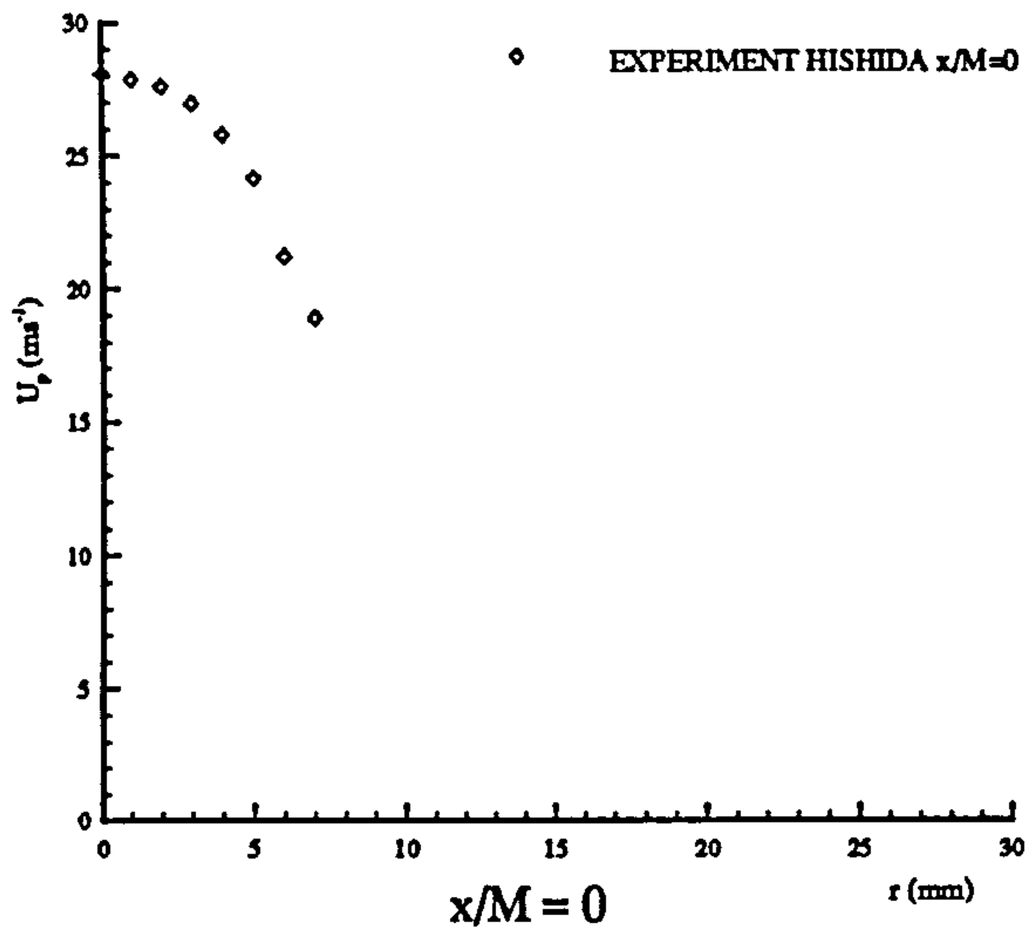

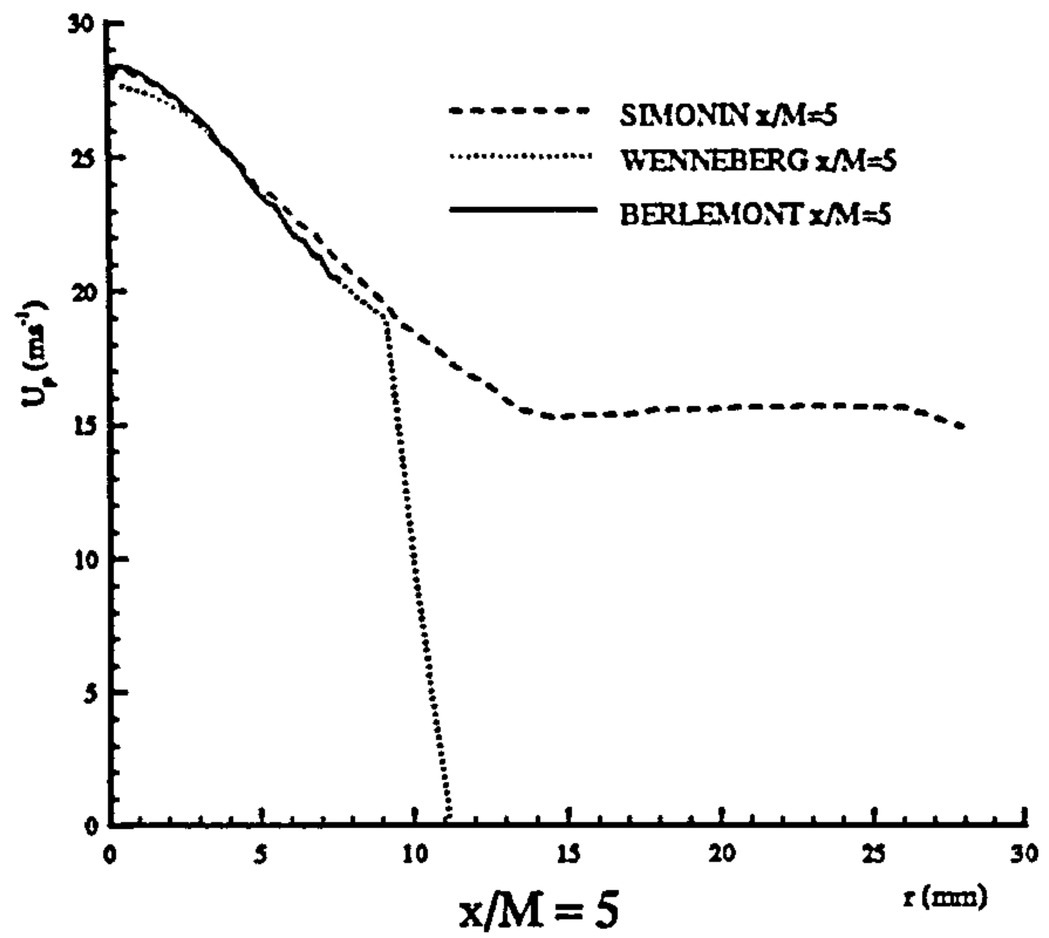

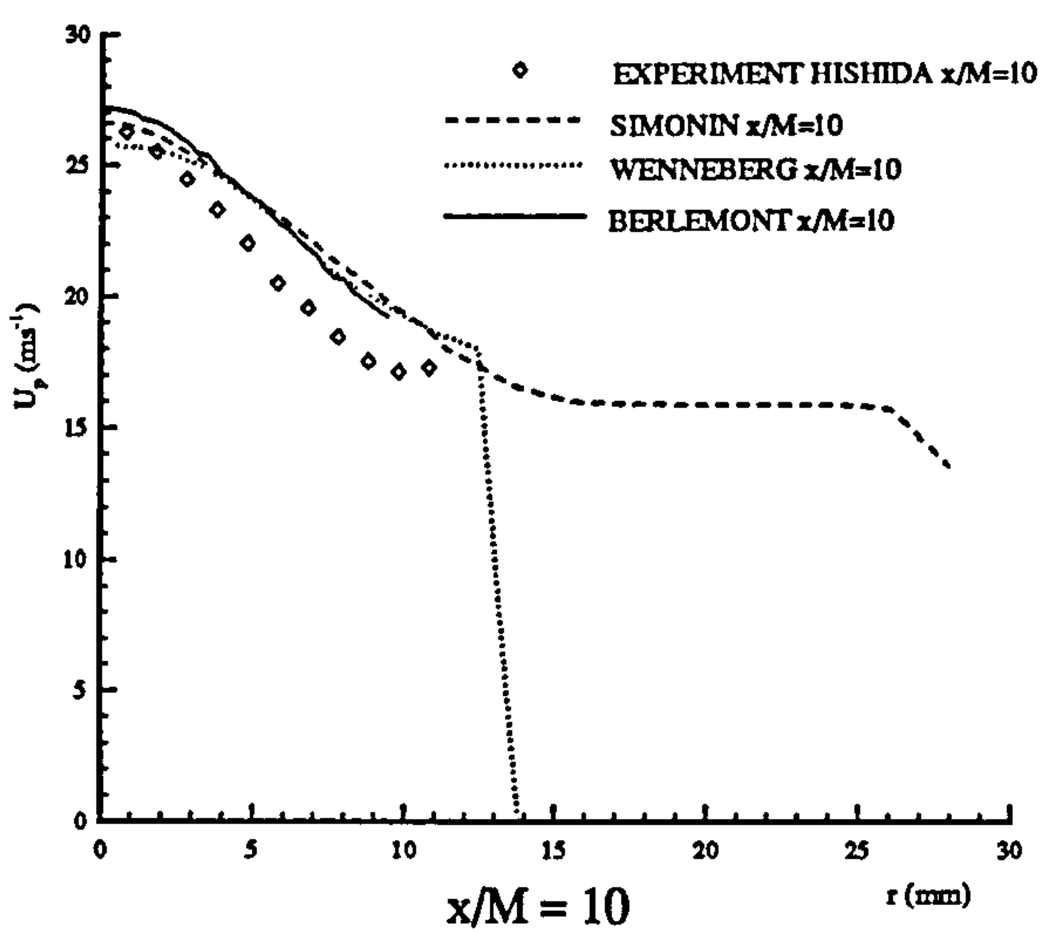

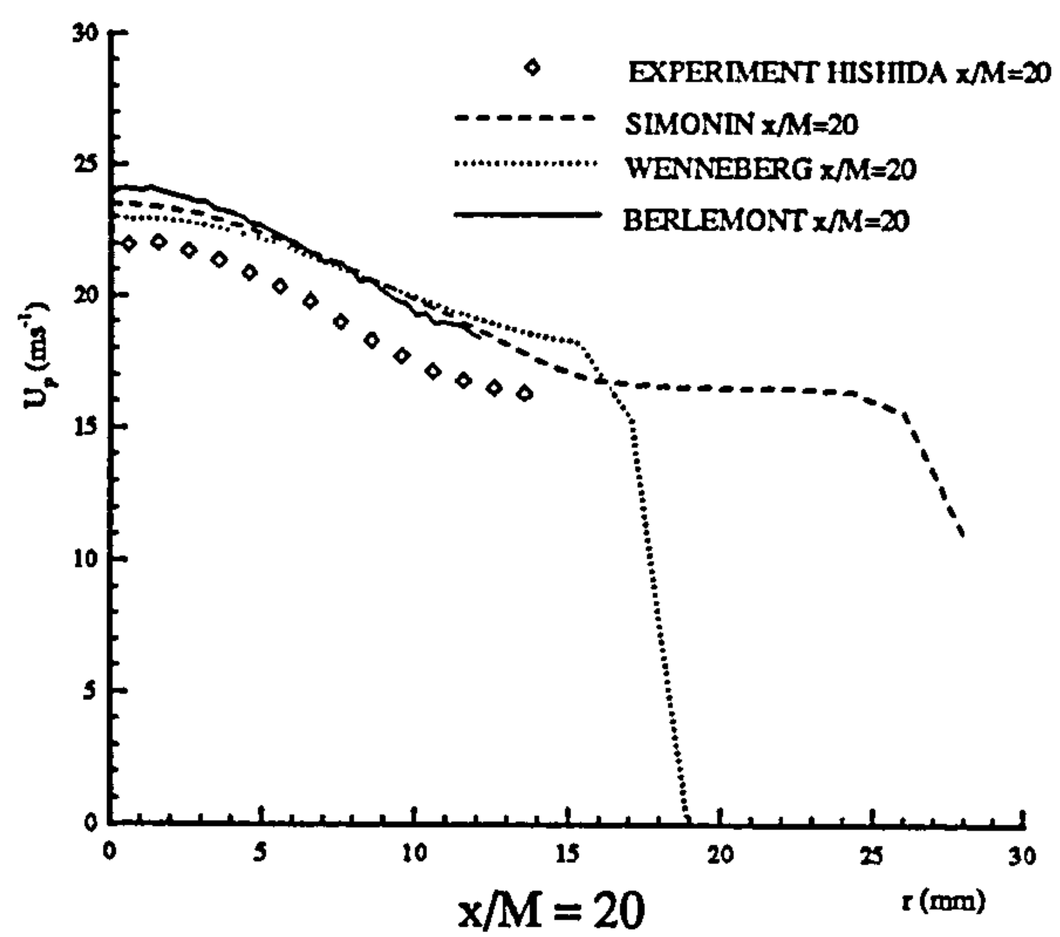

Figure 7.11 : Mean Axial Particle Velocity Profiles - Case 2 (Light Particles)

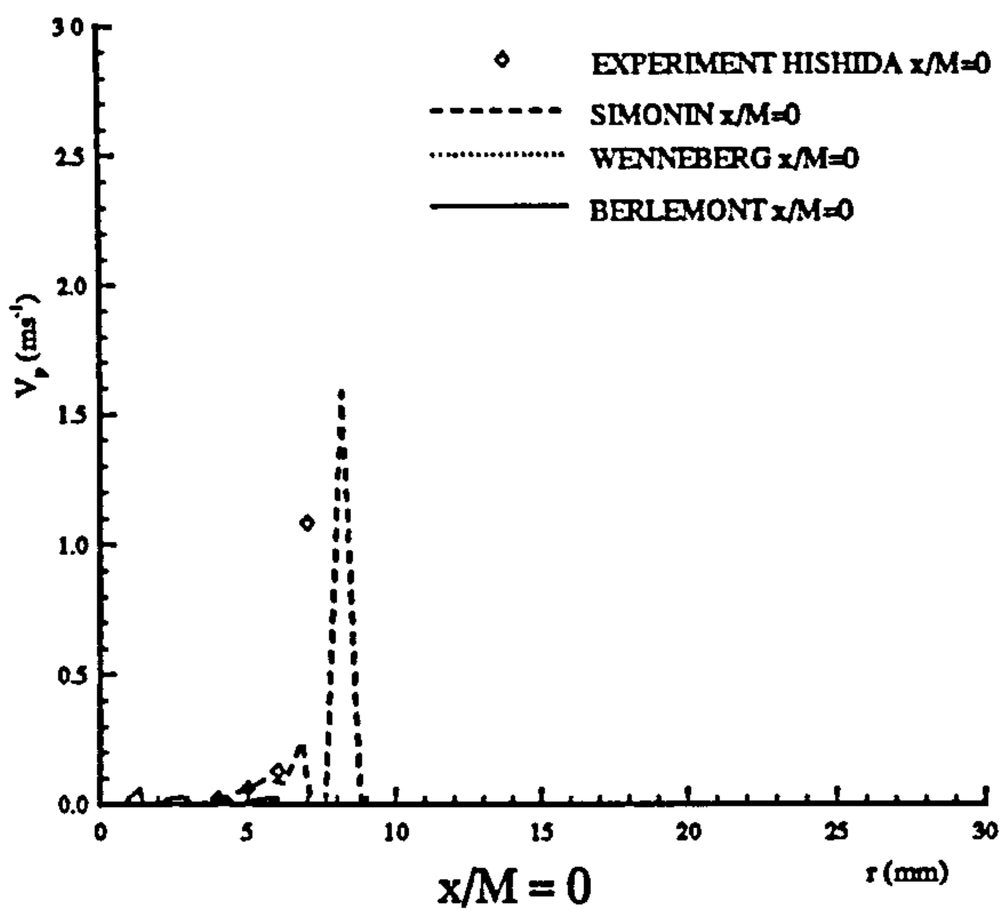

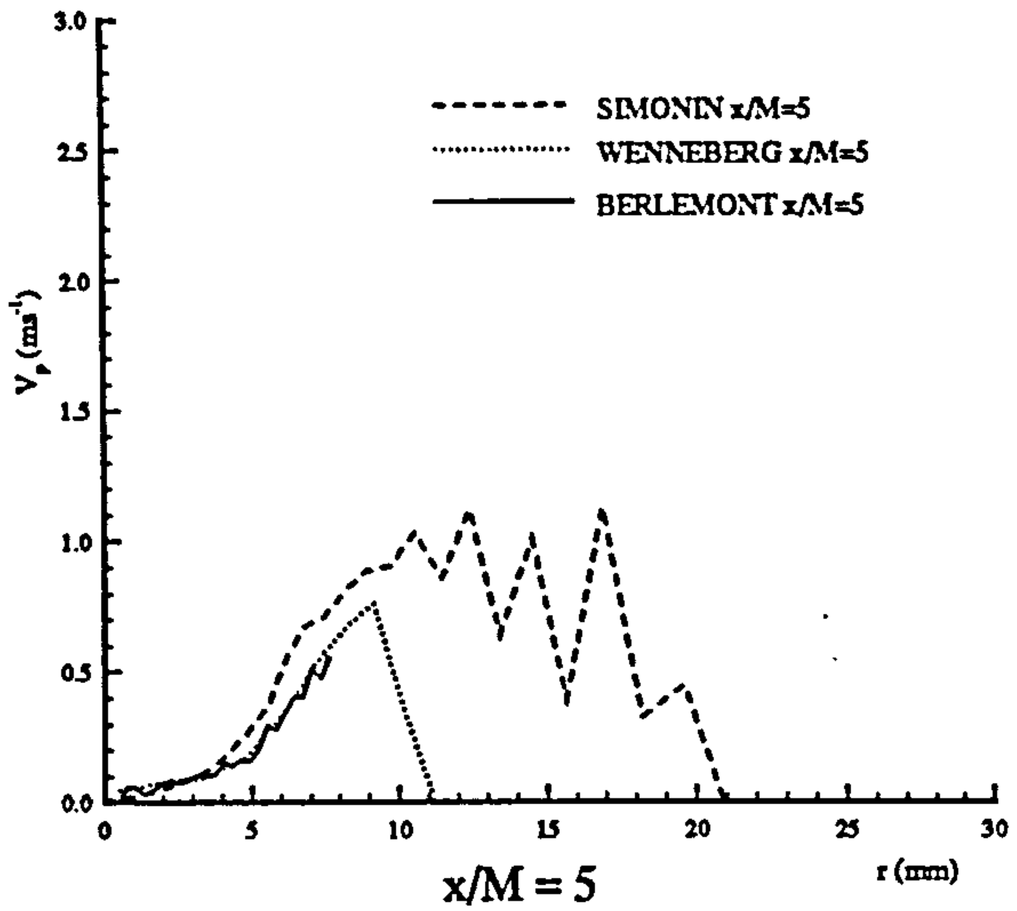

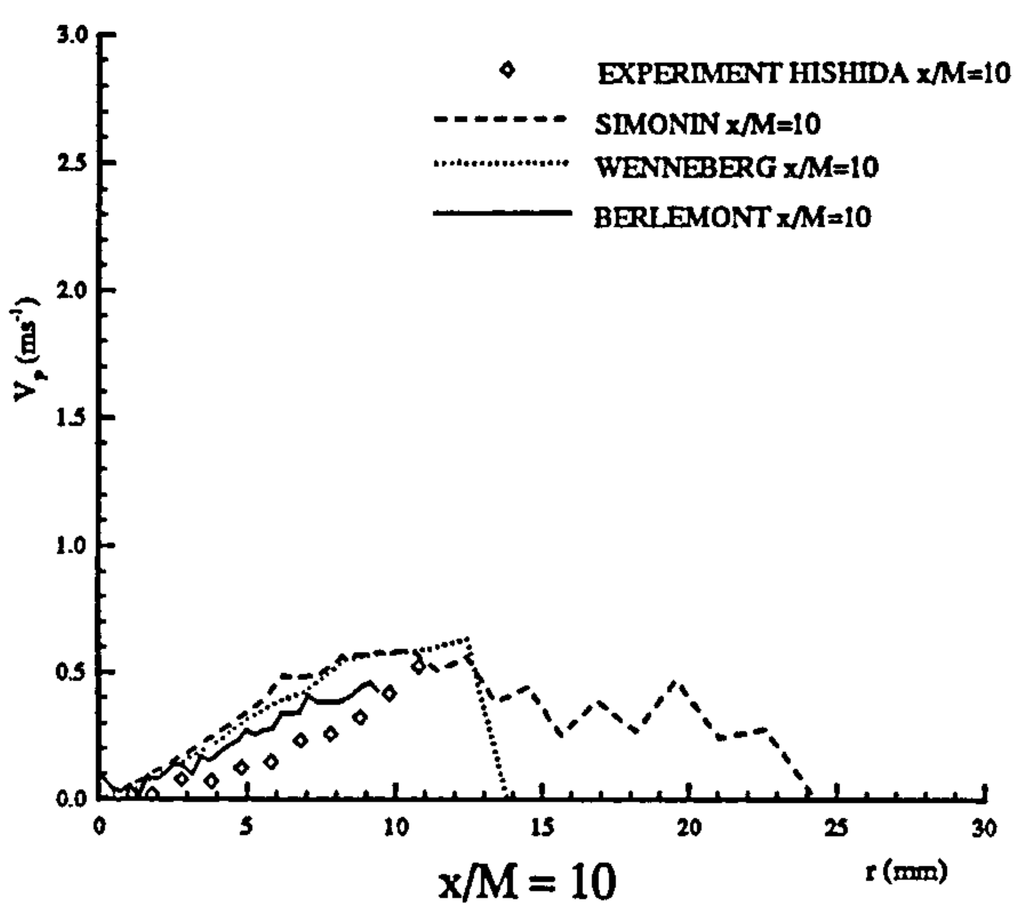

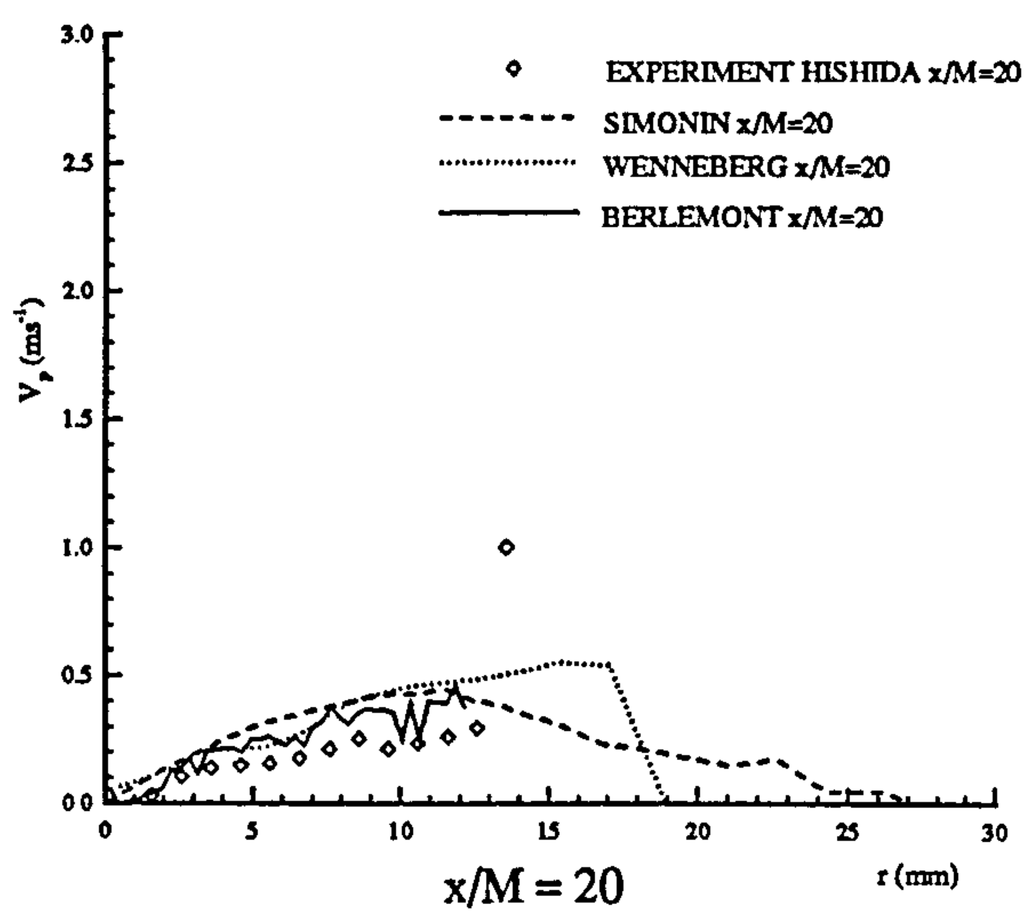

Figure 7.12 : Mean Radial Particle Velocity Profiles - Case 2 (Light Particles)

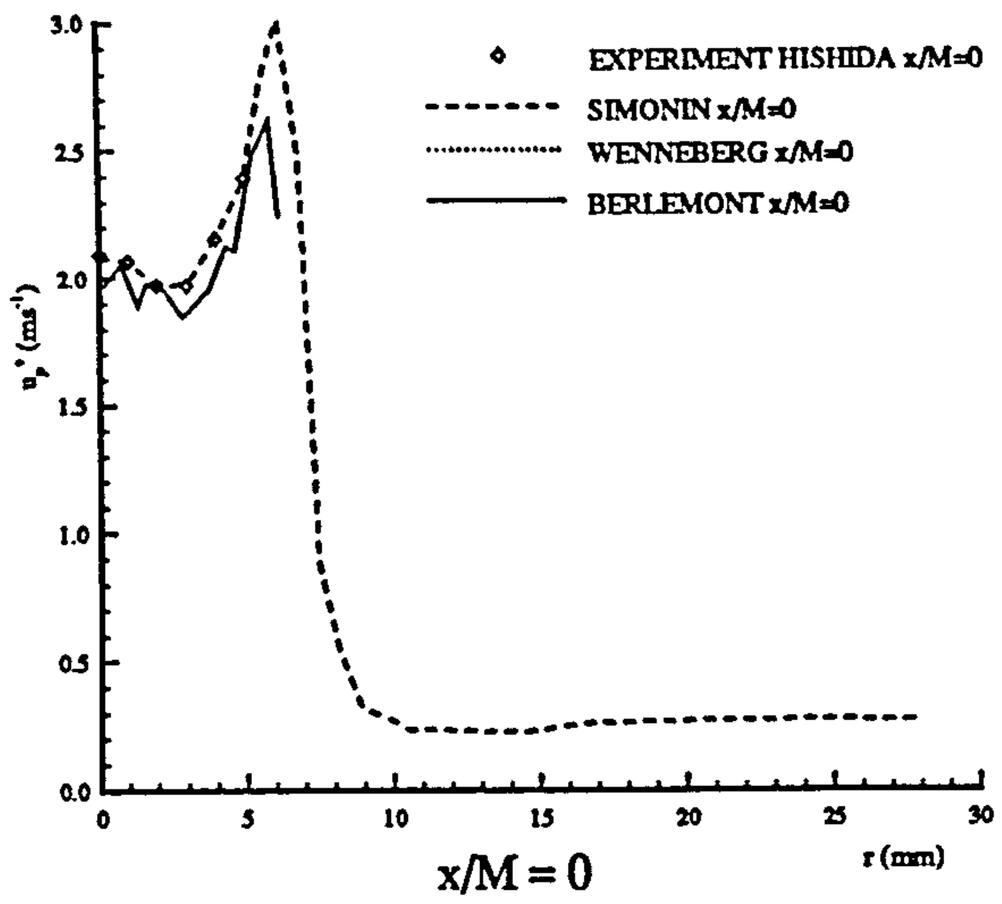

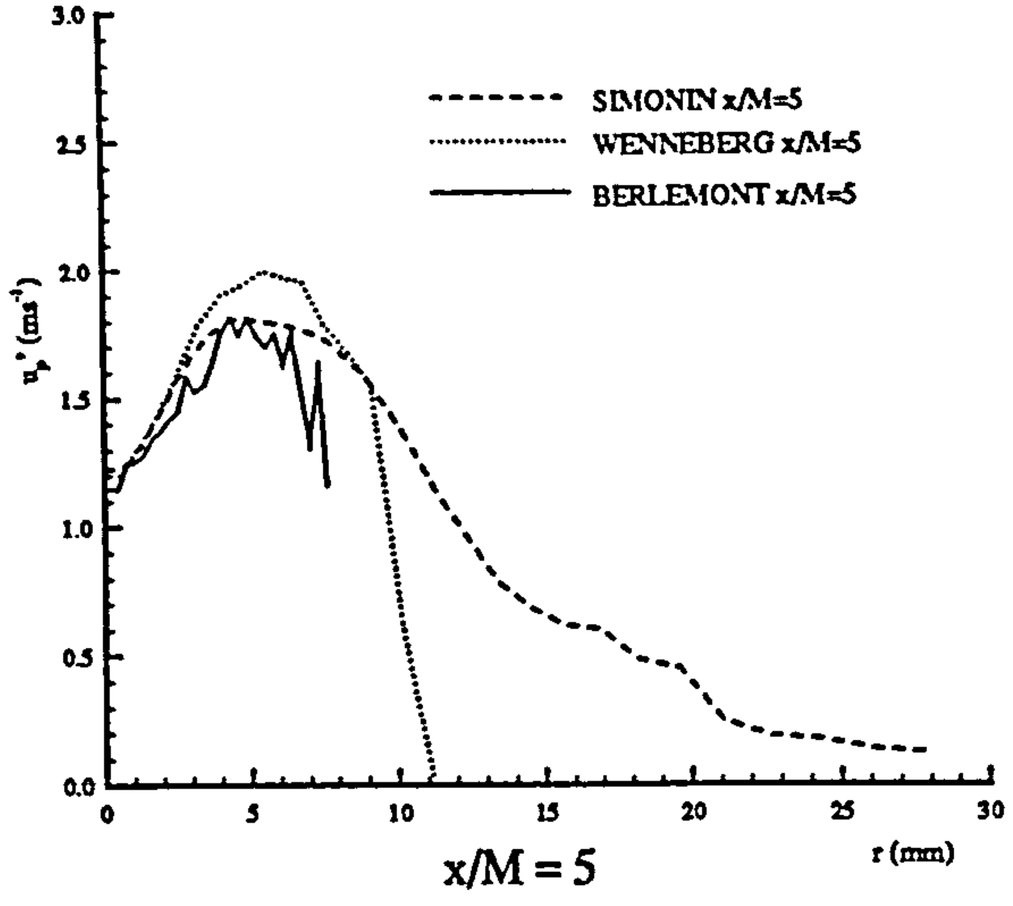

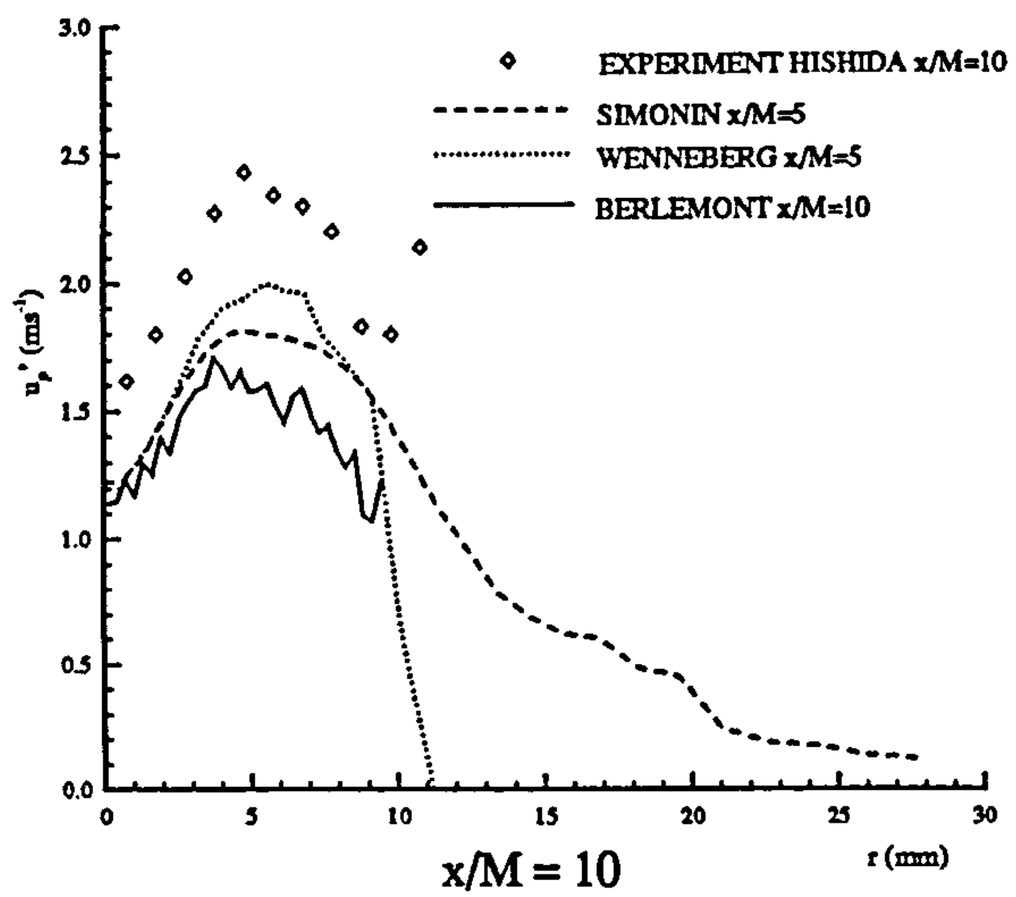

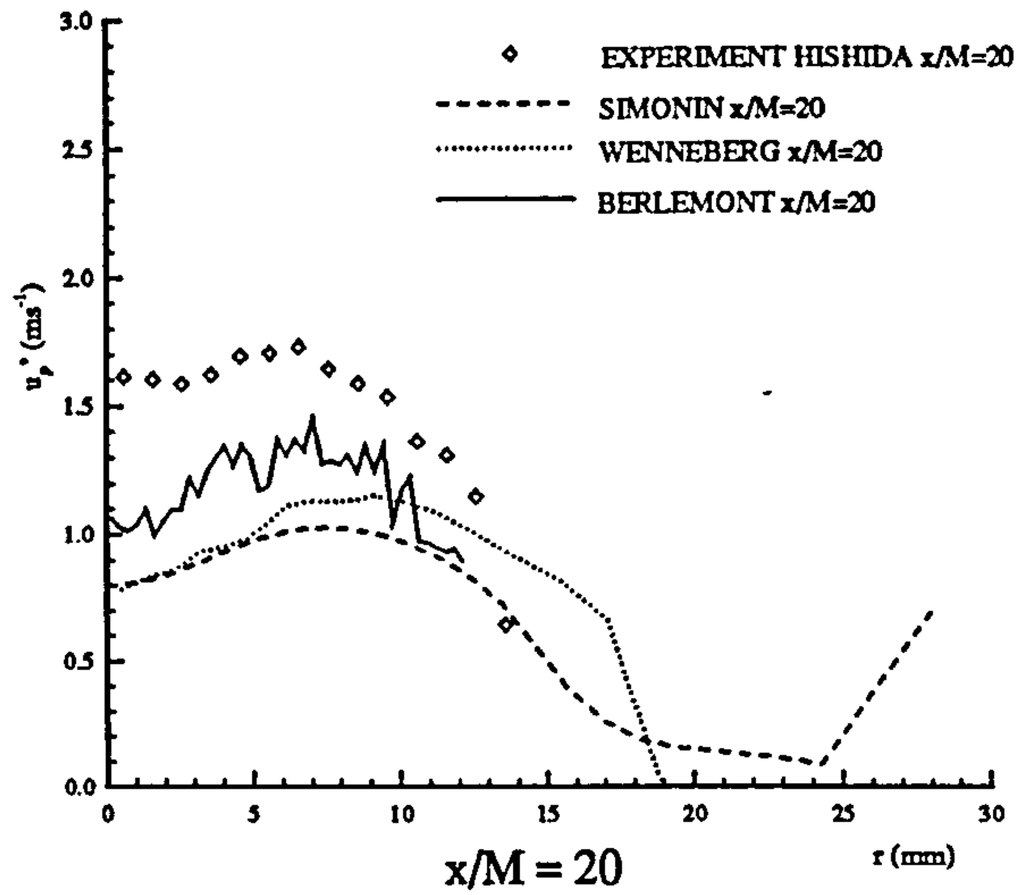

Figure 7.13 : Fluctuating Axial Particle Velocity Profiles - Case 2 (Light Particles)

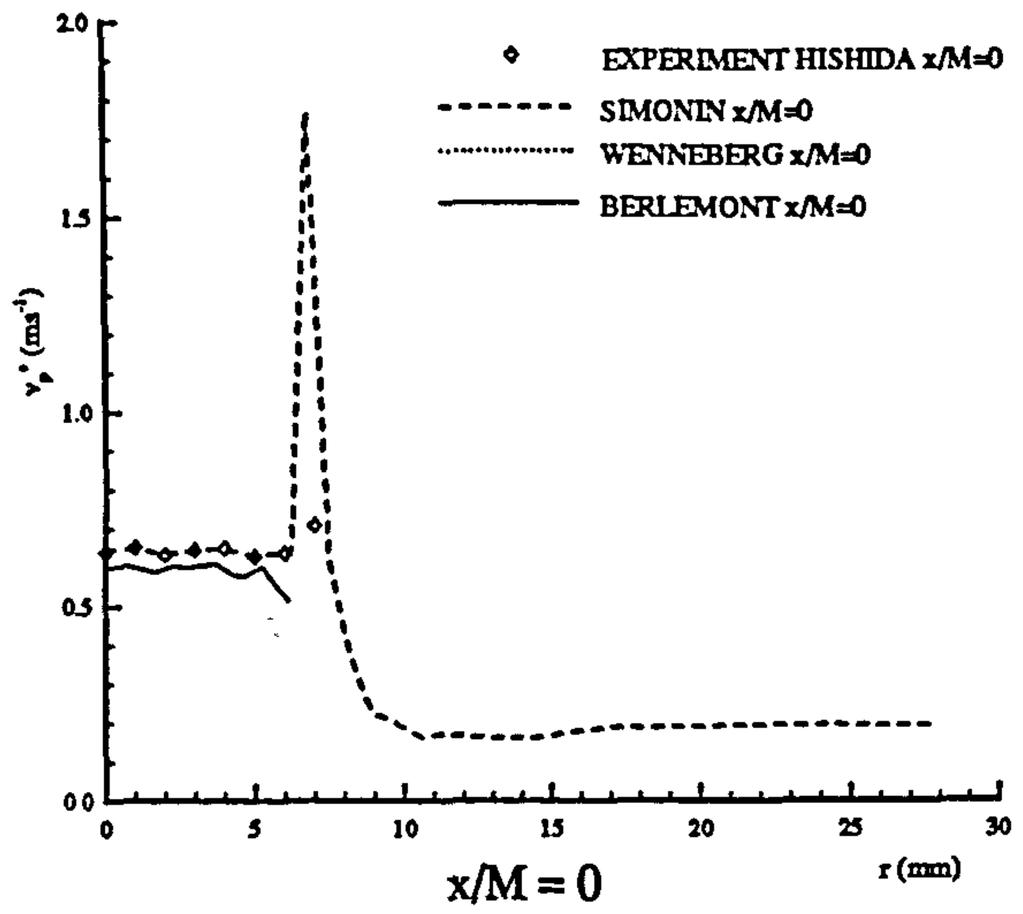

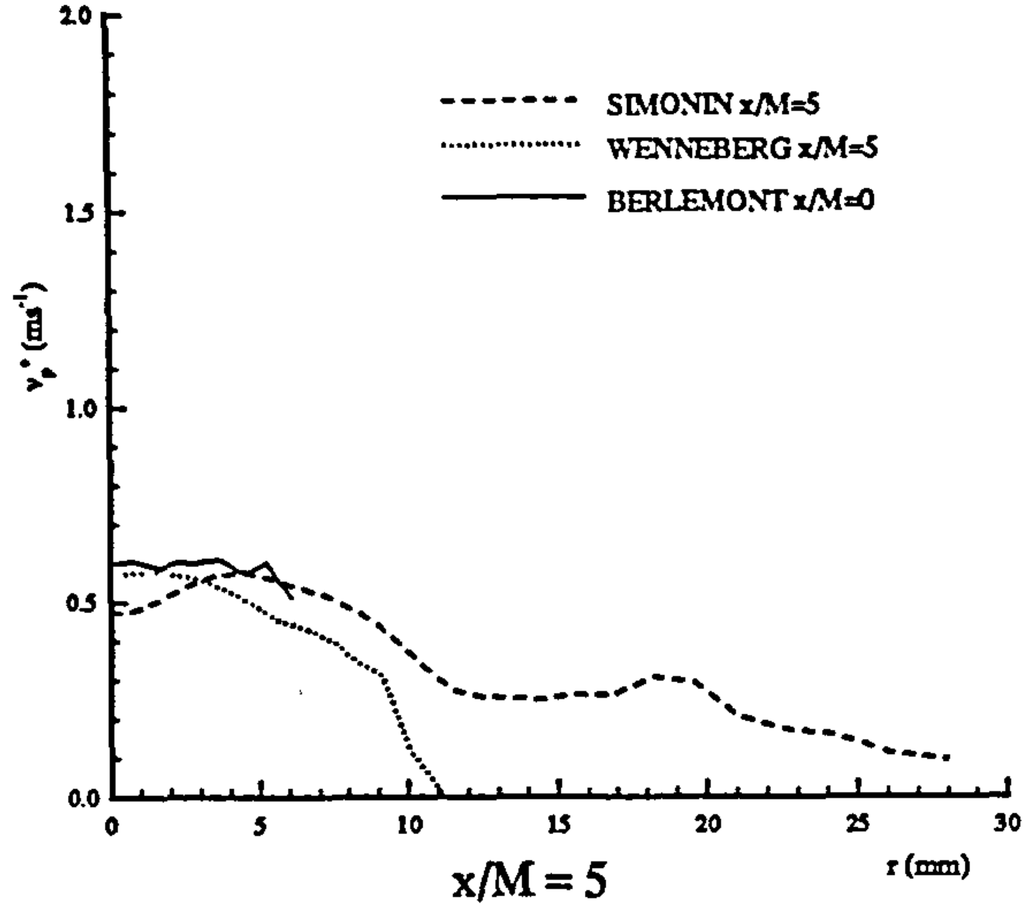

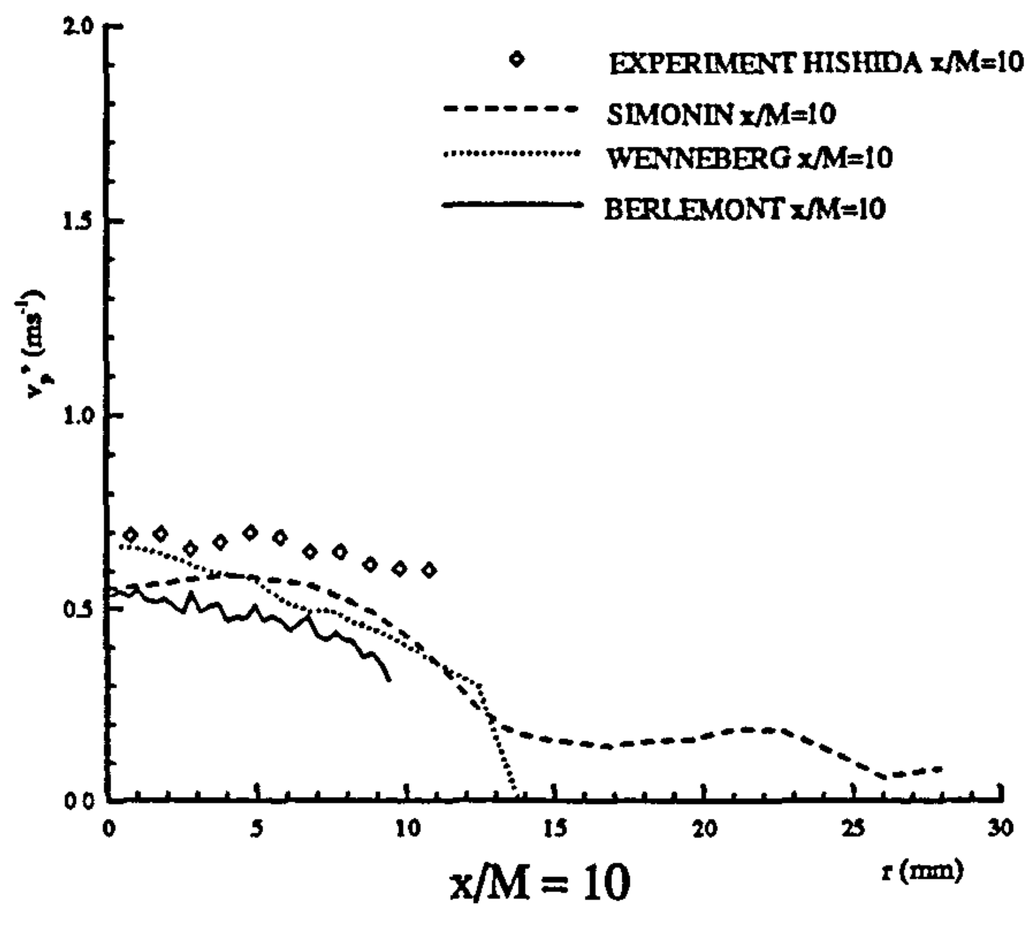

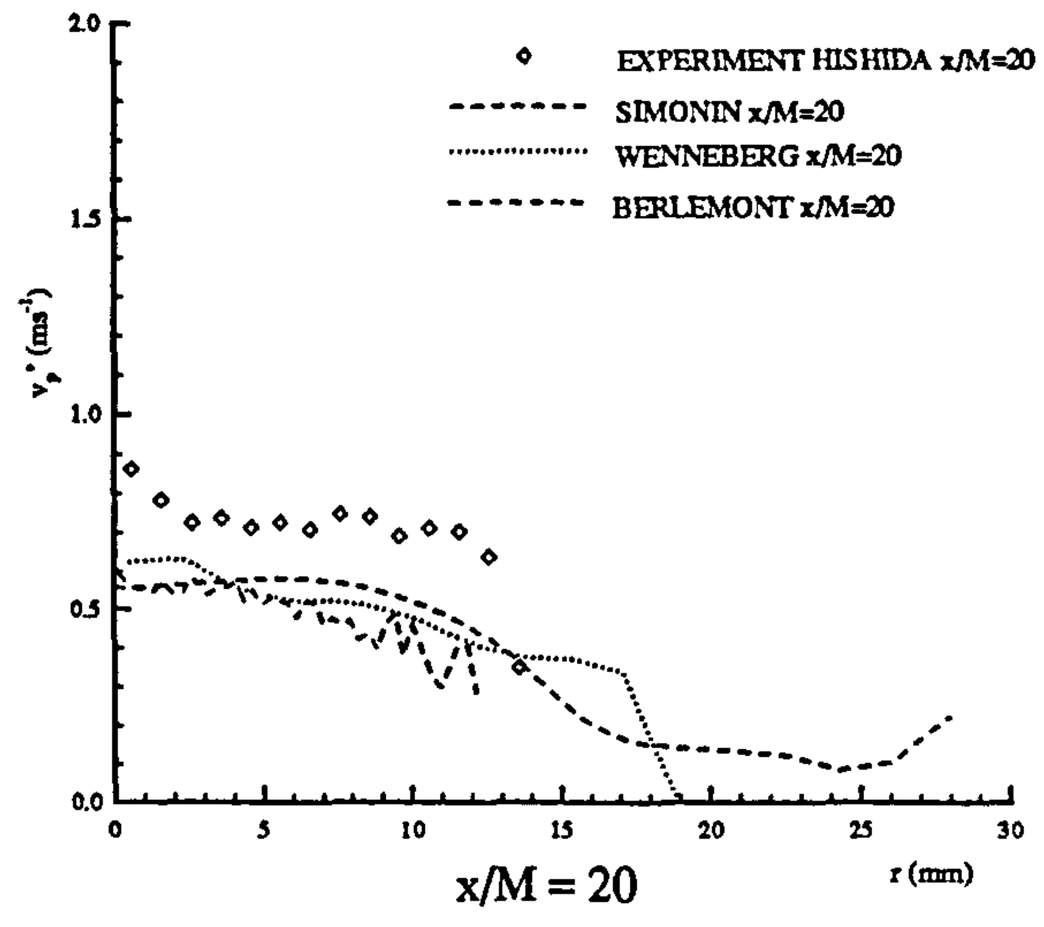

Figure 7.14 : Fluctuating Radial Particle Velocity Profiles - Case 2 (Light Particles)

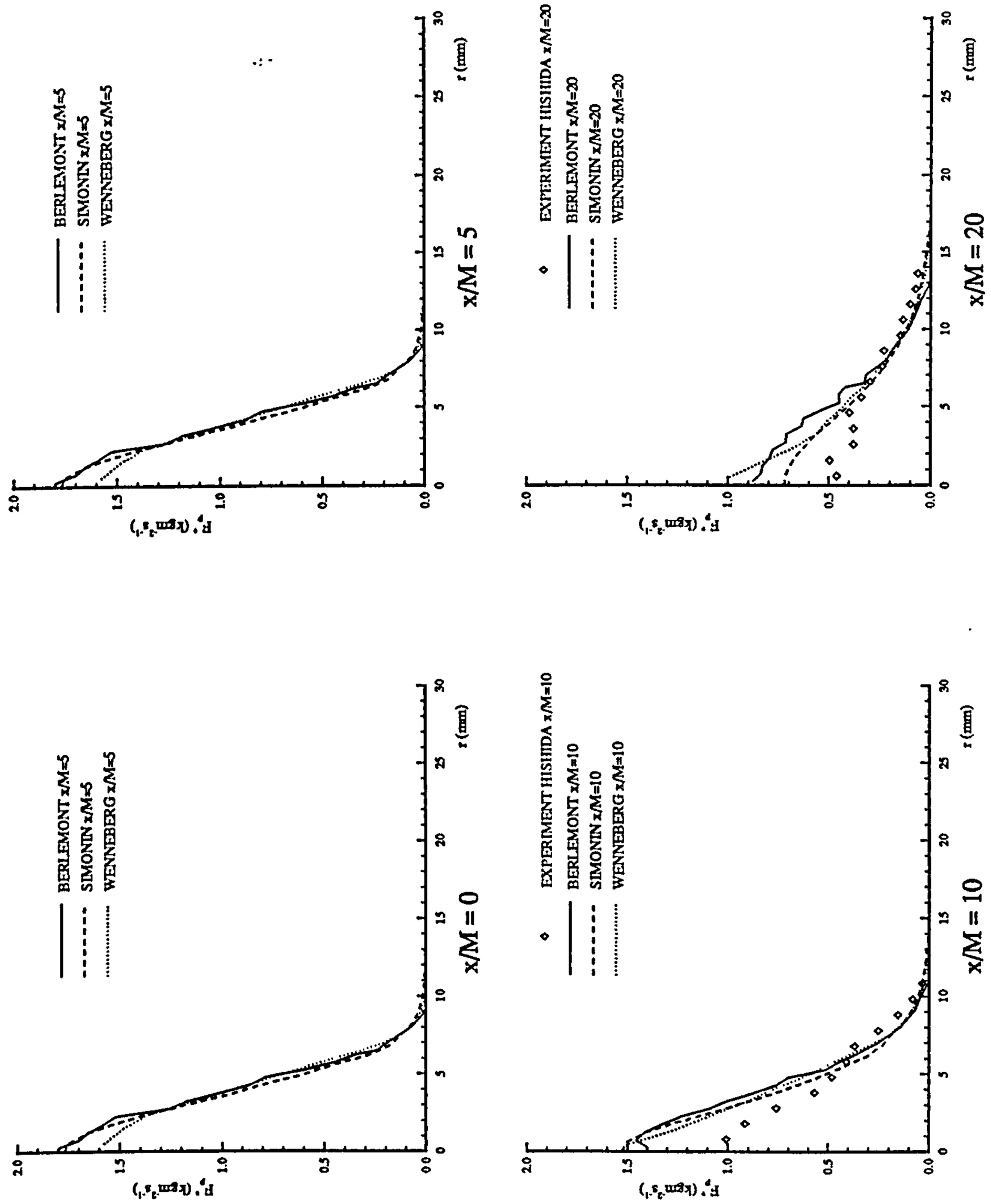

Figure 7.15 : Particle Mass Flux - Case 2 (Light Particles)

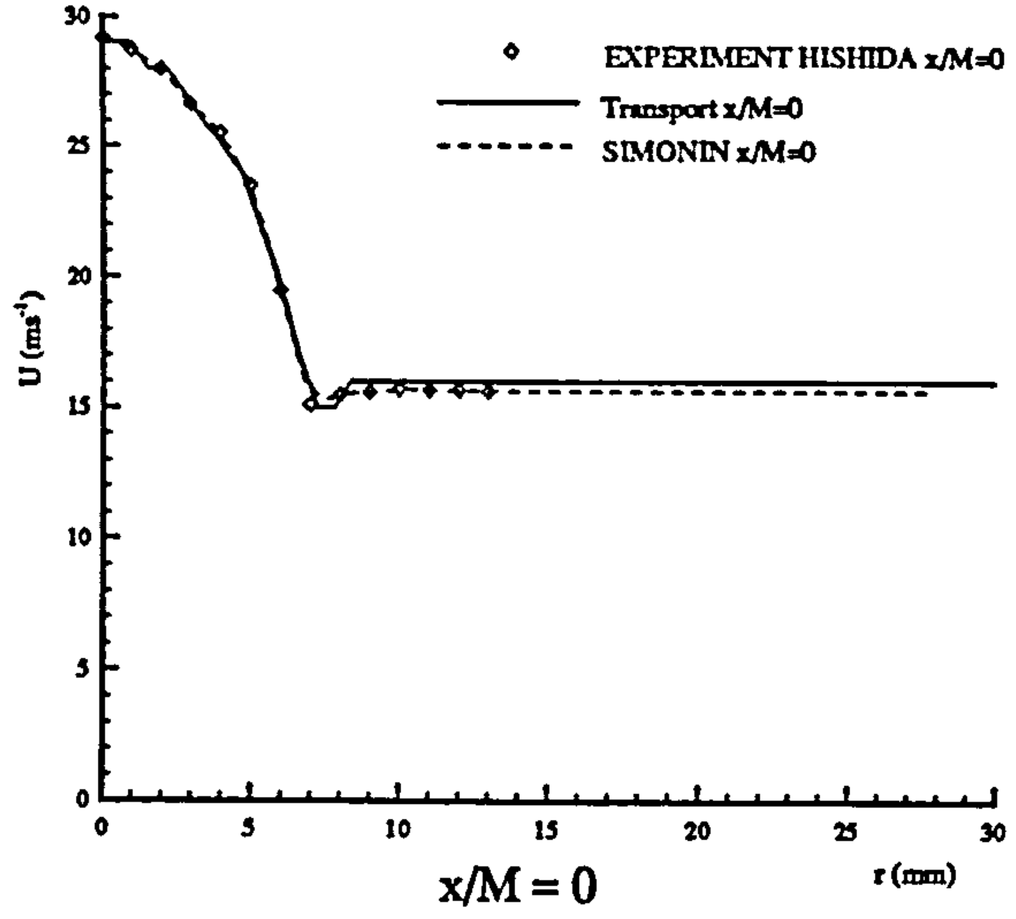

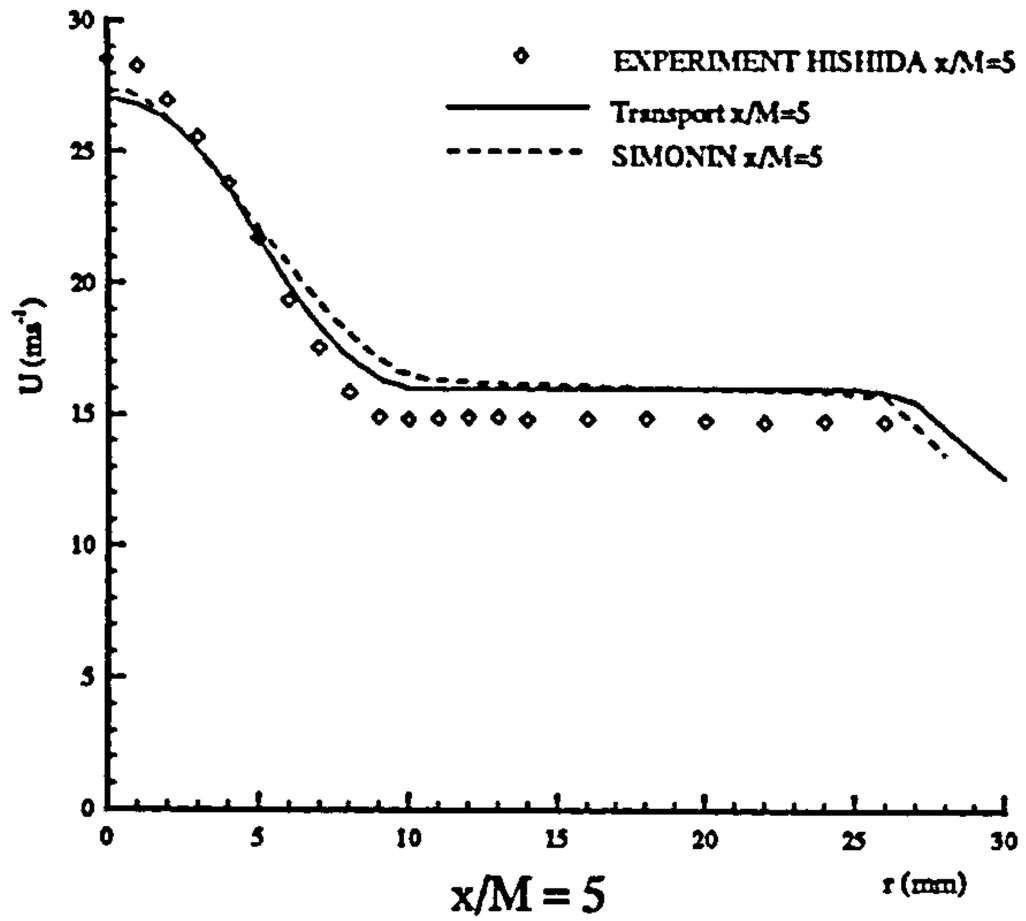

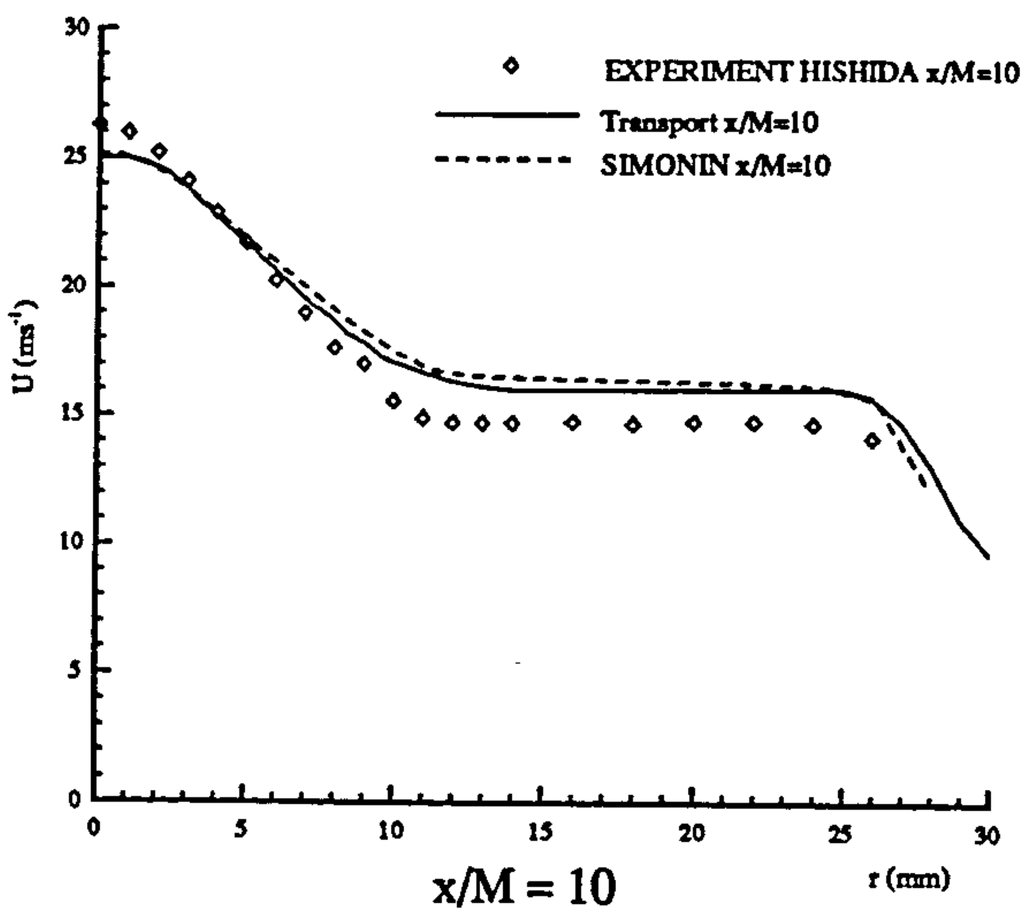

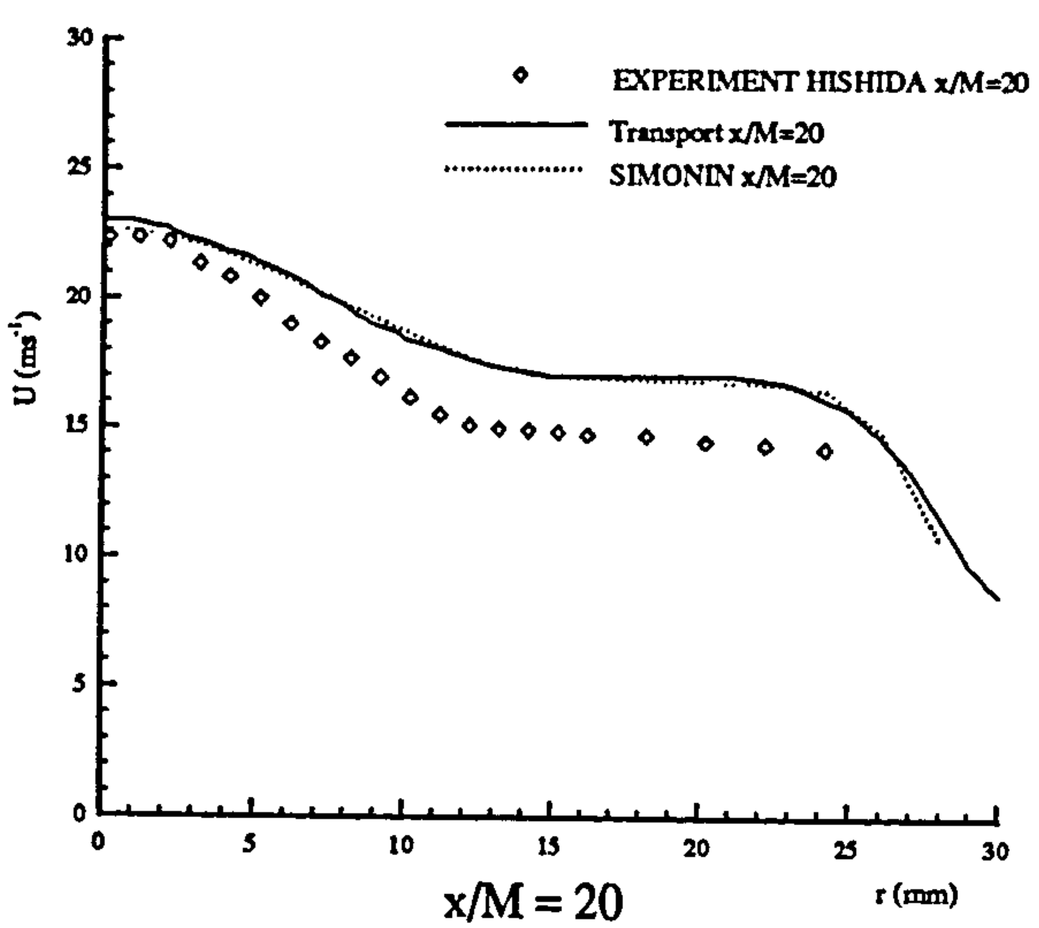

Figure 7.16 : Mean Axial Gas Velocity Profiles

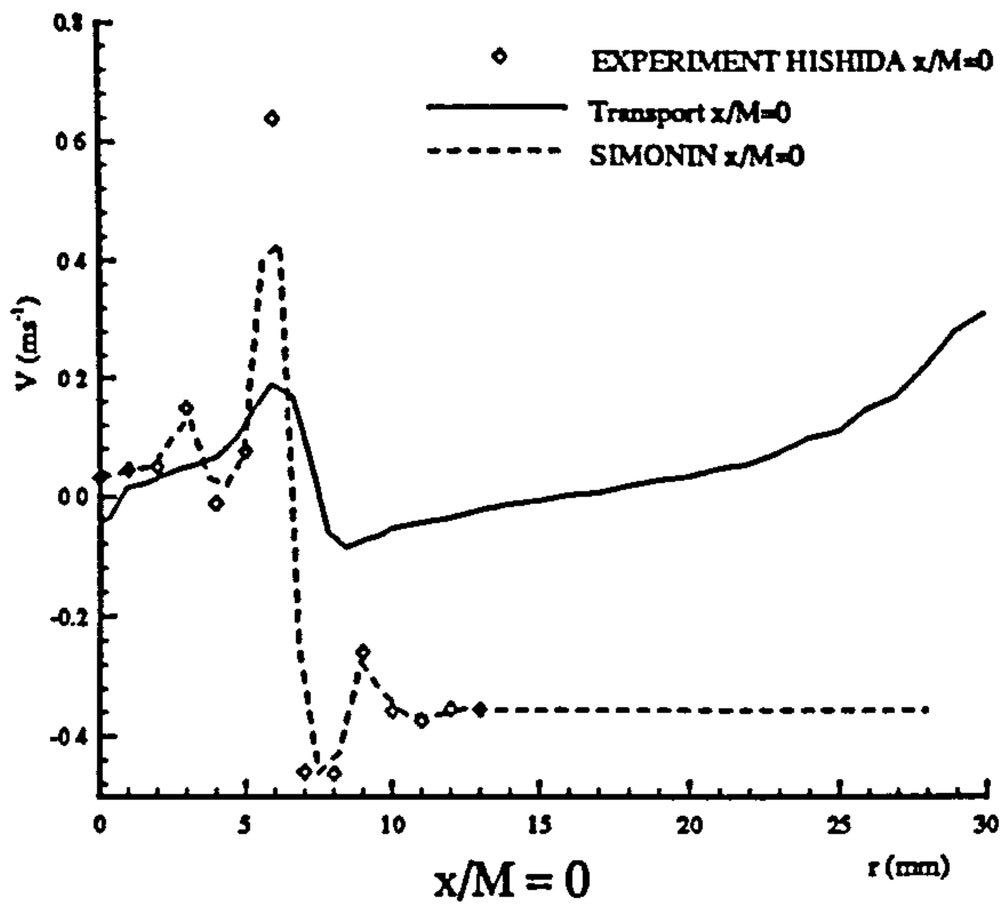

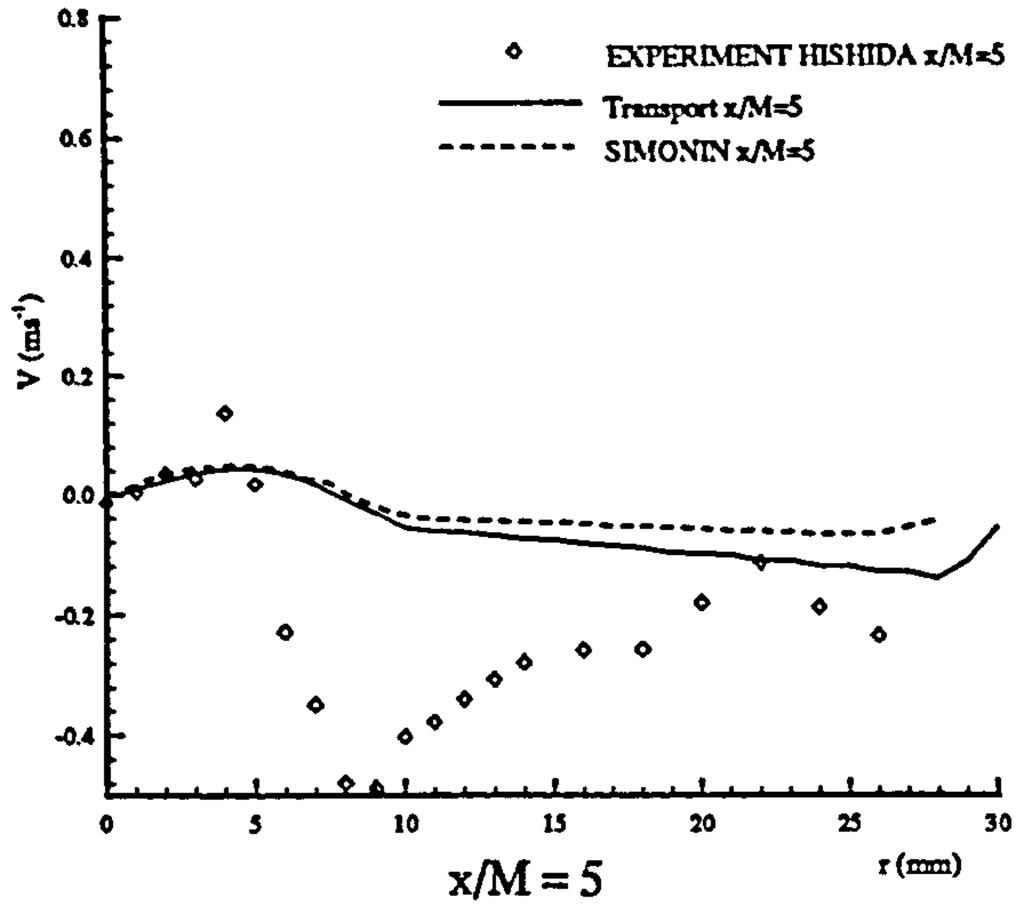

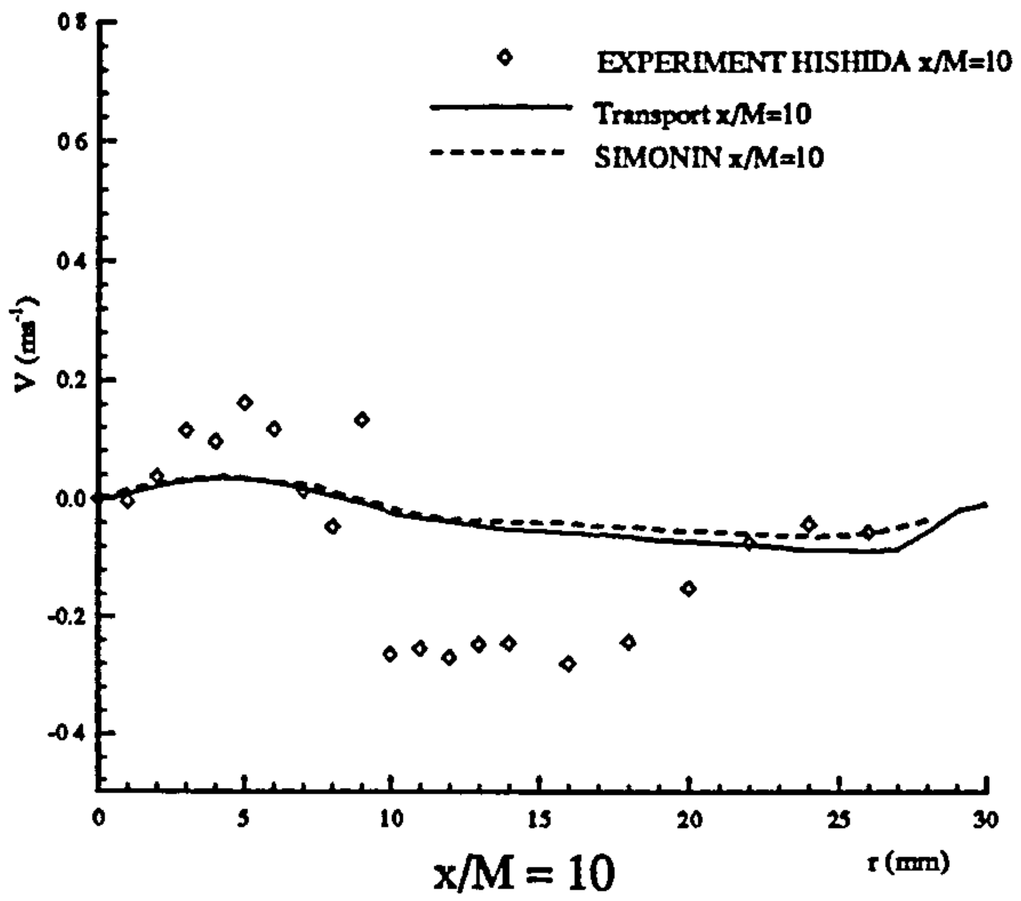

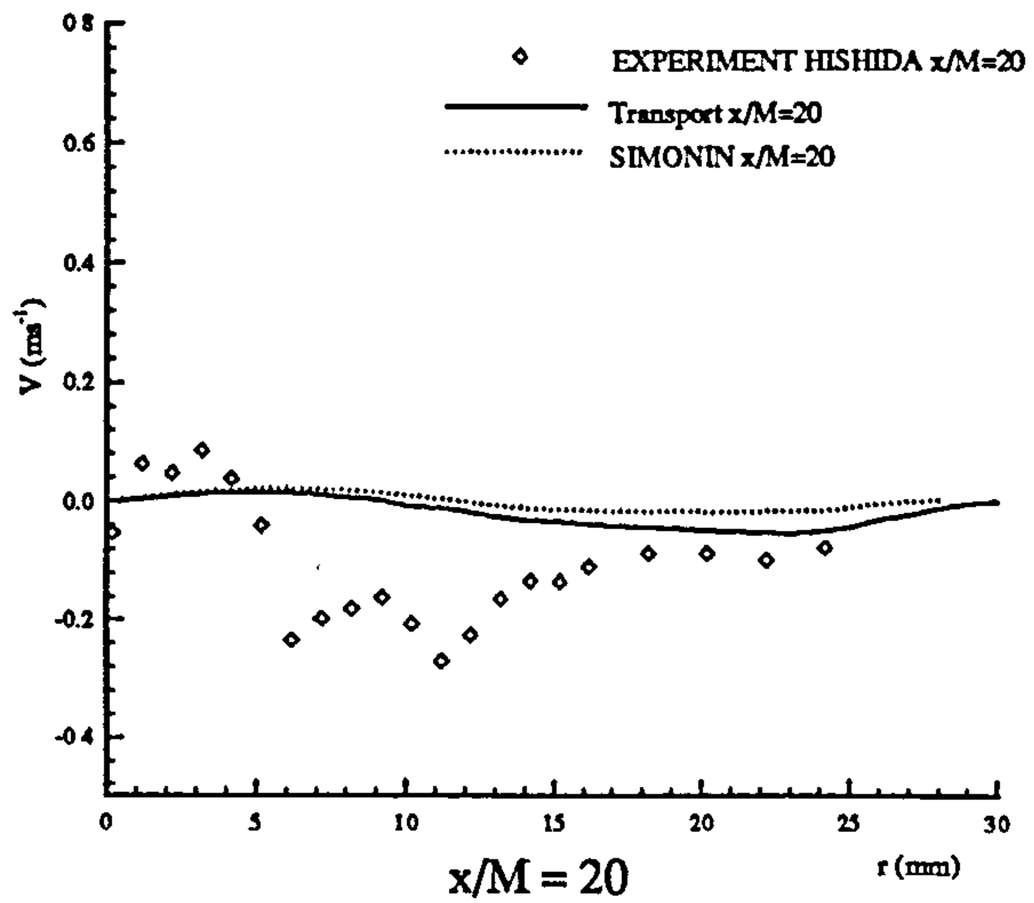

Figure 7.17 : Mean Radial Gas Velocity Profiles

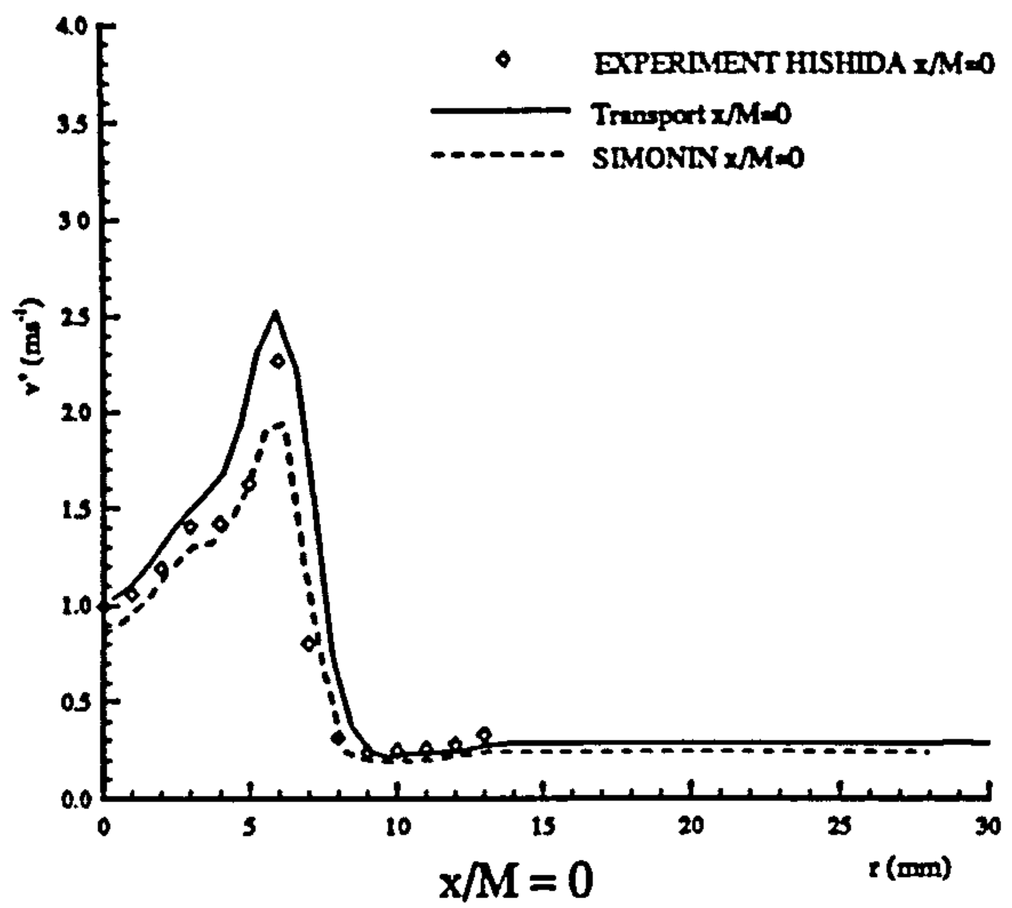

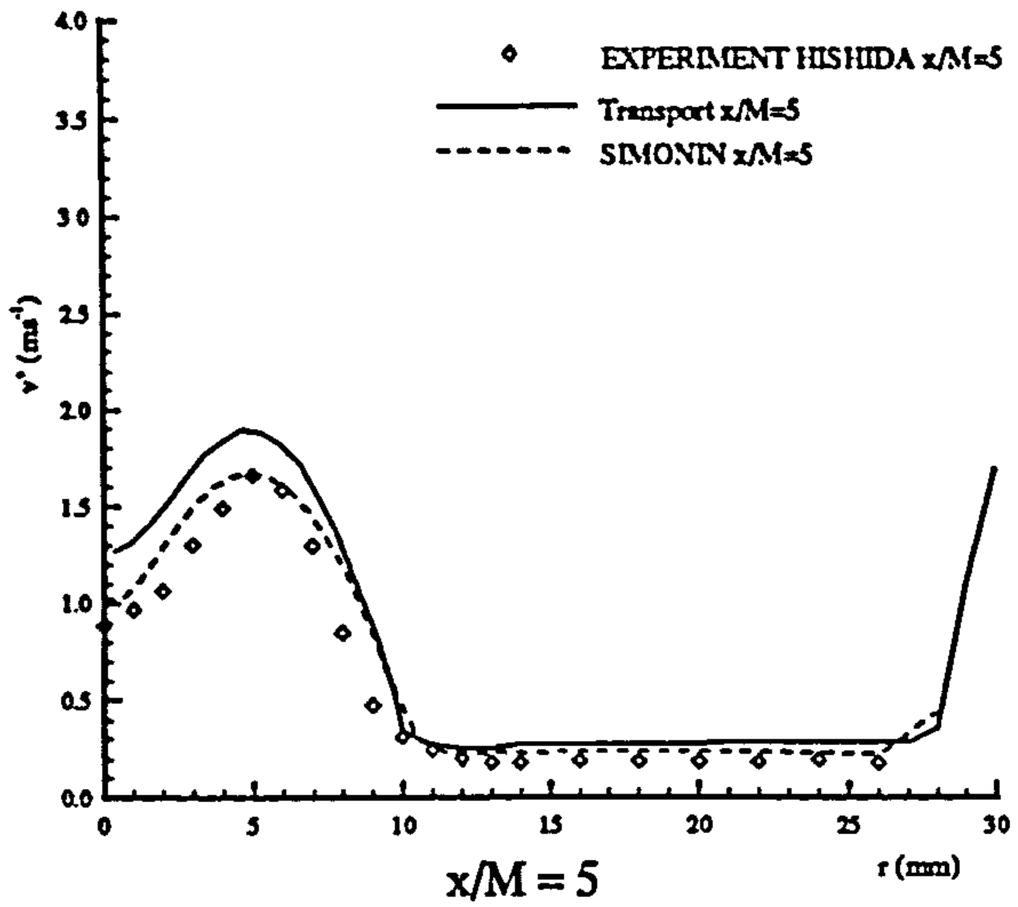

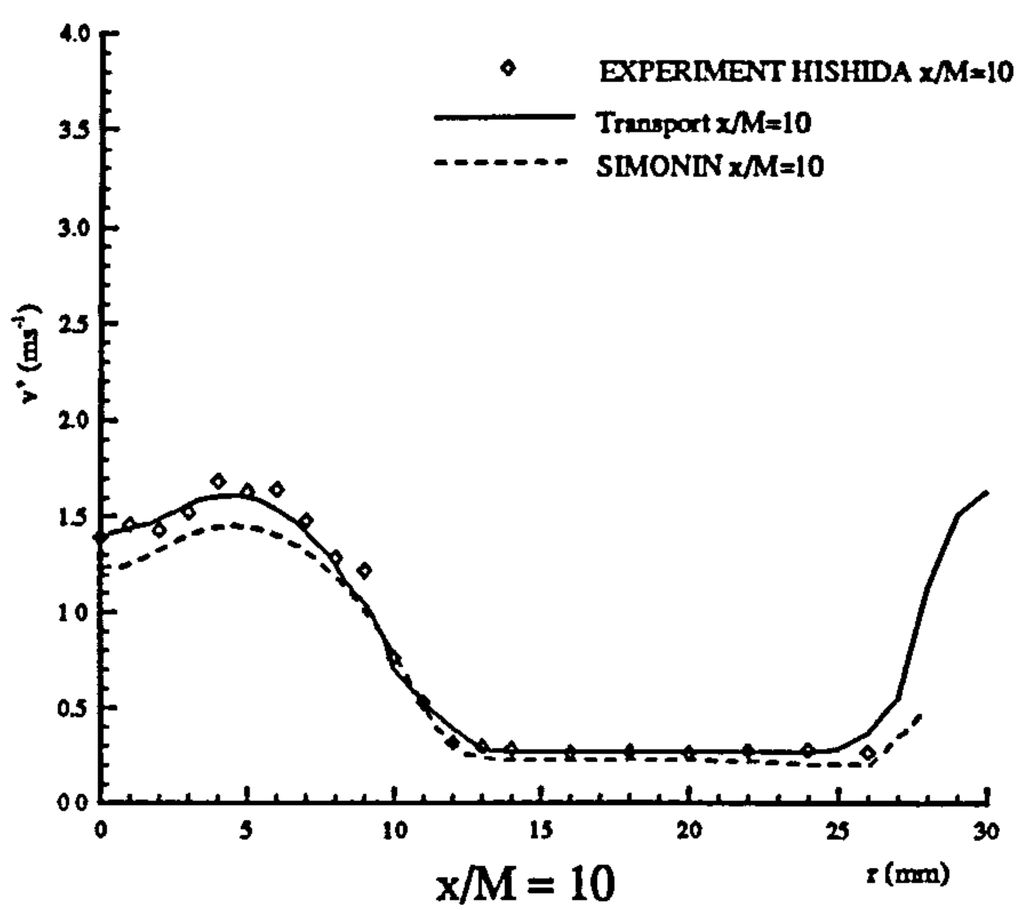

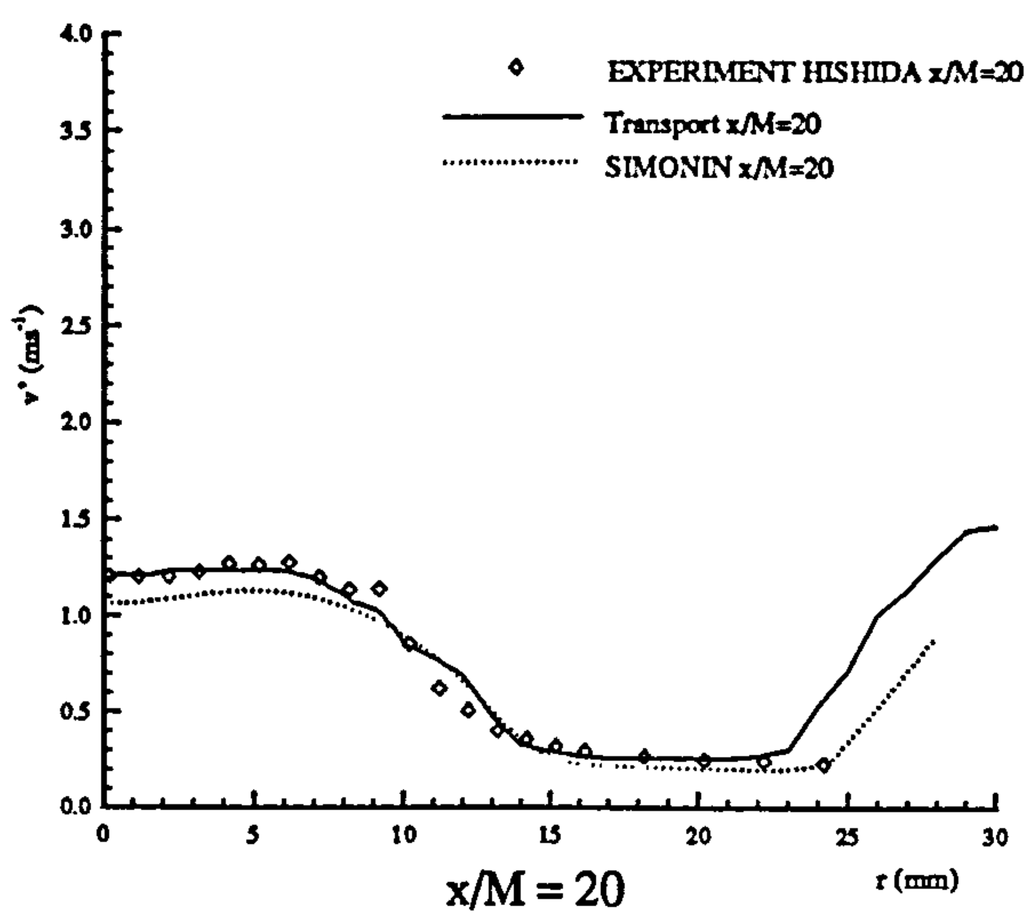

Figure 7.18 : Fluctuating Radial Gas Velocity Profiles

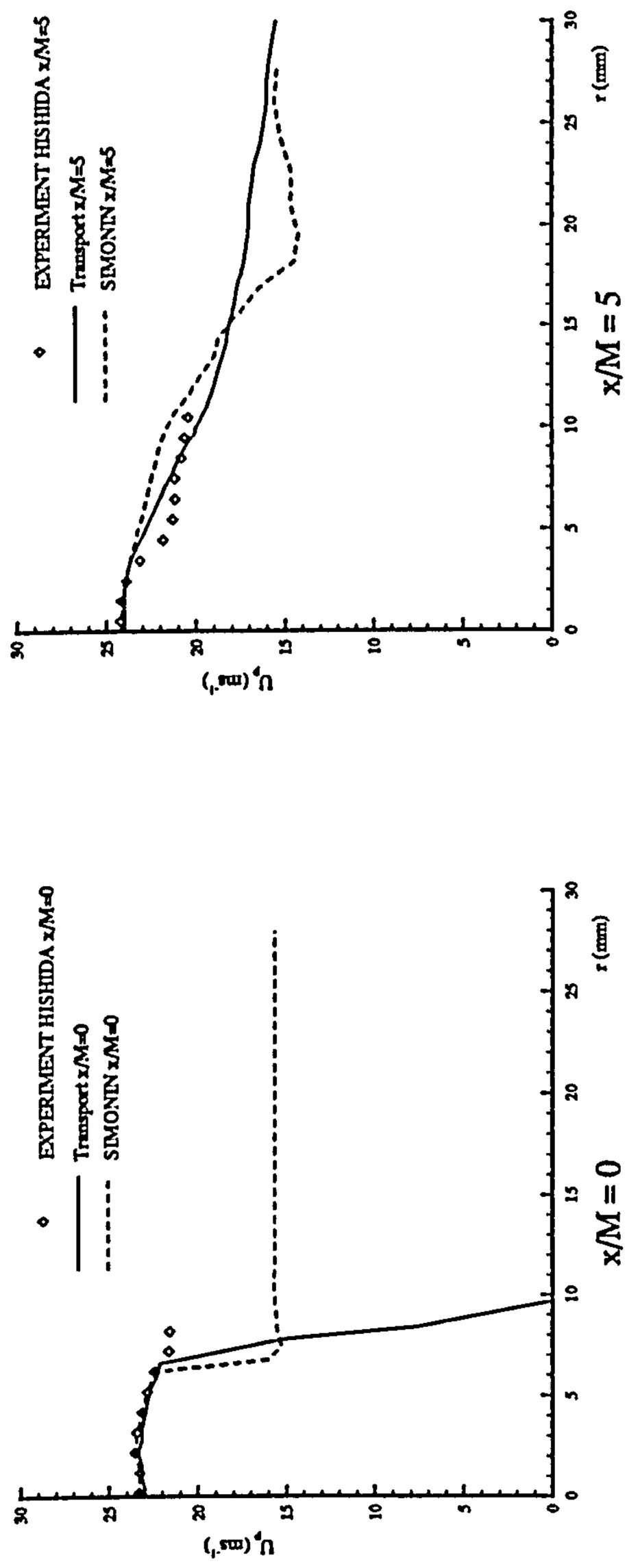

Figure 7.19 : Mean Axial Particle Velocity Profiles - Case1

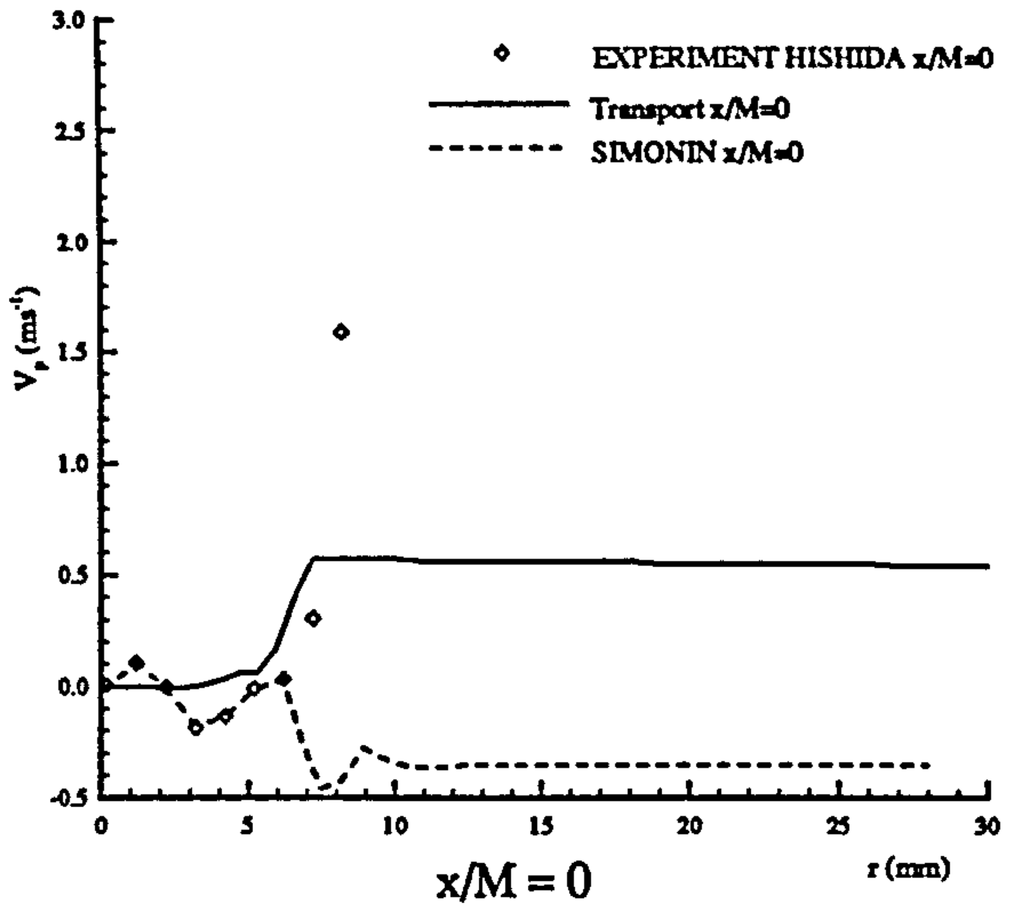

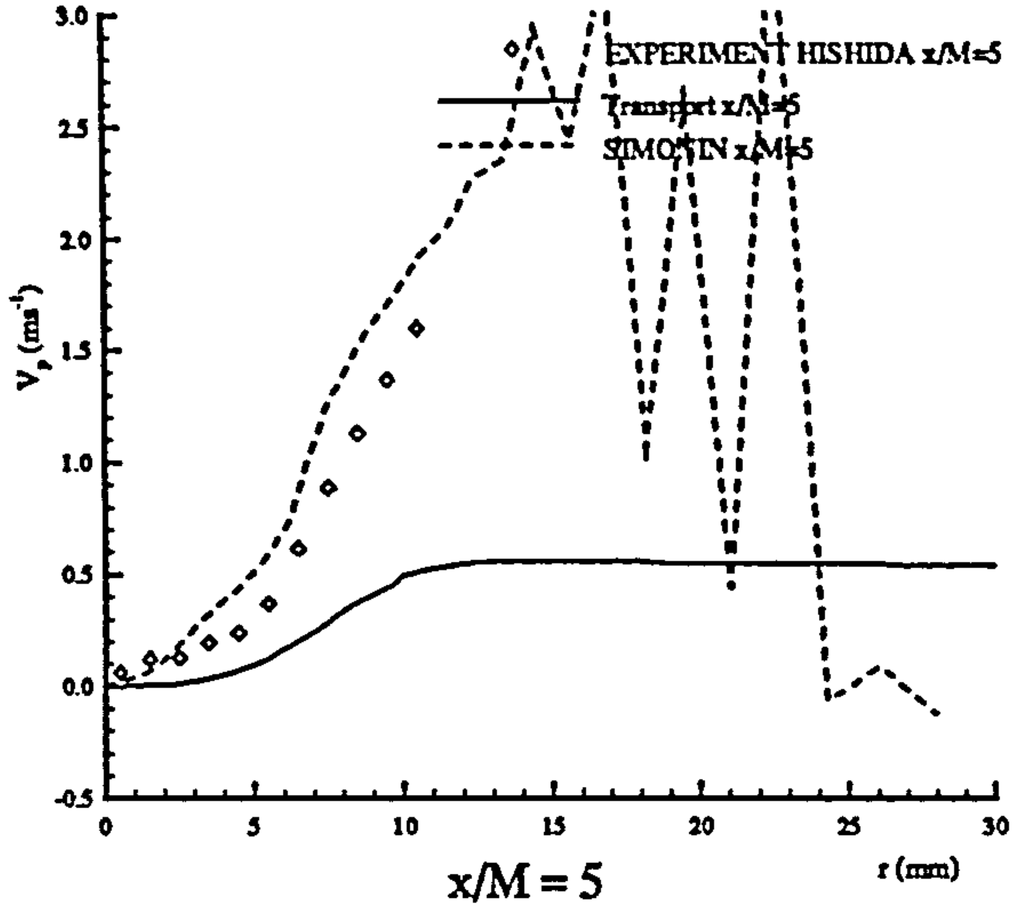

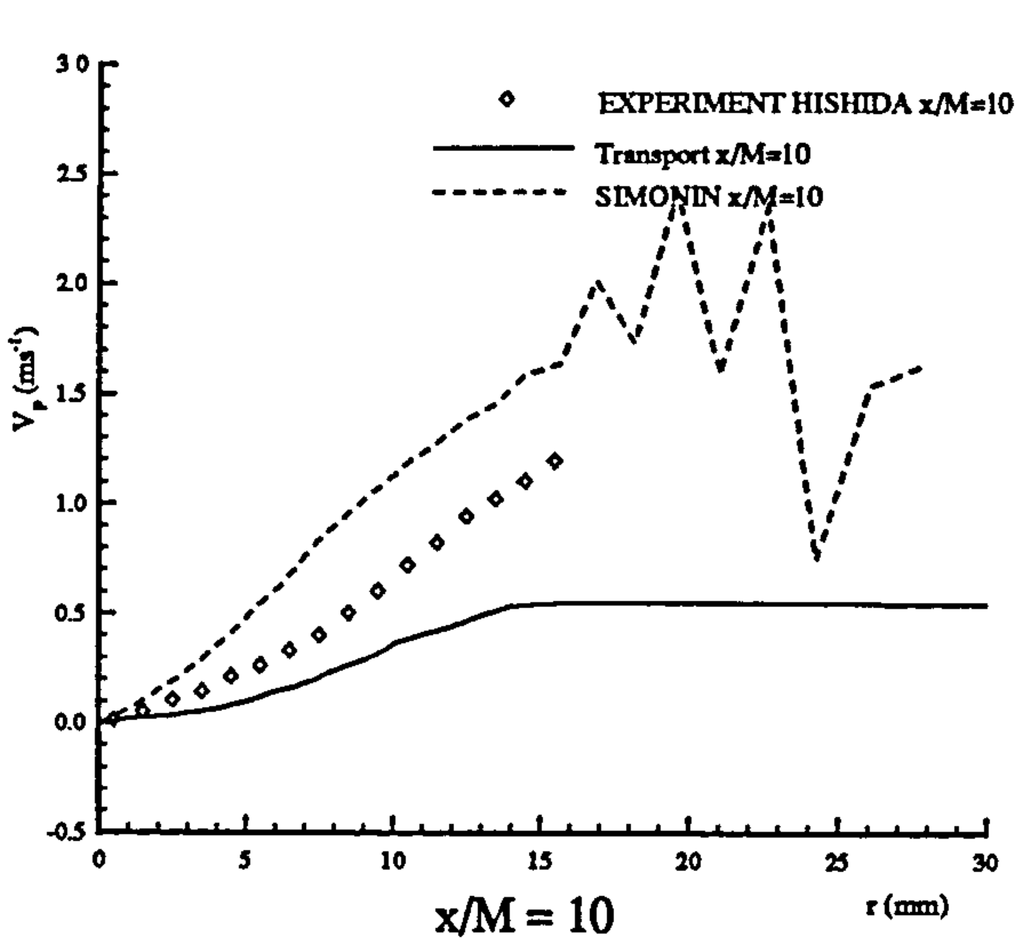

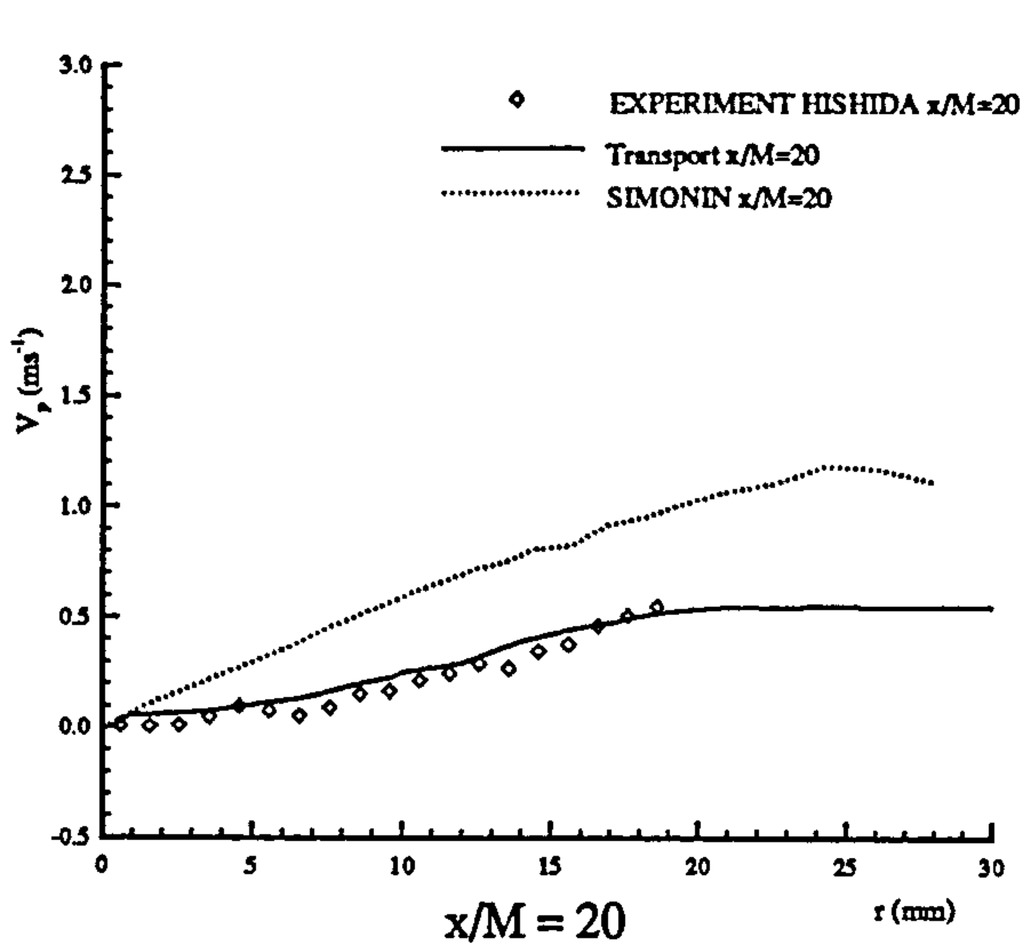

Figure 7.20 : Mean Radial Particle Velocity Profiles - Case 1

Figure 7.21 : Particle Mass Flux - Case 1

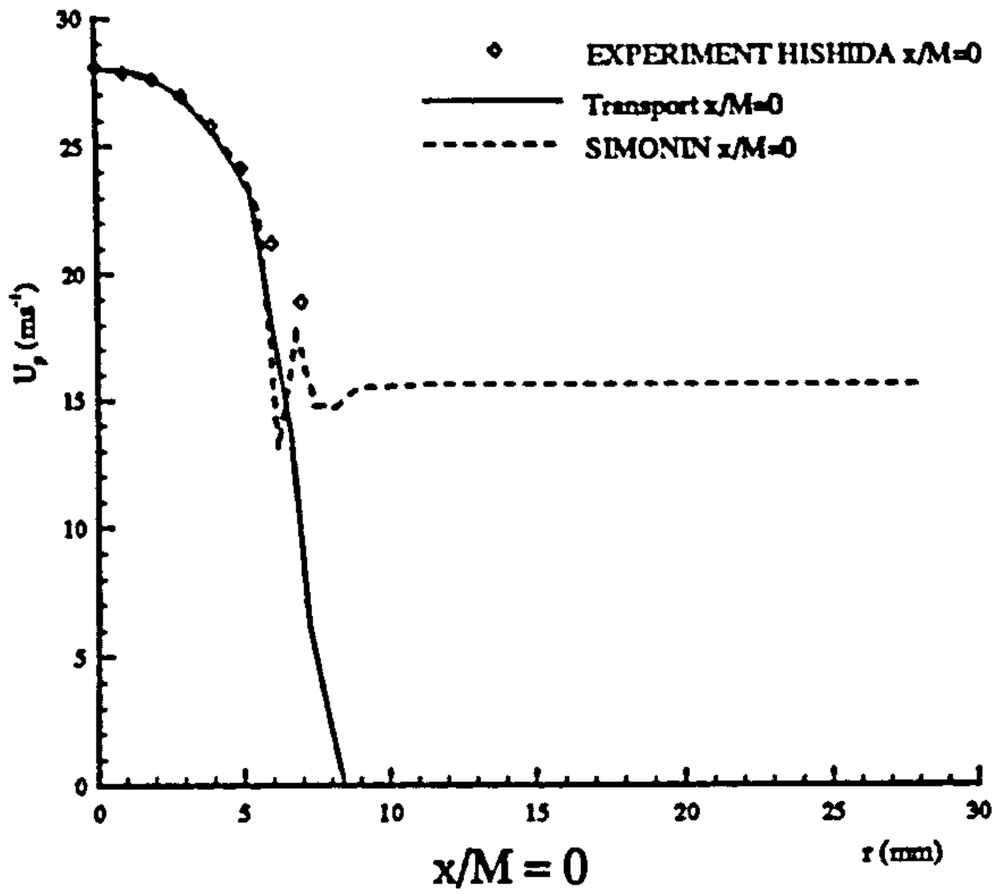

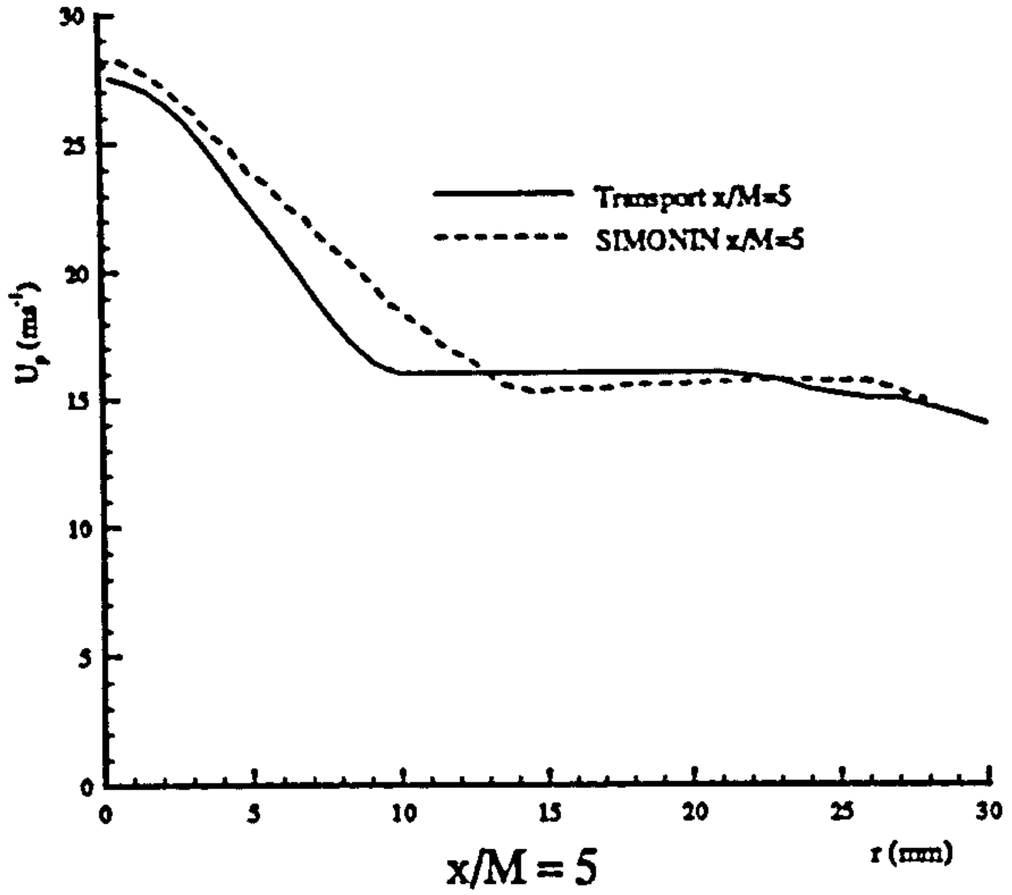

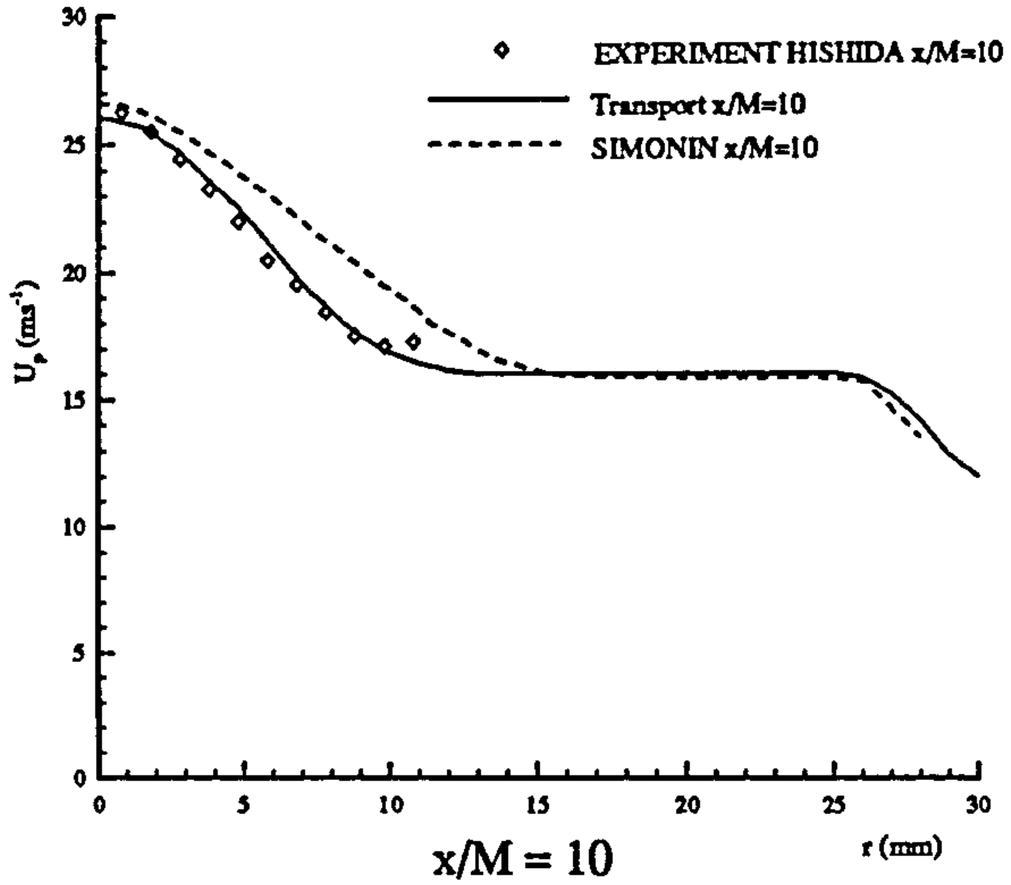

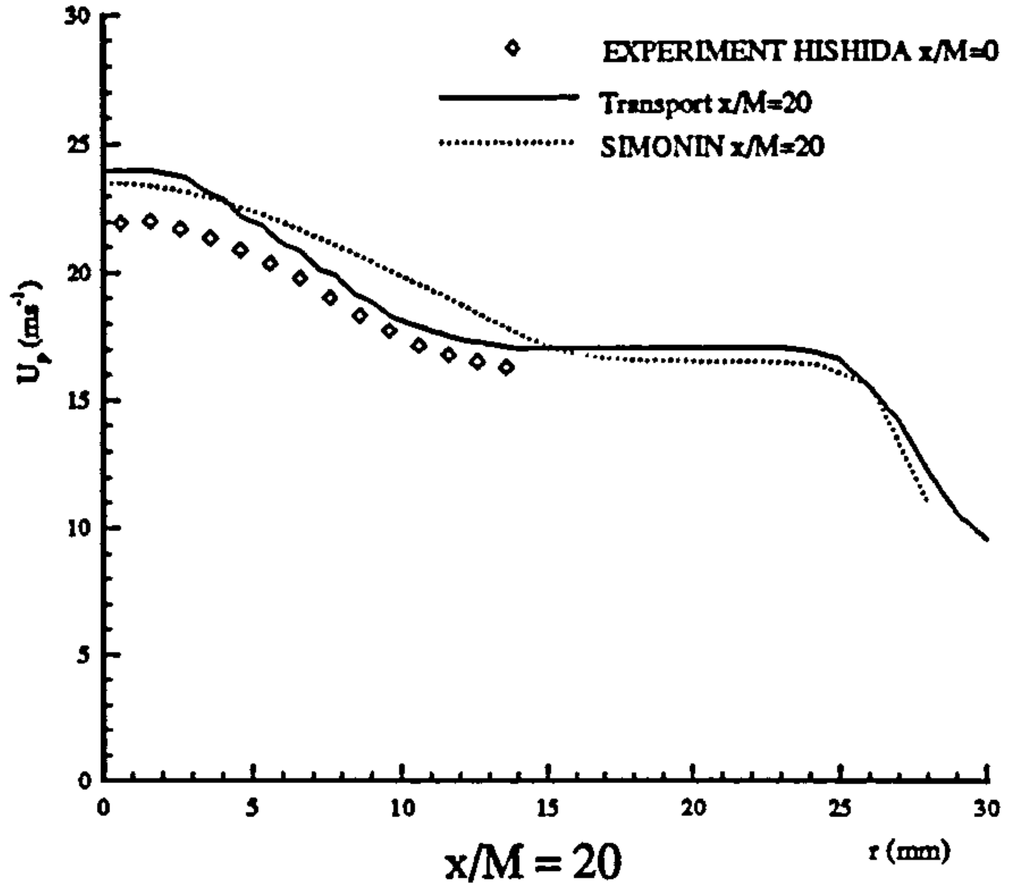

Figure 7.22 : Mean Axial Particle Velocity Profiles - Case 2

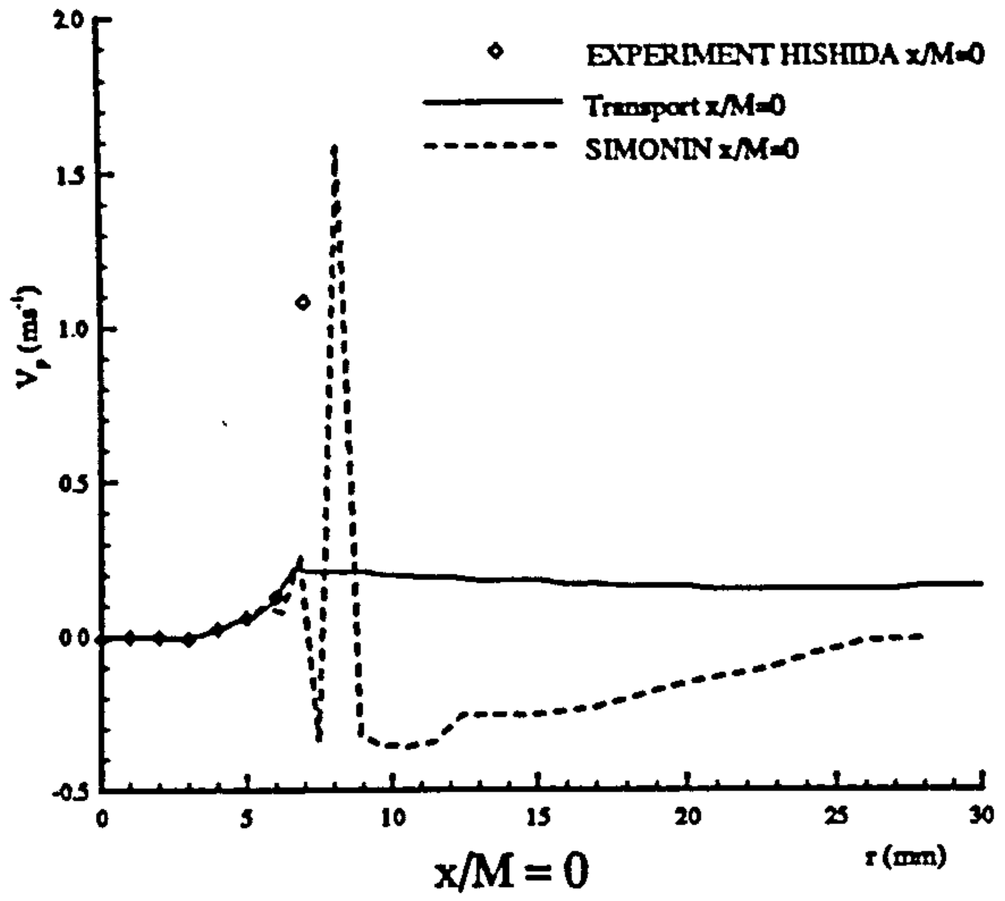

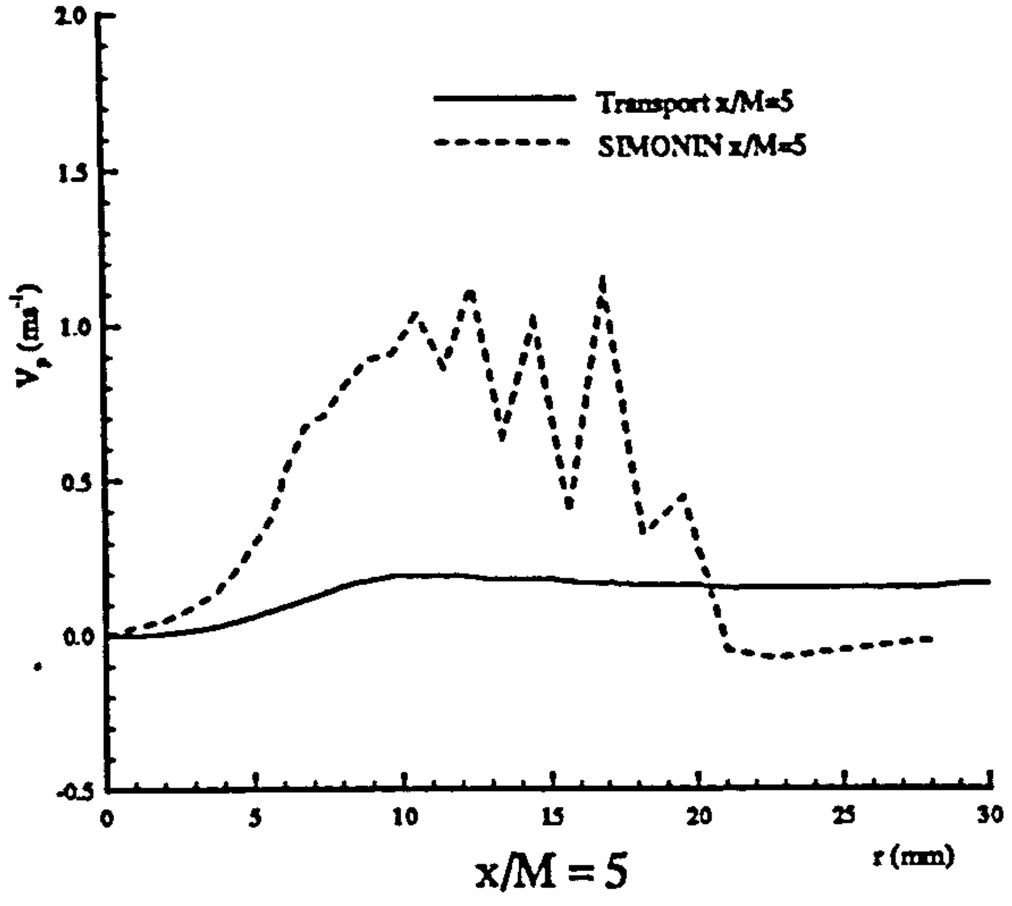

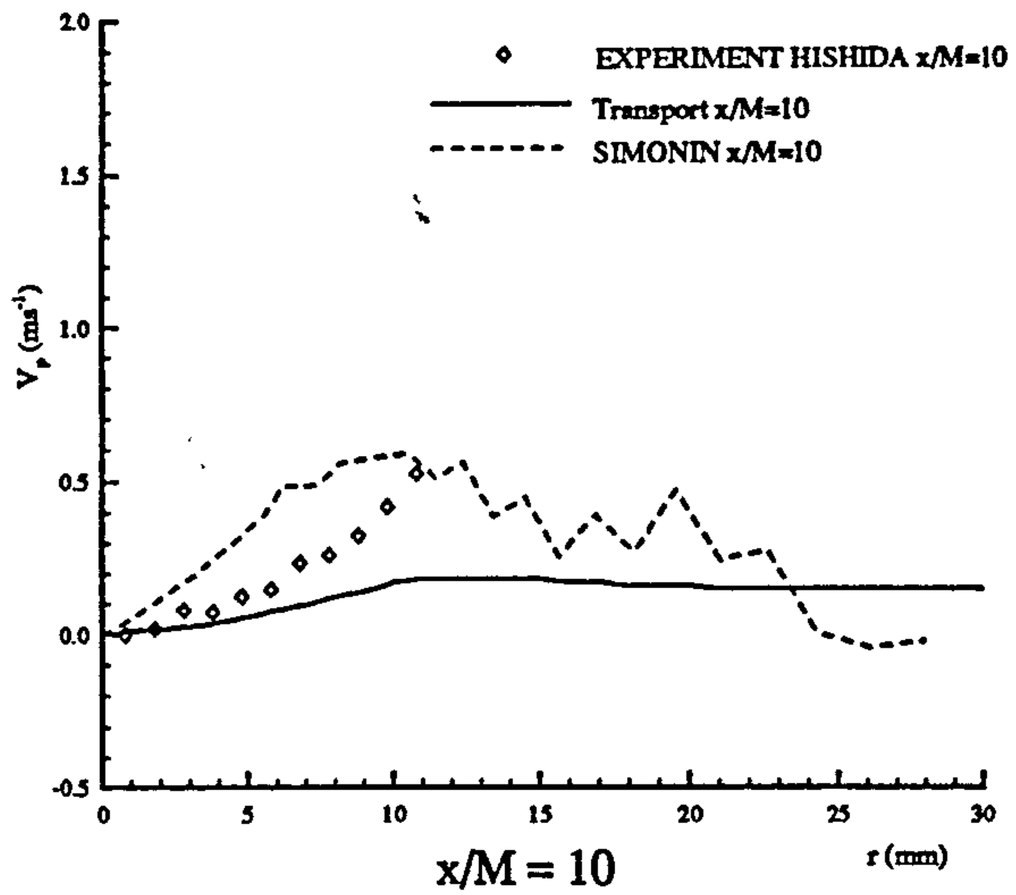

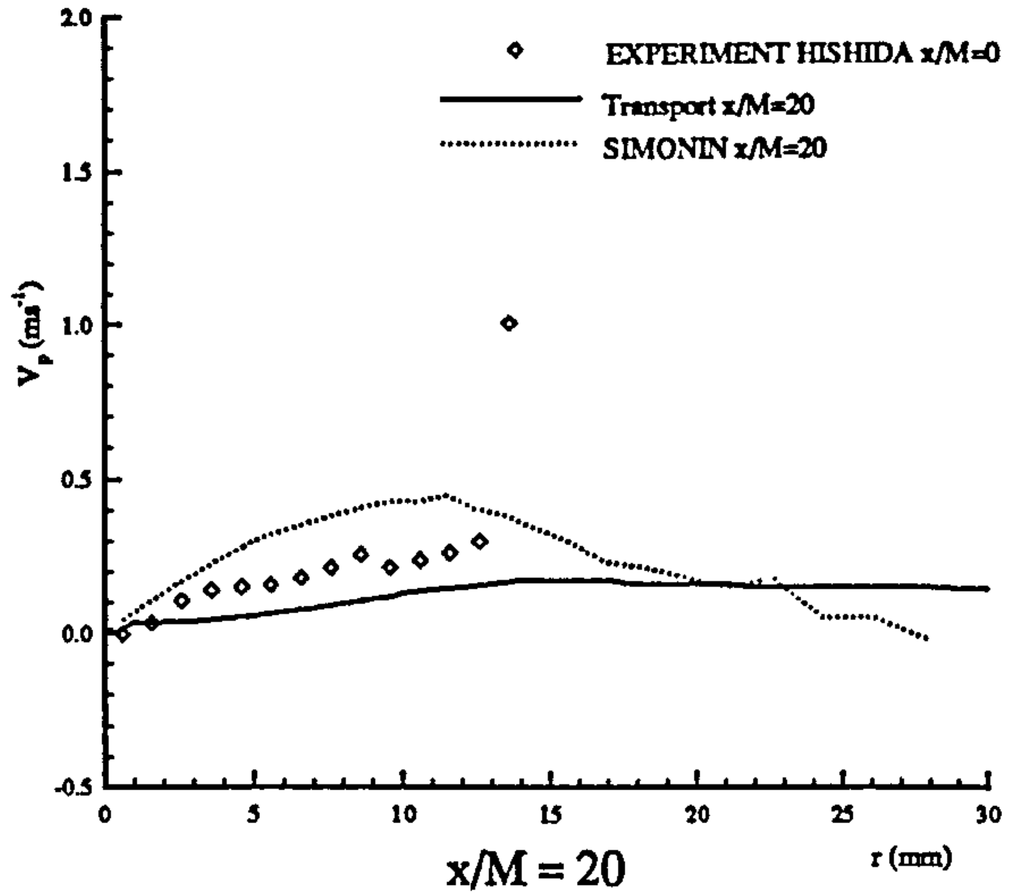

Figure 7.23 : Mean Radial Particle Velocity Profiles - Case 2

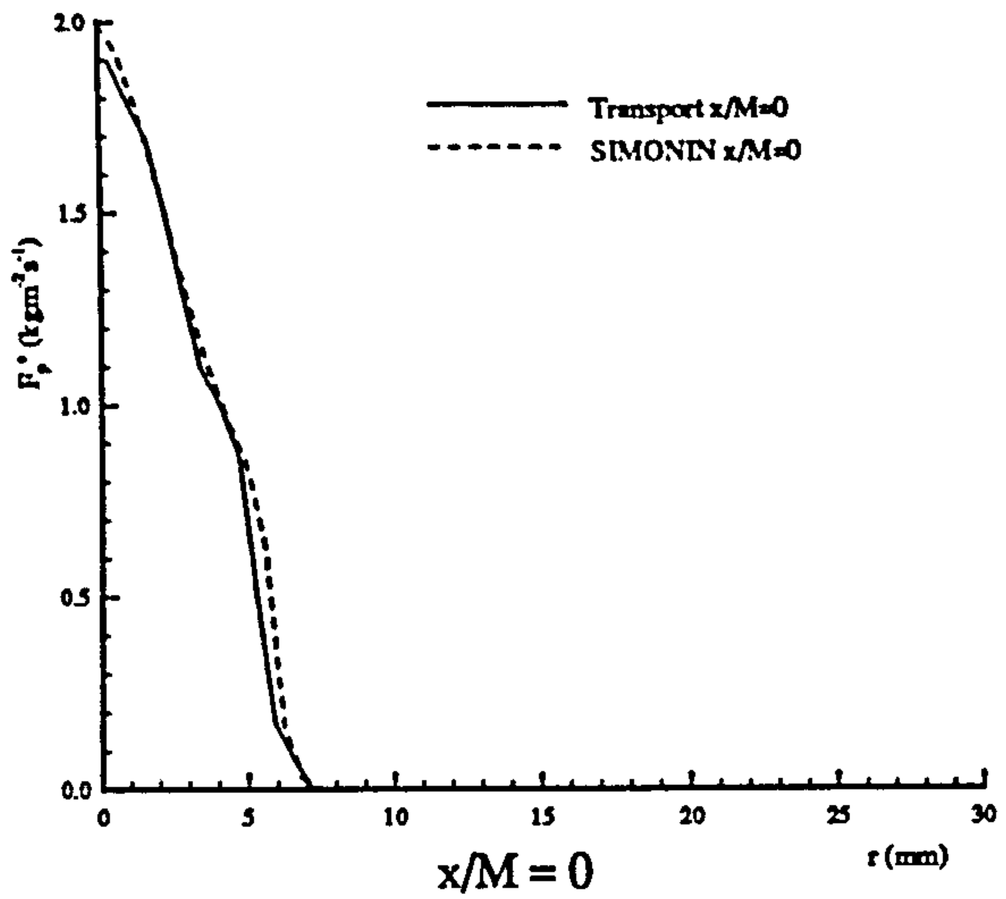

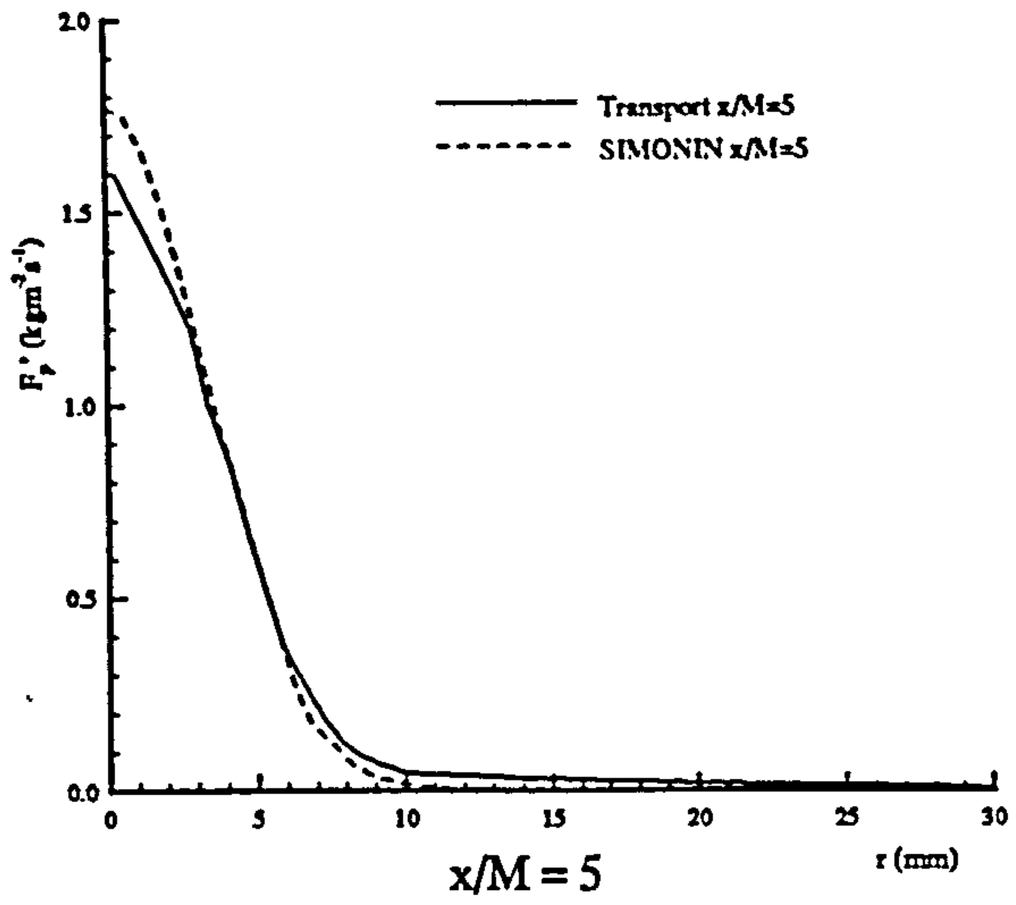

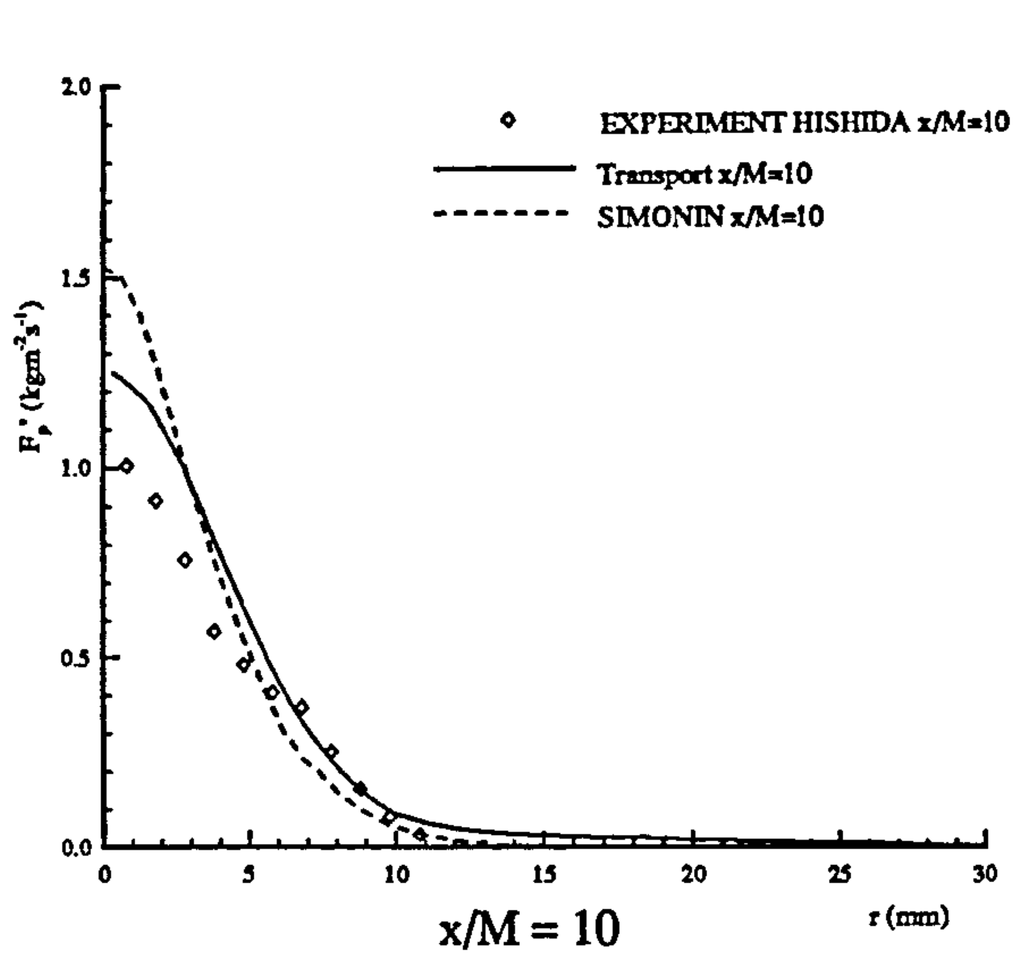

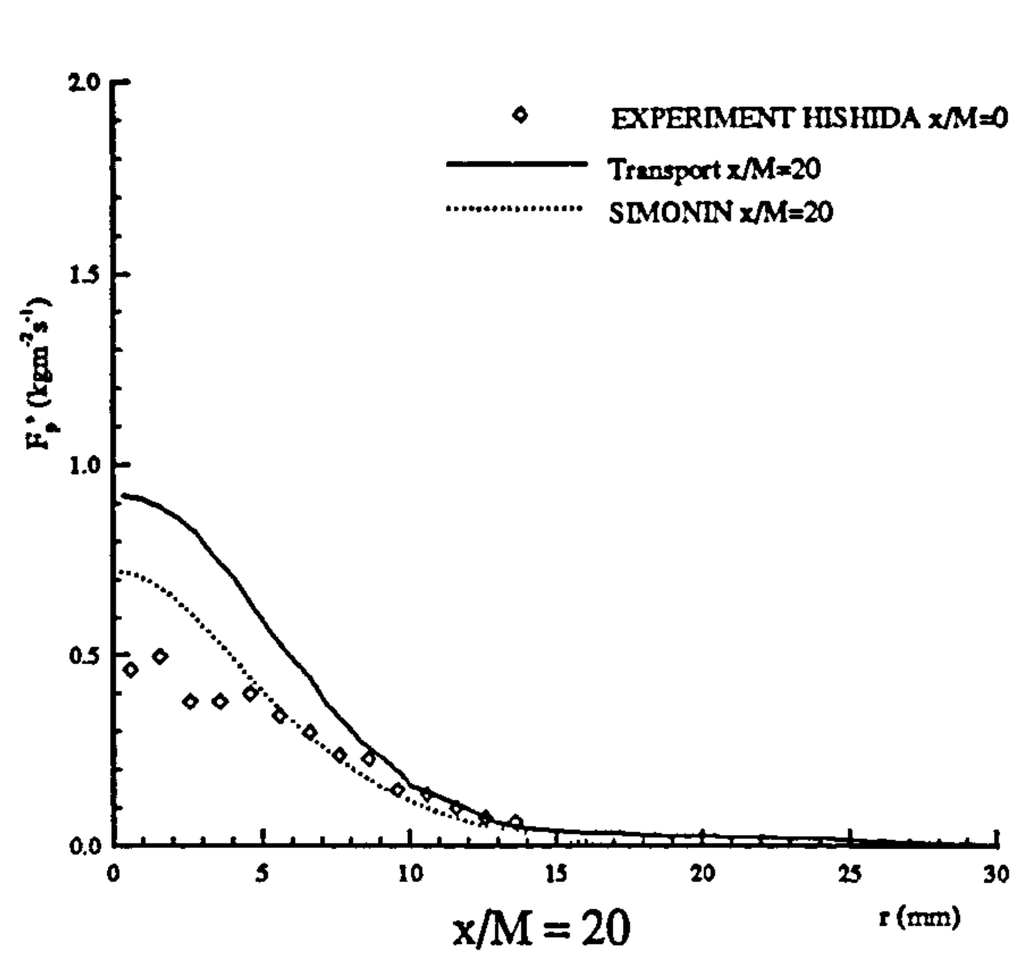

Figure 7.24 : Particle Mass Flux - Case 1

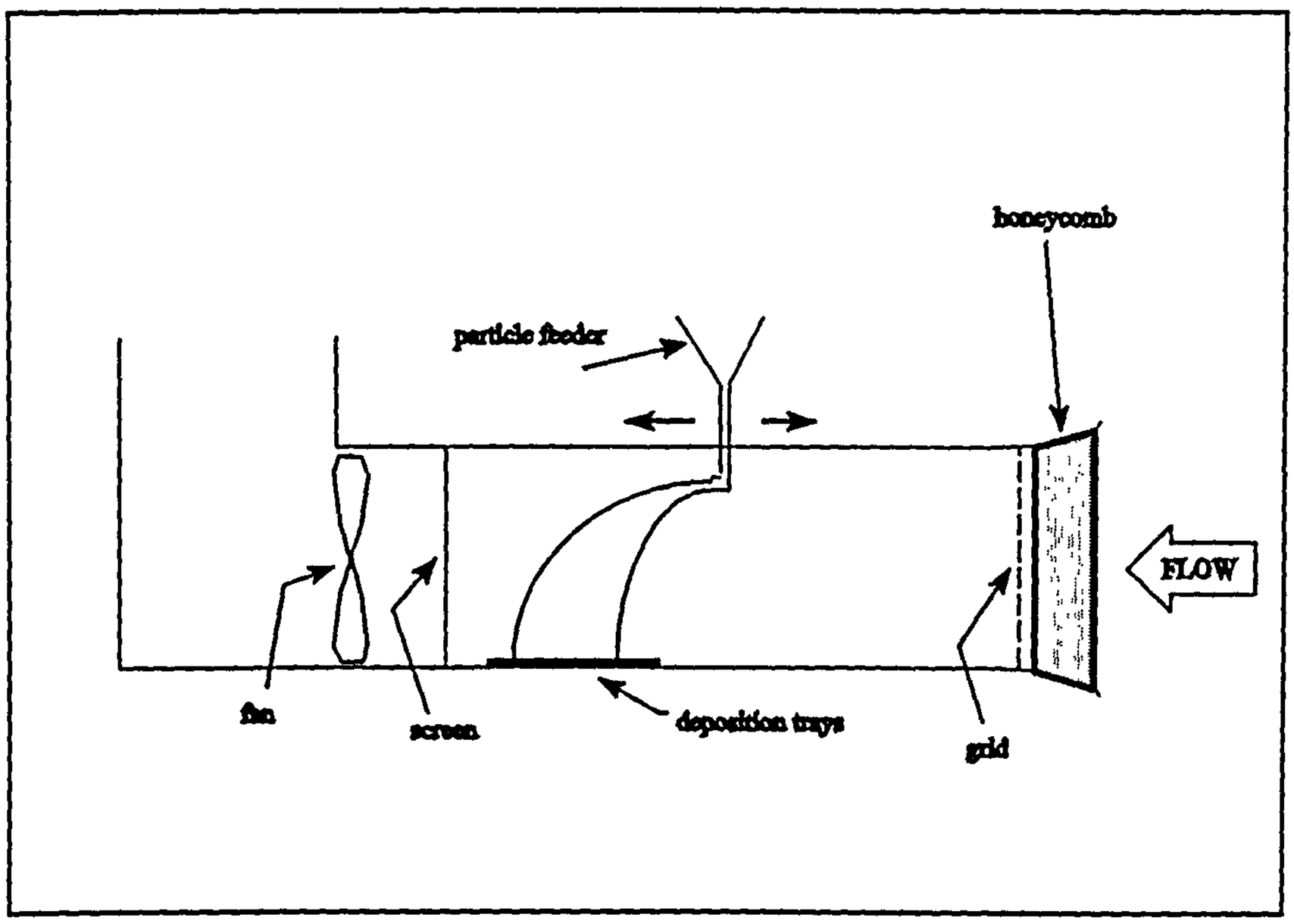

Figure 7.25 : Experimental Setup for Perkins et al

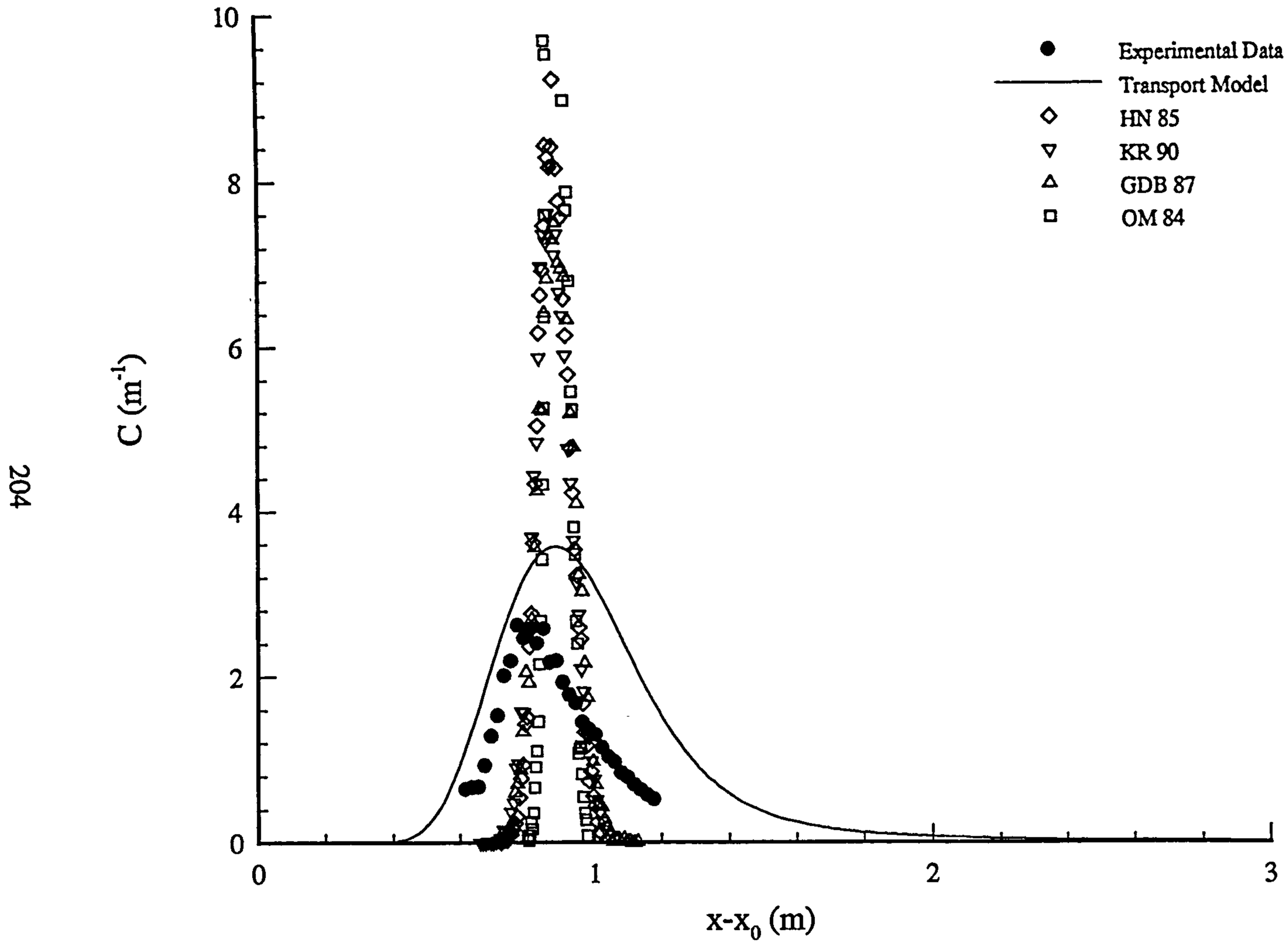

Figure 7.26 : Particle Deposition Profile Experiment D1

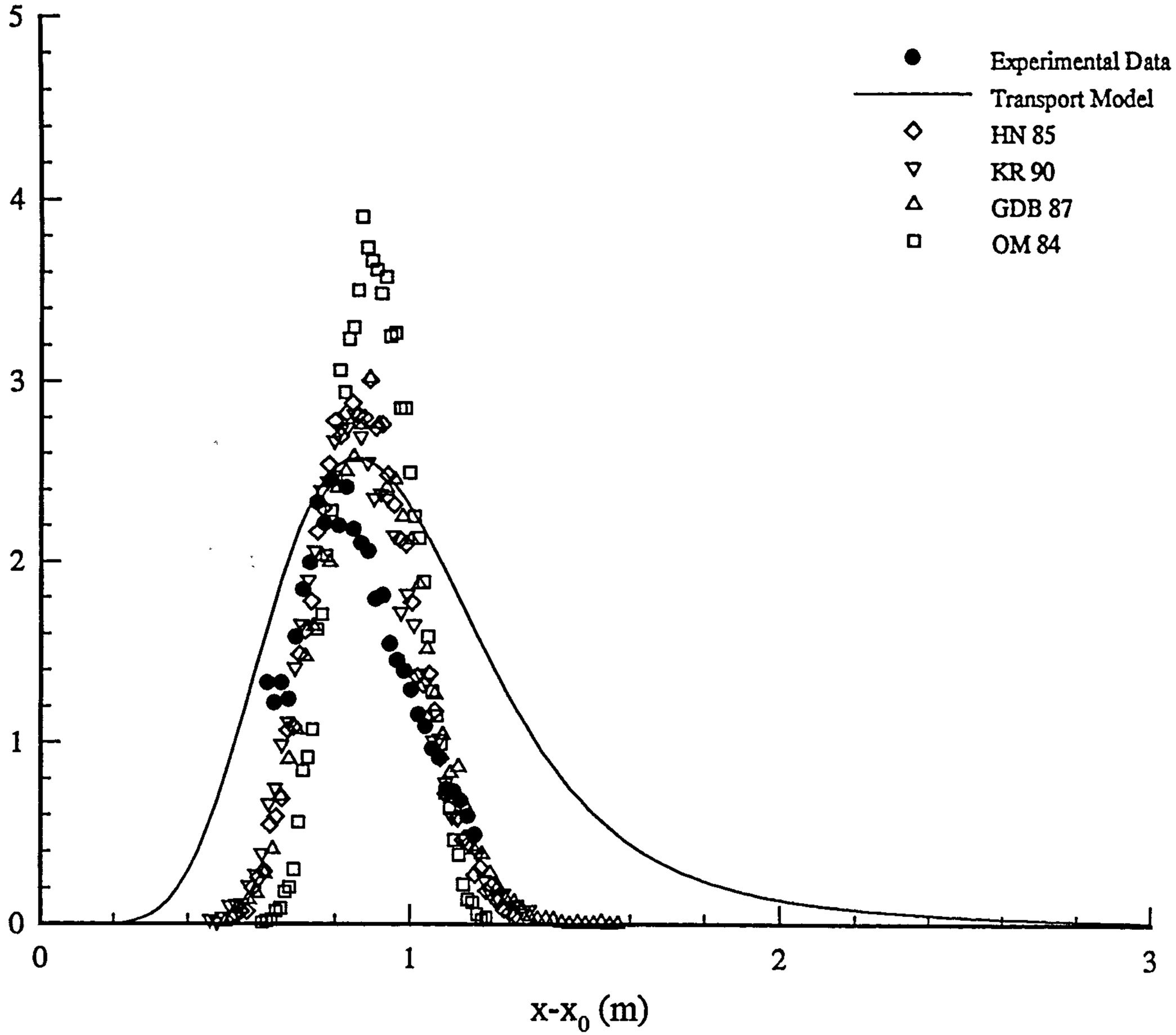

Figure 7.27 : Particle Deposition Profile Experiment D2

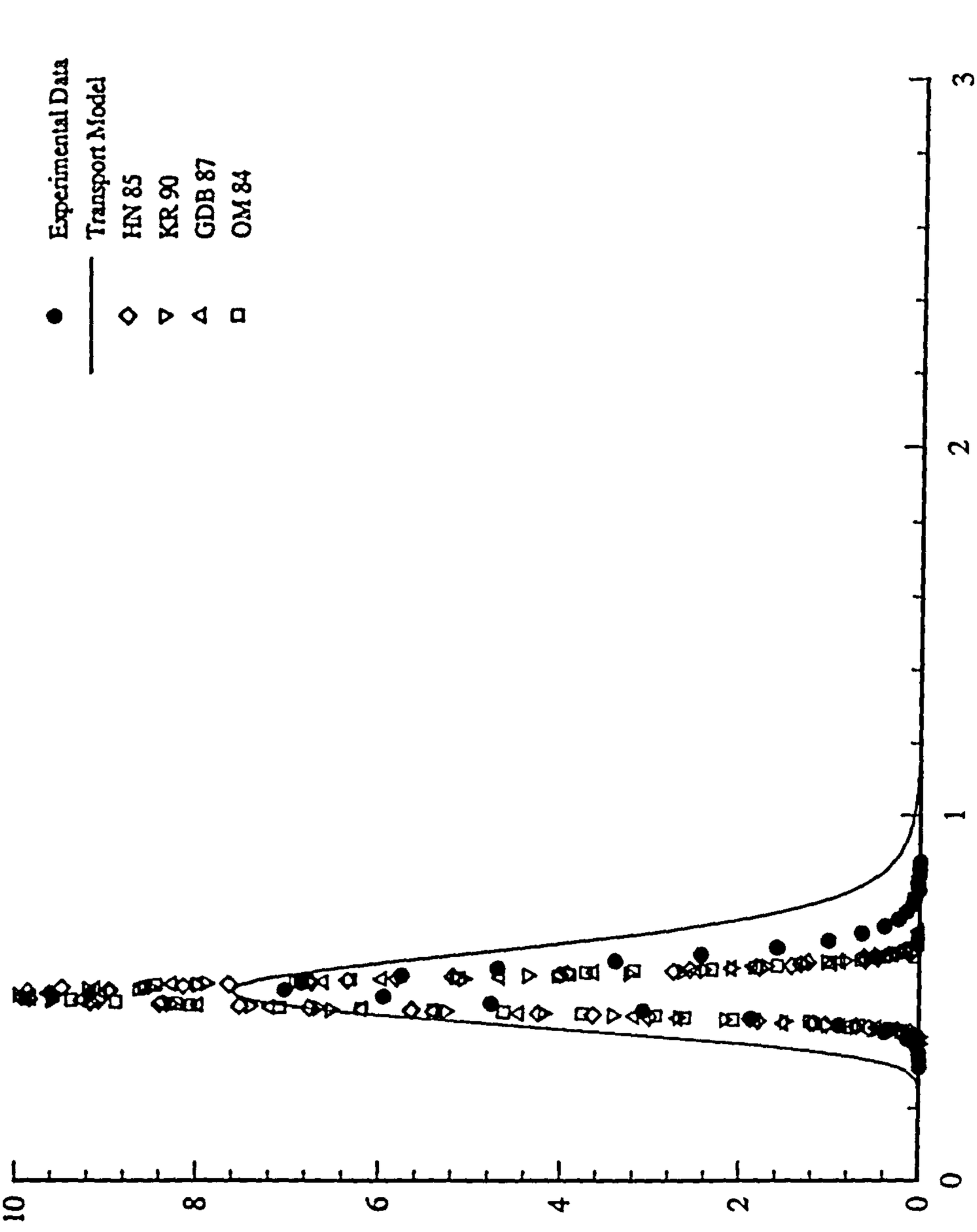

Figure 7.28 : Particle Deposition Profile Expt. D3

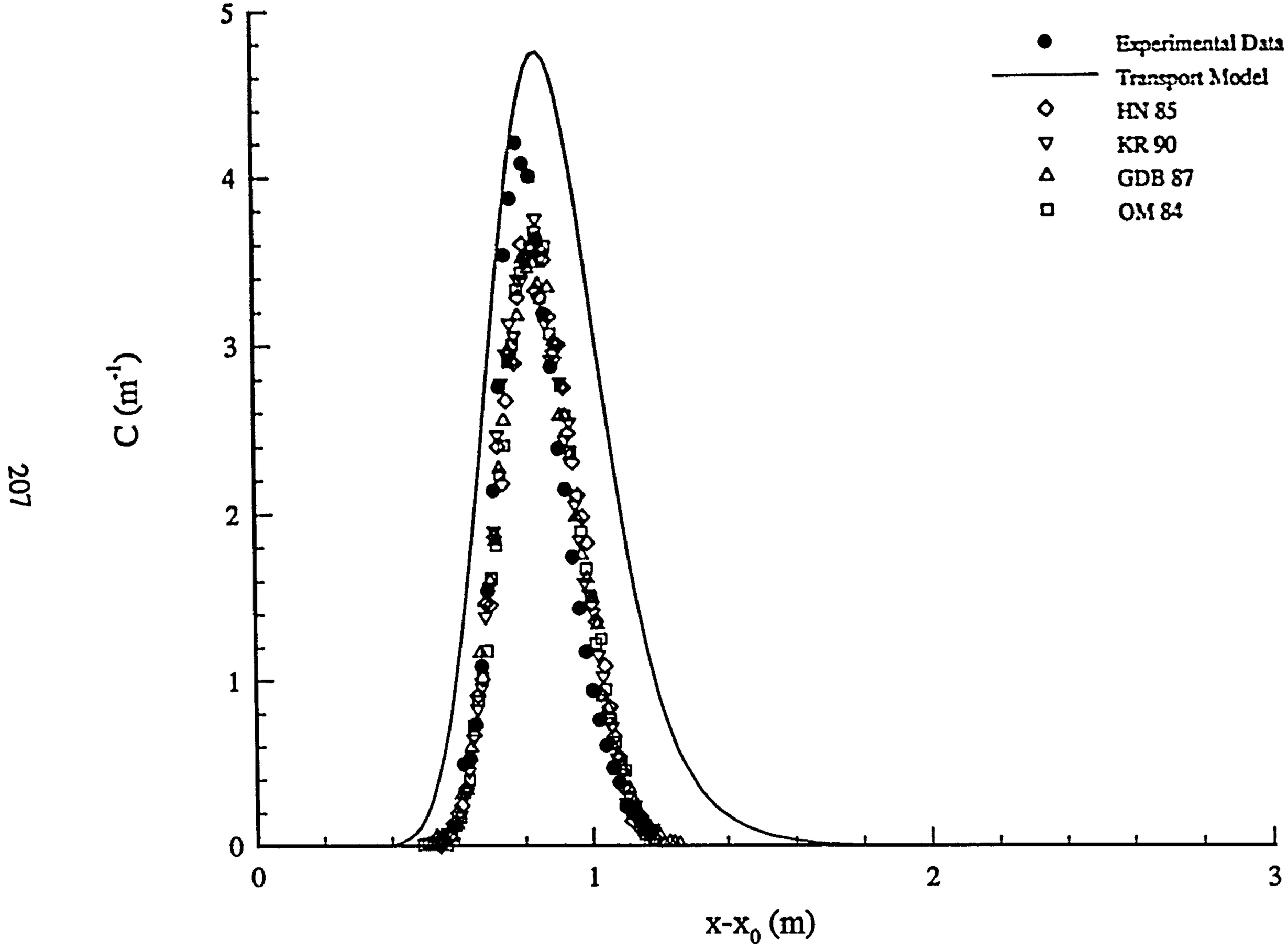

Figure 7.29 : Particle Deposition Profile Experiment D4

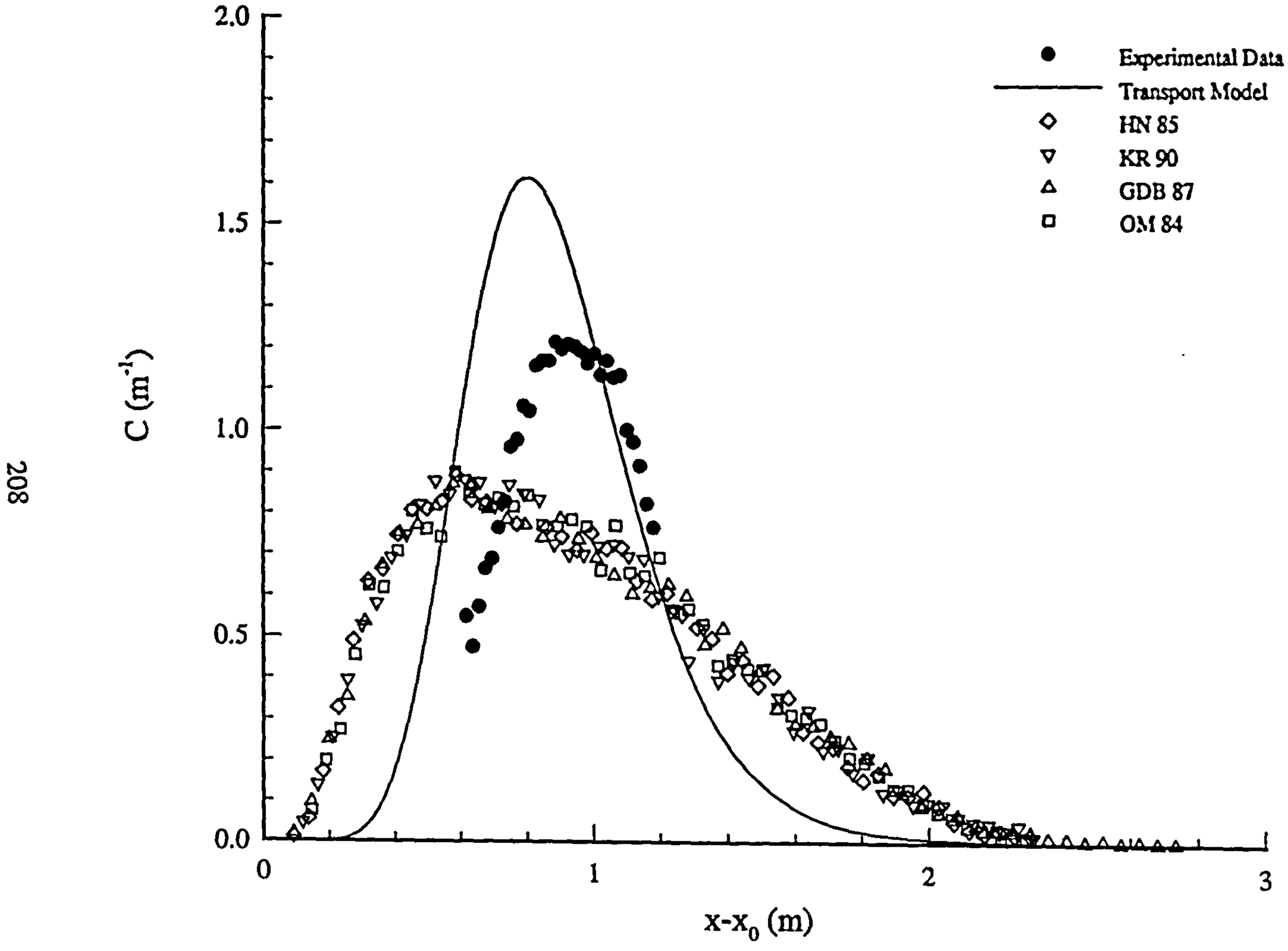

Figure 7.30 : Particle Deposition Profile Experiment D5

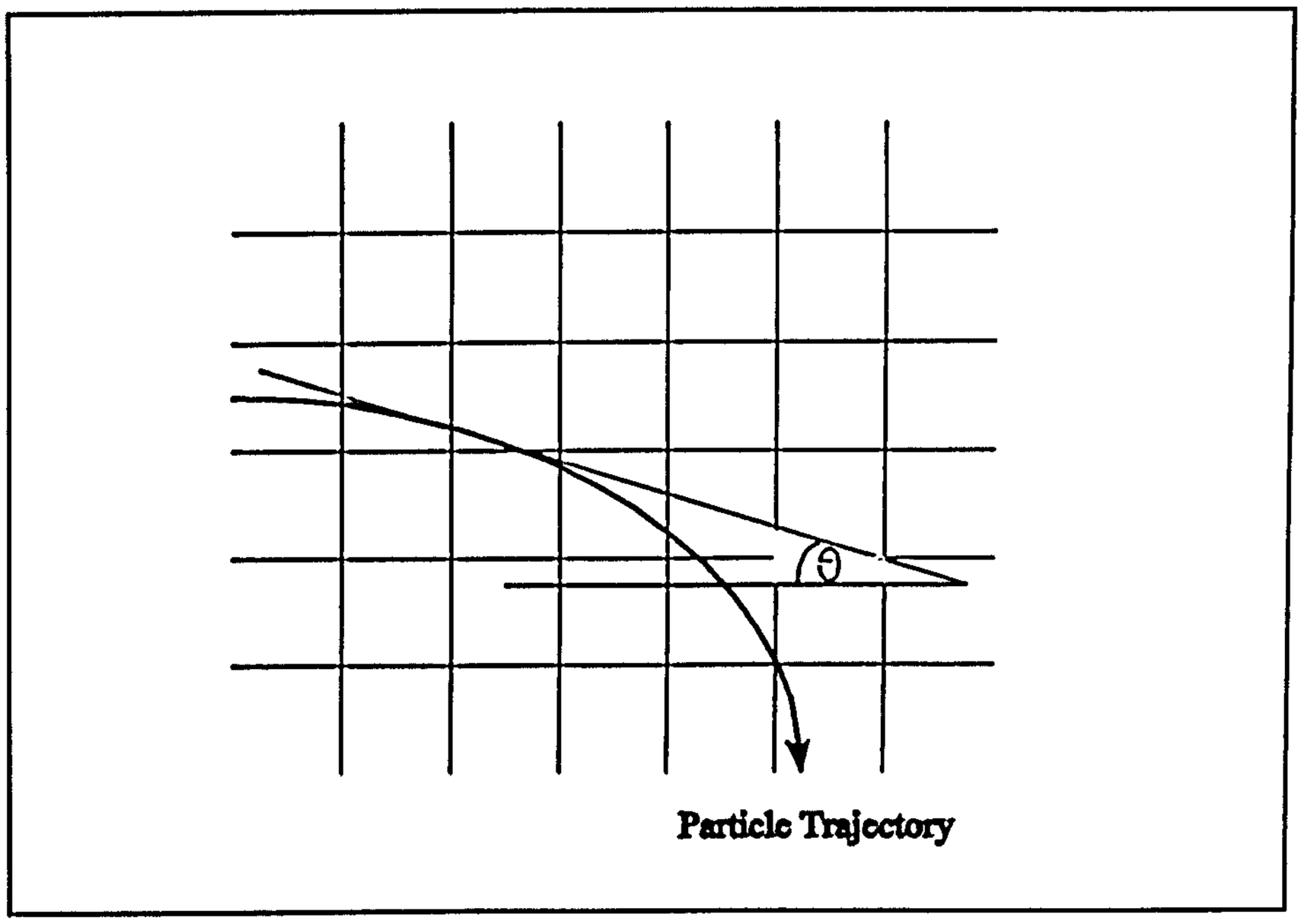

Figure 7.31 : Angle of Incidence between Particle Trajectory and Calculation Grid.

Chapter 8

Discussion, Conclusions and Recommendation for Future Work

8.1 Discussion

Some important points arising out of the above work are discussed in the following sections. Each part of the calculation is dealt with in turn. The particle diffusion coefficient calculation is discussed first, followed by the Eulerian calculations, both for the carrier and the discrete phases, and then the full calculation procedure. Finally the evaluation of the model against the experimental test cases is discussed.

8.1.1 Particle Diffusion Coefficient Calculation

Many of the most commonly used models found in the literature are based on a Lagrangian tracking technique. These models use the particle equation of motion, equation (2.3), as their foundation. Various approximations are made to (2.3) to reduce the complexity of the calculation. These techniques have been shown to give good results for the prediction of the dispersion of dilute two-phase flows. Their major drawback, however, is the computational cost involved in tracking a large number of particles necessary to obtain statistically stationary results. Simple one-way coupled calculations can be accomplished in the order of minutes. However this cost increases markedly when extra effects are added. The inclusion of two-way coupling, for example, increases the calculation time markedly (to a matter of hours). Further, the inclusion of particle-particle interaction, which usually require the simultaneous tracking of a large number of particles, increases the computational cost even more. While these solution times may be considered acceptable for research, the usefulness of this type of calculation for design is still limited.

The ability of such types of models to capture the physical effects experienced by the particle is not in doubt. Consequently the use of a simplified form of Lagrangian tracking to obtain particle diffusion coefficients is appropriate. While this retains some of the

computational overhead of the full tracking methods, the need to calculate the particle behaviour for all flow conditions is not required. The smoothness of the diffusion coefficient, together with a suitable interpolation technique, allows the full scope of particle diffusion coefficients to be represented by a suitable reduced range. This approach was discussed in chapter 6, and allows the large computational cost associated with the Lagrangian simulation to be treated separately. Unlike the above tracking models the calculation need only be performed once for a given particle type and range of flow characteristics.

The method also reduces the computational cost associated with the introduction of further effects. For example the treatment of a two-way coupled calculation would only require a single realisation of the diffusion coefficient calculation based on the initial uncoupled flow field. Introduction of the coupling between the phases would lead to modulation of the turbulence by the particles and therefore would give rise to flow characteristics already spanned by the original look-up table. Further effects of interest such as particle-particle interaction can be better handled in an Eulerian framework (though droplet breakup and coalescence would affect the particle diffusion coefficient calculation as discussed previously) and as such will be discussed later.

Though, in the majority of this work, an empirical correlation is used to calculate the particle diffusion coefficients the above arguments remain valid. The useful range for this empirical correlation has been discussed in the main body of the text (chapter 6). Though the level of error associated with its use has been shown to depend on the characteristics of the turbulence (figures 6.6-6.9), the level of agreement between the correlation and simulation was shown to be of the order of 10%. This discrepancy is consistent with other approximations made in the model and therefore is considered acceptable. The calculation is then even faster as the computational overhead associated with the Lagrangian simulation has been completely removed.

The statistics of the particle-eddy interaction process have also been investigated. It was shown that this process is non-ergodic implying the non-equivalence of time and ensemble averages. A simplified interaction, consisting of a sequence of random signs, was used to explore this behaviour. It follows from these results that care must be taken in the use of averaging to obtain particle statistics. Consequently, all averaging in this work is

based on an ensemble approach.

A procedure was then developed to extend the validity of the Lagrangian model to treat short times where a diffusion representation breaks down. Introduction of a so-called convection delay into the calculation was proposed which suppressed the initial diffusion of the particle. This delay time was calculated for a range of particles and was based of the half decay time of the particle autocorrelation function (see chapter 2). Use of this delay was shown to greatly increase the accuracy of the predictions for all times considered.

8.1.2 Single Phase Calculation

The accurate calculation of the carrier phase flow field is clearly important in the ability of any model to predict the behaviour of the discrete phase. The flow field solver used in this work was a very simple finite volume, pressure correction code (SIMPLER). Use of this type of code is widespread in the literature and its abilities and drawbacks are well known. The closure model used to represent the turbulence present in the first phase is also very important as values obtained for the turbulent kinetic energy and dissipation directly influence the diffusive behaviour of the second phase. The standard k-ϵ turbulence formalism was used to model the turbulence throughout this work. Where necessary, the adjustable coefficients were modified to achieve a good fit to measured flow fields which were considered fixed. While the inaccuracies of this turbulence model are well-known it was decided, in the development of the transport model, that its simple form with its direct translation to turbulent scales (through equations 2.10 and 2.11) outweighed its deficiencies.

The code used here to calculate the carrier phase flow field was validated using a simple pipe flow calculation (see chapter 4). The results were shown to accurately represent this well-documented flow, giving an error of less than 10%. Further, the calculations used for the first experimental test-case were shown to reproduce the measured flow field to an acceptable degree of error given the simple form of model used.

An analytical flow field was used for test-case two due to the well-established properties of decaying grid generated turbulence. This decision both removed the possibility of errors due to inaccuracies in the flow field solver and significantly reduced computation

equation contains source terms due to the momentum transfer between the two phases. This momentum transfer is assumed to take the form of quadratic drag interaction, together with gravity. This assumption is consistent with the calculation of the particle diffusion coefficient (see above), and results from the simplifications made to the particle equation of motion discussed previously (see chapter 1 and 2).

The Reynolds averaged second phase conservation equations are solved using the same method as used for the single phase calculation. The procedure is simplified by the lack of a pressure equation for the second phase. Though the calculation is post-processed in this work, simultaneous solution of the equations for both phases is possible and would be relatively straightforward to implement.

The effect of numerical dispersion on the second phase has been investigated. A false diffusion coefficient was calculated as a function of the incidence angle between the flow and the computational grid. The magnitude of this effect is discussed in detail in chapter 7 with regard to the second modeled test-case. The influence on the calculation was shown to be small even though only a low order discretisation scheme was used throughout this work.

An Eulerian approach could be expected to become a better representation of the flow field as the mass loading, of the second phase, increases, and it is exactly this type of flow where the commonly used Lagrangian tracking techniques become expensive. Thus the use of an Eulerian method would simplify the inclusion of effects such as particle-particle interactions (i.e. collision and coalescence) through the introduction of a modified drag relation (see Silverman and Sirignano (1994)). In addition the inclusion of two-way coupled calculation is much more straightforward in an Eulerian frame since it is possible to solve for both phases simultaneously, removing the need for the global iteration approach required for Lagrangian techniques.

8.1.4 Complete Calculation

Firstly the single phase flow field is calculated using the algorithm developed in chapter 4. Use is made of the available adjustable coefficients to obtain a best fit between

the measured and computed flow field, this also enables the intrinsic inclusion of the effect of the second phase on its carrier fluid. The computed flow field is then used as an initial condition for the second phase calculation

The single phase calculation also provides both the mean flow field of the carrier phase and the distribution of both kinetic energy and dissipation within the domain. These distributions enable the calculation of the turbulent scales of the flow through application of equations (2.10) and (2.11). In order to reduce the number of diffusion coefficient calculations required, use is made of the smoothness of the particle diffusion coefficient (see chapter 6). This enables the representation of the full scope of scales present in the flow by a reduced sample, which must span the range of possible scales. In this work the maximum and minimum length and velocity scales, together with eight equally spaced intermediate points were used. This leads to the calculation of one hundred particle diffusion coefficients.

To further reduce the cost of the calculation of these diffusion coefficients the empirical correlation developed in chapter 2 (equation (2.18)) was used, wherever possible, in preference to the simulation techniques discussed above. The correlation has been shown to give comparable results to the simulation (see figure 2.10). The variation between the particle dispersion calculated in a simple pipe flow using the simulation method and correlation has been shown to give errors within an acceptable range (~10%) though its range of validity is in question.

A further question mark about the use of the correlation is its inability to accurately calculate the particle mean square fluctuating velocity. This quantity is required for correct treatment of the source term arising from the repeated application of the diffusion approximation to the second phase momentum equation. The influence of this added source term, which arises from the non-zero diagonal of the second phase Reynolds stress tensor, has been investigated for the case of a simple pipe flow. The influence of this term on the dispersion of a range of particles was shown to be negligible, less than 1% (see figures 6.2-6.3). It follows from this that the poor prediction of the mean square fluctuating velocity of the particle afforded by the correlation is unimportant. Therefore, use of the correlation to calculate particle diffusion coefficients is acceptable and used throughout the majority of this work.

8.1.5 Comparison With Test-Cases

Comparison has been drawn with experimental test-cases for both the diffusion coefficient calculation and the full calculation procedure.

In order to calculate a relationship between the Eulerian scales, which are generally available for the flow field, and the Lagrangian scales required for the calculation, it is useful to consider the behaviour of a fluid point. This is especially useful in the current work since the properties of a fluid point can be specified analytically. Due to the inaccuracies noted in the dispersion of the particle chosen by Snyder and Lumley (1971) to represent this fluid point, the DNS data of Elghobashi and Truesell (1992) was used. This numerical experiment calculates the behaviour of a fluid point in the same flow as considered by Snyder and Lumley, and therefore complements the experimental data.

This numerical data, together with the analytical behaviour of the fluid point within the transport model, allowed the derivation of a relationship between the Lagrangian and Eulerian time scales present in the flow. The resulting ratio showed that the Lagrangian time scale is greater than the Eulerian scale by a factor of 1.65. This relationship, together with the Eulerian scales given by equation (2.10) allowed the required characteristics of the representative eddy to be fully specified. The resulting scales were used throughout this work.

Various forms of simulation method were implemented and compared with three well-known test-cases. First the experimental results of Snyder and Lumley were considered. The original model of Hutchinson, Hewitt and Dukler (1971) was implemented and shown to give poor results. The model was extended to include crossing trajectory effects, through the simple inclusion of a crossing time scale, again poor results were observed. The vector model was therefore developed which included the effects of crossing trajectories in a more fundamental manner. Again the initial predictions of this model were poor. Investigation into the ergodicity of the particle-eddy interaction process (see chapter 2), showed that the interaction is non-ergodic and therefore, time and ensemble averages are not equivalent. Since initially all calculations were performed using time averaging, the

developed models converted from time to ensemble averaging, which markedly improved the results. While the gradients of the dispersion curves were well predicted, the use of the diffusion approximation (which is strictly only valid for long times) in the initial interaction region led to a large over-prediction of the particle dispersion. To improve the performance of the model in this quadratic interaction region an extra time scale, the convection time, was introduced. The convection time was used to delay the start of diffusion of the particle, and was determined as a function of the particle autocorrelation functions. Introducing this added time scale greatly increased the accuracy of the calculations, which were shown to predict well the dispersion of the whole range of particle types.

A full formalism is available through integration of the particle autocorrelation functions. These autocorrelation functions were calculated using the same data set as the simulation, and used to check of self-consistency within the model. The two results showed excellent agreement for all particle types.

Secondly the experiment of Wells and Stock (1983) was considered. This experiment attempted to isolate the effects of inertia and gravity by the suspension of charged particles in a horizontally orientated flow field. The model fails to predict the measured dispersive behaviour of the particles. This is considered due to errors in the experimental data (as discussed in chapter 3).Other workers have also been unable to accurately predict measured dispersion of Wells and Stock for both particle types using a consistent flow field, Sommerfeld (private communication).

Next the full calculation procedure was applied to two experimental test-cases both of which had already been compared to other computational models. This allowed not only the evaluation of the current model against the experimental data but also with other modelling techniques.

The first test-case was that of a confined coaxial jet flow due to Hishida and Maeda (1987) which was presented at the Fifth Workshop for Two-Phase Flows in Erlangan, Germany. The predictions of both the carrier and discrete phases were shown to be good. The mass-flux however, was significantly over-predicted for both types of particles considered. The performance of the transport model was shown to be comparable to the other numerical methods presented. Due to the relatively higher speeds (~30 m/s) and small

measurement volumes (~0.26 m) the primary effects of the fluid on the particles were, therefore, convective and did not fully test the model.

The second and more challenging test-case was that of particle deposition in a horizontally orientated wind tunnel, due to Perkins et al (1994). Generally the predicted deposition profiles provided a good account of the measured data. The predictions were generally better than the Lagrangian models reported by the authors. The influence of numerical dispersion effects were investigated and shown to be small. The positions for the peak concentration were predicted well for all but the last experiment. The qualitative shape of the profiles was well captured for all cases, as was the width of the deposition profiles.

Overall, the predictions obtained from the transport model agree well with the presented experimental data. It is also shown that the results of the model are at least comparable to, and generally better than, other calculations presented for the above test-cases.

8.2 Conclusions

Though the development of the transport model presented here is at an early stage the results are encouraging. Both the diffusion coefficient calculation and the application of the full model to experimental test-cases give good agreement. Also, the relative computational cost of the model is low. The inclusion of a diffusion coefficient based on the Lagrangian properties of the particles, in an Eulerian framework enables the benefits of both modelling approaches to be exploited. In addition the model is such that its further development is straightforward.

Insight has also been obtained into the interaction process between the particle and a turbulent eddy and a relationship developed between Eulerian and Lagrangian time scales. The particle-eddy interaction process was shown to be non-ergodic. This is an interesting and somewhat surprising result the implications of which have not yet been fully explored.

The model has been validated against available experimental data and compared with other modelling approaches. The comparative performance was shown to be good.

From the above conclusions, development of the model would be advantageous, the

inclusion of many other effects is also possible and is discussed in more detail below.

8.3 Recommendations for Future Work

The model presented here is still in an early stage of development. Consequently, there are many avenues for future work. Some of the more interesting, and important, extensions are discussed here.

The expansion of the work into more industrially important flow situations would clearly be of great interest. The first step in accomplishing this would be to extend the calculation to a coupled form, that is to include the influence of the dispersed phase on its carrier fluid.

The choice of solution method used in this work allows the two phases to be calculated simultaneously. Though this procedure would be straightforward, the need for the particle diffusion coefficients (and mean square fluctuating velocity) at each calculation point, which would vary between iterations, complicates matters. Due to the high cost of computing the particle statistics through simulation, it would be impractical to solve for them simultaneously with the flow fields. However, due to the relative insensitivity of the dispersion of a particle to its diffusion coefficient (a result of the square root dependency) it would not be necessary to calculate the new diffusion coefficient field for each global iteration. Further, the slowly varying nature of the diffusion coefficient would allow the possibility of using a single look-up table for all realisations of the flow, since it would be possible to extrapolate for values which lie slightly beyond the span of the given look-up table. Alternatively, the use of the empirical correlation to obtain these properties would remove the above problems as it would enable the calculation of these properties simultaneously with the flow fields.

A second useful extension would be to include evaporative effects into the calculation. This would greatly increase the applicability of the model to industrial situations, allowing its use to model to such processes as spray drying and venturi scrubbers. Evaporation would lead to a reduction of the diameter of the particle during the calculation. This would introduce the need for a calculation which could deal with a poly-dispersed

distribution of particle sizes. Also, the influence of the evaporation of vapour from the droplet surface would lead to a modification of the particle drag coefficient. The inclusion of poly-dispersed flows would considerably influence the dimension of the particle look-up table. It would be possible to reduce this effect by representing the full range of possible particle sizes by perhaps three size ranges. These would correspond to (i) large droplets for which inertial effects dominate and therefore react relatively little to the turbulence; (ii) intermediate droplets which are both influenced by the turbulence of the carrier fluid and inertial effects and (iii) small droplets which closely follow the fluctuations of the carrier gas. Whether three size ranges are sufficient or if the intermediate size ranges would need to be further broken down would require investigation.

The extension of the code to enable greater mass loading would be of great interest, as this would allow the calculation to be performed nearer the spray nozzle and possibly the development of a method to link spray breakup and dispersion. As mentioned above one main advantage of Eulerian techniques is their possible extension into dense flow regions where particle-particle interactions become important. The inclusion of models for collision effects, rebound for particles and possible coalescence and break-up for droplets, should be possible. Similarly more advanced particle-wall interactions would also be of great interest especially in situations where deposition is a dominant factor.

References

Abbot M.B. and Basco D. R., *Computational Fluid Dynamics: An Introduction for Engineers*, Longman, 1989

Adeniji-Fashola, A " Comprehensive Modeling of Turbulent Particulate Flows using Eulerian and Lagrangian Schemes" *AIAA 19th Fluid Dym., Plasma Dym. Lasers Conf*, Hawaii, 1987

Ahamadi, G. and Goldschmidt, V.W. " Motion of Particles in a Turbulent Fluid - The Basset History Term." *J. Appl. Mech.*, p. 561, 1971

Andresen, E. "Statistical Approach to a Continuum Model for the Disperse Phase in Gas-Particle Flows", *Proc.5th Work. Two-Phase Flows*, Erlangen, Germany, p. 89, 1990

Auton, T.R " The Dynamics of Bubbles, Drops and Particles in Motion in Liquids", *PhD Thesis*, Cambridge Uni., 1983

Baines, W. D. and Peterson, E. G "An Investigation of Flow Through Screens", *Trans. ASME*, Vol. 73, p. 467, 1951

Basset, A.B *A Treatise on Hydrodynamics*, Dover, Vol. 2, p. 285, 1888

Batchelor, *The Theory of Homogeneous Turbulence*, Cambridge Univ. Press, Cambridge, 1953

Bendig, L., Konimann, J. and Kamenz, G " Droplet Size Distribution Analysis on a Twin Fluid Atomizer with Twin Gas Jets for Spray Drying", *ILASS Conf.*, Guilford U.K., 1991

Berlemont, A., Desjonqueres,, P. and Gouesbet, G "Particle Lagrangian Simulation inTurbulent Flows", *Int. J. Multi. Flows*, Vol. 16, No. 1, p.19, 1990

Boothroyd, R.G. " Pressure Drop in Duct Flow of Gaseous Suspensions of Fine Particles." *Trans. instu. Chem. Eng.*, Vol. 44, p. 306, 1966

Boussinesq, J *Theorie Analytique de la Chaleur* (in French), Paris, Vol 2, p 224, 1903

Buevich, Y.A " Motion Resistance of a Particle Suspended in a Turbulent Medium", *Fluid Dynam.* (AN SSSR, *Mekhanika Zhidkosti i Gaza*, Vol. 1, No. 6, p. 182, 1966)

Chadrasekar, S "Stochastic Problems in Physics and Astronomy", *Rev. Mod. Phys.*, Vol 15, No.1, 1943

Chen, C.P. and Wood, P.E. " A Turbulence Closure Modeling for Dilute Gas-Particle Flows." *The Can. J. ChE.*, Vol. 63, p. 931, 1983

Chiang, C. H., Raju, M. S. and Sirignano, W. A "Numerical Analysis of Convecting, Vaporising Fuel Droplets with Variable Properties", *Int. J. Heat Mass Trans.*, Vol. 35, p. 1307, 1992

Choi, Y.D and Chung, M.K "Analysis of Turbulent Gas-Solid Suspension Flow in a Pipe", *J. Fluids Eng.*, Vol 105, p 329, 1983

Chung, J.N. and Troutt, T.R. " Simulation of Particle Dispersion in an Axi-symmetric Jet." *J. Fluid Mech.*,Vol. 186, p. 199, 1988

Chung, M.K., Sung, H.J. and Lee, K.B. " Computational Study of Turbulent Gas-Particle Flow in a Venturi." *J. Fluid Eng.*, Vol. 108, p. 248, 1986

Corrsin, S. and Lumley, J. L, *Appl. Sci. Research*, Vol 6A, p. 114, 1956

Corrsin, S "Estimates of the Relations between Eulerian and Lagrangian Scales in Large Reynolds Number Turbulence", *J. Atmos. Sci.*, Vol. 20, p. 115, March 1963

Courant, R., Isaacson, E. and Rees, M "On the Solution of Non-Linear Hyperbolli Differential Equations by Finite Differences", *Comm. Pure Appl. Math*, Vol. 5, p. 24, 1952

Crowe, C.T., Sharma, M.P. and Stock, D.E " The Particle-Source-In Cell (PSI-Cell) Model for Gas Droplet Flows", *J. Fluids Eng.*, Vol. 99, p. 325, 1977

Csanady, G.T. "On the Energy Balance off a Turbulent Mixing Layer", *J. Fluid Mech.*, Vol. 15, P. 545, 1963

Dannon, H., Wolfshtein, M. and Hestroni, G. " Numerical Calculations of Two-Phase Turbulent Round Jet." *Int. J. Multi. Flow*, Vol. 3, p. 223, 1977

de Vahl Davis, G. and Mallinson, G. D "False Diffusion in Numerical Fluid Mechanics", *Report 1972/FMT/1*, Univ. of New South Wales, Sch. Mech. Ind. Eng., 1972

Desjonqueres, P., Berlemont, A. and Gouesbet, G "A Lagrangian Approach for the Prediction of Particle Dispersion in Turbulrnt Flows", *J. Aerosol Sci.*, Vol 19, No. 1, p. 99, 1988

Durst, F., Milojevic, D. and Schonung, B. " Eulerian and Lagrangian Predictions of Particulate Two-Phase Flows : A Numerical Study." *Appl. Math. Model.* Vol 8, p. 101, 1984

Elghobashi, S.E. and Abou-Arab, T.W. " A Two-Equation Closure for Two-Phase Flows." *Phys. Fluids*, Vol. 26, p. 931, 1983

Elghobashi, S.E. and Truesdell, G.C " Direct Simulation of Particle Dispersion in a Decaying Isotropic Turbulence", *J. Fluid Mech.*, Vol. 22, p 655, 1992

Fick, A., *Annln. Phys.*, Vol. 170, p. 59, 1855

Finlayson, B.A., *The Method of Weighted Residuals and Variational Principles*, Academic, New York, 1972

Fleckhaus, D., Hishida, K. and Maeda, M " Effect of Laden Solid Particles on the Turbulent low Structure of a Round Free Jet", *Expt. Fluids*, Vol. 5, p. 323, 1987

Frenkiel, F. N "Etude Statistique de la Turbulence - Fonctions Spectrales et Coefficients de Corrélation", *Rapport Technique, ONERA*, No. 34, 1948

Gosman, A.D. and Ioannides, E. " Aspects of Computer Simulation of Liquid-Fuelled Combustors." *J. Energy*,Vol. 7, No. 6, p 482, 1983

Gouesbet, G., Berlement, A. and Picart, A "Dispersion of Discrete Particles by Turbulent Continuous Motions. Extensive Discussion of Tchen's Theory using a Two Parameter Family of Lagrangian Correlation Functions", *Phys. Fluids*, Vol. 27, p. 827, 1984

Govan, A. H., Hewitt, G. F. and Ngan, C. F "Particle Motion in a Turbulent Pipe Flow", *Int. J. Multi. Flow*, Vol. 15, No. 3, p. 471, 1989

Govan, A. H "A Simple Equation for the Diffusion Coefficient of Large Particles in a Turbulent Gas Flow", *Int. J. Multi. Flow*, Vol. 15, No. 2, p.287, 1989

Graham, D. I "Eulerian Time Correlations in Eddy Interaction Models", *Research Report MS-94-02*, School of Mathematics and Statistics, Uni. of Plymouth, U.K., 1994

Graham, D. I. and James, P. W. "Turbulent Dispersion of Particles using Eddy Interaction Models", *Research Report MS-94-01*, School of Mathematics and Statistics, Uni. of Plymouth, U.K., 1994

Harlow, F. H. and Welch, J. E "Numerical Calculation of Time-Dependent Viscous Incompressible Flow of Fluid with Free Surfaces", *Phys Fluids*, Vol. 8, p. 2182, 1965

Hinze, J.O *Turbulence*, McGraw-Hill, New York, 1975

Hinze, J.O. " Turbulent Fluid and Particle Interaction." *Prog. Heat Mass Trans.*, Vol. 6, 1972

Hishida, K. and Maeda, M. " Turbulent Characteristics of Gas-Solids Confined Jet : Effect of Particle Density" (in Japanese), *Japanese J. Multi. Flow*, Vol. 1, No. 1, p. 56, 1987

Hishida, K. et al " Turbulent Flow Characteristics of Dispersed Two Phase Flow in Plane Shear Layer", *Proc. th Int. Sym. Appl. Laser Anem. Fluid Mech.*, Portugal, 1988

Hishida,K. et al "Turbulence Characteristics of Liquid-Solids Two-Phase Circular Confined Jet" (in Japanese),*Trans. JSME*, Vol. 511, p. 68, 1989

Hjelmfelt, A.T and Mockros, L.F. " Motion of Discrete Particles in a Turbulent Fluid." *Appl. Sci. Res.*,Vol. 16, p. 149, 1966

Hunt, J. C. R. and Nalpanis, P "Saltating and Suspending Particles over Flat and Sloping Surfaces. I. Modelling Concepts", *Proc. Int. Work. Phys. Blown Sand*, Aarhus, Denmark, 1985

Hutchinson, P. and Brown, D.J. " Particle Motion in Turbulent Flow Fields." *AERE-R7813*, 1974

Hutchinson, P., Hewitt, G.F. and Dukler, A.E. " Deposition of Liquid or Solid Suspensions from a Turbulent Gas Stream : A Stochastic Model." *Chem. Eng. Sci.*, Vol. 26, p 419, 1971

Kallio, G. A. and Reeks, M. W "A Numerical Simulation of Particle Deposition in Turbulent Boundary Layers", *Int. J. Multi. Flows*, Vol. 15, No. 3, p. 433, 1988

Kampé de Fériet, J.M "Les Fonctions Aléatoires Stationaries et la Théorie Statistique de la Turbulence Homogène", Ann. Soc. Sci. (Bruxelles), Vol. 59, p. 145, 1939

Kawazoe, H., Ohsawa, K. and Fujikake, K. " LDA Measurement o Fuel Droplet Sizes and Velocities in a Combution Field", *Comb. and Flame*, Vol. 82, p. 151, 1990

Kennedy, D. A., *Ph.D Dissertation*, Dept. Mech., The Johns Hopkkins Uni., 1965

Kim, I., Elghobashi S.E and Sirignano, W.A " Three-Dimensional Droplet Interactions in Dense Sprays", *AIAA 29th Aero. Sci. Meet.*, Nevada, 1991.

Kim, I., Elghobahi, S. and Sirignano, W. A "Three-Dimensional Flow Over Two Spheres in Parallel Side-by-Side Motion", *J. Fluid Mech.*, Vol. 246, p. 465, 1993

Kim, I., Elghobahi, S. and Sirignano, W. A "Three-Dimensional Flow Computation for Two Interacting, Moving Droplets", *AIAA Paper 92-0343*, 1992

Laufer, J "The Structure of Turbulence in Fully Developed Pipe Flow", *NACA TR-R-1174*, 1954

Launder, B.E and Spalding, D.B " The Numerical Computation of Turbulent Flows", *Comp. Meth. Appl. Mech. Eng.*, Vol. 3, p. 269, 1974

Launder, B.E., *Lecture Series No 76*, Von Kármán Inst., Belgium, 1975

Launder, B. E "Second-Moment Closure and its Use in Modelling Turbulent Industrial Flows", *Int. J. Num. Meth. Fluids*, Vol. 9, p. 963, 1989

Litchford R. J. and Jeng, S-M "Evaluation of an Efficient Statistical Transport Model for Turbulent Droplet Dispersion in Dilute Combusting Sprays", *AIAA-91/2509*, 1991

Lumley, J.L "Some Problems Connected with the Motion of Small Particles in a Turbulent Fluid", *PhD Thesis*, Johns Hopkins Uni., 1957

Lumley, J.L. " Two-Phase and Non-Newtonian Flows", *Topics Phys.*, Vol. 12, p. 22, 1978a

Lumley, J.L., *Phys. Fluids*, Vol. 18, p.619, 1975.

Lumley, J.L., *Adv. Appl. Mech.*, Vol. 18, p. 135,1978b

Marble, F.E. " Dynamics of Dusty Gases." *Ann. Rev. Fluid Mech.*, Vol. 2, p. 397, 1970

Owen, P.R. " Pneumatic Transport. " *J. Fluid Mech.*,Vol. 39, p. 407, 1969

Maxey, M.R. and Riley, J.L. " Equation of motion for a Small Rigid Sphere in a Nonuniform Flow." *Phys. Fluids.*, Vol. 24, No. 4,1983

Meeks, C.C and Jones, B.G "Studies of the Behaviour of Heavy Particles in a Turbulent Fluid Flow.", *J. Atmos. Sci.*, Vol 30, p 239, 1973

Michaelides, E.E. " A Model for the Flow of Solid Particles in Gases." *Int. J. Mult. Flow*, Vol. 10, p. 61, 1984

Mickelson, W.R " An Experimental Comparison of the Lagrangian and Eulerian Correlation Coefficients in Homogeneous Isotropic Turbulence", *NACA TN3570* ,1955

Milojevic, D " Lagrangian Stochastic-Deterministic (LSD) Prediction of Particle Dispersion in Turbulence" *Part. and Part. Sys. Char.*, Vol. 7, p. 181, 1990

Monin, A.S. and Yaglom, A.M. *Statistical Fluid Mechanics : Mechanics of Turbulence.*, Vol 1, Cambridge, MIT Press, 1971

Mostafa, A.A and Montigia, H.C. " On the Modelling of Turbulent Evaporation of Sprays: Eulerian vs Lagrangian Approach." *Int. J. Heat Mass Trans.*, Vol. 30, No. 12, p. 2583, 1987

Nallasamy, M "Turbulence Models and Their Applications to the Prediction of Internal Flows: A Review", *Comp. Fluids*, Vol. 15, No. 2, p. 151, 1987

Naudrasher, E. and Farrell, C "Unified Analysis of Grid Turbulence", *J. Eng. Mech. Div. ASCE*, Vol. 96 (EM2), p. 121, 1970

Neumann, P. and Umbauer, H. " Characterization of the Spatial Distribution of Particles Transported by a Turbulent Flow", *Expt. Fluids*, Vol. 12, p. 125, 1991

Nir and Pisman " The effect off Steady Drift on the Dispersion of a Particle in a Turbulent Fluid", *J. Fluid Mech.*, Vol. 94, p. 369, 1979

O'Brien, R.W " A Method for the Calculation of Effective Transport Properties of Suspensions of Interacting Particles", *J. Fluid Mech.*, Vol. 91, Part 1, p. 17, 1979

Ormancey, A. and Martinon, J "Prediction of Particle Dispersion in Turbulent Flows", *PhysicoChemical Hydro.*, Vol. 5, No. 3, p. 229, 1984

Oseen, C.W "Über die Stokes'sche formel, und über eine verwandte aufgabe in der hydrodynamik" (in German), Leipzig, *Hydromechanik*, Vol 82, 1927

Owen, P. R, "Pnematic Transport", *J. Fluid Mech.*, Vol 39, p. 407, 1969

Papoulis , A., Probability, *Random Variables and Stochastic Processes*, 2nd Edn., McGraw-Hill, 1984

Patankar, S. V *Numerical Heat Transfer and Fluid Flow*, McGraw-Hill, New York, 1980

Patankar, S. V. and Spalding, D. B "Simultaneous Prediction of Flow Pattern and Radiation for Three-Dimensional Flames", Chap. 4, Heat Transfer in Flames, Hemisphere, Washinton D.C, 1974b

Patankar, S. V. and Spalding, D. B., *Heat and Mass Transfer in Boundary Layers*, 2nd Edn., Intertext, London, 1970

Patankar, S. V. and Spalding, D. B "A Calculation Procedure for the Transient and Steady-State Behaviour of Shell-and-Tube Heat Exhangers", Chap. 7, *Heat Exchangers: Design abd Theory Sourcebook*, Hemisphere, Washington D.C., 1974a

Patankar, S. V. and Spalding, D. B "A Computer Model for Three-Dimensional Flow in Furnaces", *Proc. 14th Sym. (Int.) Comb.*, The Combustion Inst., p. 605, 1972b

Patankar, S. V. and Spalding, D. B "A Calculation Procedure for Heat, Mass and Momentum, Transfer in Three-Dimensional Parabolic Flows", *Int. J. Heat Mass Trans.*, Vol. 15, p. 1787, 1972a

Patankar, S. V. and Spalding, D. B "Computer Analysis of the Three-Dimensional Flow and Heat Transfer in a Steam Generator", *Forsch. Ingenieurwes*, Vol. 44, p. 4, 1978

Perkins, R.J, Vassilicos, J.C and Hunt, J.C.R " Aerosol Transport, Deposition and Resuspension in the LWR Circuit and Containment", Final Report Contract No. 4120 90-10

ED ISP GB, Dept. App. Math. Theor. Phys, Uni. Cambridge, 1994

Peskin, R.L " Some Fundamental Research Problems in Gas-Solid Flows", *AICHE Sym.* ,Vol. 71, No. 147, p. 52, 1975

Phythian, R. " Dispersion by Random Velocity Fields." *J. Fluid Mech.*, Vol. 67, Part 1, p 145, 1975

Pisman and Nir " On the Motion of Suspended Particles in Stationary Homogeneous Turbulence", *J. Fluid Mech.*, Vol. 84, p. 193, 1978

Prandtl, L., *2nd Int. Cong. Appl. Mech.*, Zurich, (see also *NACA TM-435*), 1926

Procededings, *5th Workshop onTwo-Phase Flow Predictions*, Erlangen, March 1990 (ISBN 3-89336-066-2), 1990

Raju, M.S. and Sirignano, W.A " Interaction Between Two Vaporizing Droplets in an Intermediate Reynolds Number Flow", *Phys. Fluids A*, Vol. 2, No. 10, p. 1780, 1990

Reeks, M.W. " On the Dispersion of Small Particles Suspended in an Isotropic Turbulent Fluid." *J. Fluid Mech.*, Vol. 83, Part 3, p. 529, 1977

Reif, F., *Fundementals of Statistical and Thermal Physics*, Mc-Graw-Hill, 1965

Rodi, W.,*Turbulence Models and Their Applications in Hydaulics - A State of the Art Review*, 2nd Edn. Int. Ass. Hyd. Res., Deft, 1984

Sabnis, J.S et al " A Combined Eulerian-Lagrangian Analysis for Computation of Two-Phase Flows", *AIAA 19th Fluid Dym., Plasma Dym. Lasers Conf*, Hawaii, 1987

Sabnis, J.S et al " Computaion of Two-phase Shear-Layer Flow Using and Eulerian-Lagrangian Analysis", *AIAA/ASME/SAE/ASEE 24th Joint Prop. Conf.*, Boston, 1988

Scarborough, J. B., *Numerical Mathematical Analysis*, 4th Edn., Johns Hopkins Press, Baltimore, 1958

Sheun, J.S. et al " Structure of Particle-Source-In-Cell Method for Gas Droplet Flows", *AIAA J.*, Vol. 23, p. 396, 1985

Shih, T-H and Lumley, J.L " Second-Order Modelling of Particle Dispersion in a Turbulent Flow", *J. Fluid Mech.*, Vol. 163, p. 39, 1986

Silverman, I. and Sirignano, W.A. " Multi-Droplet Interaction Effects in Dense Sprays", *Int. J. Multi. Flow*, Vol. 20, No. 1, p. 99, 1994

Simonin, O. and Viollet, P. L "Numerical Study on Phase Dispersion Mechanisms in Turbulent Bubbly Flows", *Proc. Int. Conf. Mech. Two-Phase Flows*, Taipei, Taiwan, June 1989

Simonin, O. "Eulerian Formulation for the Particle Dispersion in Turbulent Two-Phase Flows", *Proc. 5th Workshop Two-Phase Flow Pred.*, Erlangen, Germany, 1990

Simonin, O. and Viollet, P. L "Prediction of an Oxygen Droplet Pulverisation in a Compressible Subsonic Coflowing Hydrogen Flow", *Proc. Symp. Num. Meth. Multi. Flows*, Tronoto, Canada, June 1990

Sirignano, W. A "Fuel Droplet Vaporisation and Spray Combustion Theory", *Prog. Energy Combust. Sci.*, Vol. 9, p. 291, 1983

Snyder, W.H. and Lumley, J.L " Some Measurements of Particle Velocity Autocorrelation

Functions in a Turbulent Flow", *J. Fluid Mech.*, Vol. 48, p. 41, 1971

Sommerfeld, M. "Modelling of Particle-Wall Collisions in Confined Gas-Particle Flows", *Int. J. Multi. Flow*, Vol. 18, No. 6, p. 905, 1992

Sommerfeld, M. and Krebs, W. "Particle Dispersion in a Swirling Confined Jet Flow", *Part. Syst. Charact.*, Vol. 7, p. 16, 1990

Sommerfeld, M. " Numerical Simulation of the Particle Dispersion in Turbulent Flow : The Importance of the Particle Lift Forces and Particle/Wall Collision Models", *Num. Meth. Multi. Flow*, Vol. 91, 1990

Sommerfeld, M. and Qiu, H-H "Detailed Measurements in a Swirling Particulate Two-Phase Flow by Phase-Doppler Anemometer", *Int. J. Heat and Fluid Flow*, Vol. 12, No. 1, p. 20, 1991

Sommerfeld, M., Hohnen, G. and Rüger " Some Open Questions and Inconsistencies of Lagrangian Particle Dispersion Models", *9th Sym. Turb. Shear Flow*, Japan, 1993

Sommerfeld, M., *Private communication*, 1993.

Soo, S.L " Statistical Properties of Momentum Transfer in Two Phase Flow", *Chem. Eng. Sci*, Vol. 5, p. 57, 1956

Stokes, *Trans. Camb. Phil. Soc.*, Vol. IX.

Taylor, G.I. " Diffusion by Continuous Movement", *Proc. London Math. Soc*, Vol. A 20, p.196, 1921

Tchen, C.M " Mean Value and Correlation Problems Connected with the Motion of Small

Particles Suspended in a Turbulent Fluid" *PhD Thesis*, Delft University, The Hague : Martinus Nijhoff, 1947

Vames, J.S. and Hanratty, T.J " Turbulent Dispersion of Droplets for Air Flow in a Pipe", *Expt. Fluids*, Vol. 6, p. 94, 1988

Vojir, D. J. and Michaelides, E. E "Effect of History Term on the Motion of Rigid Spheres in a Viscous Fluid", *Int. J. Multi. Flow*,Vol. 20, No.3, p. 547, 1994

Wells, M.R and Stock, D.E " The Effects of Crossing Trajectories on the Dispersion of Particles in a Turbulent Flow", *J. Fluid Mech.*, Vol. 136, p. 31, 1983

Wennerberg, D "Numerical Aspects on the Calculation of Confined Swwirling Flows with Internal Recirculation", *LSTM Report LSTM 253/N/89*, 1989

Yudine, M.I " Physical Considerations on Heavy-Particle Diffusion", *Adv. Geophys.*, Vol. 6, p. 185, 1959

APPENDIX I - DERIVATION OF VECTOR MODEL.

The reduced vectorial form of the BBO equation is given as

$$\frac{d\vec{u}_p}{dt} = A_1(\vec{u}_g - \vec{u}_p)\,|\vec{u}_g - \vec{u}_p| + \vec{g}$$

where

$$A_1 = \frac{3}{4}\frac{\rho_g}{\rho_p}\frac{1}{d_p}C_D(Re_p)$$

Consider the relative velocity

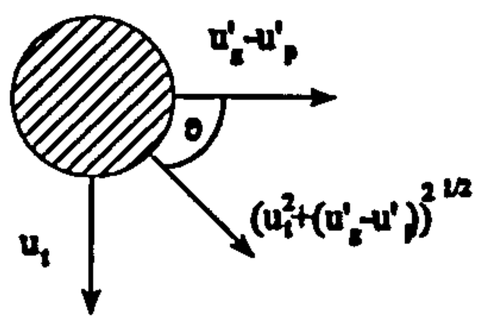

$$(\vec{u}_g - \vec{u}_p) = (U-(U-u_t), u'_g - u'_p)$$

$$= (u_t, u'_g - u'_p)$$

Hence

$$|\vec{u}_g - \vec{u}_p| = (u_t^2 + (u'_g - u'_p)^2)^{\frac{1}{2}}$$

The component of the drag force orthogonal to gravity, is given by

$$A_t(u'_g-u'_p)^2 = A_t(u_t^2+(u'_g-u'_p)^2)\cos\theta$$

with

$$\cos\theta = \frac{u'_g-u'_p}{(u_t^2+(u'_g-u'_p)^2)^{\frac{1}{2}}}$$

$$A_t(u'_g-u'_p)^2 = A_t(u_t^2+(u'_g-u'_p)^2)\frac{u'_g-u'_p}{(u_t^2+(u'_g-u'_p)^2)^{\frac{1}{2}}}$$

Hence

$$A_t(u'_g-u'_p)^2 = A_t(u_t^2+(u'_g-u'_p)^2)^{\frac{1}{2}}(u'_g-u'_p)$$

Dropping the primes gives

$$\frac{du_p}{dt} = A_t(u_t^2+(u_g-u_p)^2)^{\frac{1}{2}}(u_g-u_p)$$

Letting

$$x = |u_g-u_p| = s_t(u_g-u_p) \quad \rightarrow \quad dx = -s_t du_p$$

where s_t represents the sign of the relative velocity.

Hence

$$-\frac{dx}{dt} = A_t(u_t^2+x^2)^{\frac{1}{2}}x$$

$$-\int_{x_{t-1}}^{x_t} \frac{1}{(u_t^2+x^2)^{\frac{1}{2}}x}dx = \int_0^{\tau} A_t dt$$

$$\frac{1}{u_t}\left[\ln\left|\frac{u_t+(u_t^2+x^2)^{\frac{1}{2}}}{x}\right|\right]_{x_t}^{x_{t-1}} = A_t\tau$$

$$\frac{1}{u_t}\ln\left|\frac{\dfrac{u_t+(u_t^2+x_t^2)^{\frac{1}{2}}}{x_t}}{\dfrac{u_t+(u_t^2+x_{t-1}^2)^{\frac{1}{2}}}{x_{t-1}}}\right| = A_t\tau$$

Since no change of sign of relative velocity is possible within an eddy the sign of the internal term in the logarithm is always positive and hence the modulus sign can be dropped giving

$$\frac{\dfrac{u_t+(u_t^2+x_t^2)^{\frac{1}{2}}}{x_t}}{\dfrac{u_t+(u_t^2+x_{t-1}^2)^{\frac{1}{2}}}{x_{t-1}}} = e^{A_t\tau u_t}$$

Letting

$$\alpha = \frac{u_t + (u_t^2 + x_{t-1}^2)^{\frac{1}{2}}}{x_{t-1}} \qquad \& \qquad \beta = A_t u_t$$

It follows that

$$\frac{u_t + (u_t^2 + x_i^2)^{\frac{1}{2}}}{x_i} = \alpha e^{\beta \tau}$$

Thus letting

$$c = \alpha e^{\beta \tau}$$

we get

$$u_t + (u_t^2 + x_i^2)^{\frac{1}{2}} = c x_i$$

which leads to

$$x_i = -\frac{2 u_t c}{1 - c^2}$$

Re-substituting for x_i and introducing the particle velocity during interaction i u_{p_i} gives

$$s_i(u_g - u_{pi}) = -\frac{2 u_t c}{1 - c^2}$$

Hence

$$u_{pi} = u_g + \frac{2 u_t s_i c}{1 - c^2}$$

The displacement equation is

$$l_{pl} = \int_0^{\tau} u_{pl}\,dt = \int_0^{\tau} \left(u_g + \frac{2\,u_t s_t c}{1-c^2} \right) dt$$

Thus

$$l_{pl} = u_g \tau + \int_0^{\tau} \frac{2\,u_t s_t c}{1-c^2}\,dt$$

where

$$c = \alpha\, e^{\beta t} \quad \rightarrow \quad dc = \beta\, c\, dt$$

Hence consideration of the second term on the RHS of the above equation gives

$$\frac{1}{\beta} \int_{\alpha}^{\alpha e^{\beta\tau}} \frac{2 s_t u_t}{1-c^2}\,dc = \frac{2\,u_t s_t}{\beta} \int_{\alpha}^{\alpha e^{\beta\tau}} \frac{1}{1-c^2}\,dc$$

The integral on the RHS is a standard integral which leads to

$$\frac{2\,u_t s_t}{\beta} \int_{\alpha}^{\alpha e^{\beta\tau}} \frac{1}{1-c^2}\,dc = \frac{u_t s_t}{\beta} \int_{\alpha}^{\alpha e^{\beta\tau}} \left(\frac{1}{1+c} + \frac{1}{1-c} \right) dc$$

$$= \frac{u_t s_t}{\beta} \left[\ln|1+c| - \ln|1-c| \right]_{\alpha}^{\alpha e^{\beta\tau}}$$

$$= \frac{u_t s_t}{\beta} \left[\ln\left|\frac{1+c}{1-c}\right| \right]_{\alpha}^{\alpha e^{\beta\tau}}$$

Hence

$$l_{pl} = u_g \tau + \frac{u_t s_t}{\beta} \left\{ \ln\left|\frac{1+\alpha\, e^{\beta\tau}}{1-\alpha\, e^{\beta\tau}}\right| - \ln\left|\frac{1+\alpha}{1-\alpha}\right| \right\}$$

Thus

$$l_{pl} = u_g \tau + \frac{u_t s_t}{\beta} \ln \left| \frac{1 + \alpha e^{\beta t}}{1 - \alpha e^{\beta t}} \frac{1 - \alpha}{1 + \alpha} \right|$$

The relative displacement is used to calculate the interaction time. The interaction is over when the relative displacement is equal to the eddy size.

$$l_e = \left| \int_0^\tau R_v dt \right| \qquad , \qquad R_v = u_g - u_p$$

$$= \int_0^\tau |R_v| dt = \int_0^\tau |u_g - u_p| dt$$

Since the sign of the particle velocity cannot change within an eddy the sign of $(u_g - u_p)$ is known. Denoting this sign by s_i, thus

$$l_e = s_i \int_0^\tau (u_g - u_p) dt$$

u_p is given from above, hence

$$l_e = s_i \int_0^\tau \left(u_g - (u_g + \frac{2 u_t s_i c}{1 - c^2}) \right) dt = - \int_0^\tau \frac{2 u_t c}{1 - c^2} dt$$

again since

$$c = \alpha e^{\beta t} \qquad ; \qquad dc = \beta c dt$$

thus

$$l_e = -\frac{2u_t}{\beta}\int_{\alpha}^{\alpha e^{\beta\tau}} \frac{1}{1-c^2}dc = -\frac{u_t}{\beta}\ln\left|\frac{1+\alpha e^{\beta\tau}}{1-\alpha e^{\beta\tau}}\frac{1-\alpha}{1+\alpha}\right|$$

from previous calculation. Thus solving for τ gives

$$\ln\left|\frac{1+\alpha e^{\beta\tau}}{1-\alpha e^{\beta\tau}}\frac{1-\alpha}{1+\alpha}\right| = -\frac{s_t\beta l_e}{u_t}$$

Taking the negative sign inside the logarithm we get

$$\ln\left|\frac{\alpha e^{\beta\tau}-1}{\alpha e^{\beta\tau}+1}\frac{\alpha+1}{\alpha-1}\right| = \frac{\beta l_e}{u_t}$$

Since both α & $e^{\beta\tau}$ are always greater than or equal to 1 the sign of the interior of the logarithm is always positive so the modulus sign can be dropped to give

$$\frac{\alpha e^{\beta\tau}-1}{\alpha e^{\beta\tau}+1}\frac{\alpha+1}{\alpha-1} = e^{\frac{\beta l_e}{u_t}}$$

letting

$$\epsilon = \frac{1+\alpha}{1-\alpha} \qquad \& \qquad \gamma = -\frac{\beta l_e}{u_t} = -A_t l_e$$

thus

$$\frac{1+\alpha e^{\beta\tau}}{1-\alpha e^{\beta\tau}} = \epsilon e^{\gamma}$$

$$1+\alpha e^{\beta\tau} = (1-\alpha e^{\beta\tau})\epsilon e^{\gamma}$$

$$\alpha e^{\beta\tau}(1+\epsilon e^{\gamma}) = (\epsilon e^{\gamma}-1)$$

We get

$$\tau = \frac{1}{\beta}\ln\left|\frac{1}{\alpha}\frac{\epsilon e^{\gamma}-1}{\epsilon e^{\gamma}+1}\right|$$

Limiting Cases

Derivation of Original model (u_t=0)

The starting point is the reduced BBO equation

$$\frac{du_p}{dt} = A_1(u_g-u_p)\,|u_g-u_p|$$

where

$$A_1 = \frac{3}{4}\frac{\rho_g}{\rho_p}\frac{1}{d_p}C_D(Re_p)$$

Letting

$$s_1 = sign\,(u_g-u_p)$$

we get

$$\frac{du_p}{dt} = A_1 s_1 (u_g-u_p)^2$$

making the substituion

$$x = (u_g-u_p) \qquad \Rightarrow \qquad dx = -du_p$$

Hence

$$-\frac{dx}{dt} = A_i s_i x^2$$

integrating gives

$$\left[\frac{1}{x}\right]_{x_{i-1}}^{x_i} = A_i s_i \tau$$

which gives

$$x_i = \frac{x_{i-1}}{1 + A_i s_i x_{i-1} \tau}$$

resubstituting for x gives

$$(u_g - u_{p_i}) = \frac{u_g - u_{p_{i-1}}}{1 + A_i s_i (u_g - u_{p_{i-1}}) \tau}$$

which gives the solution

$$u_{p_i} = u_g - \frac{u_g - u_{p_{i-1}}}{1 + A_i s_i (u_g - u_{p_{i-1}}) \tau}$$

This needs to be integrated again to obtain the displacement

$$l_{p_i} = \int_0^\tau u_{p_i} dt$$

$$l_{p_i} = \int_0^\tau \left[u_g - \frac{u_g - u_{p_{i-1}}}{1 + A_i s_i (u_g - u_{p_{i-1}}) t} \right] dt$$

the solution of which is simply

$$l_{p_t} = u_g \tau - \frac{S_t}{A_t} \ln\left(1 + A_t S_t (u_g - u_{p_{t-1}})\,\tau\right)$$

Interaction is over when the relative displacement equals the eddy length scale, i.e.

$$l_e = \left| \int_0^\tau (u_g - u_p)\,dt \right| = \int_0^\tau |u_g - u_p|\,dt = s_t \int_0^\tau (u_g - u_p)\,dt$$

Hence

$$l_e = s_t \int_0^\tau u_g - \left(u_g - \frac{u_g - u_{p_{t-1}}}{1 + A_t S_t (u_g - u_{p_{t-1}})\,\tau}\right) dt = s_t \int_0^\tau \frac{u_g - u_{p_{t-1}}}{1 + A_t S_t (u_g - u_{p_{t-1}})\,\tau}\,dt$$

$$l_e = \frac{S_t}{A_t S_t} \ln\left(1 + A_t S_t (u_g u_{p_{tt}})\,\tau\right)$$

Solving for τ gives

$$\tau = \frac{e^{L_e A_t} - 1}{A_t S_t (u_g - u_{p_{t-1}})}$$

Derivation of limit $u_t >> (u_g - u_p)$

The initial equation reduces to

$$\frac{du_p}{dt} = A_t \mu_t (u_g - u_p)$$

making substitution

$$x = |u_g - u_p| = s_t(u_g - u_p) \quad \rightarrow \quad dx = -s_t dt$$

we get

$$-\int_{x_{t-1}}^{x_t} \frac{1}{x} dx = \int_0^{\tau} A_t \mu_t dt$$

$$-\ln \left| \frac{x_t}{x_{t-1}} \right| = A_t \mu_t \tau$$

$$\frac{x_t}{x_{t-1}} = e^{-A_t \mu_t \tau}$$

which gives the solution

$$u_{p_t} = u_g - (u_g - u_{p_{t-1}}) e^{-A_t \mu_t \tau}$$

integrating to give displacement

$$l_{p_t} = u_g \tau - \int_0^{\tau} (u_g - u_{p_{t-1}}) e^{-A_t \mu_t t} dt$$

$$= u_g \tau + \frac{(u_g - u_{p_{t-1}})}{A_t u_t} (e^{-A_t \mu_t \tau} - 1)$$

Hence

$$l_{p_t} = u_g \tau + \frac{(u_g - u_{p_{t-1}})}{A_t u_t} (e^{-A_t u_t \tau} - 1)$$

Using the same method as above the interaction time is given by

$$\tau = -\frac{1}{A_t \mu_t} \ln \left| \frac{(u_g - u_{p_{t-1}})}{(u_g - u_{p_{t-1}}) - l_e A_t u_t} \right|$$

Limiting case $u_t \to 0$

Firstly consider

$$\frac{1}{u_t}\ln\left|\frac{u_t+(u_t^2+x^2)^{\frac{1}{2}}}{x}\right| = A_t\tau$$

interior of logarithm as $u_t \to 0$

$$\frac{u_t+(u_t^2+x^2)^{\frac{1}{2}}}{x} = \frac{u_t}{x}+(1+O(u_t^2))^{\frac{1}{2}}$$

$$= \frac{u_t}{x}+1$$

assuming $O(u_t^2)$ terms can be neglected in the limit $u_t \to 0$

Expanding the log gives

$$\frac{1}{u_t}\ln\left|1+\frac{u_t}{x}\right| = \frac{1}{u_t}\frac{u_t}{x} = \frac{1}{x}$$

hence

$$\frac{1}{x} = A_t\tau$$

resubtituting for x

$$\frac{1}{(u_g - u_p)} = A_i \tau$$

which is the same result as in the original model

Skipping to the solution of u_{pi}

$$u_p = u_g + \frac{2cu_t}{(1-c^2)}$$

With

$$c = \frac{u_t + (u_t^2 + x_{i-1}^2)^{\frac{1}{2}}}{x_{i-1}} e^{A_i \mu_i \tau}$$

taking the limit of second term on RHS as $u_t \to 0$

$$u_t \to 0 \qquad c \to (\frac{u_t}{x} + 1)(1 + A_i \mu_i \tau) = 1 + u_t(\frac{1}{x_{i-1}} + A_i \mu_i \tau) + O(u_t^2)$$

$$c^2 \to 1 + 2u_t(\frac{1}{x_{i-1}} + A_i \mu_i \tau) + O(u_t^2)$$

hence

$$2u_t \left(\frac{1 + u_t(\frac{1}{x_{i-1}} + A_i \mu_i \tau)}{1 + 2u_t(\frac{1}{x_{i-1}} + A_i \mu_i \tau) - 1} \right)$$

$$= u_t\left(\frac{1}{u_t\left(\frac{1}{x_{t-1}}+A_t\mu_t\tau\right)}+1\right)$$

$$= \frac{(u_g-u_{p_{t-1}})}{1+A_t(u_g-u_{p_{t-1}})\tau}$$

which gives

$$u_{p_t} = u_g - \frac{(u_g-u_{p_{t-1}})}{1+A_tS_t(u_g-u_{p_{t-1}})\tau}$$

which is the original result, as required

Check solution of displacement integral as $u_t \to 0$

$$\alpha e^{\beta t} \to 1+u_t\left(\frac{1}{x_{t-1}}+A_t\tau\right) \qquad , \qquad \alpha \to 1+\frac{u_t}{x_{t-1}}$$

equation to consider is

$$l_{p_t} = u_g\tau + \frac{s_t}{A_t}\ln\left|\frac{1+\alpha e^{\beta t}}{1-\alpha e^{\beta t}}\frac{1-\alpha}{1+\alpha}\right|$$

in the limit the term inside the log becomes

$$\frac{1+\alpha e^{\beta t}}{1-\alpha e^{\beta t}}\frac{1-\alpha}{1+\alpha} \to \frac{2+1+u_t\left(\frac{1}{x_{t-1}}+A_t\tau\right)}{u_t\left(\frac{1}{x_{t-1}}+A_t\tau\right)}\frac{\frac{u_t}{x_{t-1}}}{2+\frac{u_t}{x_{t-1}}}$$

$$= \frac{\frac{2u_t}{x_{t-1}} + O(u_t^2)}{2u_t\left(\frac{1}{x_{t-1}} + A_t\tau\right) + O(u_t^2)}$$

$$= \frac{1}{1 + A_t x_{t-1}\tau}$$

substitute into above equation

$$l_{p_t} = u_g\tau + \frac{s_t}{A_t}\ln\left(\frac{1}{1 + A_t s_t(u_g - u_{p_{t-1}})\tau}\right)$$

$$l_{p_t} = u_g\tau - \frac{s_t}{A_t}\ln\left(1 + A_t s_t(u_g - u_{p_{t-1}})\tau\right)$$

Which is the desired result.

Finally consider the time equation

$$\tau = \frac{1}{\beta}\ln\left|\frac{1}{\alpha}\frac{\epsilon e^{\gamma} - 1}{\epsilon e^{\gamma} + 1}\right|$$

where

$$\epsilon = \frac{1+\alpha}{1-\alpha} \qquad \& \qquad \gamma = A_t l_e$$

In the limit $u_t \to 0$

Again consider the interior of the logarithm

$$\left|\frac{1}{\alpha}\frac{\epsilon e^{\gamma}-1}{\epsilon e^{\gamma}+1}\right|$$

As before

$$\alpha \to 1+\frac{u_t}{x_{t-1}}+O(u_t^2) \quad \& \quad \epsilon \to -\frac{2}{\frac{u_t}{x_{t-1}}}-1$$

letting $\theta = \frac{u_t}{x_{t-1}}$

$$\Rightarrow \alpha \to 1+\theta \quad \& \quad \epsilon \to -\frac{2}{\theta}-1$$

Thus

$$\left|\frac{1}{\alpha}\frac{\epsilon e^{\gamma}-1}{\epsilon e^{\gamma}+1}\right| \to \left|\frac{1}{1+\theta}\frac{(-\frac{2}{\theta}-1)e^{\gamma}-1}{(-\frac{2}{\theta}-1)e^{\gamma}+1}\right|$$

$$= \left|\frac{1}{1+\theta}\frac{(1+\frac{\theta}{2})e^{\gamma}+\frac{\theta}{2}}{(1+\frac{\theta}{2})e^{\gamma}-\frac{\theta}{2}}\right|$$

$$= \left|\frac{1}{1+\theta}\frac{\frac{\theta}{2}(1+e^{-\gamma})+1}{\frac{\theta}{2}(1+e^{-\gamma})-1}\right|$$

Taking the limit $u_t \to 0$

$$\to \quad \theta,\ \frac{\theta}{2}(1+e^{-\gamma}),\ \frac{\theta}{2}(1-e^{-\gamma}) \to 0$$

Thus

$$|(1-\theta)(\tfrac{\theta}{2}(e^{-\gamma}+1)+1)(1-\tfrac{\theta}{2}(1-e^{-\gamma}))| = |\theta(e^{-\gamma}-1)+1|$$

Taking the limit of the logarithm as $\theta \to 0$

$$\ln|\theta(e^{-\gamma}-1)+1| \to \theta(e^{-\gamma}-1)$$

Thus resubtituting for θ and x we get

$$\tau = \frac{e^{A_t l_s}-1}{A_t s_t (u_g - u_{p_{t-1}})}$$

Which is the required result.

Limiting Case $1/u_t \to 0$ (i.e. $u_t >> (u_g - u_p)$)

Firstly consider the velocity equation

$$u_p = u_g + \frac{2 s_t u_t c}{1-c^2}$$

With $c = \alpha e^{\beta\tau}$, for definitions of α and β see earlier.

In the limit of $1/u_t \to 0$ we get

$$\alpha \to \frac{2u_t}{x_{t-1}} \quad \Rightarrow \quad c \to \frac{2u_t}{x_{t-1}} e^{\beta\tau}$$

Consider the second term in the above velocity equation

$$\frac{2 s_t u_t c}{1-c^2} \to \frac{2 s_t u_t (\frac{2u_t}{x_{t-1}} e^{\beta\tau})}{1-(\frac{2u_t}{x_{t-1}} e^{\beta\tau})^2}$$

Which, after some algebraic manipulation, gives

$$-s_i x_{i-1} e^{-\beta\tau}$$

Resubstituting for x_{i-1} and β we get

$$u_p = u_g - (u_g - u_{p_{i-1}}) e^{-A_i u_i \tau}$$

As required

Secondly consider the displacement equation

$$l_p = u_g \tau + \frac{s_i u_i}{\beta} \ln \left| \frac{\alpha e^{\beta\tau} + 1}{\alpha e^{\beta\tau} - 1} \frac{\alpha - 1}{\alpha + 1} \right|$$

Consider the second term in the above equation in the required limit, using the previously defined properties and lettng $\theta = \frac{x_{i-1}}{u_i}$ and hence $\alpha \to \frac{2}{\theta}$

Hence

$$\frac{s_i u_i}{\beta} \ln \left| \frac{\alpha e^{\beta\tau} + 1}{\alpha e^{\beta\tau} - 1} \frac{\alpha - 1}{\alpha + 1} \right| \to \frac{s_i}{A_i} \ln \left| \frac{\frac{2}{\theta} e^{\beta\tau} + 1}{\frac{2}{\theta} e^{\beta\tau} - 1} \frac{\frac{2}{\theta} - 1}{\frac{2}{\theta} + 1} \right|$$

$$= \frac{s_i}{A_i} \ln \left| \frac{1 + \frac{\theta}{2} e^{-\beta\tau}}{1 - \frac{\theta}{2} e^{-\beta\tau}} \frac{1 - \frac{\theta}{2}}{1 + \frac{\theta}{2}} \right| = \frac{s_i}{A_i} \ln \left| (1 + \frac{\theta}{2} e^{-\beta\tau})^2 (1 - \frac{\theta}{2})^2 \right|$$

Taking the square out of the logarithm gives

$$\frac{2 s_i}{A_i} \ln \left| (1 + \frac{\theta}{2} e^{-\beta\tau})(1 - \frac{\theta}{2}) \right| = \frac{2 s_i}{A_i} \ln \left| 1 + \frac{\theta}{2} (e^{-\beta\tau} - 1) \right|$$

Taking the limit of the logarithm gives

$$\frac{2s_t}{A_t}\frac{\theta}{2}(e^{-\beta\tau}-1) = \frac{s_t x_{t-1}}{A_t u_t}(e^{\beta\tau}-1)$$

Hence

$$l_p = u_g\tau + \frac{(u_g - u_{p_{t-1}})}{A_t u_t}\left\{e^{A_t u_t \tau}-1\right\}$$

As required

Finally consider the time equation

$$\tau = \frac{1}{\beta}\ln\left|\frac{1}{\alpha}\frac{\epsilon e^{-\gamma}-1}{\epsilon e^{-\gamma}+1}\right|$$

Where the definitions of α and ϵ are as before, thus

$$\alpha \to \frac{2}{\theta} \quad ; \quad \epsilon \to \frac{1+\frac{2}{\theta}}{1-\frac{2}{\theta}}$$

Hence in the limit

$$\frac{\theta}{2}\frac{(1+\frac{2}{\theta})e^{-\gamma}-(1-\frac{2}{\theta})}{(1+\frac{2}{\theta})e^{-\gamma}+(1-\frac{2}{\theta})} = \frac{\theta}{2}\frac{(\theta+2)e^{-\gamma}-(\theta-2)}{(\theta+2)e^{-\gamma}+(\theta+2)}$$

Notice also that in the limit $u_t \to 0 \quad ; \quad A_t l_e \to 0 \quad \therefore \quad e^{\gamma} \to (1+\gamma)$

$$\frac{\theta}{2}\frac{(\theta+2)-(\theta-2)e^{\gamma}}{(\theta+2)-(\theta-2)e^{\gamma}} = \frac{\theta}{2}\frac{(\theta+2)-(\theta-2)(1+\gamma)}{(\theta+2)+(\theta-2)(1+\gamma)} = \frac{\theta}{2}\frac{4+2\gamma}{2\theta-2\gamma}$$

Since $4 \gg 2\gamma$ we get

$$\frac{\theta}{2}\frac{4}{2\theta-2\gamma}=\frac{\theta}{\theta-\gamma}$$

Thus

$$\frac{\frac{x_{t-1}}{u_t}}{\frac{x_{t-1}}{u_t}-A_t l_e}=\frac{x_{t-1}}{x_{t-1}-A_t l_e u_t}$$

Hence

$$\tau=\frac{1}{A_t u_t}\ln\left|\frac{u_g u_{p_{t1}}}{(u_g-u_{p_{t-1}})-A_t l_e u_t}\right|$$

As required

APPENDIX II - Quadratic Initial Form

To investigate the initial quadratic form of the displacement of a particle the following representation of the particle displacement needs to be considered

$$x(t) = \int_0^t v(\tau)\,d\tau$$

which leads to a mean square displacement of

$$\langle x^2(t)\rangle = \left\langle \left(\int_0^t v(\tau)\,d\tau\right)^2 \right\rangle = \left\langle \int_0^t \int_0^t v(\tau)\,v(T)\,d\tau\,dT \right\rangle$$

The average can be taken inside the integral signs to give

$$\langle x^2(t)\rangle = \int_0^t dT \int_0^t d\tau \langle v(\tau)v(T)\rangle$$

Introducing the autocorrelation function

$$R(\tau,T) = \langle v(\tau)v(T)\rangle$$

and assuming this is stationary i.e.

$$R(\tau,T) = R(\tau - T)$$

we get

$$\langle x^2(t)\rangle = \int_0^t dT \int_0^t d\tau\, R(\tau,T)$$

letting

$$\theta = \tau - T \quad \rightarrow \quad d\theta = d\tau$$

we get

$$\langle x^2(t) \rangle = \int_0^t dT \int_{-T}^{t-T} d\theta R(\theta)$$

The domain of the integral is

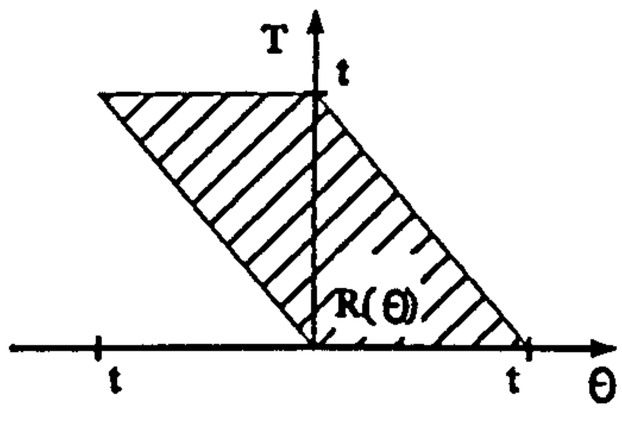

Using the definition of symmetry of the autocorrelation function

$$R(\theta) = R(-\theta)$$

To give

$$\langle x^2(t) \rangle = \int_0^t dT \int_0^{t-T} d\theta R(\theta) + \int_{-t}^0 dT \int_{-T}^t d\theta R(\theta)$$

Changing the order of integration gives

$$\langle x^2(t) \rangle = \int_0^t d\theta R(\theta)(t-\theta) + \int_0^t d\theta R(\theta)(t-\theta) = 2\int_0^t d\theta R(\theta)(t-\theta)$$

Hence

$$\langle x^2(t)\rangle = 2\int_0^t d\theta (t-\theta) R(\theta)$$

If we define the diffusion coefficient as

$$D = \frac{1}{2}\frac{d\langle x^2(t)\rangle}{dt} = \int_0^t d\theta R(\theta)$$

In the limit of large t

$$D_\infty = \frac{\langle x^2(t)\rangle}{2t} = \int_0^\infty d\theta R(\theta)$$

Special Case - Fluid Point

For the fluid point the non-dimensional autocorrelation function $R_L(t,t+\tau)$ is given by

$$R_L(t,t+\tau) = \frac{\langle v(t)\, v(t+\tau)\rangle}{\langle v^2(t)\rangle}$$

For the simple model considered this is known and given by

$$R_L(t,t+\tau) = \begin{cases} \left(1-\dfrac{\tau}{t_d}\right) & \tau \le t_d \\ 0 & \tau > t_d \end{cases}$$

Where t_d is the eddy lifetime

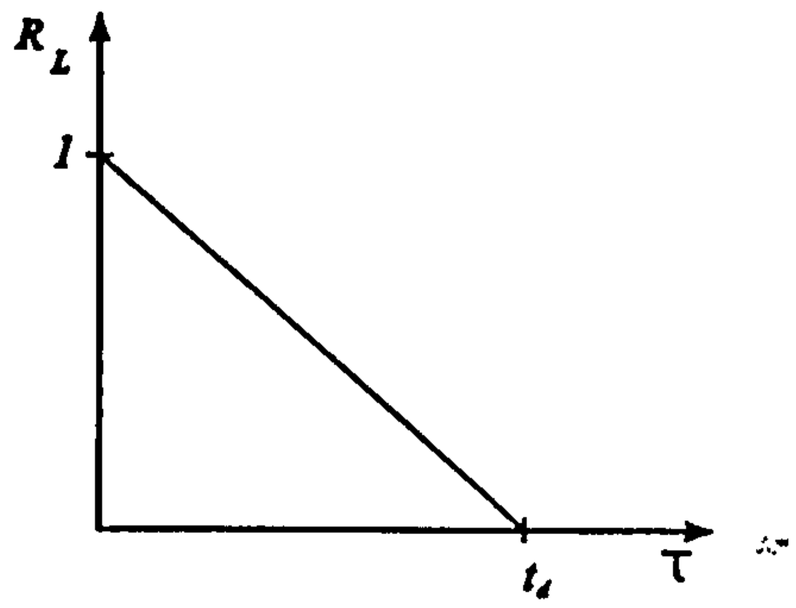

Letting τ correspond to θ we get

$$R(\theta) = \langle v^2(t) \rangle \left(1 - \frac{\theta}{t_d} \right)$$

For the fluid point $\langle v^2(t) \rangle$ is a constant given by the square of the velocity scale, u_e, thus

$$R(\theta) = u_e^2 \left(1 - \frac{\theta}{t_d} \right)$$

Thus the diffusion coefficient of the fluid point is

$$D_{fp}(t) = u_e^2 \int_0^t d\theta \left(1 - \frac{\theta}{t_d} \right) = u_e^2 t \left[1 - \frac{t}{2 t_d} \right] \qquad t \le t_d$$

Using the above definition of the fluid point autocorrelation function we can find the fluid point mean square displacement from

$$\langle x^2(t) \rangle = 2 u_e^2 \int_0^t d\theta \, (t-\theta) \left(1 - \frac{\theta}{t_e} \right) = 2 u_e^2 \left[t\theta - \frac{\theta^2}{2} \left(1 + \frac{t}{\theta} \right) + \frac{\theta^3}{3 t_e} \right]_0^t$$

Consider initial region where $t \le t_d$,we get

$$\langle x^2(t)\rangle = u_e^2 t^2\left[1-\frac{t}{t_d}+\frac{2t}{3t_e}\right] = u_e^2 t^2\left[1-\frac{t}{3t_d}\right] \qquad t \le t_d$$

Also consider the asymptotic region $t \geq t_d$, we get

$$\langle x^2(t)\rangle = u_e^2\left[tt_d-\frac{t_d^2}{2}+\frac{tt_d}{2}+\frac{t_d^2}{3}\right] = u_e^2 tt_d\left[1-\frac{t_d}{3t}\right] \qquad t \ge t_d$$

Hence

$$\langle x^2(t)\rangle = \begin{cases} u_e^2 t^2\left[1-\dfrac{t}{3t_d}\right] & t \le t_d \\ u_e^2 tt_d\left[1-\dfrac{t_d}{3t}\right] & t \ge t_d \end{cases}$$

APPENDIX III - Statistics of a Sequence of Random Signs

Presented below is an analysis of a random walk (Markov process) consisting of a sequence of random signs which occur with equal probability. The basis for the work was first given by Chandraseka (1943) in a well known paper on stochastic processes. The relevance of this analysis to the current work lies in the calculation of the particle diffusion coefficient. The following contains a proof that a sequence consisting of the square of a sum of random signs is non-ergodic. First the sequence of random signs itself is considered and shown to be ergodic.

Consider the sequence $\{\Omega_n\}$ defined by

$$\Omega_n = \frac{1}{n}\sum_{i=1}^{n} s_i$$

where s_i is a random sign with equal probability of being positive or negative.

The probability density function for the sequence of signs is denoted by $P\{\Omega,n\}$ (such that $\Omega_n = \Omega/n$), following Chandraseka

$$P\{\Omega,n\} = \frac{n!}{\left(\frac{n+m}{2}\right)!\left(\frac{n-m}{2}\right)!} = \left(\frac{1}{2}\right)^n \binom{n}{m} \qquad \text{(III-1)}$$

where

$$m = \frac{\Omega+n}{2} \quad \rightarrow \quad \Omega = 2m-n$$

and $\binom{n}{m}$ is the binomial coefficient.

Therefore, the mean of Ω_n can be written as

$$\bar{\Omega}_n = \sum_{m=1}^{n}\left(\frac{1}{m}\sum_{i=1}^{m} s_i\right) P\{\Omega,n\} \qquad \text{(III-2)}$$

In order to solve (III-2) we first consider

$$(px+q)^n = \sum_{m=1}^{n} p^m q^{n-m} x^m \binom{n}{m} \qquad \text{(III-3)}$$

where p and q are the probabilities of a + or - value of s_i and hence are given by p=q=1/2. First we differentiate (III-3) w.r.t x and set p=q=1/2 to give

$$xn(x+1)^{n-1} = \left(\frac{1}{2}\right)^n \sum_{m=1}^{n} m x^m \binom{n}{m}$$

Substituting x=1 gives

$$\frac{1}{2^n} xn(x+1)^{n-1} = \frac{n}{2} = \left(\frac{1}{2}\right)^n \sum_{m=1}^{n} m \binom{n}{m} \qquad \text{(III-4)}$$

It is useful here to continue to differentiate (III-3) pre-multiplying both sides by x before each differentiation and substituting x=1 as above. This leads to the following expressions obtained using the second, third and fourth derivative.

Second derivative

$$\frac{n^2+n}{4} = \left(\frac{1}{2}\right)^n \sum_{m=1}^{n} m^2 \binom{n}{m} \qquad \text{(III-5)}$$

Third derivative

$$\frac{n^3+3n^2}{8} = \left(\frac{1}{2}\right)^n \sum_{m=1}^{n} m^3 \binom{n}{m} \qquad \text{(III-6)}$$

Fourth derivative

$$\frac{n^4+6n^3+3n^2-2n}{16} = \left(\frac{1}{2}\right)^n \sum_{m=1}^{n} m^4 \binom{n}{m} \qquad \text{(III-7)}$$

Returning to (III-1), we can re-write the mean as

$$\bar{\Omega}_n = \sum_{i=1}^{n} \Omega_n P\{\Omega,n\} = \sum_{m=1}^{n} \frac{1}{n}(2m-n)P\{\Omega,n\}$$

It follows from (III-1) and (III-3) that

$$\bar{\Omega}_n = \frac{1}{n}(2\frac{n}{2}-n) = 0$$

Hence the mean of the sequence Ω_n is zero

In order to determine the variance of Ω_n we need to consider

$$\sigma^2_{\Omega_n} = \sum_{i=1}^{n} (\Omega_n - \bar{\Omega}_n)^2 P\{\Omega,n\}$$

Since the mean of Ω_n is zero this reduces to

$$\sigma^2_{\Omega_n} = \sum_{i=1}^{n} \Omega_n^2 P\{\Omega,n\} = \sum_{m=1}^{n} \frac{1}{n^2}\left(\sum_{i=1}^{m} s_i\right)^2 P\{\Omega,n\} \qquad \text{(III-8)}$$

We can apply the same approach as for the calculation of the mean, above. Using (III-8) and (III-5), we get

$$\sigma^2_{\Omega_n} = = \sum_{m=1}^{n} \frac{1}{n^2}(2m-n)^2 P\{\Omega,n\} = \frac{1}{n^2}(n^2+n-2n^2+n^2) = \frac{1}{n}$$

Which gives a variance for Ω_n of 1/n. Thus

$$\bar{\Omega}_n = 0 \quad , \quad \sigma^2_{\Omega_n} = \frac{1}{n} \qquad \text{(III-9)}$$

Equations (III-9) clearly show that, in the limit of a large number of samples ($n \to \infty$) the variance of Ω_n tends to zero and it follows, therefore, that the sequence Ω_n is ergodic.

Of great interest in the calculation of a diffusion process is the behaviour of the sequence

consisting of the square of the above sequence

$$\Upsilon_n^2 = \frac{1}{n}\left(\sum_{i=1}^{n} s_i\right)^2 \qquad \text{(III-10)}$$

The statistics of (III-10) can be found in a similar manner to that employed for the sequence Ω_n. The mean of (III-10) is given by

$$\overline{\Upsilon_n^2} = \sum_{m=1}^{n} \Upsilon_n^2 P\{\Upsilon,n\} = \sum_{m=1}^{n} \frac{1}{n}\left(\sum_{i=1}^{m} s_i\right)^2 P\{\Upsilon,n\} = \sum_{m=1}^{n} \frac{1}{n}(2m-n)^2 P\{\Upsilon,n\}$$

Again using (III-5) we obtain

$$\overline{\Upsilon_n^2} = \frac{1}{n}(n^2+n-2n^2+n^2) = 1$$

Hence the mean of Υ_n^2 is one.

The variance of (III-10) is given by

$$\sigma_{\Upsilon_n^2}^2 = \sum_{m=1}^{n} (\Upsilon_n^2-\overline{\Upsilon_n^2})^2 P\{\Upsilon,n\} = \sum_{m=1}^{n} \left(\frac{1}{n}\left(\sum_{i=1}^{m} s_i\right)^2 - \overline{\Upsilon_n^2}\right)^2 P\{\Upsilon,n\}$$

The mean of Υ_n^2 is one and expanding $(\Upsilon^2_n-1)^2$, we get

$$\sigma_{\Upsilon_n^2}^2 = \sum_{m=1}^{n} \{\frac{1}{n^2}(2m-n)^4 - \frac{2}{n}(2m-n)^2+1\} P\{\Upsilon,n\}$$

Expanding the products, and using (III-4), (III-5), (III-6), (III-7) we get

$$\sigma_{\Upsilon_n^2}^2 = 2-\frac{2}{n}$$

Therefore,

$$\overline{\Upsilon_n^2} = 1 \qquad , \qquad \sigma_{\Upsilon_n^2}^2 = 2-\frac{2}{n} \qquad \text{(III-11)}$$

It follows from (III-11) that in the limit of large n ($n \to \infty$) the variance of Υ_n^2 tends to a finite, but non-zero value, and hence the sequence Υ_n^2 is non-ergodic.

APPENDIX IV - Derivation of Second Phase Conservation Equations.

Mass Conservation

Consider

$$\frac{\partial c}{\partial t} + \frac{\partial}{\partial x_i}(c u_i) = 0$$

Where the zero on the RHS corresponds to zero source terms. Letting

$$c = C + c' \qquad ; \qquad u_i = U_i + u_i'$$

Reynolds averaging gives

$$\frac{\partial}{\partial t} C + \frac{\partial}{\partial x_i}\left\{ C U_i + \overline{c' u_i'} \right\} = 0$$

Applying the diffusion approximation

$$\overline{c' u_i'} = -\Gamma \frac{\partial C}{\partial x_i}$$

We get

$$\frac{\partial}{\partial t} C + \frac{\partial}{\partial x_i}(C U_i) = \frac{\partial}{\partial x_j}\left(\Gamma \frac{\partial C}{\partial x_j} \right)$$

Momentum Conservation

Consider

$$\frac{\partial}{\partial t}(c u_i) + \frac{\partial}{\partial x_j}(c u_i u_j) = F$$

Where F represents external forces. Reynolds averaging we get

$$\frac{\partial}{\partial t}(C U_i) + \frac{\partial}{\partial t}(\overline{c' u_i'}) + \frac{\partial}{\partial x_j}\left\{C U_i U_j + \overline{c' u_i'} U_j + \overline{c' u_j'} U_i + \overline{c' u_i' u_j'} + C\overline{u_i' u_j'}\right\} = \overline{F}$$

Since

$$\overline{u_i' u_j} = \delta_{ij}\overline{u_i'^2} \qquad \& \qquad \overline{c' u_i' u_j} = \Gamma^2 \frac{\partial^2 \overline{C}}{\partial x_i \partial x_j}$$

Using the above and previous approximation we get

$$C\frac{\partial U_i}{\partial t} - \frac{\partial}{\partial t}\left(\Gamma\frac{\partial C}{\partial x_j}\right) + C U_j \frac{\partial U_i}{\partial x_j} + \delta_{ij} U_i^2 \frac{\partial C}{\partial x_j} - \frac{\partial}{\partial x_j}\left(U_j \Gamma \frac{\partial C}{\partial x_j}\right) - \Gamma\frac{\partial C}{\partial x_j}\frac{\partial U_i}{\partial x_j} + \Gamma^2 \frac{\partial^3 C}{\partial x_i \partial^2 x_j} = \overline{F}$$

Conservation of $\Gamma\frac{\partial \overline{C}}{\partial x_j}$ and assuming that Γ is slowly varying gives

$$\frac{\partial}{\partial t}\left(\Gamma\frac{\partial C}{\partial x_j}\right) - \frac{\partial}{\partial x_j}\left(U_i \Gamma \frac{\partial C}{\partial x_i}\right) - \Gamma^2 \frac{\partial^3 C}{\partial x_i \partial^2 x_j} = 0$$

Hence

$$C\frac{\partial U_i}{\partial t} + C U_j \frac{\partial U_i}{\partial x_j} + \delta_{ij}\overline{u_i'^2}\frac{\partial C}{\partial x_j} - \Gamma\frac{\partial C}{\partial x_j}\frac{\partial U_i}{\partial x_j} = \overline{F}$$

If only the force of drag is considered

$$F = A_i c (u_{g_i} - u_i)\,|u_{g_i} - u_i| = A_i S_i c (u_{g_i} - u_i)^2$$

where

$$A_i = \frac{3}{4}\frac{\rho_g}{\rho_p}\frac{1}{d_p} C_D$$

and S_i is the sign of the relative velocity. Ignoring the fluctating component of the drag we get

$$\overline{F} = \overline{A_i} s_i C (U_{g_i} - U_{p_i})^2$$

Hence

$$C \frac{\partial U_i}{\partial t} + C U_j \frac{\partial U_i}{\partial x_j} + \delta_{ij} \overline{u_i'} \frac{\partial C}{\partial x_j} - \Gamma \frac{\partial C}{\partial x_j} \frac{\partial U_i}{\partial x_j} = \overline{A_i} s_i C (U_{g_i} - U_{p_i})^2$$